Numerical Methods for Hypersingular and Near-Singular Boundary Integrals in Fracture Mechanics

Earlin David Lutz
Ph.D Thesis

91-1203
May 1991

Department of Computer Science
Cornell University
Ithaca, NY 14853-7501

NUMERICAL METHODS FOR HYPERSINGULAR AND NEAR-SINGULAR BOUNDARY INTEGRALS IN FRACTURE MECHANICS

A Dissertation
Presented to the Faculty of the Graduate School
of Cornell University
in Partial Fulfillment of the Requirements for the Degree of
Doctor of Philosophy

by
Earlin David Lutz
May 1991

Numerical Methods for Hypersingular and Near-Singular Boundary Integrals in Fracture Mechanics

Earlin David Lutz, Ph.D.

Cornell University 1991

The boundary integral equation is one of several equivalent forms of governing equations that can be used to compute approximate solutions to boundary value problems in elasticity and potential flow analysis. Since it determines the entire solution in terms of values only on the boundary, there are possible order-of-magnitude advantages in solution time and geometric complexity over better known 'domain-based' methods such as finite elements and finite differences.

In practice, it has been hard to capitalize on these advantages. Many of the difficulties center around inability to perform certain numerical integrations. This thesis presents (a) a systematic 'modal' method of converting singular integrals to easier integrals over 'far' surfaces (b) an optimal quadrature method for the 'nearly singular' integration problem. An existence proof is given to show that all surface integrals arising from the 3D boundary integral can be converted to easier contour integrals if basis functions are constructed in a cartesian sense, rather than the

common parametric formulations. Stokes vectors needed to make this result useful are demonstrated for the Laplace equation and for some cases of elasticity.

Comparison to analytic benchmark cases shows that the method produces accurate stress intensity factors for 3-dimensional fracture analysis.

Biographical Sketch

Earlin David Lutz received a B.S. in Mechanical Engineering from the Pennsylvania State University (1978), an M.S. in Computer and Information Science from Rensselaer Polytechnic Institute (1981), and M.S. and Ph.D. in Computer Science from Cornell University (1991). He was employed from 1978 to 1981 as a scientific programmer for jet engine design software by United Technologies (Pratt & Whitney Aircraft), and from 1981 to 1982 by the General Electric Company as a research engineer for robotics. From 1982 to 1987 he was project leader for CAD software at Vector Automation, in Baltimore, Maryland.

To Marilyn, Melanie, and David

Acknowledgements

It has been a great privilege to study at Cornell for the past four years. Thesis committee members Anthony Ingraffea, David Gries, Herbert Voelcker, and Stephen Vavasis have each influenced the style and content of this research. Special thanks to David Gries for encouraging pursuit of interdepartmental research. John Hopcroft and Keith Marzullo served on an early thesis committee.

The technical material on hypersingular integration owes much to Leonard Gray and Luiz Martha. Fellow students Paul Wawrzynek, Dave Potyondy, and Jose Sousa provided the remarkable FRANSYS software. Allen Back and Vadim Shapiro have always been ready to listen to unusual ideas.

Financial support was provided by a fellowship from the Unisys Corporation. Additional funding for the Cornell Fracture Group was provided by Dowell Schlumberger and the Digitial Equipment Corporation. Computing facilities were provided by the Cornell University Program of Computer Graphics, Donald Greenberg, Director.

Finally, special thanks to Dr. and Mrs. Earlin H. Lutz and Dr. and Mrs. Robert Manning for their support and encouragement.

Table of Contents

List of Tables

List of Figures

Preface

As indicated in Fig. 0.1, Chapters 1 to 6 may be read in sequence as (a) a detailed development of a problem and (b) the theory of several increasingly detailed solutions.

Chapter 1 gives (a) an intuitive introduction to 'boundary value problems' such as stress, heat transfer, and potential flow analysis and (b) a summary of common ways of solving the problems. Chapter 2 is a detailed introduction to methods based on the boundary integral equation (BIE). Chapter 3 focuses on how the BIE becomes degenerate when a solid contains interior surfaces such as cracks. The degeneracy is, in principle, readily corrected by using a derivative (gradient) of the equation. However, the extra differentiation converts the already-troublesome singular problem of the primary BIE into an especially difficult form known as 'hypersingular' integral.

Chapter 4 describes methods that were applied to the hypersingular integration problem by prior researchers beginning in the mid-1980's. They are characterized by lengthy term-by-term manipulation of singular integrands. Chapter 5 shows that by reasoning about certain known solution modes we can systematically convert all of the difficult surface integrals to easier integrals over other surfaces. The derivations and final results are much simpler than prior methods, and are independent of both the geometric dimension and curvature or corners in the surface geometry.

Chapter 6 gives a theorem that shows that the modal results can, in principle, be

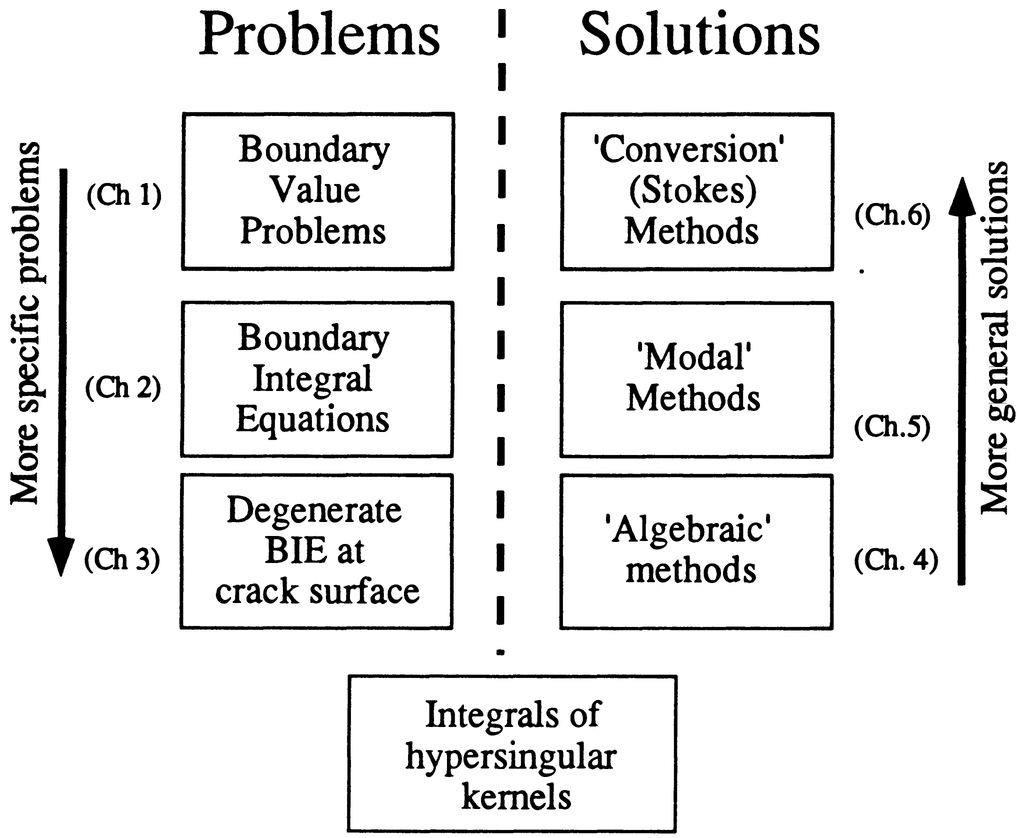

Figure 0.1: Organization of chapters leading up to and addressing hypersingular integration

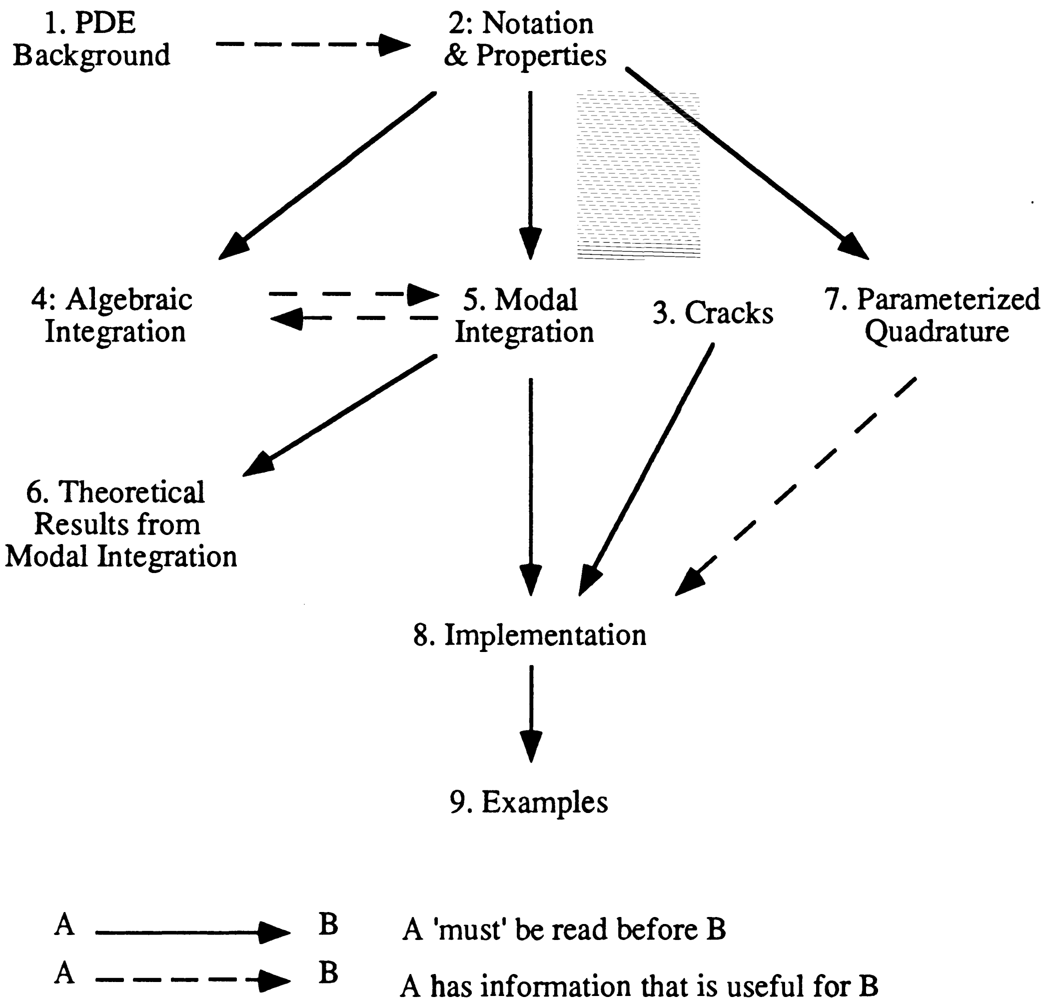

Figure 0.2: Chapter dependencies

even further simplified by Stokes theorem, which will convert the surface integrals to easier contour integrals. Attaining this simplification requires that certain vector expressions be determined. At the time of this writing, these vectors have been determined for several cases of the Laplace equation, but unfortunately not for elasticity.

An unfortunate side effect of the modal method is that its implementation requires computation of many 'nearly singular' integrals that have historically been very problematic numerically. Chapter 7 gives a new method of computing these integrals by using a family of Gaussian quadrature formulas that vary continuously with respect to a certain geometric parameter.

Chapter 8 describes an implementation based on the theory of Chapters 5 and 7. Chapter 9 gives numerical examples of results.

Fig. 0.2 indicates further dependencies among the Chapters. Because Chapter 1 is highly intuitive, it can be skipped by readers familiar with boundary value problems and boundary integrals. Chapter 2 introduces the technical material needed for all later chapters. The main path from this to the computational results is through Chapters 5 and 8. The historical information in Chapter 4 is useful but not necessary for understanding the new methods in Chapter 5. Chapter 6 contains conjectures about *future* implementations, and hence is not necessary for the current one. Chapters 3 is important in setting up the general problem, and Chapter 7 contributes to a particular integration problem that arises in the implementation.

Chapter 1

Intuitive Notions of Boundary Value Problems

This chapter gives an overview of boundary value problems and various methods of solving them. Compared to the more detailed mathematics of later chapters, this chapter is rather informal. The goal is to establish an intuitive notion of (a) how physical processes 'carry' information from the boundary of a solid to the interior, and (b) how this process is captured mathematically by approximate solution methods, particularly those based on the boundary integral equation. Within this intuitive presentation, we can identify several areas where the pure mathematical behavior of this integral equation has been difficult to mimic in real computation. Subsequent chapters will restate these problems in more formal form and propose new solutions.

1.1 Boundary Value Problems

A basic problem of engineering and science is to compute *field properties* such as temperature or stress distribution in a solid. That is, we are given an object, such as the hinge mount in Fig. 1.1, and asked questions such as:

> What is the maximum stress at in the corner at the front of the pin lug when a force is applied at the hole?
>
> If a small crack starts, will it grow, and if so in what direction?

The crack propagation question is highly relevant to this part, which is part of a door hinge on the American space shuttles. At the time that this thesis is being written, cracks in these hinges are causing significant concern for the safety of these vehicles [Lea91]. The computational methods in this thesis are directed at analysis of cracks of this type.

The essential mathematical issues of the crack problem also arise in the mathematically simpler problems of heat transfer, potential fluid flow, and electrostatics, all of which are represented by the Laplace partial differential equation.

This chapter treats all of these problems on an informal basis, attempting to give an intuitive feel for how various physical quantities are related to one another.

In each of these problems, there is some 'primary quantity' whose value varies (smoothly) throughout the interior. In the stress analysis and crack propagation problems, the primary quantity is the 'displacement' of each interior point from its original location. For the thermal problem, the primary quantity is temperature.

Engineering decisions – for example, selection of material or dimensions for the part – are usually not driven by the primary unknown itself. They more commonly depend on the derivatives (gradients) of the primary quantity. In elasticity, linear combinations of the derivatives have physical meaning of stresses and strains. In thermal and electrical potential problems, these derivatives have the physical meaning of heat and charge flux.

Gradient quantities can be interpreted as motion or flow. The single-valued primary quantity at each point in the solution field gives rise to different gradients

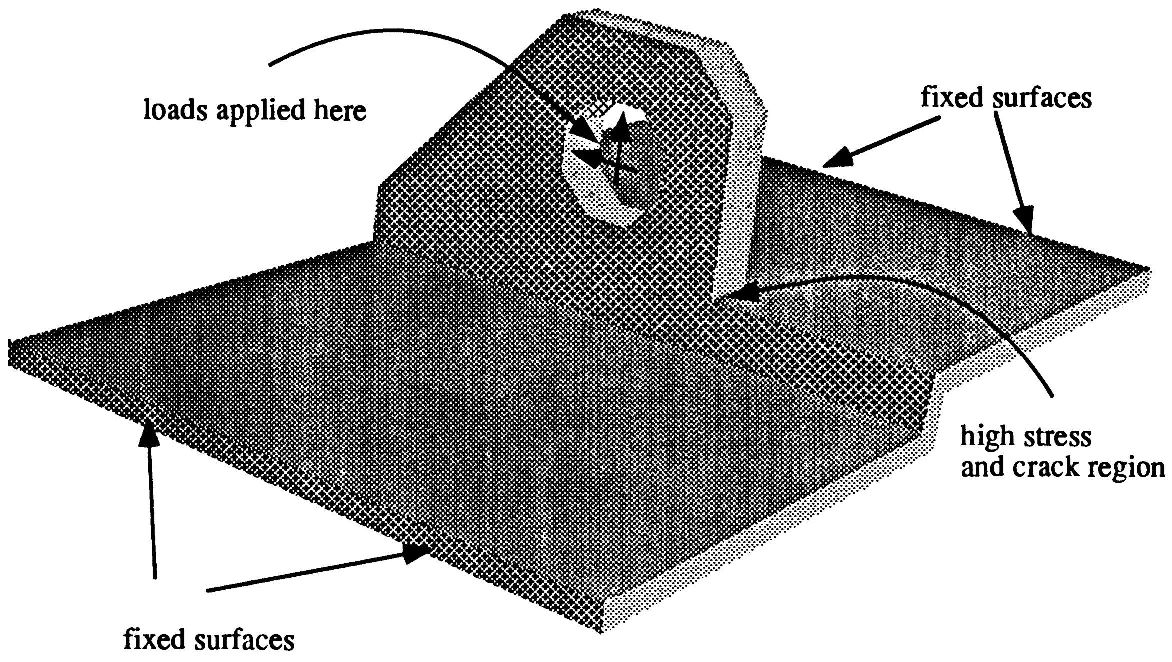

Figure 1.1: Space shuttle fuel door hinge

– flow rates – in different directions. At a surface point, the main derivative of interest is usually the one in the direction normal to the surface.

We must carefully distinguish among among the 'interior primary quantity', the 'surface primary quantity', and the 'surface normal derivative' quantity, and how each participates in the solution process.

To discuss this distinction, consider the schematic view in Fig. 1.2. The middle region of the figure represents the interior of the body. Two narrow bands are wrapped around the boundary. Shading in the interior region indicates a state in which values of the primary quantity are known everywhere in the interior. Shading in the inner boundary band indicates that the primary quantity values are known on the surface itself. Shading in the outer band indicates that the gradient quantity is known 'in the direction normal to the surface'.

Using this schematic, a field problem is a problem in which (a) a schematic is given with only some of the shaded regions shaded and (b) we are asked to fill in the unshaded regions.

The underlying physics and mathematics of these problems provide conditions (Ames [Ame77], Stakgold [Sta79]) under which this request can and cannot be satisfied:

If at every boundary point (see Fig. 1.3) (a) there is exactly one linear constraint imposed involving one or both of the two boundary bands and (b) those constraints include at least enough primary constraints to rule out multiple solutions that differ only by a 'rigid body motion', the problem will have a unique solution everywhere.

If the *interior primary values* are all known (see Fig. 1.4a), the problem is essentially solved already. Interior gradients can be determined by differentiating the given primary function. Both primary and

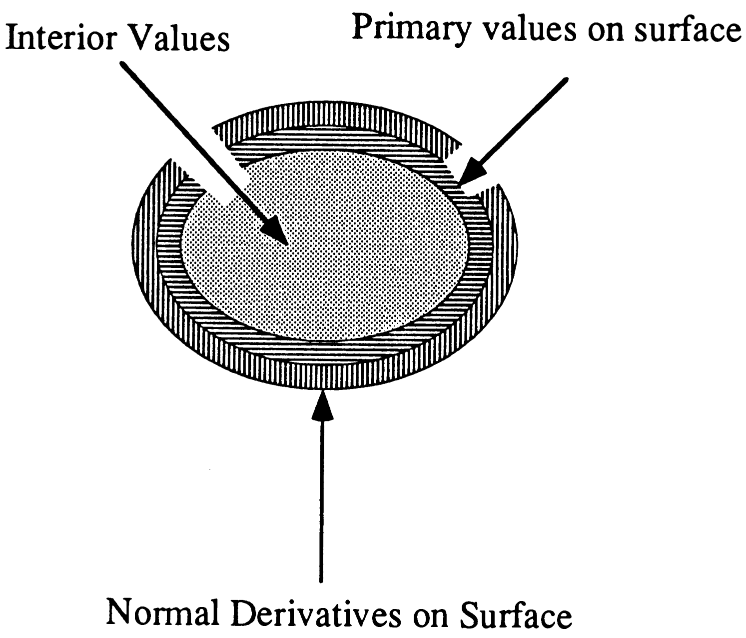

Figure 1.2: Schematic abstraction of interior values, surface values, and surface gradients of a field function.

gradient values at surface points can be determined by evaluating the limit of the interior values at points approaching the surface.

If boundary values are given in any combination other than as described in the previous cases, the problem is either over- or underspecified. If there is a portion of the boundary with neither band filled in (see Fig 1.4c), there are an infinite number of interior solutions that can satisfy the remaining boundary values. If there is a boundary portion with both bands filled in (see Fig 1.4b), there is generally no solution.

The essential property of a well posed problem is that exactly one constraint is imposed at each boundary point. Under these conditions, we can imagine that nature has some black box algorithm which, in one uninterrupted step, 'computes' all the interior values and the unspecified boundary value, as in Fig. 1.5.

Approximate methods for Solving Boundary Value Problems Unfortunately, the workings of the hypothetical black box can only be reproduced exactly for very simple geometries and boundary conditions. Analysis of real engineering structures depends on computations that (a) use only a finite number of degrees of freedom to approximate the infinite-degree-of-freedom solution and (b) allow quantities that should be identically 0 at an infinite number of points or when integrated over any of the infinite number of subsets of the given geometry to be nonzero at all except for only a finite number of points or subsets.

The fundamental step in devising an approximate solution method is to find a mathematical expression that couples the unknown part of the solution to the known parts in the boundary conditions. In the widely used finite difference and finite element methods, the chosen expressions are, respectively, the partial differential equation and an integrated error minimization condition. The conditions are

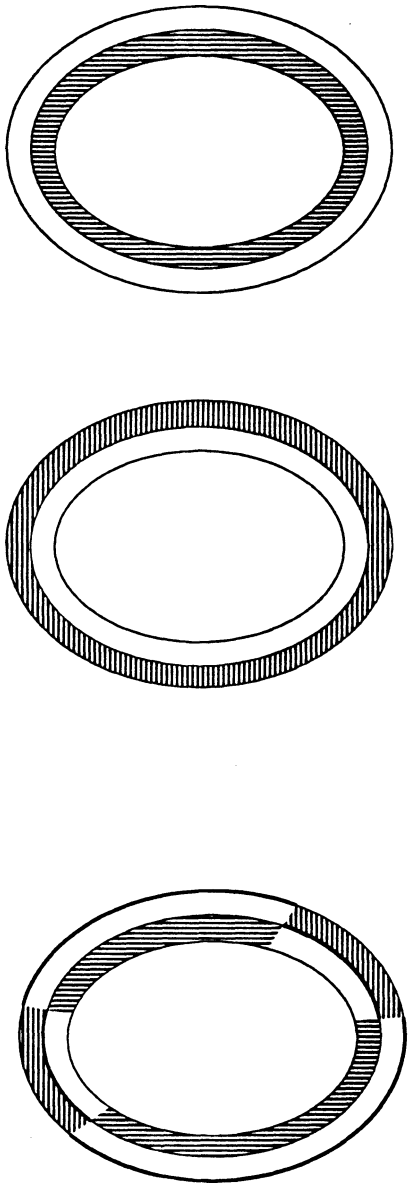

Primary Quantity Known at all boundary points

Normal derivative quantity known at all boundary points

General case: 1 of 2 values constrained (either by explicit value or as a function of the other) at each boundary point. Any boundary crossing must encounter 1 known value.

Figure 1.3: Well posed problems

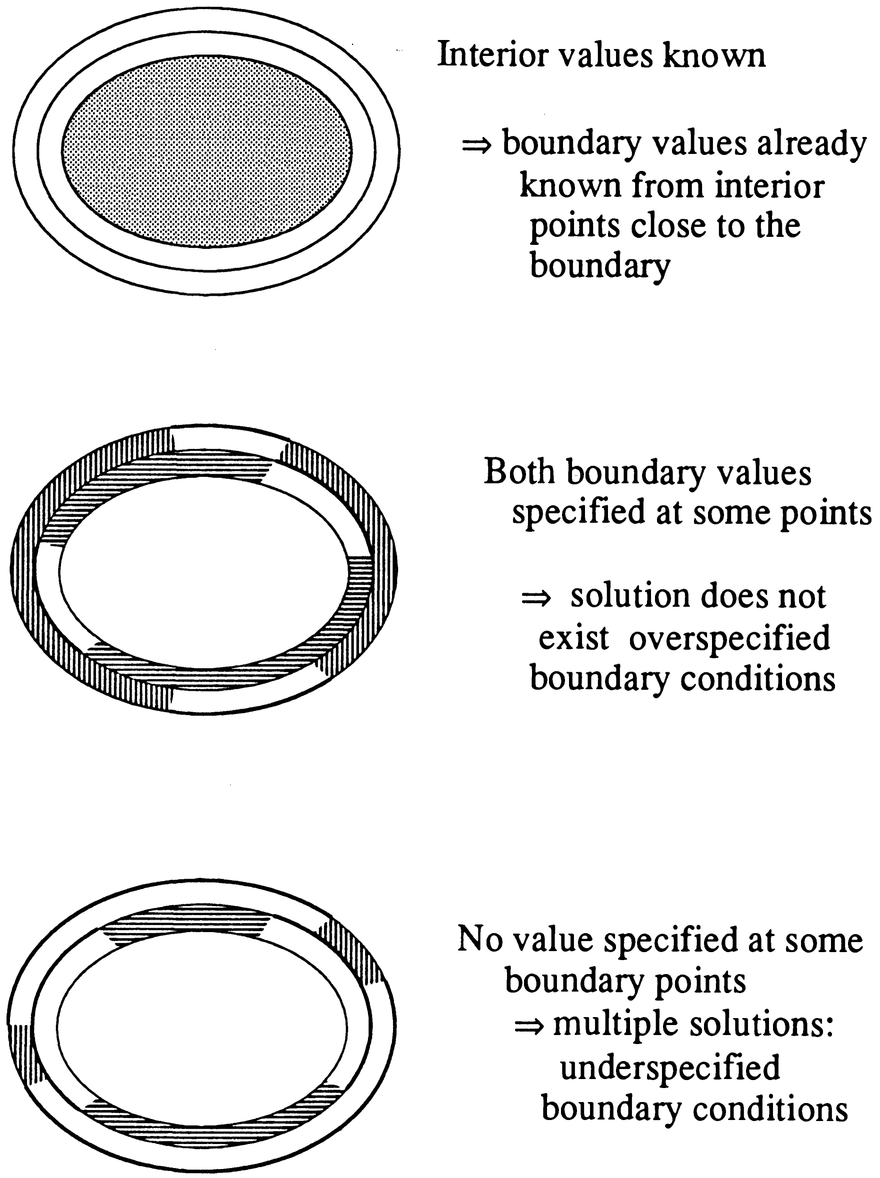

Figure 1.4: Ill posed problems

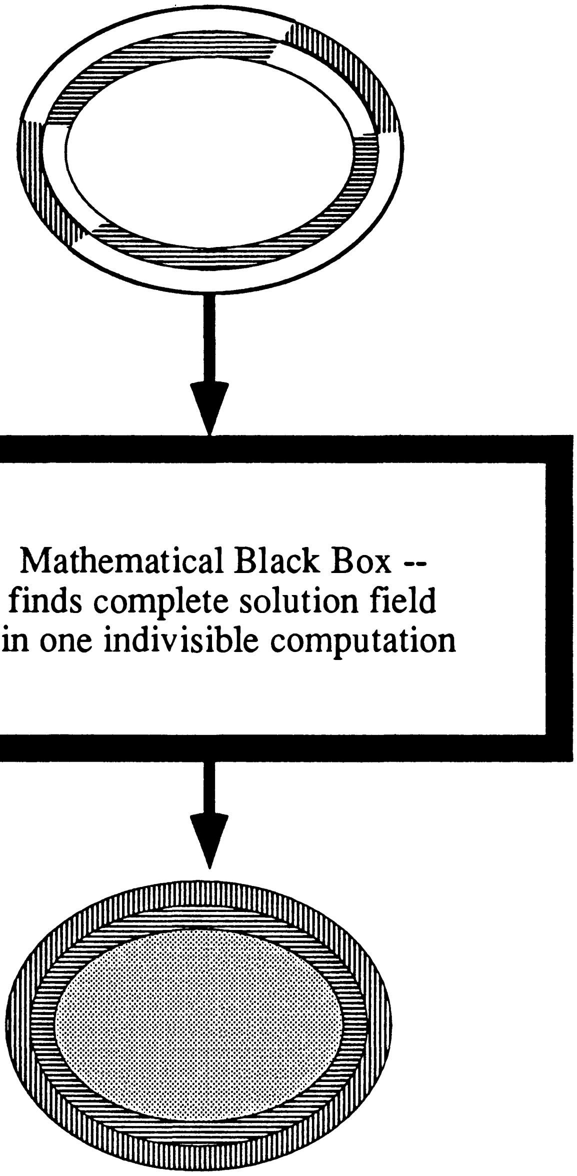

Figure 1.5: Exact, one-step solution process carried out by pure mathematics

enforced on a local basis (i.e. at individual points and on small volumes) at points distributed throughout the *volume* of the region. These methods implicitly assume that in order to find a field solution that (nearly) mimics the true material behavior 'everywhere' it is necessary to actively enforce some condition 'nearly everywhere'.

This thesis is concerned with a less-well-known solution method in which this critical first decision chooses a *boundary integral* condition. This is mathematically equivalent to the volumetric conditions, but provides an explicit formula for any interior-point field value as as integral that involves (a) the boundary geometry and (b) the values of *both the primary and gradient quantities on the boundary.* The entire construction is carried out using only the surface. Regardless of the complexity of the region or distance from an interior point to the surface, all information about how the solution field 'flows' through the interior is captured analytically by the integral formulation.

Fig. 1.6 uses the boundary band schematic to illustrate essential features of these three methods. In the finite difference method, solution of a linear system that emulates the partial differential equation on a point-by-point basis throughout the volume produces approximate function values at distinct nodal points in the interior. The construction provides no explicit indication of function values *between* the solution points. A finite element solution produces a similar grid of nodal values, but the analysis is explicitly based on a piecewise polynomial interpolation within each cell of the grid. The initial calculation can therefore be followed by evaluation of the polynomials to obtain a piecewise-smooth function throughout the interior. The initial boundary element solution produces solution values only at certain points on the surface. However, the linear system construction explicitly defines a polynomial interpolation so that the surface node values also define a piecewise smooth function everywhere on the surface. In addition, the integral formulation defines a further formula so that the solution field has a smooth, infinitely

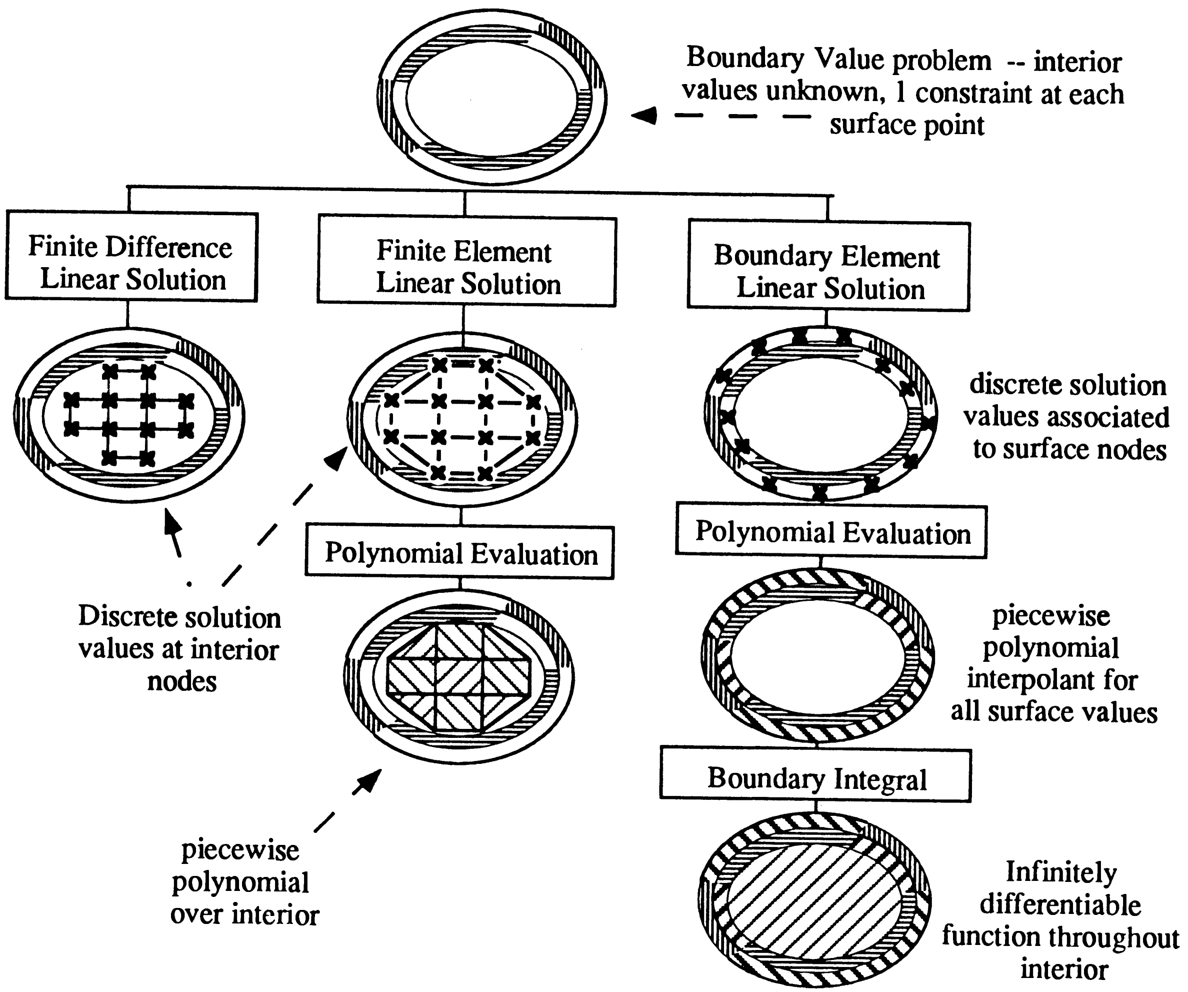

Figure 1.6: Schematic characteristics of finite difference, finite element, and boundary integral solution methods

differentiable representation everywhere in the interior.

1.1.1 Approximate Solution Methods

Despite the differences among the finite difference, finite element, and boundary element methods, there are significant similarities in the path from the abstract field problem to practical method. Certain key issues appear in all methods. In particular, each method is characterized by the following decisions:

1. Choose one of the numerous mathematical/physical conditions that are uniquely and exactly satisfied by the true solution.
2. Replace this exact expression by one that is identical except that the solution function is replaced by a linear combination of some yet-to-be-determined basis functions multiplied by undetermined functions.
3. Choose a representation of the geometry.
4. Choose a finite number of basis functions to insert in the linearized expression.
5. Express the boundary conditions in terms of the chosen geometry and basis functions.
6. Choose some method of enforcing the chosen physical condition the same number of times as there are unknown degrees of freedom.

The first two steps do *not* involve approximations. The initial choice among equivalent mathematical expressions does not lose anything contained in other expressions because an exact solution to one expression is an exact solution to all of them. The linearization (*before* choice of basis functions) is at least abstractly exact if given an infinite number of basis functions. It is therefore desirable to perform as much manipulation as possible in one of these two forms, prior to introduction of specific representation of geometry.

The following paragraphs present a brief summary of how each of these decisions is made in the finite element, finite difference, and boundary element methods.

Finite Difference Method The physical principle chosen is the partial differential equation of the material. The linearized form replaces each derivative in the PDE by a difference expression approximating the derivative as a linear combination of function values at distinct points. The geometry is represented by a collection of node points associated to neighbors in a grid structure. The basis functions are finite difference formulas or 'computational molecules' ([Ame77]) that specify what geometric values are to be extracted from the grid and used as coefficients of the approximated derivatives. Values of the primary function at boundary nodes are given by the nodal values; gradient boundary conditions are given by additional computational molecules.

The results of a finite difference solution are function values at *discrete* points. There is no intrinsic notion of what values the function has between these points, or of derivatives other than the particular ones that appear in the PDE. Gradients are extracted by application of additional computational molecules other than those in the original PDE differencing.

Finite Element Method There are numerous interpretations of the physical principle enforced by the finite element method. For elasticity, one interpretation is that the approximate solution is the one that has minimum energy among a set of functions that obey compatibility and constitutive laws (e.g. do not introduce non-physical behavior such as appearance of voids) and boundary conditions. The linearized form replaces the exact solution (which has an infinite number of possible shapes or modes) by a linear combination of particular (but still continuous) modes of deformation. Geometry is represented as a collection of simple cells (elements) mapped by a parametric coordinate system; the free surface of the approximate geometry may be different from that of the true geometry. The basis functions are low-order polynomials in the parametric coordinate system of each cell. Boundary displacements are expressed directly by the basis functions. Boundary gradients are expressed by integrating the gradients of the displacement function to obtain 'work equivalent nodal loads'

The construction of elements and basis functions provides a parameterized deformation function at all points on the approximate solid. This function is infinitely differentiable at all points other than the boundaries between elements. Most implementations enforce C^0 continuity between elements, and have discontinuities in all derivatives at element boundaries.

Boundary Element Method Material behavior is expressed by a *boundary integral* that expresses the solution value at each interior point as an integral (weighted average) of values of the function and its normal gradient quantity on the boundary. The linearization replaces *surface* function values by linear combinations of other functions that are continuous on the surface but not necessarily defined elsewhere. Surface geometry is represented by quasi-disjoint cells (boundary elements) mapped to parametric coordinates; the surface formed by these cells may be different from the true surface. Basis functions are low-order polynomials in the parametric coordinate system of each cell. Boundary conditions are expressed directly in terms of these values.

The construction of elements and basis functions provides a parameterized deformation function at all points of the *surface*. Most implementations enforce C^0 continuity between elements. The surface functions themselves are infinitely differentiable at the interior of the surface elements, but has derivative discontinuities at element boundaries. In addition, the basic formulation defines an explicit (albeit expensive) integration formula that produces an infinitely differentiable function at all interior points of the solid.

1.2 Benefits and Problems of the Boundary Integral Methods

The boundary integral equation offer two types of advantage over volume-based methods. The first is geometric simplification. In 2D, meshing is reduced to subdivision of lines and curves; in 3D, volume meshing is replaced by surface meshing. The second benefit is possible efficiency gains due to dealing with less geometry. Appendix A shows that for analysis of a regularly meshed cube – arguably an example that favors the boundary element method because there is little surface relative to the cube's volume – a boundary element solution requires $O(n^6)$ arithmetic operations, while a finite element solution requires $O(n^7)$, where n is the number of nodes placed along each edge. However, some constant factors are so greatly in favor of the finite element method that the boundary element method has more arithmetic operations up to n=144, i.e. 125,000 boundary elements or 3 million finite elements. Solution of this system (for the elasticity equation) would require approximately a year on a 1-gigaflop computer.

Practical use of boundary element methods has been hampered by several other factors. Aside from the non-technical factor of having been developed 10 to 15 years after the finite element method, the boundary element method is significantly more difficult to implement. The standard implementation is notably lacking in convergence proofs and intuitive physical analogies that are so readily available for finite elements.

1.2.1 Integration Problems

Among the implementation difficulties of boundary element methods, the most basic one is computation of certain singular integrals. Although these integrals are well defined at all interior points, they are quite difficult to carry out for points either close to or on the surface. Derivatives of the solution are even more difficult, and have been carefully avoided in practice. This thesis addresses these problems as follows:

- **Hypersingular integration** Evaluation of gradients at points on the surface gives rise to 'hypersingular' integrals. Chapter 4 and Chapter 5 present a systematic analysis of these integrals. Chapter 4 expands on the 'limit from the interior' method proposed by Gray, Martha, and Ingraffea [GMI90], and proposes that it be used as the primary method of analyzing both the hypersingular integral and the more familiar Cauchy and weak singularities. Chapter 5 shows that the extensive algebraic difficulties of Gray's method can be overcome by use of 'modal' methods that replace the difficult integrals by easier integrals over other surfaces.

- **Near-singular integration** Points that are *near* but not exactly on the surface do not present the same analytic difficulties as the hypersingular problem. However, they are numerically very poorly behaved. Chapter 7 presents a method of evaluating these integrals using a family of Gaussian quadrature rules that are 'parameterized by' distance to the surface. These optimal rules prove to be quite valuable in implementing the modal method of hypersingular integrals, because that method frequently calls for many near-singular integrals.

With these integration methods, we are able to address another problem of the boundary element method, namely the fact that basic boundary integral is degenerate at points on a crack face and cannot be used as the basis of numerical solution. Using the hypersingular integration methods, we are able to apply a gradient condition on the crack face and obtain elastic field solutions without resorting to 'multidomain' methods that have been used in the past.

1.2.2 Historical Notes

Independent of any application, there is is extensive mathematical analysis of the 'indirect' or 'generalized potential methods' by Russian academics such as Mikhlin [Mik65]), Muskhelishivili [Mus63], and Kupradze [Kup65]. Aside from the intrinsic difficulty of the material, the generalized potential methods are difficult to interpret because they express the unknown solution quantities as distributions of 'surface densities' that do not relate directly to physical quantities.

Practical use began when Jaswon [Jas63] and Rizzo [Riz69] converted the integral formulations so that all unknowns were physically meaningful values of the primary and gradient functions on the surface. This 'direct potential method' produced promising results in the 1960's and 1970's, such as given in Cruse [Cru69].

In the late 1970's, terminology and programming details were revised to make use of isoparametric mapping methods borrowed from the finite element method. The integral methods became known as the boundary element method. The contemporary formulation for elasticity problems follows the structure described in Lachet and Watson [LW76] and Rudolphi [Rud83].

Chapter 2

The Boundary Integral Equation

This chapter gives the rigorous (and unfortunately lengthy) mathematical notation for boundary integral problems. Basic properties of boundary integrals are presented, and the near-field and hypersingular integration problems to be addressed in later chapters are restated in the more formal notation.

The terms *boundary integral equation* (BIE), *linearized boundary integral equation*, and *boundary element method* have particular meanings. As indicated in Fig. 2.1, the BIE is a high level mathematical abstraction in which both the geometry and the solution function appear in exact form. The *linearized* BIE is an intermediate form in which the solution function is replaced by a linear combination of as-yet-unspecified basis functions multiplied by coefficients. The *boundary element method* is a specific implementation of the linearized BIE after the further decision to represent both geometry and solution functions by low-order parametric polynomial mappings over a set of 'boundary elements' that form the boundary of the region.

The intended application is elasticity, which has cumbersome subscript manipulation. In order to simplify the mathematics and make the results more general,

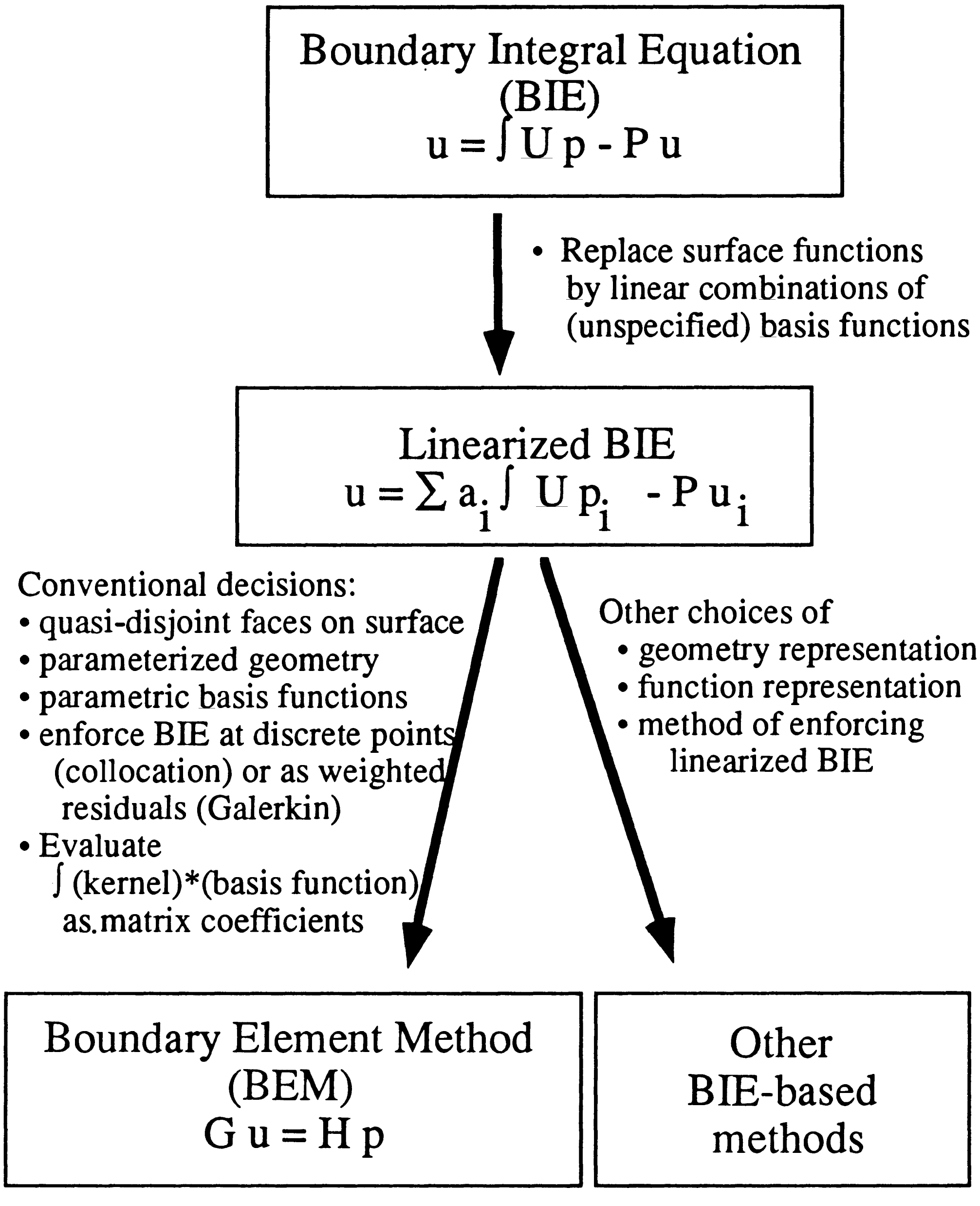

Figure 2.1: Levels of abstraction for boundary integrals

most derivations are done with either (a) unsubscripted tensor notation that applies to both elasticity and the Laplace equation or (b) only for the simpler Laplace equation.

2.0.1 Geometric Notation

Lower case $\mathbf{x}$ and $\mathbf{y}$ denote geometric points in d-dimensional Euclidean space E^d, with $d = 2$ and $d = 3$. V is some volume with boundary (surface) S. Point $\mathbf{x}$ is *never* on the boundary, but may approach some limit point $\overline{\mathbf{x}}$ that is on the boundary. Point $\mathbf{y}$ is an integration variable, i.e. ranges over the surface during integrations.[1] Vector $\mathbf{r}$ and scalar r are defined as

$$\mathbf{r} = \mathbf{y} - \mathbf{x} \tag{2.1}$$

$$r = |\mathbf{r}| = \sqrt{(y_1 - x_1)^2 + \cdots + (y_d - x_d)^2} \tag{2.2}$$

Boldface vectors and points, e.g. $\mathbf{x}$, $\mathbf{y}$, and $\mathbf{r}$, are independent of coordinate systems. Scalar components with respect to coordinate axes are subscripted as x_i, y_i, r_i. Unless otherwise specified, subscripts appearing more than once in an expression or equation follow the standard convention of implied summation:

> If the subscript appears on both sides of an equality, the entire equality is replicated once with each possible value of the subscript.
>
> If the subscript appears on only one side of an equality, the highest level operation containing all appearances of the subscript is summed over all values of the subscript.

A comma preceding a subscript denotes partial differentiation with respect to that axis or unit vector, e.g.

$$r_{,i} = \frac{\partial}{\partial r_i} r \quad \text{and} \quad r_{,\mathbf{n}} = \frac{\partial}{\partial \mathbf{n}} r = \textstyle\sum_{1 \le i \le d} n_i r_{,i} = r_{,i} n_i \tag{2.3}$$

---

[1] $\mathbf{y}$ is an interior point for a few volume integrals.

This notation is potentially ambiguous, for the expansion of **r** shows that the i direction is determined as r_i=y_i-x_i, and the meaning of $r_{,i}$ could be either $\frac{\partial}{\partial x_i}r = -1$ or $\frac{\partial}{\partial y_i}r = +1$. To resolve the ambiguity, we use the convention that *comma notation on any expression that involves both* $\mathbf{x}$ *and* $\mathbf{y}$ *always indicates differentiation with respect to* y_i. That is,

$$r_{,i} = \frac{\partial}{\partial y_i}r = -\frac{\partial}{\partial x_i}r \tag{2.4}$$

Differentiation with respect to x_i is always written out with the formal prefix $\frac{\partial}{\partial x_i}$. In order to shorten such an expression by use of comma notation, we must apply (2.4), which introduces a negative sign. Similarly, $\nabla_{\mathbf{x}}$ (with $\mathbf{x}$ explicitly present in the subscript) is the vector $[\frac{\partial}{\partial x_1}, \frac{\partial}{\partial x_2}, \frac{\partial}{\partial x_3}]$ while the (unsubscripted) ∇ is the gradient operator with differentiation at $\mathbf{y}$, i.e. $\nabla \equiv [\frac{\partial}{\partial y_1}, \frac{\partial}{\partial y_2}, \frac{\partial}{\partial y_3}]$.

In equations that apply to both elasticity and the Laplace equation, we use boldface $\mathbf{u}(\mathbf{y})$ for the primary unknown quantity at point $\mathbf{y}$. $\nabla\mathbf{u}$ is the gradient (vector of directional derivatives along coordinate axes). $\mathbf{p}(\mathbf{y},\mathbf{n})$ is the physical gradient quantity on a surface with normal $\mathbf{n}$, related to $\nabla\mathbf{u}$ by

$$\mathbf{p}(\mathbf{y},\mathbf{n}) = \mathbf{E}\nabla\mathbf{u}(\mathbf{y})\mathbf{n} \tag{2.5}$$

where $\mathbf{E}$ is a tensor of material properties. The complete tensor of physical gradients in all axis directions is

$$\sigma(\mathbf{y}) = \left[\mathbf{p}(\mathbf{y},\mathbf{e}_1)\cdots\mathbf{p}(\mathbf{y},\mathbf{e}_d)\right] = \mathbf{E}\nabla\mathbf{u}(\mathbf{y}) \tag{2.6}$$

The choice of $\mathbf{u}$, $\mathbf{p}$, $\mathbf{E}$, and σ reflect common usage in elasticity, where they are the displacement vector, traction vector, elastic properties tensor, and the stress tensor. In a Laplace equation problem, $\mathbf{u}$ is the (scalar) potential, $\mathbf{p}$ a flux, $\mathbf{E}$ is just an identity operator, and σ is the vector of fluxes along coordinate axes.

Upper case **U**, **P**, **D**, and **S** are kernels functions to be defined. Products **Up** and **Pu** are defined and are of the same tensor order as **u** and **p**. Products **Dp** and **Su** are defined and have the same tensor order as σ. These boldface quantities are coordinate-system independent tensors in the sense of Spencer [Spe80]. The more-or-less standard subscripted equivalents u_i, p_i, E_{ijmn}, σ_{ij}, U_{ik}, P_{ik}, D_{ijk}, and S_{ijk} are used in developments specific to elasticity, and u, $\frac{\partial u}{\partial \mathbf{n}}$, δ_{ij}, ∇u, G, H, ∇G, and ∇H for developments specific to Laplace.

2.0.2 Formula Manipulation

Multistep formula manipulations are done in a format developed by Dijkstra and Scholten [DS90]. The format was originally developed for predicate calculus reasoning about computer programs, but it applies equally well to continuous mathematics.

The goal is to give systematic rules for intermixing formulas and explanatory text. A proof is written as a sequence of expressions E_0, E_1,..E_n separated by connectives and 'hints'. The sequence is given in the vertical format, as the following derivation of the frequently-used conversion of a partial derivative of r to a ratio:

Property: (Partial derivatives of r) $\frac{\partial}{\partial r_i} r = r_i / r$

$$\frac{\partial}{\partial r_i} r \tag{2.7}$$

$$= \quad \{ \text{ Expand definition of } r \quad \} \tag{2.8}$$

$$\frac{\partial}{\partial r_i} (\Sigma_{1 \leq j \leq d} r_j{}^2)^{\frac{1}{2}} \tag{2.9}$$

$$= \quad \{ \text{ Chain rule } \quad \} \tag{2.10}$$

$$\tfrac{1}{2} (\Sigma_{1 \leq j \leq d} r_j{}^2)^{-\frac{1}{2}} (2 r_i) \tag{2.11}$$

$$= \quad \{ \text{ Algebra and definition of } r \quad \} \tag{2.12}$$

$$\frac{r_i}{r} \tag{2.13}$$

The reader is encouraged to skip directly from any step to any other, reading only the connectives along the left side, to make a linkage such as $\frac{\partial}{\partial r_i} r = .. = \frac{r_i}{r}$. Numeric expressions may be connected by numeric relational operators $=$, $\geq$, $\leq$, $<$, $>$, or $\approx$, and boolean expressions (including numeric equations which use $=$ internally in a numeric sense) may be connected by $\Leftrightarrow$, $\Rightarrow$, and $\Leftarrow$.

In simple examples, the format sometimes uses more vertical space than a mixture of text and equations within a paragraph. However, more complicated formulas benefit from the clear connection between the hint and the affected expressions. There is never any question of whether explanations come before, after or in between expressions – they are always in between. Gries [Gri90] presents further examples of how this format aids clarity of presentation.

2.1 The Primary BIE

When a primary unknown quantity $\mathbf{u}(\mathbf{x})$ for interior points $\mathbf{x}$ in a region Ω bounded by surface S is governed by certain differential operators L, i.e.,

$$L\mathbf{u}(\mathbf{x}) = 0 \tag{2.14}$$

it can be shown that there is a completely equivalent formulation that expresses $\mathbf{u}(\mathbf{x})$ at any non-boundary point $\mathbf{x}$ as an integral that involves only the surface geometry, the primary unknown $\mathbf{u}$ evaluated at boundary points, and a derivative quantity $\mathbf{p}$ at boundary points. The form of this integral is

$$\gamma(\mathbf{x})\mathbf{u}(\mathbf{x}) = \int_S \mathbf{U}(\mathbf{x},\mathbf{y})\mathbf{p}(\mathbf{y},\mathbf{n}(\mathbf{y})) - \mathbf{P}(\mathbf{x},\mathbf{y},\mathbf{n}(\mathbf{y}))\mathbf{u}(\mathbf{y})\, dS(\mathbf{y}) \tag{2.15}$$

Referring to Fig. 2.2, the symbols in this expression are:

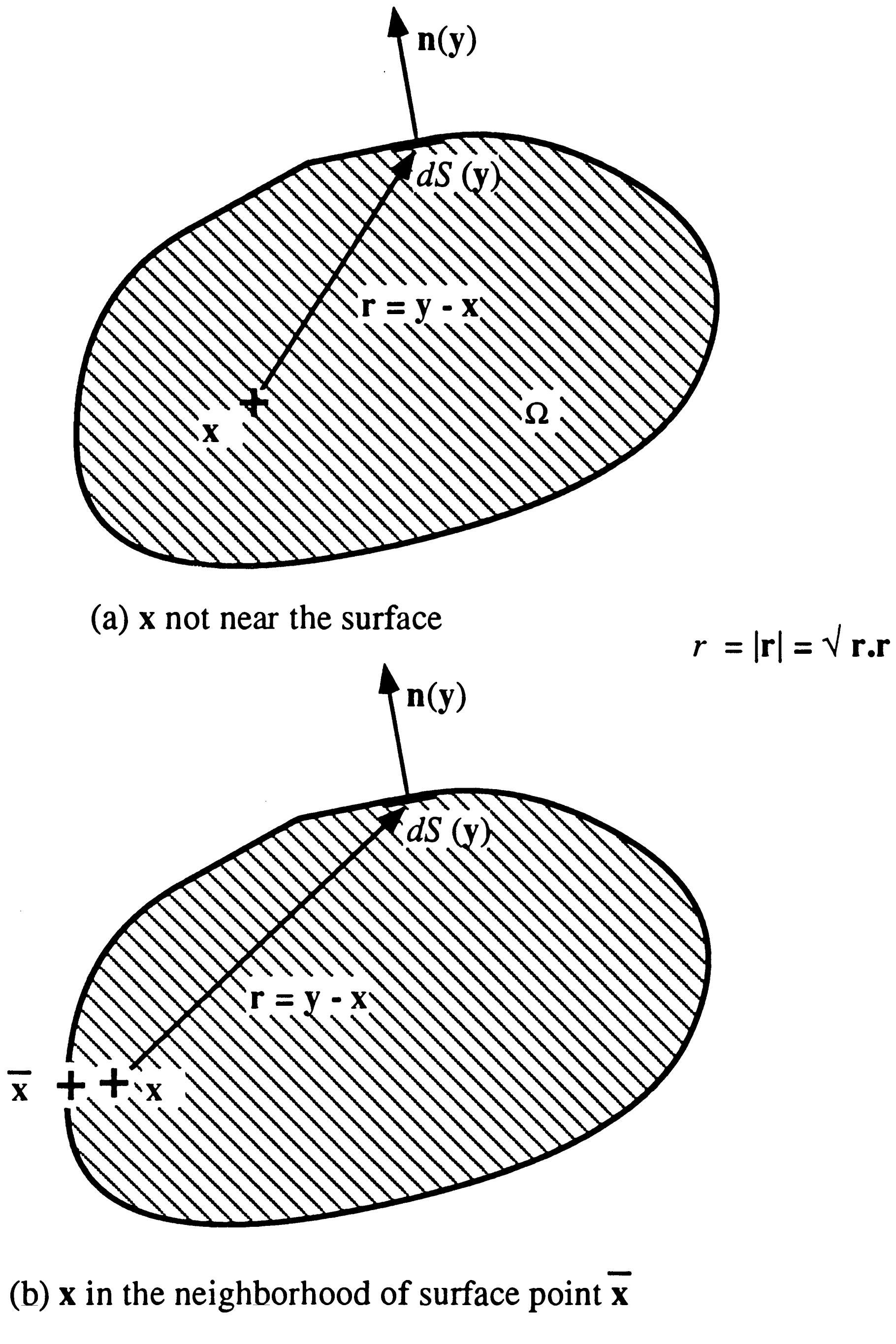

Figure 2.2: Geometric notation

$\mathbf{x}$	any point *not on the boundary of the region*
$\mathbf{y}$	a point that varies over the boundary during the integration
$\gamma(\mathbf{x})$	is the 'point membership classification' (Requicha and Voelcker[RV85]): $\gamma = \begin{cases} 1 & \text{for } \mathbf{x} \text{ inside } \Omega \\ 0 & \text{for } \mathbf{x} \text{ outside } \Omega \end{cases}$ γ is undefined on the boundary.
$\mathbf{u}(\mathbf{x})$, $\mathbf{u}(\mathbf{y})$	the primary unknown quantity at $\mathbf{x}$ and $\mathbf{y}$
$dS(\mathbf{y})$	a differential piece of surface at $\mathbf{y}$
$\mathbf{n}(\mathbf{y})$	the outward surface normal at $\mathbf{y}$
$\mathbf{p}(\mathbf{y},\mathbf{n})$	a gradient quantity (linear combination of directional derivatives) with respect to direction $\mathbf{n}$ at point $\mathbf{y}$.
$\mathbf{U}(\mathbf{x},\mathbf{y})$, $\mathbf{P}(\mathbf{x},\mathbf{y},\mathbf{n})$	certain kernel functions derived from the differential operator

Whenever possible, we will omit geometric arguments $\mathbf{x}$, $\mathbf{y}$, and $\mathbf{n}$. The much-shortened BIE is then

$$\gamma\mathbf{u} = \int_S \mathbf{U}\mathbf{p} - \mathbf{P}\mathbf{u}\, dS \tag{2.16}$$

Functions $\mathbf{u}$, $\mathbf{p}$, $\mathbf{U}$, and $\mathbf{P}$ 'within the integral' have their arguments implicitly bound to $\mathbf{x}$, $\mathbf{y}$, and $\mathbf{n}(\mathbf{y})$, and γ and $\mathbf{u}$ 'outside the integral' are at $\mathbf{x}$. This simplification is possible (i.e. does not cause ambiguity) because complicated expansions of the BIE typically arise from splitting the integrals into sums of other integrals, rather than combining integrals at multiple $\mathbf{x}$ points.

The following paragraphs outline some of the numerous subtle points in these definitions.

0. Fixed versus Moving Point. Points $\mathbf{x}$ and $\mathbf{y}$ have very specific roles in the equation. Point $\mathbf{x}$ is fixed. The main purpose of the equation is to give a value to the function $\mathbf{u}$ at this fixed point. Point $\mathbf{y}$ ranges over the entire surface of the body. At each point on the surface, $\mathbf{n}(\mathbf{y})$ is determined by the body geometry.

1. Origin of the kernel $\mathbf{U}$. The primary kernel $\mathbf{U}$ is unique to the differential operator L. For each differential equation considered, one must find (systematically or otherwise) definitions of $\mathbf{U}$ and its gradient $\mathbf{P}$ that make the boundary integral true. The two critical properties that are required for this are that:

- $\mathbf{U}(\mathbf{x},\mathbf{y})$ satisfies the differential equation when $\mathbf{x}$ is fixed and $\mathbf{y}$ varies, i.e.

$$L_{\mathbf{y}}\mathbf{U}(\mathbf{x},\mathbf{y}) = 0 \text{ when } \mathbf{x} \neq \mathbf{y} \tag{2.17}$$

- $L_{\mathbf{y}}\mathbf{U}$ is a Dirac delta function, i.e. for any smooth function $\mathbf{u}(\mathbf{y})$ we can write the volume integral

$$\int_{\Omega} L_{\mathbf{y}}\mathbf{U}(\mathbf{x},\mathbf{y})\mathbf{u}(\mathbf{y})d\Omega(\mathbf{y}) = \begin{cases} \mathbf{u}(\mathbf{x}) & \text{when } \mathbf{x} \text{ is in } \Omega \\ 0 & \text{when } \mathbf{x} \text{ is outside of } \Omega \end{cases} \tag{2.18}$$

The case when $\mathbf{x}$ is on the boundary is again left undefined.

2. Origin of the $\mathbf{P}$ *kernel.* The $\mathbf{P}$ kernel at surface point $\mathbf{y}$ with normal $\mathbf{n}$ is the gradient of the $\mathbf{U}$ field in direction $\mathbf{n}$. That is,

$$\mathbf{P}(\mathbf{x},\mathbf{y},\mathbf{n}) = \mathbf{E}\nabla\mathbf{U}(\mathbf{x},\mathbf{y})\mathbf{n} \tag{2.19}$$

3. Kernels are Singular at $\mathbf{y}=\mathbf{x}$. In order to produce the Dirac delta function property, kernels must be singular be at $\mathbf{x}$. Evaluation of the kernel functions requires division by the magnitude r of the vector $\mathbf{r} = \mathbf{y} - \mathbf{x}$. The presence of high powers of r^{-1} in the integrals is a persistent problem in implementation of the boundary element method. Chapters 4, 5, and 6 are devoted to analysis of the case where $\mathbf{x}$ is considered to be 'on' the surface. Chapter 7 considers numerical issues occurring when $\mathbf{x}$ is a finite but small distance from the boundary.

4. Symmetry Properties. Because they are formed from spatial derivatives, the solution gradient $\mathbf{p}$ and the gradient kernel $\mathbf{P}$ must change sign when $\mathbf{n}$ is reversed. Since $\mathbf{U}$ and $\mathbf{u}$ are determined entirely by $\mathbf{x}$ and $\mathbf{y}$, but not by $\mathbf{n}$, we can add an artificial argument $\mathbf{n}$ and write

$$\mathbf{U} \text{ is symmetric with respect to } \mathbf{n}: \quad \mathbf{U}(\mathbf{x},\mathbf{y},-\mathbf{n}) = \mathbf{U}(\mathbf{x},\mathbf{y},\mathbf{n}) \tag{2.20}$$

$$\mathbf{u} \text{ is symmetric with respect to } \mathbf{n}: \quad \mathbf{u}(\mathbf{y},-\mathbf{n}) = \mathbf{u}(\mathbf{y},\mathbf{n}) \tag{2.21}$$

$$\mathbf{P} \text{ is antisymmetric with respect to } \mathbf{n}: \quad \mathbf{P}(\mathbf{x},\mathbf{y},-\mathbf{n}) = -\mathbf{P}(\mathbf{x},\mathbf{y},\mathbf{n}) \tag{2.22}$$

$$\mathbf{p} \text{ is antisymmetric with respect to } \mathbf{n}: \quad \mathbf{p}(\mathbf{y},-\mathbf{n}) = -\mathbf{p}(\mathbf{y},\mathbf{n}) \tag{2.23}$$

Hence the primary BIE integrand $\mathbf{Up} - \mathbf{Pu}$ is antisymmetric; integrating over the same surface points (i.e. a crack) with opposing normals reverses the sign of the result.

5. Orientation of Integration. The differential surface unit $dS(\mathbf{y})$ in the integrals is an *unsigned* quantity. The integrations themselves are independent of any notion of inside and outside. *Orientation effects arise from the direction of the normal vector used in computing the integrands.*

6. Class of PDE's Considered. This thesis considers only the Laplace and elasticity equations, which are steady-state, second-order PDE's with constant coefficients and no body (volume) loads. Additional applications may be found in [Muh82] and [BTW84].

7. Derivation of the Boundary Integral for Laplace' Equation. For the Laplace equation, Green's second theorem [Gas58] provides an initial relationship between boundary and volume integrals of a pair of functions $u(\mathbf{y})$ and $G(\mathbf{x},\mathbf{y})$. We choose u as the desired solution field and G as

$$G(\mathbf{x},\mathbf{y}) = \tfrac{1}{4\pi} r^{-1} \qquad (r = |\mathbf{y} - \mathbf{x}|) \tag{2.24}$$

This leads to the primary BIE via

$$
\begin{aligned}
& \int_S G(\mathbf{y})\frac{\partial}{\partial \mathbf{n}}u(\mathbf{y}) - u(\mathbf{y})\frac{\partial}{\partial \mathbf{n}}G(\mathbf{y})\, dS(\mathbf{y}) && (2.25)\\
= \ & \left\{ \begin{array}{l}\text{Green's second theorem, applicable to } \textit{any} \\ \text{functions } u \text{ and } G \end{array} \right\} && (2.26)\\
& \int_\Omega u(\mathbf{y})\nabla^2 G(\mathbf{x},\mathbf{y}) - G(\mathbf{x},\mathbf{y})\nabla^2 u(\mathbf{y})\, d\Omega(\mathbf{y}) && (2.27)\\
= \ & \{ \text{ Assume } \nabla^2 u = 0 \text{ throughout the interior } \} && (2.28)\\
& \int_\Omega u(\mathbf{y})\nabla^2 G(\mathbf{x},\mathbf{y})\, d\Omega(\mathbf{y}) && (2.29)\\
= \ & \left\{ \text{ Dirac delta function property of } G = \tfrac{1}{4\pi} r^{-1} \right\} && (2.30)\\
& \gamma(\mathbf{x})u(\mathbf{x}) && (2.31)
\end{aligned}
$$

The first and last entries are the primary BIE.

A physical interpretation of the Green's function is that $G(\mathbf{x},\mathbf{y})$ is the potential field produced by a point source that introduces a unit amount of flow into an infinitesimal area at $\mathbf{x}$.

An alternate derivation in terms of weighted residuals is found in Brebbia and Dominguez [BD88].

8. Derivation of the Boundary Integral for Elasticity.

The pure mathematics of generalizations to other differential equations have been intensively studied under the title of 'generalized potential theory'. A very general formula to obtain kernels for any 2nd order differential operator for which the coefficients of each derivative are given is found in Mikhlin [Mik65]. This formulation has seen little practical use because it results in boundary integrals in which the surface function in the boundary integrals is a generalized mathematical 'density' rather than a meaningful physical quantity. The density can be related back to the actual gradient $\mathbf{p}$ on the boundary by additional integrals.

Practical use of integral equations for elasticity became possible when Rizzo [Riz69] used the kernels of the generalized potential theory with Betti's reciprocal theorem to obtain the integral (Eq. 2.15 or 2.16).

The derivation requires an expression for U_{ik}(x,y), interpreted as the direction-i displacement induced at each point **y** of a hypothetical infinite elastic medium by a unit load in direction-k concentrated at point **x** of the solid. For 3D elasticity, this expression is

$$U_{ik}(\mathbf{x},\mathbf{y}) = \frac{1}{16\pi(1-\nu)r}\left\{(3-4\nu)\delta_{ik} + r_{,i}r_{,k}\right\} \tag{2.32}$$

Differentiating this field and recombining according to stress-strain relationships of elasticity produces the tensor P_{ik}(x,y,n) (see Fig. 2.4 for algebraic expression) that is understood as the direction-i component of the traction vector on a surface passing through point, again due to the direction-k component of the point load.

Since both (a) the U_{ik} and P_{ik} tensors and (b) the desired solution functions u_k(y) and its surface traction p_k(y,n) are equilibrium elastic fields, Betti's reciprocal theorem specifies an equality between the work done by the tractions and body forces of each field acting on the other field's displacements. This leads to the boundary integral by the steps

$$\int_S U_{ik}(\mathbf{x},\mathbf{y})p_k(\mathbf{y}) - P_{ik}(\mathbf{x},\mathbf{y})u_k(\mathbf{y})\,dS(\mathbf{y}) \tag{2.33}$$

$$= \left\{\begin{array}{l}\text{Betti's reciprocal theorem equates reciprocal}\\ \text{work by surface tractions to reciprocal work}\\ \text{by body forces } b_k \text{ of the solution field and}\\ B_k \text{ of the fundamental solution}\end{array}\right\} \tag{2.34}$$

$$\int_\Omega u_i(\mathbf{x})B_k(\mathbf{y}) - U_{ik}(\mathbf{x},\mathbf{y})b_k(\mathbf{y})\,d\Omega(\mathbf{y}) \tag{2.35}$$

$$= \left\{\text{Assume body forces } b_k \equiv 0\right\} \tag{2.36}$$

$$\int_\Omega u_i(\mathbf{y})B_k(\mathbf{y})\,d\Omega(\mathbf{y}) \tag{2.37}$$

$$= \left\{\begin{array}{l}\text{The force field } B_k(\mathbf{y}) \text{ for a point load at } \mathbf{x} \text{ is}\\ \text{a Dirac delta function}\end{array}\right\} \tag{2.38}$$

$$\gamma(\mathbf{x})u_i(\mathbf{x}) \tag{2.39}$$

2.2 The Gradient BIE

A very important property of the BIE is that it may be interpreted in strict right-to-left fashion to define function $\mathbf{u}(\mathbf{x})$ at all points on the interior of the region. That is, if we consider only interior points, the coefficient γ is uniformly one and the right side is a direct expression for interior values as an integral of boundary values.

Since the function is defined everywhere, and not just at isolated points, it can be differentiated with respect to coordinates of point $\mathbf{x}$. Partial differentiation $\frac{\partial}{\partial x_n}$ of the integrals with respect to a coordinate of $\mathbf{x}$ may be taken inside the integrals, where they apply to $\mathbf{U}$ and $\mathbf{P}$ but not to $\mathbf{u}$ or $\mathbf{p}$ (which are functions of the integration variable $\mathbf{y}$):

$$\begin{aligned} \frac{\partial}{\partial x_n}\mathbf{u} &= \frac{\partial}{\partial \mathbf{x}_n}\int_S \mathbf{U}\mathbf{p} - \mathbf{P}u\,dS & (2.40) \\ &= \int_0^1 (\frac{\partial}{\partial x_n}\mathbf{U})\mathbf{p} - (\frac{\partial}{\partial x_n}\mathbf{P})\mathbf{u}\,ds & (2.41) \end{aligned}$$

Taking these derivatives in all directions and applying the material properties in $\mathbf{E}$, we define

$$\begin{aligned} \sigma(\mathbf{x}) &= \mathbf{E}\nabla_{\mathbf{x}}\mathbf{u}(x) & (2.42) \\ \mathbf{D} &= \mathbf{E}\nabla_{\mathbf{x}}\mathbf{U} & (2.43) \\ \mathbf{S} &= \mathbf{E}\nabla_{\mathbf{x}}\mathbf{P} & (2.44) \end{aligned}$$

to define "the" gradient BIE

$$\gamma\sigma = \int_S \mathbf{D}\mathbf{p} - \mathbf{S}\mathbf{u}\,dS \tag{2.45}$$

The algebraic expansions of $\mathbf{D}$ and $\mathbf{S}$ are given in Fig. 2.4 and Fig. 2.3.

The gradient kernels $\mathbf{D}$ and $\mathbf{S}$ have symmetry properties corresponding to $\mathbf{U}$ and $\mathbf{P}$:

$$\mathbf{S} \text{ is antisymmetric with respect to } \mathbf{n}: \tag{2.46}$$

$$\mathbf{S}(\mathbf{x},\mathbf{y},-\mathbf{n}) = -\mathbf{S}(\mathbf{x},\mathbf{y},\mathbf{n}) \tag{2.47}$$

$$\mathbf{D} \text{ is symmetric with respect to } \mathbf{n}: \tag{2.48}$$

$$\mathbf{D}(\mathbf{x},\mathbf{y},-\mathbf{n}) = \mathbf{D}(\mathbf{x},\mathbf{y},-\mathbf{n}) \tag{2.49}$$

$$\mathbf{Dp} - \mathbf{Su} \text{ is antisymmetric with respect to } \mathbf{n}: \tag{2.50}$$

$$\int_S \mathbf{D}(\mathbf{x},\mathbf{y})\mathbf{p}(\mathbf{y},-\mathbf{n}(\mathbf{y})) - \mathbf{S}(\mathbf{x},\mathbf{y},-\mathbf{n})\mathbf{u}\, dS \tag{2.51}$$

$$= -\int_S \mathbf{D}(\mathbf{x},\mathbf{y})\mathbf{p}(\mathbf{y},\mathbf{n}(\mathbf{y})) - \mathbf{S}(\mathbf{x},\mathbf{y},\mathbf{n})\mathbf{u}\, dS \tag{2.52}$$

2.3 Summary of Kernel Relationships

The BIE development involves (a) several differentiations of the initial $\mathbf{U}$ kernel, and (b) linear combinations of the derivatives to convert to physically meaningful gradient quantities.

Fig. 2.5 contains a detailed summary of the relationships of the various kernels. Starting from the initial $\mathbf{U}$ kernel, downward vertical transitions reflect differentiation. Horizontal transitions to the right mean linear combinations using elasticity constants or normal vectors. Diagonal transition will be explained below and in Chapter 6.

Order of Singularities Differentiation of the singular kernels has two effects on the algebraic expression for the kernel. First, it raises the order of singularity by one power of r^{-1} In addition, due to chain- and product-rule action, the kernels are multiplied by increasingly complicated chains of non-singular factors.

(a) Notation and Governing Equations

Primary Quantity	$u(\mathbf{x})$	potential or temperature at $\mathbf{x}$
Derivative Quantity	$q_j = \frac{\partial u(\mathbf{x})}{\partial x_j}$	velocity or flux in direction j
PDE		$\nabla^2 u = 0$
Primary BIE		$\gamma u = \int_S G\frac{\partial u}{\partial \mathbf{n}} - Hu\, dS$
Gradient BIE		$\gamma q_j = \gamma\frac{\partial u}{\partial x_j} = \int_S \frac{\partial G}{\partial x_j}\frac{\partial u}{\partial \mathbf{n}} - \frac{\partial H}{\partial x_j} u\, dS = \int_S -G_{,j}\frac{\partial u}{\partial \mathbf{n}} + H_{,j} u\, dS$

(b) Kernel Expressions

Kernel	2D	3D
G	$\frac{1}{2\pi}\ln(\frac{1}{r})$	$\frac{1}{4\pi}\frac{1}{r}$
H	$-\frac{1}{2\pi}\frac{1}{r}\frac{\partial r}{\partial \mathbf{n}}$	$-\frac{1}{4\pi}\frac{1}{r^2}\frac{\partial r}{\partial \mathbf{n}}$
$-\frac{\partial G}{\partial x_j} = G_{,j}$	$-\frac{1}{2\pi}\frac{1}{r}r_{,j}$	$-\frac{1}{4\pi}\frac{1}{r^2}r_{,j}$
$-\frac{\partial H}{\partial x_j} = H_{,j}$	$-\frac{1}{2\pi}\frac{1}{r^2}(n_j - 2\frac{\partial r}{\partial \mathbf{n}}r_{,j})$	$-\frac{1}{4\pi}\frac{1}{r^3}(n_j - 3\frac{\partial r}{\partial \mathbf{n}}r_{,j})$

Figure 2.3: Conventional notation for the Laplace equation

(a) Notation and Governing Equations

Primary Quantity	u_i	displacement in direction i
Derivative Quantity	$\sigma_{ij} = E_{ijkl}\frac{\partial u_k}{\partial x_l}$ $p_i = \sigma_{ij}n_j$	stress tensor traction on surface with normal components n_j
PDE		$\sigma_{ij,j} = 0$
Primary BIE		$\gamma u = \int_S U_{ik}p_k - P_{ik}u_k \, dS$
Gradient BIE		$\gamma\sigma_{ij} = \int_S D_{ijk}p_k - S_{ijk}u_k \, dS$ $\gamma p_i(\mathbf{N}) =$ $\int_S D_{ijk}N_jp_k - S_{ijk}N_ju_k \, dS$
Physical Constants	E_{ijkl}	Constitutive tensor (Incorporates μ = Poisson's ratio ν = Shear modulus)

Figure 2.4: Conventional notation for elasticity

(continued on next page)

(b) Kernel Expressions

Kernel	Expression
$U_{ik}(2D)$	$\frac{1}{8\alpha\pi\mu(1-\nu)} \quad \left[(3-4\nu)\delta_{ik}\ln(1/r) + r_{,i}r_{,k}\right]$
$U_{ik}(3D)$	$\frac{1}{8\alpha\pi\mu(1-\nu)} \quad \frac{1}{r}\left[(3-4\nu)\delta_{ik} + r_{,i}r_{,k}\right]$
P_{ik}	$\frac{1}{4\alpha\pi(1-\nu)}\frac{1}{r^{\alpha}} \quad \left\{\frac{\partial r}{\partial \mathrm{n}}\left[(1-2\nu)\delta_{ik} + \beta r_{,i}r_{,k}\right] + (1-2\nu)(n_i r_{,k} - n_k r_{,i})\right\}$
D_{ijk}	$\frac{1}{4\pi\alpha(1-\nu)}\frac{1}{r^{\alpha}} \quad \left[(1-2\nu)\left(\delta_{ki}r_{,j} + \delta_{kj}r_{,i} - \delta_{ij}r_{,k}\right) + \beta r_{,i}r_{,j}r_{,k}\right]$
S_{ijk}	$\frac{1}{4\alpha\pi(1-\nu)}\frac{1}{r^{\beta}} \quad \left\{\beta\frac{\partial r}{\partial \mathrm{n}}\left[(1-2\nu)\delta_{ij}r_{,k} + \nu(\delta_{ik}r_{,j} + \delta_{jk}r_{,i}) - \gamma r_{,i}r_{,j}r_{,k}\right] + \beta\nu(n_i r_{,j}r_{,k} + n_j r_{,i}r_{,k}) + (1-2\nu)(\beta n_k r_{,i}r_{,j} + n_j\delta_{ik} + n_i\delta_{jk}) - (1-4\nu)n_k\delta_{ij}\right\}$

(c) Kernel Notation Depending on Geometric Dimension

dimension	α	β	γ
2D	1	2	4
3D	2	3	5

Fig. 2.4 (continued from previous page) BIE Summary for Elasticity

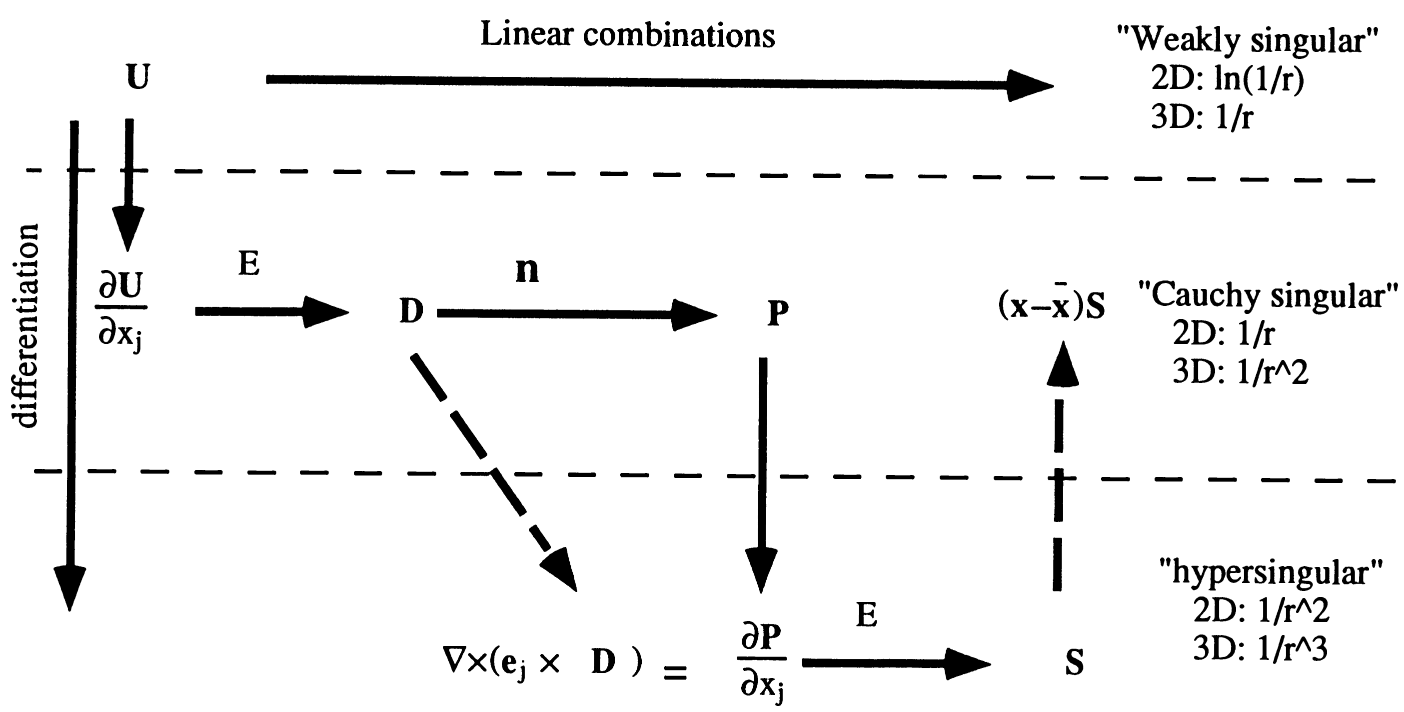

Figure 2.5: Relationships among generalized kernels.

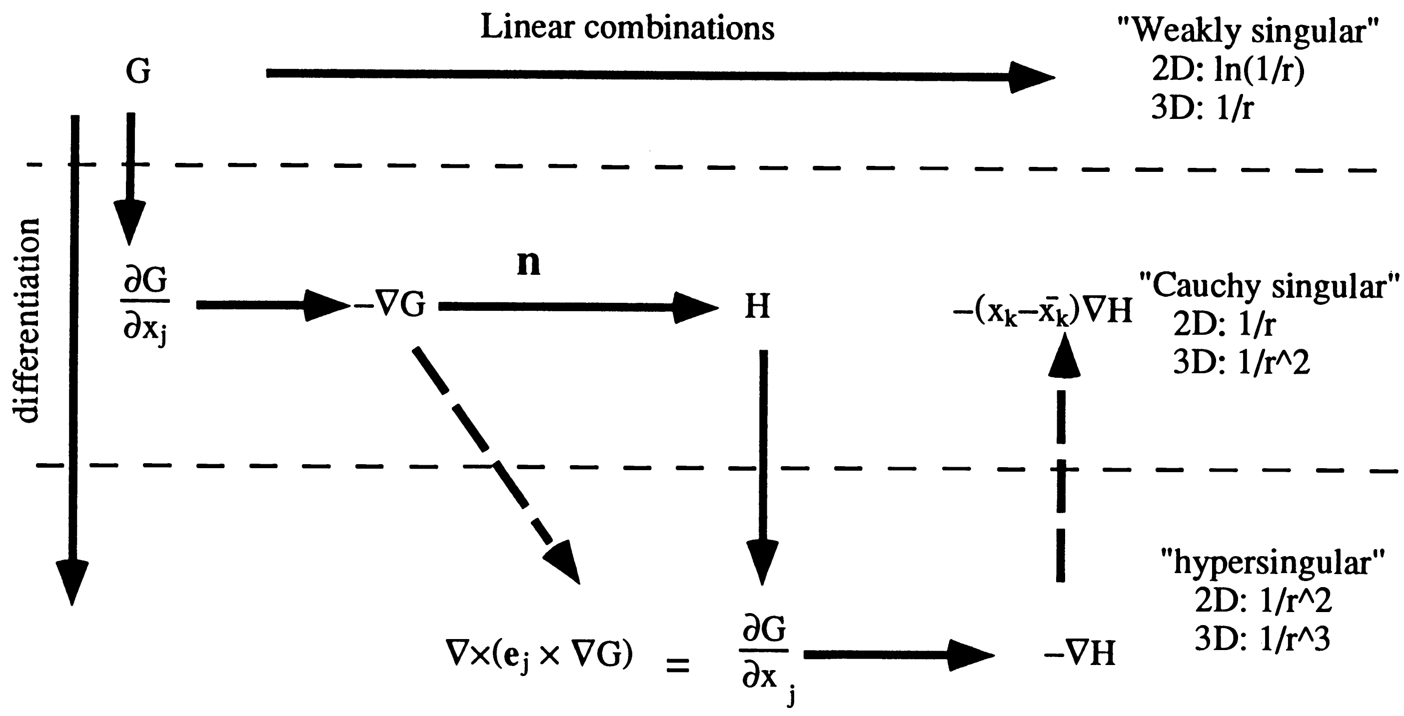

Figure 2.6: Relationships among Laplace kernels.

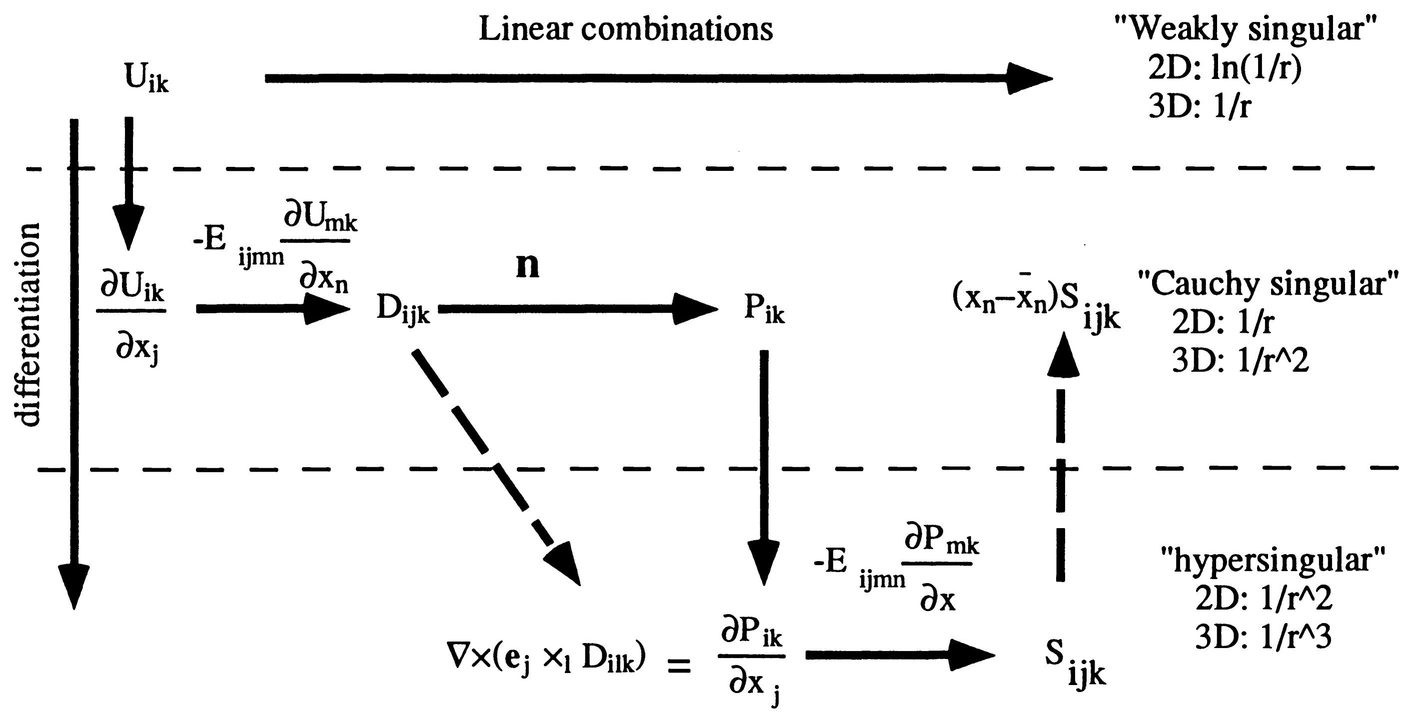

Figure 2.7: Relationships among elasticity kernels.

The traditional naming convention for the integration of 'leading' singularities (i.e. the kernels stripped of the non-singular factors) when the BIE fixed point $\mathbf{x}$ approaches surface point $\overline{\mathbf{x}}$ is:

- The initial $\mathbf{U}$ singularity ($\ln(r^{-1})$ in 2D, r^{-1} in 3D) is analyzed by a simple exclusion zone argument and is considered 'weak'.
- The singularities in $\frac{\partial \mathbf{U}}{\partial x_j}$, $\mathbf{D}$, and $\mathbf{P}$ (order r^{-1} in 2D, r^{-2} in 3D) are analyzed by an exclusion zone and a 'Cauchy principal value' interpretation of the integration.
- The singularities in $\frac{\partial \mathbf{P}}{\partial x_j}$ and S (order r^{-2} in 2D, r^{-3} in 3D) have been very poorly understood. They are loosely termed 'hypersingular'.

An additional case to be considered is that multiplying any kernel by a linear function of vector $\mathbf{x} - \overline{\mathbf{x}}$, reduces its effective singularity by one order. For the hypersingular kernels, the product $\mathbf{S}(\mathbf{x} - \overline{\mathbf{x}})$ is still Cauchy singular. These softening effects are noted on the kernel figures by upward diagonals to the level of the weakened singularity.

2.4 Regularization

The BIE does not directly call for integration of the bare kernels. Rather, they are multiplied by surface functions $\mathbf{p}(\mathbf{y})$ and $\mathbf{u}(\mathbf{y})$. To isolate (regularize) the kernel from the general surface function, write $\mathbf{u}(\mathbf{y})$ in a series expansion about the singular point $\overline{\mathbf{x}}$, e.g.

$$\mathbf{u}(\mathbf{y}) = \overline{\mathbf{u}} + \overline{\mathbf{A}}(\mathbf{y} - \overline{\mathbf{x}}) + ... + \overline{\mathbf{v}}^{(k)}(\mathbf{y}) \tag{2.53}$$

where barred quantities $\overline{\mathbf{u}}$ and $\overline{\mathbf{A}}$ are series coefficients at the singular point and $\overline{\mathbf{v}}^{(k)}(\mathbf{y})$ contains all terms of size $O(|\mathbf{y} - \overline{\mathbf{x}}|^k)$ or higher.

For the primary BIE, the Cauchy singularity in $\mathbf{P}$ is isolated by setting $k = 1$ and writing

$$\gamma(\mathbf{x})\mathbf{u}(\mathbf{x}) = \int_S \mathbf{U}\mathbf{p} - \mathbf{P}\mathbf{u}\, dS \tag{2.54}$$

$$\Leftrightarrow \quad \left\{ \begin{array}{l} \text{Series expansion } \mathbf{u}(\mathbf{y}) = \overline{\mathbf{u}} + \overline{\mathbf{v}}^{(1)}(\mathbf{y}) \text{ both} \\ \text{within the integrals and at the fixed point} \end{array} \right\} \tag{2.55}$$

$$\gamma(\mathbf{x})(\overline{\mathbf{u}} + \overline{\mathbf{v}}^{(1)}(\mathbf{x})) = \int_S \mathbf{U}\mathbf{p} - \mathbf{P}\overline{\mathbf{v}}^{(1)}(\mathbf{y})\, dS - \overline{\mathbf{u}}\int_S \mathbf{P}\, dS \tag{2.56}$$

$$\Rightarrow \quad \left\{ \begin{array}{l} \text{Take limit as } \mathbf{x} \text{ goes to } \overline{\mathbf{x}} \text{ on a path where} \\ \gamma(\mathbf{x}) \text{ does not change} \end{array} \right\} \tag{2.57}$$

$$\gamma\overline{\mathbf{u}} = \lim_{\mathbf{x}\to\overline{\mathbf{x}}}\int_S \mathbf{U}\mathbf{p} - \mathbf{P}\overline{\mathbf{v}}^{(1)}(\mathbf{y})\, dS - \tag{2.58}$$

$$\overline{\mathbf{u}}\boxed{\lim_{\mathbf{x}\to\overline{\mathbf{x}}}\int_S \mathbf{P}\, dS} \tag{2.59}$$

In the hypersingular gradient BIE, it becomes very important that the expansion is done in a d-dimensional *cartesian* sense, i.e. defines the displacement function at all space points $\mathbf{y}$, rather than just those on the surface. As a result, the surface gradient $\mathbf{p}(\mathbf{y})$ is *not* independent of $\mathbf{u}(\mathbf{y})$, as is assumed in the isoparametric boundary element methods. Rather, given the series expansion of $\mathbf{u}$ and a surface normal $\mathbf{n}(\mathbf{y})$ the local gradient tensor is

$$\sigma(\mathbf{y}) = \mathbf{E}(\nabla\mathbf{u}(\mathbf{y})) = \mathbf{E}(\overline{\mathbf{A}} + \overline{\mathbf{w}}^{(2)}(\mathbf{y})) \tag{2.60}$$

and the gradient in specific direction $\mathbf{n}$ is

$$\mathbf{p}(\mathbf{y}) = \sigma\mathbf{n} = \mathbf{E}(\overline{\mathbf{A}} + \overline{\mathbf{w}}^{(2)}(\mathbf{y}))\mathbf{n} \tag{2.61}$$

where $\overline{\mathbf{w}}^{(2)}(\mathbf{y})$ contains derivatives of the remainder terms $\overline{\mathbf{v}}^{(2)}(\mathbf{y})$ of the series expansion of $\mathbf{u}$ and is $O(|\mathbf{y} - \mathbf{x}|)$. The regularized gradient BIE is then

$$\sigma(\mathbf{x}) = \int_S \mathbf{D}\mathbf{p} - \mathbf{S}\mathbf{u}\, dS \tag{2.62}$$

$$\Leftrightarrow \quad \{ \text{ Series expansion on both sides } \} \tag{2.63}$$

$$\gamma(\mathbf{x})(\mathbf{E}(\overline{\mathbf{A}}+\overline{\mathbf{w}}^{(2)}(\mathbf{x}))= \tag{2.64}$$

$$\int_S \mathbf{DE}(\overline{\mathbf{A}}+\overline{\mathbf{w}}^{(2)}(\mathbf{y}))\mathbf{n}-\mathbf{S}(\overline{\mathbf{u}}+\overline{\mathbf{A}}(\mathbf{y}-\overline{\mathbf{x}})+\overline{\mathbf{v}}^{(2)}(\mathbf{y}))\,dS \tag{2.65}$$

$$\Leftrightarrow \quad \{\text{ Isolate singular parts of integrals } \} \tag{2.66}$$

$$\gamma(\mathbf{x})(E(\overline{\mathbf{A}}+\overline{\mathbf{w}}^{(2)}(\mathbf{x}))= \tag{2.67}$$

$$\int_S \mathbf{DE}\overline{\mathbf{w}}^{(2)}(\mathbf{y})\mathbf{n}-\mathbf{S}\overline{\mathbf{v}}^{(2)}(\mathbf{y})\,dS \tag{2.68}$$

$$-\overline{\mathbf{u}}\int_S \mathbf{S}\,dS \tag{2.69}$$

$$+\int_S \mathbf{DE}\overline{\mathbf{A}}\mathbf{n}-\mathbf{S}\overline{\mathbf{A}}(\mathbf{y}-\overline{\mathbf{x}})\,dS \tag{2.70}$$

$$\Rightarrow \quad \left\{\begin{array}{l}\text{Take limit as } \mathbf{x} \text{ approaches } \overline{\mathbf{x}} \text{ on a path}\\ \text{where } \gamma(\mathbf{x}) \text{ does not change sign}\end{array}\right\} \tag{2.71}$$

$$\gamma(\mathbf{x}) \quad \overline{\sigma}= \tag{2.72}$$

$$\int_S \mathbf{DE}\overline{\mathbf{w}}^{(2)}(\mathbf{y})\mathbf{n}-\mathbf{S}\overline{\mathbf{v}}^{(2)}(\mathbf{y})\,dS \tag{2.73}$$

$$-\overline{\mathbf{u}}\boxed{\lim_{\mathbf{x}\to\overline{\mathbf{x}}}\int_S \mathbf{S}\,dS} \tag{2.74}$$

$$+\overline{\mathbf{A}}\boxed{\lim_{\mathbf{x}\to\overline{\mathbf{x}}}\int_S \mathbf{DEn}-\mathbf{S}(\mathbf{y}-\overline{\mathbf{x}})\,dS} \tag{2.75}$$

In (2.58) and (2.73), integrals of 'higher order terms' involving $\overline{\mathbf{v}}^{(k)}(\mathbf{y})$ and $\overline{\mathbf{w}}^{(k)}(\mathbf{y})$ are at most weakly singular and can be integrated. The integrals in (2.59) and (2.75) are Cauchy singular, and the boxed terms of (2.74) are hypersingular. Fully subscripted forms for the Laplace and elasticity equations are given in Fig. 2.8 and Fig. 2.9.

Chapter 4 will describe direct attack on these integrals using the kernel expressions in Fig. 2.3 and Fig. 2.4. Chapter 5 will give solutions using much shorter arguments that do *not* depend on expanding the kernel expressions. An important point in both types of analyses is that the integral $\int_S \mathbf{DEn}-\mathbf{S}(\mathbf{y}-\overline{\mathbf{x}})\,dS$ is analyzed as a unit; it is not possible to compute $\int_S \mathbf{DEn}\,dS$ and $\int_S \mathbf{y}-\overline{\mathbf{x}}\,dS$ independently at corners.

1. Constant Term of Primary BIE (Cauchy singular)

$$I = \int_{S_1} H \, dS \tag{2.76}$$

2. Constant term of Gradient BIE (Hypersingular)

$$I_j = \int_{S_1} H_{,j} \, dS \tag{2.77}$$

3. Linear term of Gradient BIE (Cauchy singular)

$$I_{jk} = \int_{S_1} G_{,j} n_k - H_{,j} (y_k - \overline{x_k}) \, dS \tag{2.78}$$

Figure 2.8: Singular integrals in the Laplace equation

Singular Integration Problems – Elasticity

1. Constant Term of Primary BIE (Cauchy singular)

$$I_{ik} = \int_{S_1} P_{ik} \, dS \tag{2.79}$$

2. Constant term of Gradient BIE (Hypersingular)

$$I_{ijk} = \int_{S_1} S_{ijk} \, dS \tag{2.80}$$

3. Linear term of Gradient BIE (Cauchy singular)

$$I_{ijmn} = \int_{S_1} D_{ijk} E_{klmn} n_l - S_{ijm} (\mathrm{x}_n - \overline{x_n}) \, dS \tag{2.81}$$

Figure 2.9: Singular integrals in the elasticity equation

2.5 The Linearized BIE

In order to make the BIE useful for numerical computation, the abstract surface functions $\mathbf{u}(\mathbf{y})$ and $\mathbf{p}(\mathbf{y})$ must be discretized, i.e. converted to a form with only a finite number of degrees of freedom.

Without committing to a representation of basis functions, we write $\mathbf{u}$ and $\mathbf{p}$ by linear combinations of $N_{\mathbf{u}}$ and $N_{\mathbf{p}}$ yet-to-be-determined basis functions. The surface functions $\mathbf{u}(\mathbf{y})$ and $\mathbf{p}(\mathbf{y})$ themselves are rewritten as

$$\mathbf{u}(\mathbf{y}) \approx \sum_{i}^{N_{\mathbf{u}}} \mathbf{a}_i \mathbf{u}_i(\mathbf{y}) \tag{2.82}$$

$$\mathbf{p}(\mathbf{y}) \approx \sum_{j}^{N_{\mathbf{p}}} \mathbf{b}_j \mathbf{p}_j(\mathbf{y}) \tag{2.83}$$

and we define

$$\mathcal{U}_j(\mathbf{x}) = \int_S \mathbf{U}\mathbf{p}_j(\mathbf{y})\, dS \tag{2.84}$$

$$\mathcal{P}_i(\mathbf{x}) = \int_S \mathbf{P}\mathbf{u}_i(\mathbf{y})\, dS \tag{2.85}$$

to represent frequently occurring integrations of the basis functions multiplied by kernels. Note that at this stage the basis functions are considered to be (a) defined everywhere on the surface, and (b) functions of the surface point $\mathbf{y}$ in a coordinate-system independent way, i.e are not parametrized functions. However, we make no assumptions about (a) whether or not the basis functions are defined at non-surface points and (b) whether the $\mathbf{a}_i$ and $\mathbf{b}_j$ can be interpreted as specific physical displacements and tractions. They are simply generalized degrees of freedom multiplying generalized basis functions to approximate $\mathbf{u}$ and $\mathbf{p}$.

The BIE then for point $\mathbf{x}$ the becomes

$$\gamma(\mathbf{x})\mathbf{u}(\mathbf{x}) \quad \int_S \mathbf{U}\mathbf{p} - \mathbf{P}\mathbf{u}\, dS \tag{2.86}$$

$$\begin{array}{lll}
\approx & \{ \text{ Substitute summations} \quad \} & (2.87) \\
& \int_S \mathbf{U}(\sum_j^{N_\mathbf{p}} \mathbf{b}_j \mathbf{p}_j(\mathbf{y})) - \mathbf{P}(\sum_i^{N_\mathbf{u}} \mathbf{a}_i \mathbf{u}_i(\mathbf{y}))\, dS & (2.88) \\
= & \{ \text{ Take coefficients outside integrals} \quad \} & (2.89) \\
& \sum_j^{N_\mathbf{p}} \mathbf{b}_j \int_S \mathbf{U}\mathbf{p}_j(\mathbf{y})\, dS - \sum_i^{N_\mathbf{u}} \mathbf{a}_i \int_S \mathbf{P}\mathbf{u}_i(\mathbf{y})\, dS & (2.90) \\
= & \left\{ \begin{array}{l} \text{Substitute symbols for integrated basis} \\ \text{functions} \end{array} \right\} & (2.91) \\
& \sum_j^{N_\mathbf{p}} \mathbf{b}_j \mathcal{U}_j(\mathbf{x}) - \sum_i^{N_\mathbf{u}} \mathbf{a}_i \mathcal{P}_i(\mathbf{x}) & (2.92)
\end{array}$$

The terms $\mathcal{P}_i(\mathbf{x})$ and $\mathcal{U}_j(\mathbf{x})$ are, respectively, the integrals of the i'th displacement function $\mathbf{u}_i(\mathbf{y})$ and the j'th traction function $\mathbf{p}_j(\mathbf{y})$ over the entire surface, using the particular point $\mathbf{x}$ as a fixed point. Each point $\mathbf{x}$ generates a different set of values of $\mathcal{P}_i(\mathbf{x})$ and $\mathcal{U}_j(\mathbf{x})$.

2.6 Constructing Linear Equations to Solve the Boundary Value Problem

For the exact BIE, integrated values $\mathbf{u}(\mathbf{x})$ at interior points $\mathbf{x}$ that are near some surface point $\overline{\mathbf{x}}$ will converge in the limit to the surface value $\mathbf{u}(\overline{\mathbf{x}}) = \sum_i^{N_\mathbf{u}} \mathbf{a}_i \mathbf{u}_i(\overline{\mathbf{x}})$. When $\mathbf{u}(\mathbf{y})$ and $\mathbf{p}(\mathbf{y})$ are represented only approximately, this equality does not hold exactly. Rather, at each surface point $\overline{\mathbf{x}}$ there will be some residual error $\mathbf{v}(\overline{\mathbf{x}})$

$$\mathbf{v}(\overline{\mathbf{x}}) = (\sum_i^{N_\mathbf{u}} \mathbf{a}_i \mathbf{u}_i(\overline{\mathbf{x}})) - \lim_{\mathbf{x}\to\overline{\mathbf{x}}} \left[\sum_j^{N_\mathbf{p}} \mathbf{b}_j \mathcal{U}_j(\mathbf{x}) - \sum_i^{N_\mathbf{u}} \mathbf{a}_i \mathcal{P}_i(\mathbf{x}) \right] \quad (2.93)$$

In a well posed boundary value problem, boundary conditions will constrain exactly one of the two surface values $\mathbf{u}(\mathbf{y})$ and $\mathbf{p}(\mathbf{y})$ at each boundary point to either take on some value or be linearly dependent on the other. This in turn provides constraints on roughly half of the unknown quantities $\mathbf{a}_i$ and $\mathbf{b}_j$. (Most presentations make the simpler statement 'Boundary conditions prescribe the *values* of half of the unknowns'. This is *not* correct, since it precludes (a) mixed boundary conditions and (b) surface function values that are linear combinations of degrees of freedom, rather than individual d.o.f. values. The implementation in Chapter 8 provides a more general framework for this problem.

Standard Linear System Construction: Collocation The standard method of constructing a linear system is to assume that among the $N_{\mathbf{u}}+N_{\mathbf{p}}$ unknowns of the linearized BEM, some number, say $N_{\mathbf{u}}+N_{\mathbf{p}}$-$N$ are given explicit values by boundary conditions, while N remain unconstrained. To constrain the remaining degrees of freedom, the residual $\mathbf{v}(\overline{\mathbf{x}_c})$ is computed at each of N collocation points $\overline{\mathbf{x}_c}$. This produces N equations

$$\begin{array}{llllll}
(\sum_i^{N_{\mathbf{u}}} \mathbf{a}_i \mathbf{u}_i(\overline{\mathbf{x}}_1)) & -\mathcal{U}_1(\mathbf{x}_1)\mathbf{b}_1 & -\mathcal{U}_2(\mathbf{x}_1)\mathbf{b}_2 & \cdots & & \\
 & +\mathcal{P}_1(\mathbf{x}_1)\mathbf{a}_1 & +\mathcal{P}_2(\mathbf{x}_1)\mathbf{a}_2 & \cdots & = & 0 \\
\vdots & & & & & \vdots \\
(\sum_i^{N_{\mathbf{u}}} \mathbf{a}_i \mathbf{u}_i(\overline{\mathbf{x}}_N)) & -\mathcal{U}_1(\mathbf{x}_N)\mathbf{b}_1 & -\mathcal{U}_2(\mathbf{x}_N)\mathbf{b}_2 & \cdots & & \\
 & +\mathcal{P}_1(\mathbf{x}_N)\mathbf{a}_1 & +\mathcal{P}_2(\mathbf{x}_N)\mathbf{a}_2 & \cdots & = & 0
\end{array} \tag{2.94}$$

Collecting terms in matrices and vectors, we can write

$$\left[\mathbf{u}_i(\overline{\mathbf{x}}_c) + \mathcal{P}_i(\mathbf{x}_c)\right]\left[\mathbf{a}_i\right] - \left[\mathcal{U}_j(\mathbf{x}_c)\right]\left[\mathbf{b}_j\right] = [0] \tag{2.95}$$

The 'textbook' formulation of the boundary element method (e.g. Brebbia and Dominguez [BD88]) further simplifies this equation in the following ways:

- The generalized unknowns $\mathbf{a}_i$ are chosen to be the actual physical displacement precisely at the collocation points $\overline{\mathbf{x}_c}$. Similarly, the $\mathbf{b}_j$ unknowns are chosen to be tractions at those points; there may be several distinct $\mathbf{b}_j$ values at a single point if the surface geometry has a corner or edge or if the applied tractions are discontinuous.

- The basis functions are chosen to have *local support.* That is, each $\mathbf{u}_i(\mathbf{y})$ and $\mathbf{p}_j(\mathbf{y})$ is nonzero over only a small portion of surface.

- Except for some recent research using B-splines (Cabral, Wrobel, and Brebbia [CWB90]), engineering codes have used basis functions $\mathbf{u}_i(\mathbf{y})$ and $\mathbf{p}_j(\mathbf{y})$ with the Lagrangian property that at each $\overline{\mathbf{x}_c}$ there is a distinguished basis function whose value is one while all others are zero at that point. This reduces the matrix $\left[\mathbf{u}_i(\overline{\mathbf{x}}_c)\right]$ to an identity matrix.

- Boundary conditions are specified so that at each $\overline{\mathbf{x}_c}$ all but one of the $\mathbf{a}_i$ and $\mathbf{b}_j$ unknowns is given a value, and the remaining one is completely unconstrained. The matrix columns multiplying known values can be taken immediately to the right side of the system.

- Because there is only one displacement basis function $\mathbf{a}_i$ with a nonzero constant term of its Taylor expansion at each $\overline{\mathbf{x}_c}$, the singularities in the integrations required for all remaining basis functions $\mathcal{P}_i(\mathbf{x}_{\overline{\mathbf{x}_c}})$ at that point are weakened by one degree. The Cauchy singularity of the remaining integral does not need to be explicitly computed, for a rigid body motion argument determines that the sum of the $\mathcal{P}_i(\mathbf{x}_{\overline{\mathbf{x}_c}})$ entries across the row must be one.

These are appropriate simplifications for many problems. However, the beneficial matching of the position and number of collocation points with points at which the unknowns are given physical interpretations cannot always be obtained in more complex problems involving cracks and multiple materials. A generalized implementation must be prepared to deal with (a) collocation points $\overline{\mathbf{x}_c}$ that do *not* correspond to points where nodal unknowns are defined and (b) evaluation of Cauchy and hypersingular integrals at points where many basis functions contribute to the approximated solution.

Of all these assumptions, the only one carried without reservation in the implementation described in Chapter 8 is that basis functions will have local support. This has the important effect that each matrix coefficient $\mathcal{P}_i(\mathbf{x}_C)$ and $\mathcal{U}_j(\mathbf{x}_C)$ is an integral over only small portions, say S_i and S_j, of the overall surface. *The computation of one such integral – a particular basis function over its associated surface patch – is the fundamental operation of the boundary element method.*

A more standard presentation of the boundary element method would choose a slightly lower level 'fundamental operation', namely the integral over a single boundary element (which is only a subset of the S_i and S_j); the summation operation that combines several single-element integrals is considered a trivial issue.

Non-Standard Linear System Formulations Essentially all practical use of the BIE has been based on collocation, i.e. forcing the residual to be exactly 0 at one point per unknown coefficient, with no effort to measure and/or constrain it at points in between. This is in sharp contrast to the finite element method, which has always been based on forcing its corresponding residual quantity to be zero in an average (Galerkin) sense that can be interpreted as finding the minimum energy solution among those feasible with the given basis functions. Since the BEM has produced accurate results in practice, the lack of an energy interpretation and corresponding convergence guarantees is not a *de facto* flaw in the method.

The most important practical problem caused by collocation is that the linear systems it produces are non-symmetric. This makes it difficult to combine finite and boundary element analysis in the same model, since finite element programs often depend in a basic way on the symmetric, positive definite character of the linear system the FEM produces.

Several Galerkin formulations of linear systems for the BIE have been proposed. Lean [Lea81] has applied the general Bubnov-Galerkin analysis found in Mikhlin

[Mik64] to obtain a positive-definite linear system from the Laplace BIE for electromagnetics. This enforces a global minimization of the residual function $\mathbf{v}(\overline{\mathbf{x}})$ defined above; there may or may not be an energy-based interpretation of the corresponding formulation of elasticity. Polizzotto [Pol88] has described an elasticity formulation that can be explicitly interpreted as energy minimization. This requires computation of both the displacement residual as defined above and a residual of the gradient BIE, i.e. the hypersingular kernels addressed in Chapter 5.

Practical use of Galerkin methods is restricted by the fact that they require residuals to be computed at far more points than collocation. The added computation is approximately a factor of 3 to 5 in 2 dimensions and 9 to 25 in 3 dimensions, depending on the accuracy of calculation of the integrated residuals. The researchers involved generally claim that there are accuracy improvements in return for the added computation. However, since integration generally constitutes about half the computation time of a BEM solution, the additional factor is currently a significant impediment to use of the Galerkin method.

Chapter 3

The BIE in a Cracked Solid

A crack is a $d-1$ dimensional geometric feature in the interior of a d dimensional region, i.e. a surface in the interior of a 3D solid or a line in the interior of a 2D area. In a field problem, a crack is significant if it causes the solution to behave differently on opposite sides. In elasticity, this takes the very tangible form that the crack can open and expose two distinct surfaces. In electrostatics, a thin, non-conducting sheet in a conducting 3D medium causes a discontinuity in the electric field.

Fig. 3.1 illustrates terminology related to a 3D crack. The *crack face* is the interior of the 2D surface. The edge where new material is exposed as the crack grows is the *crack front.* An edge where the crack joins a free surface is a *free surface edge* or simply a *crack edge.* The points where a crack front joins a free surface are the *crack tips.*

When the BIE is applied to a crack, the integration variable 'sweeps over' both crack faces as if the crack were open, i.e. the body is topologically a manifold. However, surface coordinates in the integration are those of the closed crack. This ambiguity has a severe effect on the boundary integral equation. Close inspection

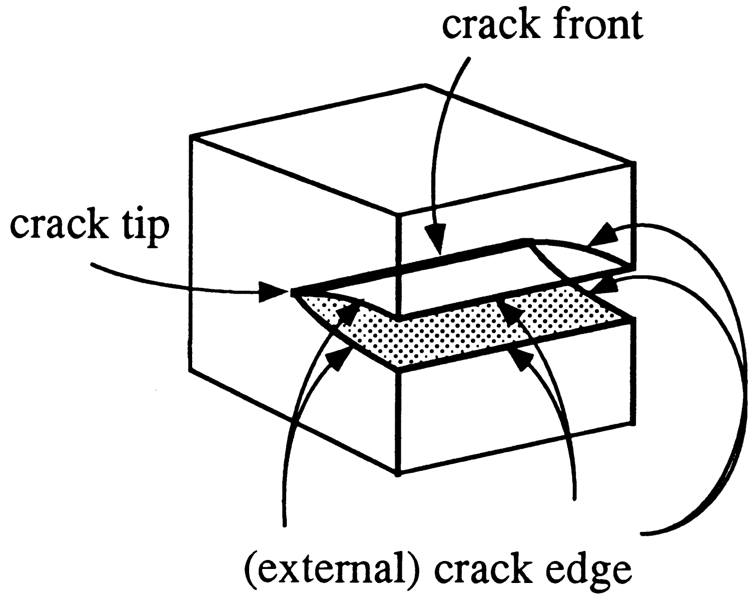

Figure 3.1: Crack terminology

of how surface coordinates and normals appear in the BIE shows that the surface traction term is completely canceled from the integrands of both the primary and gradient BIE. If we consider surface traction to be an *input* to the problem, the primary BIE is thus no longer a viable governing equation, for the canceled traction is the only appearance of the crack surface traction.

Section 1 gives the derivation of this degeneracy. Section 2 describes the established *multidomain* solution method, which bypasses the problem by geometric subdivision of the solid. Section 3 describes the principles of applying the *gradient* BIE, which has crack tractions appearing (uncanceled) on the left side, as a substitute equation. This preserves the boundary-only character of the BIE, but introduces the severe integration problems treated in subsequent chapters.

3.1 Singularity of the Primary BIE at a Crack

As given by Cruse [Cru88], careful application of the symmetry and anti-symmetry properties (Section 2.5) causes the traction distribution on the crack face to disappear entirely from the equation. We will repeat the derivation here to emphasize the nature of the degeneracy.

As in Fig. 3.2, label the non-crack surface S^{far}, label one crack face as S^{+}, and the other S^{-}, and also attach the same superscripts to all quantities involving points on those surfaces. Any surface integral must sweep through each point $\mathbf{y}$ of the crack twice, once as part of S^{+}(with an upward normal in the figure) and once as part of S^{-}. Superscripts distinguish surface functions and kernel evaluations as follows:

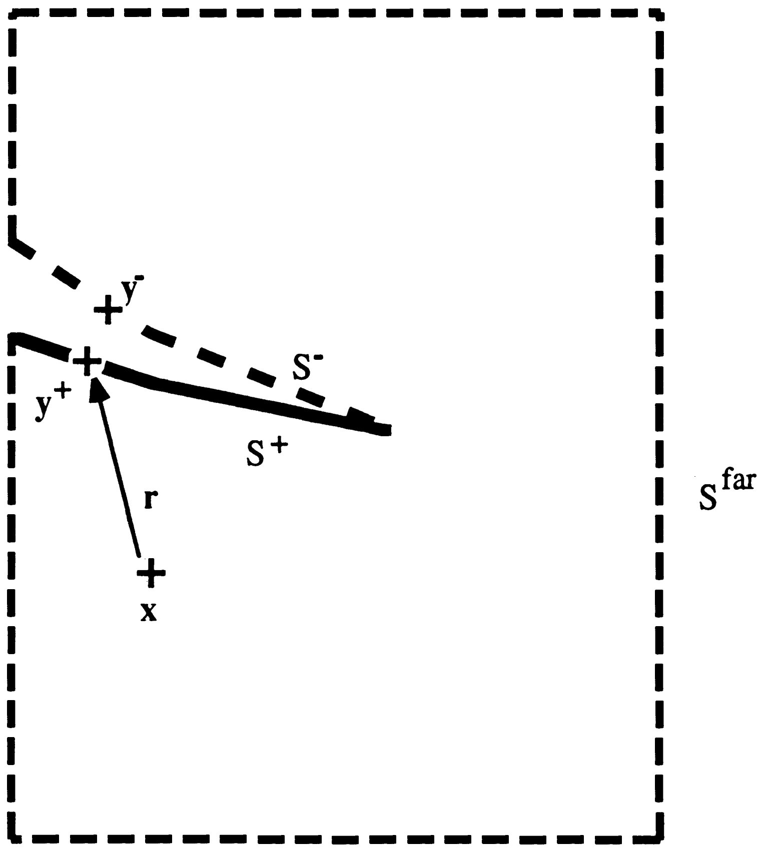

Figure 3.2: Notation for integration in a crack

$\mathbf{y}^+,\mathbf{y}^-$	= point $\mathbf{y}$ treated as part of S^+,S^-
$\mathbf{n}^+,\mathbf{n}^-$	= surface normal to S^+,S^-at $\mathbf{y}$
$\mathbf{u}^+,\mathbf{u}^-$	= displacements of $\mathbf{y}^+,\mathbf{y}^-$at $\mathbf{y}$
$\mathbf{p}^+,\mathbf{p}^-$	= tractions acting on $S^+,S^-\mathbf{y}$
$\mathbf{U}^+,\mathbf{U}^-$, $\mathbf{P}^+,\mathbf{P}^-$	= value of the primary and gradient kernels (Green's functions) when evaluated between fixed point $\mathbf{x}$ and points $\mathbf{y}^+$, $\mathbf{y}^-$using corresponding normals $\mathbf{n}^+$, $\mathbf{n}^-$

Now, with the physically reasonable assumption that tractions on the two crack faces have equal magnitude and opposite direction, proceed from the basic boundary integral as follows:

$$\gamma\mathbf{u} = \int_S \mathbf{Up} - \mathbf{Pu}\, dS(\mathbf{y}) \tag{3.1}$$

$$= \left\{ \begin{array}{l} \text{Replace the full integral by a sum of integrals} \\ \text{over } S^+,\ S^-, \text{ and } S^{\text{far}} \end{array} \right\} \tag{3.2}$$

$$\int_{S^{\text{far}}} \mathbf{Up} - \mathbf{Pu}\, dS(\mathbf{y}) \tag{3.3}$$

$$+ \int_{S^+} \mathbf{U}^+\mathbf{p}^+ - \mathbf{P}^+\mathbf{u}^+\, dS(\mathbf{y}) \tag{3.4}$$

$$+ \int_{S^-} \mathbf{U}^-\mathbf{p}^- - \mathbf{P}^-\mathbf{u}^-\, dS(\mathbf{y}) \tag{3.5}$$

$$= \{ \text{ Symmetry properties } \mathbf{U}^+ = \mathbf{U}^-,\ \mathbf{P}^+ = -\mathbf{P}^- \ \} \tag{3.6}$$

$$\int_{S^{\text{far}}} \mathbf{Up} - \mathbf{Pu}\, dS(\mathbf{y}) \tag{3.7}$$

$$+ \int_{S^+} \mathbf{U}^+\mathbf{p}^+ - \mathbf{P}^+\mathbf{u}^+\, dS(\mathbf{y}) \tag{3.8}$$

$$+ \int_{S^-} \mathbf{U}^+\mathbf{p}^- + \mathbf{P}^+\mathbf{u}^-\, dS(\mathbf{y}) \tag{3.9}$$

$$= \left\{ \begin{array}{l} \text{Combine crack surface integrals over identical} \\ \text{points} \end{array} \right\} \tag{3.10}$$

$$= \int_{S^{\text{far}}} \mathbf{Up} - \mathbf{Pu}\, dS(\mathbf{y}) \tag{3.11}$$

$$+ \int_{S^+} \mathbf{U}^+(\mathbf{p}^+ + \mathbf{p}^-) - \mathbf{P}^+(\mathbf{u}^+ - \mathbf{u}^-)\, dS(\mathbf{y}) \tag{3.12}$$

$$= \quad \{ \text{ Apply traction condition } \mathbf{p}^+ - \mathbf{p}^- = 0 \qquad \} \tag{3.13}$$

$$= \int_{S^{\text{far}}} \mathbf{U}\mathbf{p} - \mathbf{P}\mathbf{u}\, dS(\mathbf{y}) \tag{3.14}$$

$$+ \int_{S^+} -\mathbf{P}^+(\mathbf{u}^+ - \mathbf{u}^-)\, dS(\mathbf{y}) \tag{3.15}$$

Expression (3.15) is completely equivalent to the original BIE, but no longer has any crack surface traction terms. If equation is used to determine the crack opening induced by a certain surface pressure in the crack, there is no place to apply the crack-surface pressure input. The numerical manifestation is that when the primary BIE is written simultaneously for two corresponding collocation points on opposing crack faces, the matrix columns of the second point are linearly dependent on those of the first point.

It is important that the degeneracy occurs in the original BIE. Martha [Mar89] gives an informal proof of the singularity of the final matrix of a BEM implementation, based on reasoning about columns of the linear system. Although its conclusion is correct, the matrix-level proof offers no evidence that minor modifications such as placing collocation points at different locations on the mating faces would also fail.

3.2 Multiregion Solution Methods

The established method of addressing this singularity is to (a) subdivide the body into two regions such that only one crack face is in each region, (b) write the BIE independently in each region, and (c) enforce displacement and traction continuity as 'boundary conditions' on the interface between the two regions. Implementation of multidomain method was described for 2D by Blandford, Ingraffea, and Liggett [BIL81] and for 3D by Perucchio [Per84] and Martha [Mar89].

Although it overcomes the ambiguity in the boundary integral, the multidomain method introduces several new problems. First, one must determine where to introduce the artificial interface. This adds to the preliminary effort of constructing the geometric model.

More importantly, there are numerical problems that are dependent on the geometry of the interface. In a series expansion [Bro82] of the displacement field around a crack tip, the leading term of each displacement component varies as $\sqrt{r}$, where r is the distance to the crack tip. When this is differentiated to obtain stresses, all stress components are dominated by $1/\sqrt{r}$. This goes to infinity as r vanishes. These unbounded stresses become surface tractions on the artificial subdivision surface. Hence the artificial surface is being added in the most sensitive part of the stress field.

3.3 Traction BIE Formulations

Rather than altering the geometry to seek a well posed problem, one may look for a different integral formulation that involves the surface traction in a non-degenerate way. Gray, Martha, and Ingraffea [GMI90] showed that it is feasible to replace the degenerate collocation equation by a collocation of the normal component of the gradient BIE. That is, choose a point $\overline{\mathbf{x}}$ on the crack surface and consider two interior points $\mathbf{x}^+$ and $\mathbf{x}^-$ approaching from opposite sides. At $\mathbf{x}^+$, enforce the limiting condition

$$\gamma(\mathbf{x}^+)\mathbf{u}^+(\overline{\mathbf{x}}) = \lim_{\mathbf{x}^+ \to \overline{\mathbf{x}}} \int_S \mathbf{U}\mathbf{p} - \mathbf{P}\mathbf{u}\, dS \tag{3.16}$$

and at $\mathbf{x}^-$ enforce the limiting condition

$$\gamma(\mathbf{x}^-)\mathbf{p}^-(\overline{\mathbf{x}}) = \mathbf{n}^-(\overline{\mathbf{x}}) \lim_{\mathbf{x}^- \to \overline{\mathbf{x}}} \int_S \mathbf{D}\mathbf{p} - \mathbf{S}\mathbf{u}\, dS \tag{3.17}$$

The implementation in Gray, Martha, and Ingraffea [GMI90] was for strictly planar crack surfaces[1] not intersecting any external surface. Extension to cracks with (a)

[1]i.e. contained in a single plane; the curved crack could *not* be faceted from many small planar pieces.

curved faces, (b) faceted faces, and (c) intersections with exterior surfaces requires the more complete singular integral analysis of Chapter 5.

Displacement Discontinuity (DD) Formulation Since the **D** and **S** kernels have the same symmetry properties as **U** and **P**, all steps of the derivation of the disappearance of **p** from the primary BIE apply unchanged to the gradient BIE. Hence the **Dp** integral on the right side of (3.17) vanishes in the same fashion. However, the traction term on the *left* side is not affected, and the traction condition is equivalent to

$$\gamma\sigma = \int_{S^{\mathrm{far}}} \mathbf{D}\mathbf{p} - \mathbf{S}\mathbf{u}\, dS(\mathbf{y}) + \int_{S^{+}} -\mathbf{S}^{+}(\mathbf{u}^{+} - \mathbf{u}^{-})\, dS(\mathbf{y}) \tag{3.18}$$

If the displacement discontinuity $\Delta\mathbf{u} = \mathbf{u}^{+} - \mathbf{u}^{-}$ is defined as an independent quantity, the boundary integrals no longer involve the two displacements $\mathbf{u}^{+}$ and $\mathbf{u}^{-}$ on opposite sides of the crack. Hence instead of enforcing *both* the primary and gradient integrals to fully constrain the crack surface, only the gradient needs to be enforced.

This strategy is the one currently used by Cruse *et al* and Rizzo *et al.* Since the **S** kernel still appears multiplying an unknown surface displacement function, the fundamental hypersingular integration problem remains unchanged; it becomes clear, however, that there is no need to integrate the **D** kernel on the crack surface. The DD form has the (probably very significant) advantage that there are only half as many unknowns on the crack, and has completely eliminated the primary BIE collocations on the crack. In a computer simulation involving a large crack surface and minimal non-crack surface, this would reduce the matrix dimension by a factor of two, total storage for the (square) matrix by four, and matrix factorization time by eight. A minor disadvantage is that it does not produce absolute displacements of the crack; however, they can be computed by a subsequent integration of the primary BIE. This should not generally be necessary except for purposes of visual inspection of the opened crack shape; essential computations such as stress intensity factor computation requires only the $\Delta\mathbf{u}$ terms.

Summary

This chapter has shown how surface tractions vanish from the BIE applied over a crack. This results in inability to use the BIE to solve the field problem. Three methods were given for overcoming the problem: artificial geometry subdivision (multidomain analysis), and two variants of applying the gradient BIE to enforce crack tractions. Subsequent chapters will address computation of the hypersingular integrals in the traction BIE formulations.

Chapter 4

Singular Integration I: Algebraic Methods

This is the first of three chapters dealing with the singular integrals that arise when the 'fixed point' of the primary BIE (Eq. 2.15 or 2.16) is taken to the boundary. This first chapter provides an overview of the entire topic and then reviews prior methods of singular and hypersingular integration. Chapter 5 contains the 'modal' method of analysis, which is the core of the entire thesis and the basis for our implementation. Chapter 6 contains theoretical results that follow from the modal analysis and may be important in future implementations.

There is an important distinction between this chapter and those that follow. The methods in this chapter all contain extensive 'algebraic' manipulation of the kernels. They require term-by-term analysis of the expressions in Fig. 2.3 and Fig. 2.4, often with respect to specific coordinate systems and geometries. Results appear after somewhat grueling algebraic, geometric, and integral transformations.

In contrast to the algebraic methods, both the modal analysis in the Chapter 5 and the further developments in Chapter 6 reason only about certain properties that the kernels inherit from the differential equations. We refer to this as 'generalized' analysis.

The primary goal of embarking on this analysis is the hypersingular case. However, a byproduct of the effort is that the methods used for this hardest integration are also applicable to the easier cases.

4.0.1 Overview of Hypersingular Integration

Fig. 4.1 shows a tree-like summary of the decisions leading to various methods for hypersingular integrals. The top of the tree is labeled with the main problem, hypersingular integration. The highest level branching is based on whether one deals with (a) the expanded integrand, leading to the 'algebraic' methods on the left, or (b) the unexpanded integrand, leading to the 'generalized' methods on the right. On both sides of the tree, there is a secondary branching related to the domain of integration. On the algebraic side, this branch takes the form of deciding whether or not to use an exclusion zone. On the generalized side, the modal approach converts the original surface integral to an integral over another, more tractable, surface; the Stokes theorem approach converts the hard surface integral to an integral over the *edge* of the surface.

The resulting methods are mathematically equivalent in the sense that (a) they produce the same values and (b) they all demand C^1 continuity of the solution function. There are significant practical differences among ease of derivation, range of geometries treated, and ease of implementation. Some overall comments are as follows:

- The 'modal' analysis has by far the shortest derivation, and (if certain geometric constructions are available) leads directly to concise implementation, as described in Chapter 8.

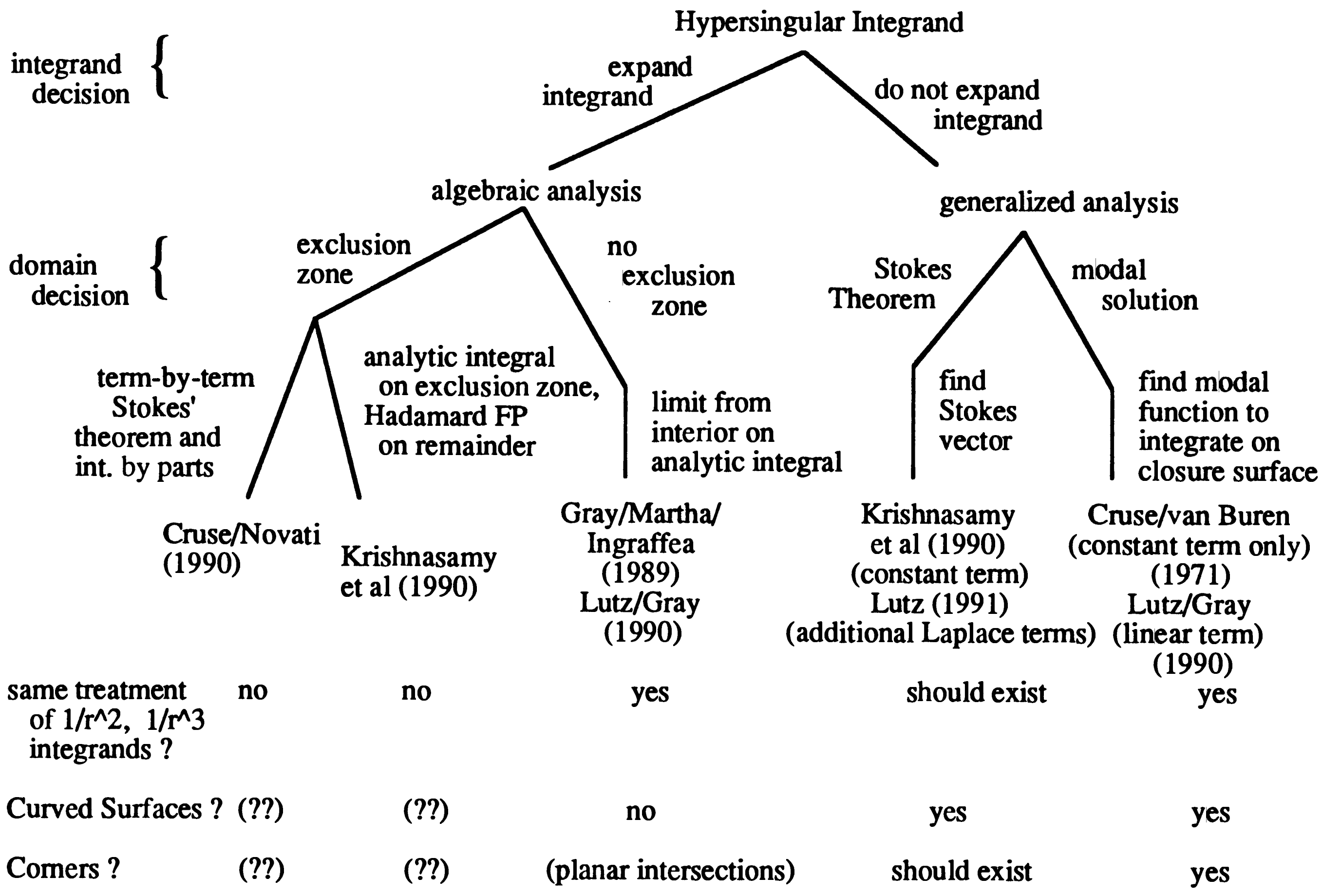

Figure 4.1: Decision tree for hypersingular integration methods

- Both derivation and coding of algebraic approaches are exacting tasks. However, the analytic results may lead to more efficient and accurate computations.

- At the time of this writing, the Stokes theorem methods are not theoretically complete. As will be discussed in Chapter 6, a corollary to the modal derivation is that *all* surface integrals in the BIE should be reducible to edge integrals by Stokes theorem. However, the 'Stokes vectors' that facilitate the conversion are only known for (a) the hypersingular case and (b) a subset of the Cauchy cases. As will be discussed in Chapter 6, this writer believes that the Stokes method will become the preferred implementation if the missing pieces are found.

4.0.2 Overview of Algebraic Analyses

Section 4.1 reviews the classical 'exclusion zone' approaches to singular integration. This approach is successful for weak and Cauchy singularities, but *not* for the hypersingular case.

Section 4.2 is a detailed presentation of the 'limit from the interior' approach, which has been developed primarily by L.J. Gray. This is a consolidated (and hopefully more consistent) version of results published in several papers by Gray, Martha, and Lutz [GMI90],[GL90] [Gra91]. A point being raised in this presentation is that 'limit from the interior' is not just a method that happens to work for the hypersingular case, but is a single, consistent approach to *all* singularities.

Section 4.3 and Section 4.4 are brief discussions of approaches by Rizzo *et al* and Cruse *et al.* These fall into the algebraic category in in most respects, but exhibit some hints of more generalized analysis.

4.1 Exclusion Zone Analysis

Exclusion zone analysis attempts to derive a singular integral value when the fixed point $\mathbf{x}$ of (Eq. 2.15 or 2.16) and Eq. 2.41 or 2.45) is *exactly on the surface.* To avoid division by 0 when the moving point $\mathbf{y}$ of the integration passes through the fixed point, an *exclusion zone* S_ϵ is introduced around the singularity. The overall integral is then defined as

$$\begin{aligned}
& \textstyle\int_S < \dots > dS &&= C + I_{S - S_\epsilon} \\
\text{where} \quad & C &&= \text{value assigned for the integral over the exclusion zone } S_\epsilon \\
& I_{S - S_\epsilon} &&= \textstyle\int_{S - S_\epsilon} < \dots > dS \\
& &&= \text{`Cauchy Principal Value' of the integral} \\
& &&= \text{Integral over surface excluding the singular point}
\end{aligned} \tag{4.1}$$

For 2D boundary integrals on a (1D) linear surface, consider the geometry shown in Fig. 4.2a. With the fixed point at the origin and an x axis along the surface to the right, the one-sided integrals over $S - S_\epsilon$ are

$$I_{S - S_\epsilon} = \lim_{\epsilon \to 0} \int_\epsilon^b \begin{bmatrix} \ln(1/x) \\ \frac{1}{x} \\ \frac{1}{x^2} \end{bmatrix} dx \tag{4.2}$$

$$= \quad \{ \text{ Expand indefinite integrals } \} \tag{4.3}$$

$$\lim_{\epsilon \to 0} \begin{bmatrix} -x\ln(x) + x \\ \ln(x) \\ -\frac{1}{x} \end{bmatrix}_\epsilon^b \tag{4.4}$$

$$= \quad \{ \text{ Take limits (where possible) } \} \tag{4.5}$$

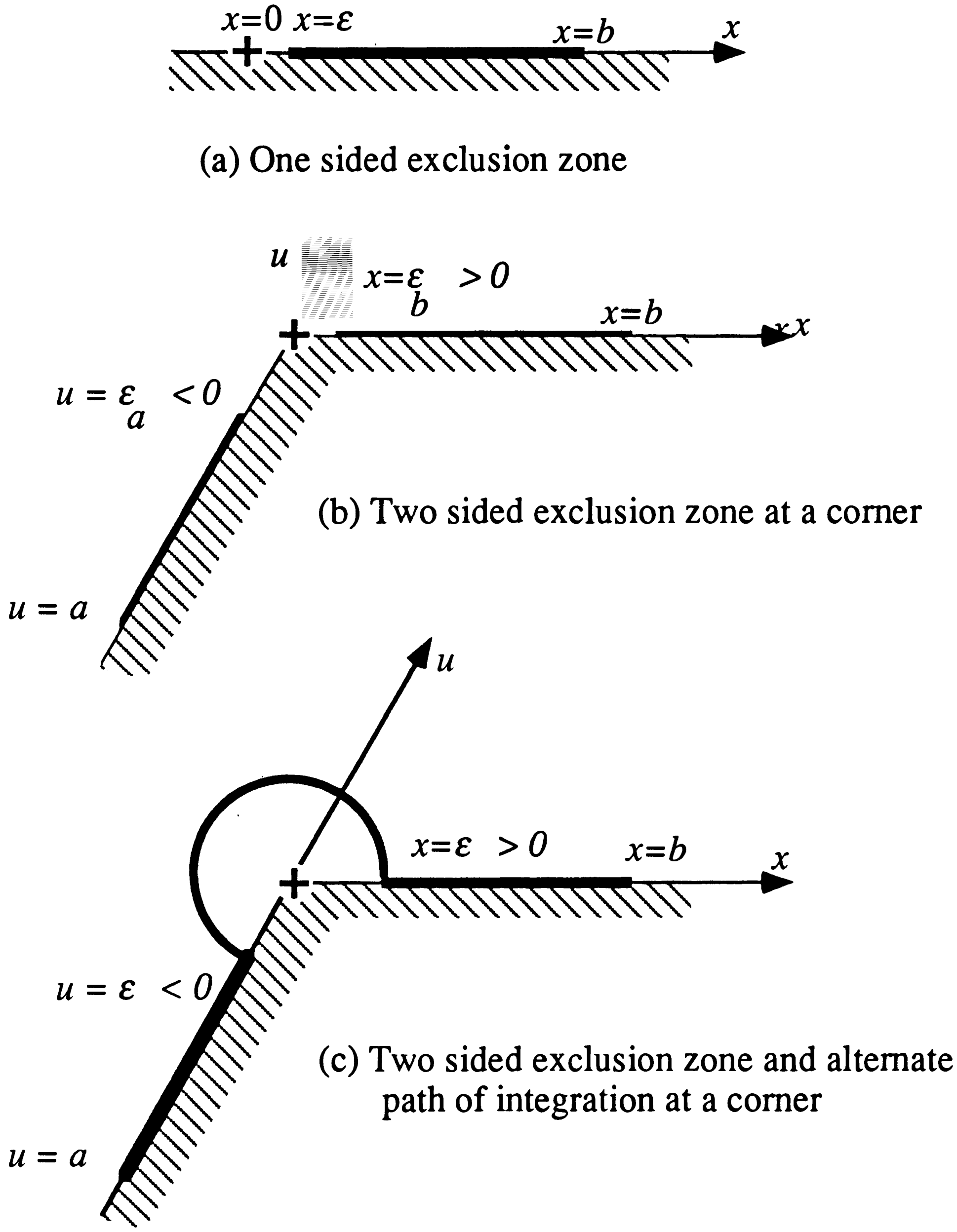

Figure 4.2: Geometry for 2D leading singularity analysis

$$\begin{bmatrix} -b\ln(1/b)+b \\ \ln(b)-\ln(\epsilon) \\ -(\frac{1}{b}-\frac{1}{\epsilon}) \end{bmatrix} \tag{4.6}$$

In the $\ln(r^{-1})$ case, the $\epsilon\ln(\epsilon)$ term vanishes in the limit; we therefore use C=0 for the $\ln(r^{-1})$ integral, i.e. ignore any contribution of the exclusion zone to the $\ln(1/x)$ integral. A similar result applies for any $\int 1/x^{\alpha}\,dx$ for any $\alpha < 1$. These 'weak' singularities can therefore be integrated separately on each edge.

The r^{-1} and r^{-2} integrals still have singular terms that cannot be ignored as ϵ vanishes. This is addressed by combining this integral with an integral over the surface approaching from the other side. Using coordinate systems[1] as in Fig. 4.2b, the Cauchy principal value part of the integrals are

$$\begin{aligned}
I_{S\,-\,S_\epsilon} &= \int_{\epsilon_a}^{a} \begin{bmatrix} \frac{1}{x} \\ \frac{1}{x^2} \end{bmatrix} dx + \int_{b}^{\epsilon_b} \begin{bmatrix} -\frac{1}{u} \\ \frac{1}{u^2} \end{bmatrix} du && (4.7)\\
&= \quad \{\text{ Expand both indefinite integrands at once } \} && (4.8)\\
&\quad \begin{bmatrix} \ln(|\epsilon_a|)-\ln(|a|)+\ln(|b|)-\ln(|\epsilon_b|) \\ -(\frac{1}{b}-\frac{1}{\epsilon_b}-\frac{1}{\epsilon_a}+\frac{1}{a}) \end{bmatrix} && (4.9)\\
&= \quad \{\text{ Simplify } \} && (4.10)\\
&\quad \begin{bmatrix} \ln(|\epsilon_a|/|\epsilon_b|)+\ln(|b|/|a|) \\ -(\frac{1}{b}+\frac{1}{a}-\frac{1}{\epsilon_b}-\frac{1}{\epsilon_a}) \end{bmatrix} && (4.11)
\end{aligned}$$

For the r^{-1} integral, the combined limits will now exist *if* ϵ_a and ϵ_b are are the same size (with opposite signs) or constrained so ϵ_a/ϵ_b is constant as they vanish. [2] For $\frac{1}{x^2}$, the combined $I_{S\,-\,S_\epsilon}$ limits vanish only if $\epsilon_a \equiv \epsilon_b$.

---

[1]Note that all values of x (and u) (including the limits of integration) are *signed*

[2]Even when ϵ_a and ϵ_b are constrained to be equal, differently parameterized surface representations on opposite sides can lead to terms containing the logarithm of a ratio of epsilons of the two surfaces, as treated in Guiggiani and Casalini [GC87].

To determine the C term, replace the exclusion zone surface by a circular arc of radius ϵ, as in Fig. 4.2c. The C term is then

$$\int_{S_\epsilon} \begin{bmatrix} r^{-1} \\ r^{-2} \end{bmatrix} dS = \int_0^\theta \begin{bmatrix} \frac{1}{\epsilon} \\ \frac{1}{\epsilon^2} \end{bmatrix} \epsilon \, d\theta = \begin{bmatrix} \theta \\ \theta/\epsilon \end{bmatrix} \tag{4.12}$$

The θ result for the r^{-1} case is called the 'corner' or (in an analogous treatment of a spherical surface around a singular point in 3D) 'solid angle' term. Carrying out the same analysis for the complete kernels (including finite factors such as $\frac{\partial r}{\partial \mathbf{n}}$) produces variations in the particular results, but the characteristic angular term is usually present.

A full justification of the Cauchy principal value interpretation is found in Muskhelishivili [Mus63] and Calderon and Zygmond [CZ57]. Attempts to produce a corresponding interpretation of the r^{-2} singularities are found in Krishnasawamy, Schmerr, Rudolphi, and Rizzo [KSRR90]90 and Ioakimidis and Pitta [IP88].

4.2 Limit from the Interior

Numerous boundary element publications contain phrases something like the following one from Rizzo's original paper [Riz69] deriving the direct BIE for elasticity [3]:

> "If ...
>
> $$\lim_{\mathbf{x} \to \overline{\mathbf{x}}} \int_S P_{ik}(\mathbf{x}, \mathbf{y}) u_k \, dS = \int_S P_{ik}(\overline{\mathbf{x}}, \mathbf{y}) u_k \, dS$$
>
> then letting $\mathbf{x} \to \overline{\mathbf{x}}$ ... yields
>
> $$\int_S P_{ik}(\overline{\mathbf{x}}, \mathbf{y}) u_k) \, dS = \frac{1}{2} u_i(\overline{\mathbf{x}}) + \int_S T_{ik}(\overline{\mathbf{x}}, \mathbf{y}) u_k \, dS$$

[3] page 86, Written in 1965 but not published until 1969. Some notation in the quote is changed to agree with Chapter 2.

> This result is readily verified provided u_i is assumed to satisfy a Hõolder condition on C and provided the singular integral is understood in the sense of a Cauchy Principal Value. "

However, the subsequent analysis bypasses the 'approach' process and proceeds directly to the on-surface case. The result is correct, but the arbitrary separation of the exclusion zone integral and the Cauchy principal value turn out to be unnecessary if, as in this section, the distance-to-surface is retained as a (small but nonzero) parameter c in all kernel expressions and (b) the resulting expressions are examined to find simplifications that arise as c vanishes.

As in Fig. 4.3a, consider a point at coordinates (0,-c) approaching a surface aligned with the x axis from (signed) coordinates x=a to x=b, where a and b are both finitely large. [4] Writing out the full Laplace equation G and $\frac{\partial G}{\partial \mathbf{n}}$ kernels from Fig. 2.3, we have

$$\int_S \begin{bmatrix} G \\ \frac{\partial G}{\partial \mathbf{n}} \end{bmatrix} dS = \lim_{c\to 0}\int_a^b \begin{bmatrix} \ln(1/r) \\ -\frac{\mathbf{r}\cdot\mathbf{n}}{r^2} \end{bmatrix} dS \tag{4.13}$$

$$= \quad \{ \text{ Write } \mathbf{r},\, r, \text{ and } \mathbf{n} \text{ in local coordinates } \} \tag{4.14}$$

$$\lim_{c\to 0}\int_a^b \begin{bmatrix} -\frac{1}{2}\ln(x^2+c^2) \\ \frac{c}{x^2+c^2} \end{bmatrix} dx \tag{4.15}$$

$$= \quad \{ \text{ Expand integrals analytically } \} \tag{4.16}$$

$$\lim_{c\to 0}\begin{bmatrix} -\frac{1}{2}(x\ln(x^2+c^2) - 2x + 2c\,\mathrm{atan}\frac{x}{|c|}) \\ -\frac{c}{|c|}\,\mathrm{atan}\frac{x}{|c|} \end{bmatrix}_a^b \tag{4.17}$$

$$= \quad \{ \text{ Apply limits for small } c, \text{ finite } a \text{ and } b \} \tag{4.18}$$

$$\begin{bmatrix} -\frac{1}{2}(b\ln(b) - 2b - a\ln(a) + 2a) \\ \frac{c}{|c|}\pi \end{bmatrix} \tag{4.19}$$

---

[4]Note that c is also a signed quantity.

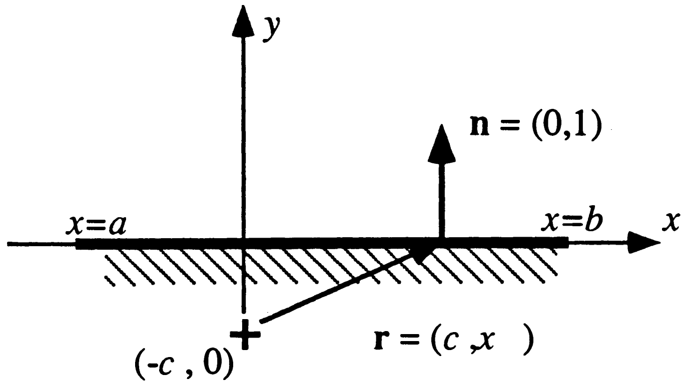

(a) Integration on a single edge

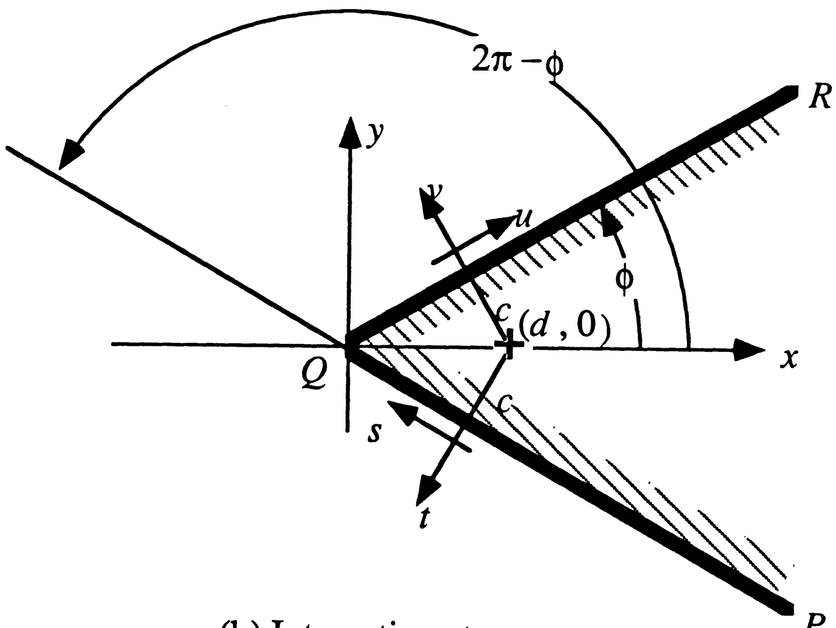

(b) Integration at a corner

Figure 4.3: Geometry for 2D 'limit from the interior' analysis

This is the same result as exclusion zone methods, but required nothing but the algebraic kernel expansion followed by straightforward limit analysis.

The same process applies, with some additional algebra due to coordinate transformations, when approaching a corner point. As in Fig. 4.3b, place the fixed point at coordinates $(d, 0)$ on an x axis that bisects the corner angle. [5] As the point moves to the corner, distance c to each surface vanishes. When integrals are carried out in the local st and uv coordinate systems, the u and s coordinates of the integration limits associated with the corner are not finite large, but vanish proportionally with c. In the uv system, the limiting integral over QR evaluates to

$$
\begin{aligned}
& [(4.17)]_a^b && (4.20)\\
= \quad & \left\{ \begin{array}{l} \text{Apply geometry: } a = -c\tan(\phi), \\ b = |QR| - c\tan(\phi) \gg 0 \end{array} \right\} && (4.21)\\
& \lim_{c\to 0} \left[\begin{array}{c} -\frac{1}{2}(b\ln(b^2+c^2) - 2b + 2c\,\mathrm{atan}\frac{b}{|c|} \\ + c\tan(\phi)\ln(x^2+c^2) - 2c\tan(\phi) \\ + 2c\,\mathrm{atan}\frac{-c\tan(\phi)}{|c|}) \\ -\frac{c}{|c|}(\mathrm{atan}\frac{b}{|c|} - \mathrm{atan}\frac{-c\tan(\phi)}{|c|}) \end{array} \right] && (4.22)\\
= \quad & \{ \text{ Take limit } \} && (4.23)\\
& \left[\begin{array}{c} -\frac{1}{2}(b\ln(b) - 2b) \\ \frac{c}{|c|}(\pi + \phi) \end{array} \right] && (4.24)
\end{aligned}
$$

Adding the other edge gives the same result as exclusion zone analysis Cauchy analysis.

Corresponding reduction of the gradient BIE kernels, using the same geometry, appears in Fig. 4.4 and Fig. 4.5.

In summary, we have shown that although the integrands are unbounded as one approaches the singular point, a direct analysis of *all* terms of the kernels leads to

[5] It is not necessary that the approach line be the bisector of the angle.

cancellation of all infinities, even at a corner, for all of the kernels (weak, Cauchy, and hypersingular) in both the primary and gradient BIE's for the Laplace equation.

4.3 Limit from the Interior for 3D Laplace Kernels

This section repeats the steps of the previous section for a point approaching a 3D surface.

The boundary integral for 3D potential problems is

$$u(\mathbf{x}) = \frac{1}{4\pi}\int_S \frac{1}{r}\frac{\partial u}{\partial \mathbf{n}} - \frac{-\mathbf{r}\cdot\mathbf{n}}{r^3}u(\mathbf{y})\,dS(\mathbf{y}) \tag{4.25}$$

where $\mathbf{r} = (r_x, r_y, r_z) = \mathbf{y} - \mathbf{x}$ and $r = \sqrt{{r_x}^2 + {r_y}^2 + {r_z}^2}$. Partial derivatives with respect to xyz coordinates of $\mathbf{x}$ are

$$\begin{bmatrix} \frac{\partial}{\partial x_x} \\ \frac{\partial}{\partial x_y} \\ \frac{\partial}{\partial x_z} \end{bmatrix} u(\mathbf{x}) \tag{4.26}$$

$$= \frac{1}{4\pi}\int_S \begin{bmatrix} r_x \\ r_y \\ r_z \end{bmatrix} \frac{1}{r^3}\frac{\partial u}{\partial \mathbf{n}} - \begin{bmatrix} -n_x r^2 + 3r_x \mathbf{r}\cdot\mathbf{n} \\ -n_y r^2 + 3r_y \mathbf{r}\cdot\mathbf{n} \\ -n_z r^2 + 3r_z \mathbf{r}\cdot\mathbf{n} \end{bmatrix} \frac{1}{r^5}u(\mathbf{y})\,dS(\mathbf{y}) \tag{4.27}$$

As in Fig. 4.6, place $\mathbf{x}$ a distance c below a point $\overline{\mathbf{x}}$ on a *planar* surface patch whose boundaries do *not* pass near $\overline{\mathbf{x}}$. Place a cylindrical (ρ,θ,z) coordinate system with its origin at $\overline{\mathbf{x}}$, z axis normal to the surface, and the polar (ρ,θ) coordinates in the plane. We also refer to in-plane coordinates by xy coordinates, where x is aligned with θ=0.

Also assume that the potential field (and its associated flux) have a series expansion

$$u(\mathbf{y}) \quad = \quad \overline{u} + \overline{a_x}x + \overline{a_y}y + O(r^2) \tag{4.28}$$

$$G = \frac{1}{2\pi}\ln(r)$$

Leading constant $\frac{1}{2\pi}$ omitted throughout

$$I_j = \int_S G,_{\mathbf{n}j}\, dS$$

$$\begin{bmatrix} I_x \\ I_y \end{bmatrix} = \lim_{c\to 0}\int_a^b \begin{bmatrix} \dfrac{-2cx}{(x^2+c^2)^2} \\ \dfrac{1}{x^2+c^2} - 2\dfrac{c^2}{(x^2+c^2)^2} \end{bmatrix} dx$$

$$= \{ \text{ Indefinite integrals } \}$$

$$\lim_{c\to 0}\begin{bmatrix} \dfrac{c}{x^2+c^2} \\ -\dfrac{x}{x^2+c^2} \end{bmatrix}_a^b \quad (AA)$$

Case 1: Flat surface, i.e. $a \ll 0$ and $b \gg 0$. Taking limits leads to:

$$\begin{bmatrix} I_x \\ I_y \end{bmatrix} = \begin{bmatrix} 0 \\ \frac{1}{a} - \frac{1}{b} \end{bmatrix}$$

Case 2: Corner point. As in Fig. 4.3b, let the fixed point approach the corner along the bisector of the angle. Compute (AA) in local st coordinates on side PQ, and in uv coordinates on side QR. As d vanishes, I_t and I_u components of (AA) are singular as $\frac{1}{d\cos(\phi)}$ on each surface. Singularities vanish when mapped to the xy system (proof follows).

Figure 4.4: Laplace 2D gradient BIE hypersingular integrals

(continued on next page)

$$
\begin{aligned}
\begin{bmatrix} I_x \\ I_y \end{bmatrix} &= -\begin{bmatrix} \cos(\phi) & -\sin(\phi) \\ \sin(\phi) & \cos(\phi) \end{bmatrix} \begin{bmatrix} I_u \\ I_v \end{bmatrix}_{a = -d\cos(\phi)} \\
&\quad + \begin{bmatrix} \cos(2\pi-\phi) & -\sin(2\pi-\phi) \\ \sin(2\pi-\phi) & \cos(2\pi-\phi) \end{bmatrix} \begin{bmatrix} I_s \\ I_t \end{bmatrix}_{b = d\cos(\phi)} \\
&= \left\{ c = d\sin(\phi),\ d = \sqrt{x^2+c^2} \text{ on both faces.} \right\} \\
&\quad \frac{1}{d}\left\{ -\begin{bmatrix} \cos(\phi) & -\sin(\phi) \\ \sin(\phi) & \cos(\phi) \end{bmatrix} \begin{bmatrix} \sin(\phi) \\ -\cos(\phi) \end{bmatrix} \right. \\
&\quad \left. + \begin{bmatrix} \cos(2\pi-\phi) & -\sin(2\pi-\phi) \\ \sin(2\pi-\phi) & \cos(2\pi-\phi) \end{bmatrix} \begin{bmatrix} \sin(\phi) \\ \cos(\phi) \end{bmatrix} \right\} \\
&= \{ \cos(2\pi-\phi) = -\cos(\phi),\ \sin(2\pi-\phi) = \sin(\phi) \ \} \\
&\quad 0
\end{aligned}
$$

Fig. 4.4 (continued from previous page) Singularity cancellation for 2D Laplace hypersingular Integrals at corner

$$G = \frac{1}{2\pi}\ln(r)$$

Leading constant $\frac{1}{2\pi}$ omitted throughout

$$I_{jk} = \int_S G_{,j} n_k - (y_k - \overline{x_k}) G_{,nj}\, dS$$

$$\begin{bmatrix} I_{xx} & I_{xy} \\ I_{yx} & I_{yy} \end{bmatrix}$$

$$= \quad \lim_{c\to 0}\int_a^b \begin{bmatrix} -\frac{2cx^2}{(x^2+c^2)^2} & -\frac{x}{x^2+c^2} \\ \frac{x}{x^2+c^2} - \frac{2c^2x}{(x^2+c^2)^2} & -\frac{c}{x^2+c^2} \end{bmatrix} dx$$

$$= \quad \left\{ \text{Indefinite integrals, with } r = \sqrt{(x^2+c^2)} \right\}$$

$$\lim_{c\to 0} \begin{bmatrix} \frac{cx}{x^2+c^2} - \frac{c}{|c|}\operatorname{atan}\frac{x}{|c|} & \ln(\frac{1}{r}) \\ -\ln(\frac{1}{r}) + \frac{c^2}{x^2+c^2} & -\frac{c}{|c|}\operatorname{atan}\frac{x}{|c|} \end{bmatrix}_a^b \quad (AA)$$

Case 1: Flat surface, i.e. $a \ll 0$ and $b \gg 0$. Taking limits leads to:

$$I_{xy} \quad \begin{bmatrix} -\frac{c}{|c|}\frac{\pi}{2} & -\ln(\frac{|b|}{|a|}) \\ \ln(\frac{|b|}{|a|}) & -\frac{c}{|c|}\frac{\pi}{2} \end{bmatrix}$$

Case 2: Corner point. As in Fig. 4.3b, let the fixed point approach the corner along the bisector of the angle. Compute (AA) in local st coordinates on side PQ, and in uv coordinates on side QR. As distance d from the origin vanishes, the off-diagonal $\ln(r)$ terms of (AA) are singular. This term appears as an upper limit of the integral over PQ, and as a lower limit over QR, hence have opposite signs and cancel.

Figure 4.5: Linear terms of 2D Laplace gradient integrals

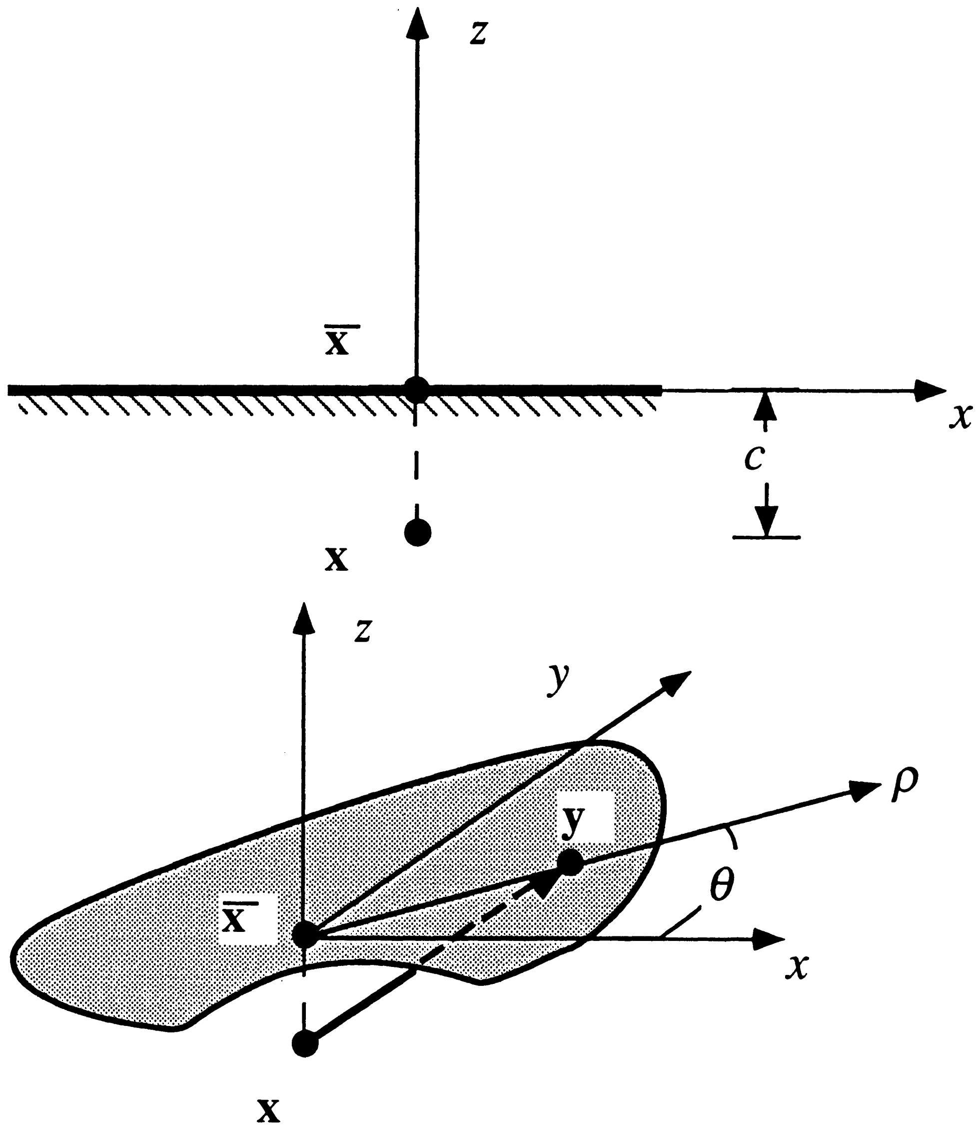

Figure 4.6: Geometry for Gray's 3D planar analysis

$\mathbf{x}$	(0,0,-c)
$\mathbf{y}$	$(\rho\cos(\theta), \rho\sin(\theta), 0)$
$\mathbf{r}$	$(\rho\cos(\theta), \rho\sin(\theta), c)$
$\mathbf{n}$	(0,0,1)
$\mathbf{r}\cdot\mathbf{n}$	c
$dS(\mathbf{y})$	$\rho\ d\rho\, d\theta$
ψ	$\frac{c}{\lvert c\rvert}$

Figure 4.7: Transformations for cylindrical coordinate system

$$= \quad \overline{u} + \overline{a_x}\rho\cos(\theta) + \overline{a_y}\rho\sin(\theta) + O(r) \tag{4.29}$$

$$\frac{\partial u}{\partial \mathbf{n}} \quad = \quad \overline{a_z} + O(r) \tag{4.30}$$

in the cylindrical coordinate system.

With these expansions and the transformations of Fig. 4.7, the gradient BIE equation (4.27) over the planar patch is

$$\begin{bmatrix} \frac{\partial}{\partial x_x} \\ \frac{\partial}{\partial x_y} \\ \frac{\partial}{\partial x_z} \end{bmatrix} u(\mathbf{x}) \tag{4.31}$$

$$= \frac{1}{4\pi}\int_{\theta=0}^{\theta=2\pi}\int_{\rho=0}^{\rho=\hat{\rho}} \begin{bmatrix} r_x \\ r_y \\ r_z \end{bmatrix} \frac{1}{r^3}(\overline{a_z} + O(r))\, d\rho\, d\theta \tag{4.32}$$

$$- \frac{1}{4\pi}\int_0^{2\pi}\int_0^{\hat{\rho}} \begin{bmatrix} 3\ \rho\cos(\theta)\mathbf{r}\cdot\mathbf{n} \\ 3\ \rho\cos(\theta)\mathbf{r}\cdot\mathbf{n} \\ -r^2 + 3c^2 \end{bmatrix} \frac{1}{r^5} \tag{4.33}$$

$$(\overline{u} + \overline{a_x}\rho\cos(\theta) + \overline{a_y}\rho\sin(\theta) + O(r^2))\, d\rho\, d\theta \tag{4.34}$$

The $O(r)$ and $O(r^2)$ terms, multiplying the kernels, weaken the all of the kernel singularities to $O(r^{-1})$. Gray's result is that the terms multiplied by $\overline{u}$, $\overline{a_x}$, $\overline{a_y}$, and $\overline{a_z}$ are also well defined, regardless of the actual outer boundaries, if one considers each integral in detail.

The proof is by manipulation of the kernel expressions during integration with respect to ρ and then θ. The outer boundary $\hat{\rho}$ remains indeterminate throughout, but cancellation of infinite terms only depends on $\hat{\rho}$ staying finitely large. If $f(\rho,\theta,c)$ is the product of one of the kernels and a surface function, and its indefinite integral with respect to ρ is $F(\rho,\theta,c)$, the integration process follows the template

$$\int_{\theta=0}^{\theta=2\pi}\int_{\rho=0}^{\rho=\hat{\rho}} f(\rho,\theta)\rho\, d\rho\, d\theta \tag{4.35}$$

$$
\begin{aligned}
&= \quad \{ \text{ Expand indefinite integral analytically } \} && (4.36)\\
&\quad \lim_{C\to 0}\int_{\theta=0}^{\theta=2\pi} [F(\rho,\theta)]_{\rho=0,r=c}^{\rho=\hat{\rho},r=\sqrt{\hat{\rho}^2+c^2}}\, d\theta && (4.37)\\
&= \quad \left\{ \begin{array}{l} \text{Expand Indefinite Integrals at specific limits} \\ \text{and move limit inside} \end{array} \right\} && (4.38)\\
&\quad \lim_{C\to 0}\int_{\theta=0}^{\theta=2\pi} F(\hat{\rho},\theta,c) - F(0,\theta,c)\, d\theta && (4.39)\\
&= \quad \{ \text{ Evaluate limits } \} && (4.40)\\
&\quad \int_{\theta=0}^{\theta=2\pi} \hat{F}(\hat{\rho},\theta,c)\, d\theta && (4.41)
\end{aligned}
$$

The final function $\hat{F}$ contains all that is left of the indefinite integrand after the limits are applied to remove terms like $\frac{1}{c}$ and $\ln(c)$ from F. The process is given for all cases in Figures 4.8 through 4.10. The various cancellation arguments are collected in Fig. 4.11, indicating how the singularity first appeared and what limiting argument had to be applied. One of the most important points in the process is whether a singular term arises from evaluation of the indefinite integrand $F(\rho,\theta)$ at the inner limit ρ=0 or the outer limit $\rho=\hat{\rho}$. When analysis is carried out at a corner or edge, the condition $\hat{\rho} \gg 0$ no longer applies and additional limit analysis must be applied, as described in Gray and Lutz [GL90].

The useful result is that the distance c vanishes completely. The final integration involves θ and the outer radius $\hat{\rho}(\theta)$ to be determined from actual geometry. That is, the supposedly infinite surface integrals have finite values that may be obtained from a path integral over the edges of the surface patch.

Restrictive Assumptions in the Derivation The assumptions that (a) $\overline{a_x}$, $\overline{a_y}$, and $\overline{a_z}$ are independent of θ, and (b) the outer surface limit $\hat{\rho}$ is always large are important restrictions.

The continuity condition is obviously necessary, because there is no way for an integral whose *result* is a gradient of the surface functions to to produce a single

$$\int_0^{2\pi}\int_0^{\hat\rho}\begin{bmatrix}\partial/\partial \mathbf{x}_x\\ \partial/\partial \mathbf{x}_y\\ \partial/\partial \mathbf{x}_z\end{bmatrix} H\rho\, d\rho\, d\theta$$

$= \{$ Cartesian forms of kernels $\}$

$$\int_0^{2\pi}\int_0^{\hat\rho}\begin{bmatrix}3\rho r_{,x} r_{,z} r^{-3}\\ 3\rho r_{,y} r_{,z} r^{-3}\\ -\rho r^{-3} + 3\rho r_{,z}{}^2 r^{-3}\end{bmatrix} d\rho\, d\theta$$

$= \{$ Convert to polar coordinates $\}$

$$\int_0^{2\pi}\int_0^{\hat\rho}\begin{bmatrix}-3z\rho^2 r^{-5}\cos(\theta)\\ -3z\rho^2 r^{-5}\sin(\theta)\\ -\rho r^{-3} + 3z^2\rho r^{-5}\end{bmatrix} d\rho\, d\theta$$

$= \{$ Integrate with respect to ρ $\}$

$$\int_{\theta=0}^{\theta=2\pi}\begin{bmatrix}-\frac{z}{|z|^2}\rho^3 r^{-3}\cos(\theta)\\ -\frac{z}{|z|^2}\rho^3 r^{-3}\sin(\theta)\\ r^{-1} - z^2 r^{-3}\end{bmatrix}_0^{\hat\rho} d\theta$$

$= \left\{\begin{array}{l}\text{expand outer and inner integration limits as}\\ z \text{ vanishes:}\end{array}\right\}$

$$\int_{\theta=0}^{\theta=2\pi}\begin{bmatrix}0\\ 0\\ \hat\rho^{-1}\end{bmatrix} d\theta \quad + \int_{\theta=0}^{\theta=2\pi}\begin{bmatrix}0\\ 0\\ 0\end{bmatrix} d\theta$$

(outer limit) (inner limit)

Figure 4.8: Integration of constant terms of ∇H kernels

$$
\begin{aligned}
& \int_0^{2\pi}\int_0^{\hat\rho}\begin{bmatrix}\partial/\partial \mathrm{x}_x\\ \partial/\partial \mathrm{x}_y\\ \partial/\partial \mathrm{x}_z\end{bmatrix} xH\rho\, d\rho\, d\theta\\
= & \quad \{\text{ Cartesian forms of kernels } \}\\
& \int_0^{2\pi}\int_0^{\hat\rho}\begin{bmatrix}3x\rho r_{,x} r_{,z} r^{-3}\\ 3x\rho r_{,y} r_{,z} r^{-3}\\ -x\rho r^{-3}+3x\rho r_{,z}{}^2 r^{-3}\end{bmatrix} d\rho\, d\theta\\
= & \quad \{\text{ Convert to polar coordinates } \}\\
& \int_0^{2\pi}\int_0^{\hat\rho}\begin{bmatrix}-3z\rho^3 r^{-5}\cos(\theta)^2\\ -3z\rho^3 r^{-5}\sin(\theta)\cos(\theta)\\ -\rho^2 r^{-3}\cos(\theta)+3z^2\rho^2 r^{-5}\cos(\theta)\end{bmatrix} d\rho\, d\theta\\
= & \quad \{\text{ Integrate with respect to } \rho \}\\
& \int_{\theta=0}^{\theta=2\pi}\begin{bmatrix}3zr^{-1}\cos(\theta)^2 - z|z|^2 r^{-3}\cos(\theta)^2\\ 3zr^{-1}\sin(\theta)\cos(\theta) - z|z|^2 r^{-3}\sin(\theta)\cos(\theta)\\ \cos(\theta)[\rho r^{-1}-\log(\rho+r)+z^2|z|^{-2}\rho^3 r^{-3}]\end{bmatrix}_0^{\hat\rho} d\theta\\
= & \quad \left\{\begin{array}{l}\text{expand outer and inner integration limits as}\\ z \text{ vanishes:}\end{array}\right\}\\
& \underbrace{\int_{\theta=0}^{\theta=2\pi}\begin{bmatrix}0\\ 0\\ -\cos(\theta)\log(2\hat\rho)\end{bmatrix} d\theta}_{\text{(outer limit)}} + \underbrace{\int_{\theta=0}^{\theta=2\pi}\begin{bmatrix}-2\psi\cos(\theta)^2\\ 0\\ 0\end{bmatrix} d\theta}_{\text{(inner limit)}}
\end{aligned}
$$

Figure 4.9: Integration of linear terms of ∇H kernels

$$\int_0^{2\pi}\int_0^{\hat\rho}\begin{bmatrix}\partial/\partial \mathbf{x}_x\\ \partial/\partial \mathbf{x}_y\\ \partial/\partial \mathbf{x}_z\end{bmatrix} G\rho\, d\rho\, d\theta$$

$=$ { Cartesian forms of kernels }

$$\int_0^{2\pi}\int_0^{\hat\rho}\begin{bmatrix}\rho r_{,x} r^{-2}\\ \rho r_{,y} r^{-2}\\ \rho r_{,z} r^{-2}\end{bmatrix} d\rho\, d\theta$$

$=$ { Convert to polar coordinates }

$$\int_0^{2\pi}\int_0^{\hat\rho}\begin{bmatrix}\rho^2 r^{-3}\cos(\theta)\\ \rho^2 r^{-3}\sin(\theta)\\ -z\rho r^{-3}\end{bmatrix} d\rho\, d\theta$$

$=$ { Integrate with respect to ρ }

$$\int_{\theta=0}^{\theta=2\pi}\begin{bmatrix}-\rho r^{-1}\cos(\theta)+\cos(\theta)\log(\rho+r)\\ -\rho r^{-1}\sin(\theta)+\sin(\theta)\log(\rho+r)\\ z r^{-1}\end{bmatrix}_0^{\hat\rho} d\theta$$

$=$ { expand outer and inner integration limits as z vanishes: }

$$\underbrace{\int_{\theta=0}^{\theta=2\pi}\begin{bmatrix}\cos(\theta)\log(2\hat\rho)\\ \sin(\theta)\log(2\hat\rho)\\ 0\end{bmatrix} d\theta}_{\text{(outer limit)}} + \underbrace{\int_{\theta=0}^{\theta=2\pi}\begin{bmatrix}0\\ 0\\ -\psi\end{bmatrix} d\theta}_{\text{(inner limit)}}$$

Figure 4.10: Integration of constant terms of ∇G kernels

Term	ρ limit	Limit Argument
(all)	$\hat{\rho}$	Simplifications as c vanishes: $\frac{1}{\hat{r}} \approx \frac{1}{\hat{\rho}}$ $\ln(\hat{\rho}+\hat{r}) \approx \ln(2\hat{\rho})$ $\frac{c}{\hat{r}} \approx 0$
$\overline{u}$	0	$\int_{\theta=0}^{\theta=2\pi} \frac{1}{c} - \frac{c}{\lvert c\rvert^2}\, d\theta$ $=$ { Coefficients of the two $\frac{1}{c}$ terms cancel } $\int_{\theta=0}^{\theta=2\pi} \frac{1}{c} - \frac{1}{c}\, d\theta$ 0
$\overline{u}$	$\hat{\rho}$	$\int_{\theta=0}^{\theta=2\pi} \frac{1}{c}\frac{\rho^3}{r^3} \cos(\theta)\, d\theta$ $\approx$ { $\frac{\rho}{r} \approx 1$ for small c. } $\int_{\theta=0}^{\theta=2\pi} \frac{1}{c} \cos(\theta)\, d\theta$ $=$ { c is constant during θ integration } $\frac{1}{c}\int_{\theta=0}^{\theta=2\pi} \cos(\theta)\, d\theta$ $=$ { Full circle integrals of odd-degree trig functions are identically 0 } 0
$\overline{a_x}, \overline{a_y}, \overline{a_z}$	0	$\int_{\theta=0}^{\theta=2\pi} \ln(2\lvert c\rvert) \cos(\theta)\, d\theta$ $=$ { c is constant during θ integration } $\ln(2\lvert c\rvert)\int_{\theta=0}^{\theta=2\pi} \cos(\theta)\, d\theta$ $=$ { Full circle integrals of odd-degree trig functions are identically 0 } 0

Figure 4.11: Consolidated limit arguments

valued result when its inputs – which are also the same gradient values – are multiply valued.

4.4 Cruse' Analyses

Cruse has made 3 separate efforts to obtain crack displacements by boundary element methods over the past 20 years. The 1971 paper with van Buren ([CVB71]) contains allusions to both the underlying problems and many of the solution methods that are just being resolved 20 years later. In this early effort, the crack-induced matrix singularity was avoided by imposing a small opening on the crack, so the two surfaces were not truly coincident. Despite accuracy limitations due to constant-displacement elements, promising results were obtained for crack-tip stress intensity factors. Displacement derivatives were obtained by finite-differences with nearby elements.

A second effort with Polch and Huang ([PCH87]) is a modern formulation enforcing a crack traction condition, as is done in this thesis, to avoid the singularity of the primary BIE. Integration of the hypersingular integrals was done by applying a regularization developed by Weaver [Wea77] and Bui [Bui77], which reduces the normal traction integrands to CPV singularities. Derivative continuity was obtained by building two separate interpolating functions, one for displacement and one for displacement derivatives, and enforcing a least squares condition to minimize the disrepancy between them.

Cruse' current approach, with Novati ([CN90]) involves a lengthy algebraic analysis of the hypersingular S_{ijk} tensor, with exclusion zone arguments to explain the disappearance of each apparently-infinite term. The need for derivative continuity is met by using non-conforming elements, allowing collocation at interior points where both the surface and the displacement functions are smooth.

Cruse' detailed analysis of the hypersingular kernels is based on rewriting the S_{ijk} tensor in the form

$$S_{ijk} = \frac{2\nu}{1-\nu}\delta_{jk}F_{,i} + \delta_{ik}F_{,j} + \delta_{ij}F_{,k} \tag{4.42}$$

$$- \frac{2}{1-\nu}n_l r_{,ijkl} + n_k \nabla^2 r_{,ij} \tag{4.43}$$

$$+ n_j \nabla^2 r_{,ik} \frac{2\nu}{1-\nu} n_i \nabla^2 r_{,kj} \tag{4.44}$$

where F is defined as

$$F = \nabla^2\left(\frac{\partial r}{\partial \mathbf{n}}\right) = \frac{\frac{\partial r}{\partial \mathbf{n}}}{r^2} \tag{4.45}$$

Each term of this expression involves 4 derivatives of r, hence is of order r^{-3} and is hypersingular. After a lengthy analysis that involves (a) integration by parts to transfer a derivative from the S_{ijk} terms to the displacement term, (b) a 'limit from the interior', and (c) an exclusion zone on the surface, each term of the surface integral

$$\int_S S_{ijk} \Delta u_k \, dS(\mathbf{y}) \tag{4.46}$$

is either shown to vanish or is converted to a product of (just) 3 derivatives of r multiplying a derivative of Δu with respect to an in-surface direction. These r^{-2} singularities are analyzed by Cauchy principal value methods.

The extensive manipulation required to determine that each term of (4.42) clearly places this in the 'algebraic' category of analysis.

4.5 Rizzo's Analyses

Rizzo *et al* [RKSR88], [KSRR90]) use hypersingular integration for acoustic wave scattering around a crack. They have pursued two approaches, which they call 'finite parts' and 'conversion'. Like Cruse, their methods focus on the r^{-3} hypersingular case, with the r^{-2} kernels left to Cauchy principal value analysis.

Their 'finite parts' analysis uses a higher order analogy to the exclusion zone, sometimes called Hadamard Finite Parts analysis. As in Cauchy principal value analysis, the total integral is divided into an exclusion zone part a non-exclusion-zone part. For *interior* of the exclusion zone, the singular point is considered to be approaching the surface in exactly the same 'limit from the interior' process as used by Gray, with the interior-distance coordinate vanishing faster than the exclusion zone radius. The integral outside the exclusion zone must be interpreted in the sense of the Hadamard finite parts analysis to eliminate infinite parts.

In [KSRR90], footnote 2 explicitly states that the exclusion zone need not vanish. Equations (C7) and (C8) are equivalent to the hypersingular analysis in Section 4.2. Thus the finite parts approach is performing essentially all of the work of section Section 4.2 within the exclusion zone, followed by additional reasoning for the remaining surface.

The 'conversion' analysis applies Stokes' theorem to convert the hypersingular part of the integrand to the sum of (a) an edge integral and (b) a spinoff surface integral. This conversion occurs at a more generalized level than the exclusion zone method and is discussed in more detail in Chapter 6.

Chapter 5

Singular Integration II: The Modal Method

The previous chapter presented the lengthy 'algebraic' approaches to existence of singular and hypersingular integrals. This chapter presents a significantly shorter 'modal' method of computing these integrals. This method applies to any geometric dimension and permits corners and curved surfaces.

We specifically need to find a formula for each of the singular integrals in Fig. 2.8 and Fig. 2.9. We will produce such formulas by a process that refers only to 'generalized' properties that the kernels share with the differential equation, independent of geometric dimension or surface geometry.

5.1 The Generic Modal Integral

Consider the geometry shown in Fig. 5.1. Point $\bar{\mathbf{x}}$ is located on surface patch S_1. Surface S_2 joins with S_1 to enclose a region. We would like to integrate some function $f(\mathbf{x},\mathbf{y})$ when (a) $\mathbf{x}$ is not on S_1 and (b) $\mathbf{y}$ varies over S_1.

Suppose that $f(\mathbf{x},\mathbf{y})$ (a) is readily evaluated anywhere (i.e. over both S_1 and

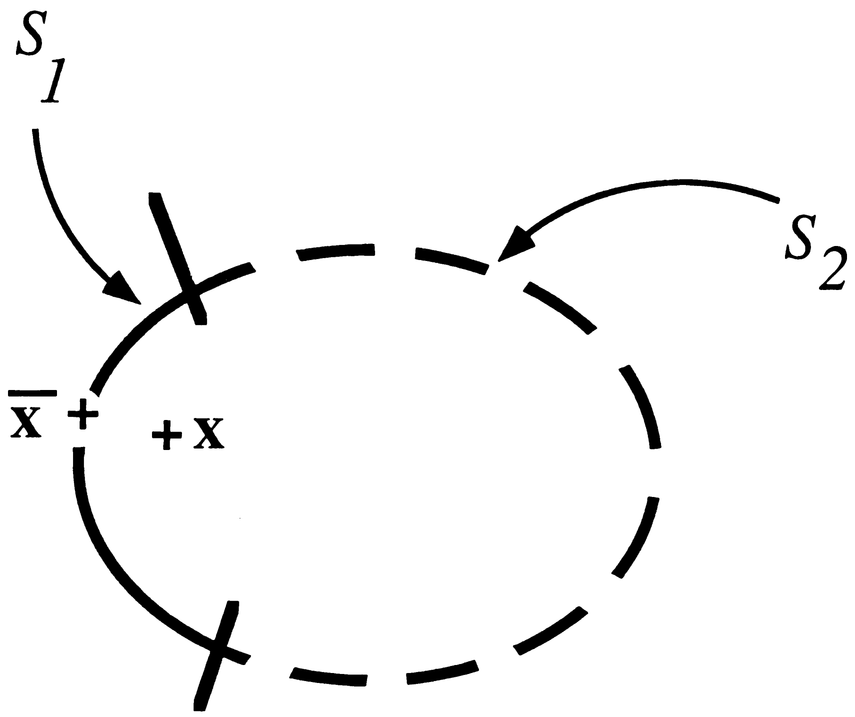

Figure 5.1: Geometry for modal integration

S_2), and (b) we happen to know that

$$\gamma(\mathbf{x})C(\mathbf{x}) = \int_S f(\mathbf{x},\mathbf{y})\, dS \tag{5.1}$$

where (a) C is some known constant or function of $\mathbf{x}$ but *not* of the surfaces, and (b) γ can be readily evaluated for any surface. Then we can split the integration domain and isolate the integral over S_1 as

$$\boxed{\int_{S_1} f(\mathbf{x},\mathbf{y})\, dS = \gamma(\mathbf{x})C - \int_{S_2} f(\mathbf{x},\mathbf{y})\, dS} \tag{5.2}$$

If the appropriate surfaces and constant C are known and f is easier to integrate over S_2 than over S_1, this gives a formula for integrating f over S_1.

The following 2 sections will demonstrate that appropriate f and C are easily produced for each of the Cauchy and hypersingular integration problems in the BIE, both for the Laplace equation and for elasticity. Each application begins with 'Consider a solution field of the form ...', followed by (a) verification that that solution field satisfies the conditions on f and C and (b) mechanical application of (5.2).

The solution fields that are required are (in elasticity terms) simply (a) a 'rigid body translation'and (b) a 'linear displacement' (uniform stress, uniform strain) deformation, as in Fig. 5.2. The rigid body case is well known in the BEM community as a means of obtaining the constant part of the **P** kernel integral, and was also suggested by Cruse and van Buren [CVB71] for the constant term of the hypersingular integral. The linear case, the construction of artificial closure surfaces, and the theoretical extensions in Chapter 6 are new material.

5.2 Modal Solutions for the Laplace Equation

Constant potential mode: Consider the potential field $u(\mathbf{x})$ defined by a 'constant potential' value $\overline{u}$. That is, for any (interior or surface) point $\mathbf{x}$ the potential

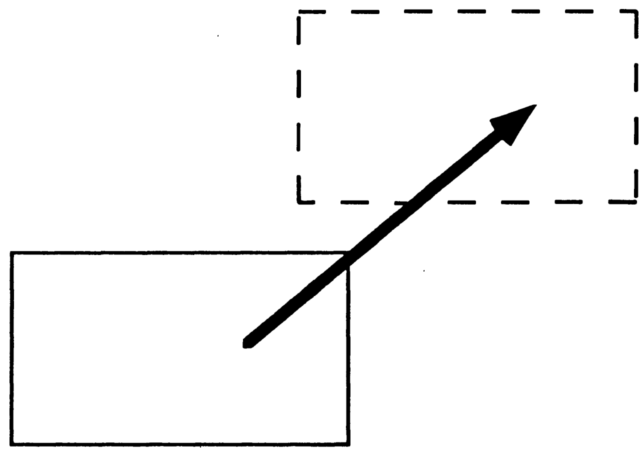

(a) Rigid body translation

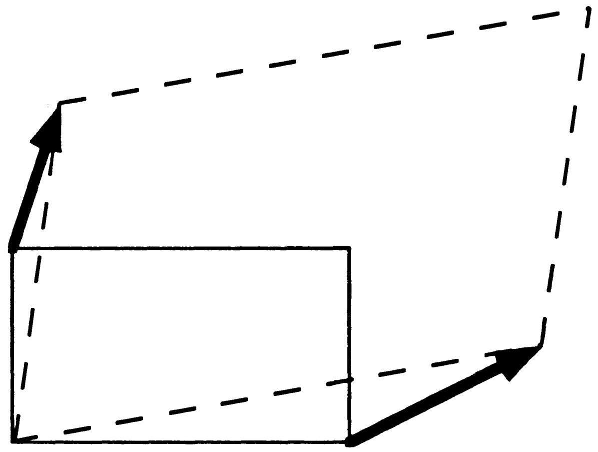

(b) Linear displacement, uniform stress

Figure 5.2: 'Rigid body translation' and 'linear displacement' modes of solution

and fluxes are given by

$$u(\mathbf{x}) \equiv \overline{u} \tag{5.3}$$

$$\frac{\partial}{\partial x_j} u(\mathbf{x}) \equiv 0 \quad \text{for } j{=}1..d \tag{5.4}$$

$$\frac{\partial}{\partial \mathbf{n}} u(\mathbf{x}) \equiv 0 \quad \text{for any direction } \mathbf{n} \tag{5.5}$$

This field identically satisfies the Laplace equation in any region. Therefore, independent of any particular field problem, we can write both the primary and boundary integrals over any surface S, using this $u(\mathbf{x})$ and its fluxes as both the left side value *and* the $u(\mathbf{y})$ and $\frac{\partial}{\partial \mathbf{n}(\mathbf{y})} u(\mathbf{y})$ values on the right. In the primary BIE this produces

$$\gamma\overline{u} \equiv \int_S G \cdot 0 - \overline{u}H \, dS \equiv \int_S -\overline{u}H \, dS \tag{5.6}$$

$$\Leftrightarrow \quad \left\{ \begin{array}{l} \text{Generic modal integral (5.2), with } f = -\overline{u}H, \\ C = \overline{u} \end{array} \right\} \tag{5.7}$$

$$\int_{S_1} -\overline{u}H \, dS = \gamma\overline{u} - \int_{S_2} -\overline{u}H \, dS \tag{5.8}$$

$$\Leftrightarrow \quad \left\{ \begin{array}{l} \text{Factor } -\overline{u} \text{ to isolate a purely geometric} \\ \text{integral} \end{array} \right\} \tag{5.9}$$

$$\boxed{\int_{S_1} H \, dS = -\gamma + \int_{S_2} H \, dS} \tag{5.10}$$

In the gradient BIE it produces, for each axis direction j,

$$\gamma\frac{\partial}{\partial x_j} u(\mathbf{x}) \equiv \gamma \cdot 0 \equiv \int_S -G_{,j} \cdot 0 + \overline{u}H_{,j} \, dS \equiv \int_S \overline{u}H_{,j} \, dS \tag{5.11}$$

$$\Leftrightarrow \quad \left\{ \begin{array}{l} \text{Generic modal integral (5.2), with } f = \overline{u}H_{,j}, \\ C = 0 \end{array} \right\} \tag{5.12}$$

$$\int_{S_1} \overline{u}H_{,j} \, dS = \gamma \cdot 0 - \int_{S_2} -\overline{u}H_{,j} \, dS \tag{5.13}$$

$$\Leftrightarrow \quad \left\{ \begin{array}{l} \text{Factor } -\overline{u} \text{ to isolate a purely geometric} \\ \text{integral} \end{array} \right\} \tag{5.14}$$

$$\boxed{\int_{S_1} H_{,j} \, dS = -\int_{S_2} H_{,j} \, dS} \tag{5.15}$$

Linear potential mode: Consider the potential field $u(\mathbf{x})$ defined to be 0 at some point $\overline{\mathbf{x}}$ and to have purely *linear* variation with respect to each coordinate direction, i.e.

$$u(\mathbf{x}) \equiv a_k(x_k - \overline{x_k}) \tag{5.16}$$

$$\frac{\partial}{\partial x_j} u(\mathbf{x}) \equiv a_j \quad \text{for each } j=1..d \tag{5.17}$$

$$\frac{\partial}{\partial \mathbf{n}} u(\mathbf{x}) \equiv a_k n_k \quad \text{for any direction } \mathbf{n} \tag{5.18}$$

This field identically satisfies the Laplace equation over any region. Therefore we can write both the primary and boundary integrals for each axis direction j and for any surface S, using this $u(\mathbf{x})$ as both the left side value *and* the $u(\mathbf{y})$ and $\frac{\partial}{\partial \mathbf{n}} u(\mathbf{y})$ on the right.

In the gradient BIE, for direction j, this produces

$$\gamma a_j \equiv \int_S -G_{,j} a_k n_k + H_{,j} a_k (y_k - \overline{x_k})\, dS \tag{5.19}$$

$$\Leftrightarrow \quad \left\{ \text{Tensor notation identity } \delta_{jk} a_k = a_j \right\} \tag{5.20}$$

$$\gamma \delta_{jk} a_k \equiv \int_S -G_{,j} a_k n_k + H_{,j} a_k (y_k - \overline{x_k})\, dS \tag{5.21}$$

$$\Leftrightarrow \quad \left\{ \begin{array}{l} \text{Generic modal integral (5.2), with} \\ f = -G_{,j} a_k n_k + H_{,j} a_k (y_k - \overline{x_k}), \\ C = \delta_{jk} a_k \end{array} \right\} \tag{5.22}$$

$$\int_{S_1} -G_{,j} a_k n_k + H_{,j} a_k (y_k - \overline{x_k})\, dS \tag{5.23}$$

$$= \gamma \delta_{jk} a_k - \int_{S_2} -G_{,j} a_k n_k + H_{,j} a_k (y_k - \overline{x_k})\, dS \tag{5.24}$$

$$\Leftrightarrow \quad \left\{ \begin{array}{l} \text{Factor } a_k \text{ to isolate a purely geometric} \\ \text{integral} \end{array} \right\} \tag{5.25}$$

$$\boxed{\begin{array}{l} \int_{S_1} -G_{,j} n_k + H_{,j} (y_k - \overline{x_k})\, dS \\ \quad = \gamma \delta_{jk} - \int_{S_2} -G_{,j} n_k + H_{,j} (y_k - \overline{x_k})\, dS \end{array}} \tag{5.26}$$

Remark: The first boundary integral is a formula for the flux in *one* direction j in terms of an integral that is summed over fluxes a_k in *all* directions (including j). The identity $\delta_{jk}a_k$ replaces the single flux value a_j on the left by a sum over *all* fluxes, with the δ_{jk} suppressing the values when $j \neq k$. The equation still applies to only one j at a time, but all terms of the identity are now summed over k, allowing subsequent factoring. The final formula is *not* summed over k; it is an identity that holds for each jk combination individually.

A linear solution field in the primary BIE will to be used in Chapter 6. The primary BIE at any point $\mathbf{x}$ is

$$\gamma a_k(x_k - \overline{x_k}) \equiv \int_S G a_k n_k - H a_k(y_k - \overline{x_k})\, dS \tag{5.27}$$

$$\Leftrightarrow \quad \left\{ \begin{array}{l} \text{Rewrite } H \text{ as a dot product with } \mathbf{n} \text{ and revise} \\ \text{subscripts to make } k \text{ appear as outer factor} \end{array} \right\} \tag{5.28}$$

$$\gamma a_k(x_k - \overline{x_k}) \equiv a_k \int_S (G\, \delta_{ik} - G_{,i}(y_k - \overline{x_k}))n_i\, dS \tag{5.29}$$

$$\Leftrightarrow \quad \left\{ \begin{array}{l} \text{Generic modal integral (5.2), with} \\ f = (G\, \delta_{ik} - G_{,i}(y_k - \overline{x_k}))n_i, \\ C = \gamma a_k(x_k - \overline{x_k}) \end{array} \right\} \tag{5.30}$$

$$a_k \int_{S_1} (G\, \delta_{ik} - G_{,i}(y_k - \overline{x_k}))n_i\, dS \tag{5.31}$$

$$= \gamma a_k(x_k - \overline{x_k}) - \int_{S_2} (G\, \delta_{ik} - G_{,i}(y_k - \overline{x_k}))n_i\, dS \tag{5.32}$$

$$\Leftrightarrow \quad \left\{ \begin{array}{l} \text{Factor } a_k \text{ to isolate a purely geometric} \\ \text{integral} \end{array} \right\} \tag{5.33}$$

$$\boxed{\begin{array}{l} \int_{S_1} (G\, \delta_{ik} - G_{,i}(y_k - \overline{x_k}))n_i\, dS \\ \quad = \gamma(x_k - \overline{x_k}) - \int_{S_2} (G\, \delta_{ik} - G_{,i}(y_k - \overline{x_k}))n_i\, dS \end{array}} \tag{5.34}$$

5.3 Modal Solutions for Elasticity

Rigid body mode Consider the displacement field $\mathbf{u}(\mathbf{x})$ associated with a 'rigid body translation' by a vector $\overline{\mathbf{u}}$ and zero traction and zero stress in all directions, i.e.

$$\begin{array}{rcll} & u_i(\mathbf{x}) & \equiv & \overline{u_i} \\ & \sigma_{ij}(\mathbf{x}) & \equiv & 0 \quad \text{for each } ij \text{ stress component} \\ p_i(\mathbf{x},\mathbf{n}) \equiv & \sigma_{ij}n_j & \equiv & 0 \quad \text{each traction component } i \text{ on a surface passing through } \mathbf{x} \text{ with normal components } n_j \end{array} \tag{5.35}$$

This deformation satisfies the elasticity equations identically in any region. Therefore, independent of any particular field problem, we can write both the primary and boundary integrals, for each direction i and over any surface S, using this $u_i(\mathbf{x})$ and its tractions as both the left side value *and* the $u_k(\mathbf{y})$ and $p_k(\mathbf{y})$ values on the right. In the primary BIE this produces

$$\gamma\overline{u_i} \equiv \int_S U_{ik} \cdot 0 - P_{ik}\overline{u_k}\, dS \equiv \int_S -P_{ik}\overline{u_k}\, dS \tag{5.36}$$

$$\Leftrightarrow \quad \left\{ \text{Tensor notation identity } \overline{u_i} = \delta_{ik}\overline{u_k} \right\} \tag{5.37}$$

$$\gamma\overline{u_i} \equiv \int_S U_{ik} \cdot 0 - P_{ik}\overline{u_k}\, dS \equiv \int_S -P_{ik}\overline{u_k}\, dS \tag{5.38}$$

$$\Leftrightarrow \quad \left\{ \begin{array}{l} \text{Generic modal integral (5.2), with} \\ f = -P_{ik}\overline{u_k},\ C = \delta_{ik}\overline{u_k} \end{array} \right\} \tag{5.39}$$

$$\int_{S_1} -P_{ik}\overline{u_k}\, dS = \gamma\delta_{ik}\overline{u_k} - \int_{S_2} -P_{ik}\overline{u_k}\, dS \tag{5.40}$$

$$\Leftrightarrow \quad \left\{ \begin{array}{l} \text{Factor } -\overline{u_k} \text{ to isolate a purely geometric} \\ \text{integral} \end{array} \right\} \tag{5.41}$$

$$\boxed{\int_{S_1} P_{ik}\, dS = -\gamma\delta_{ik} - \int_{S_2} P_{ik}\, dS} \tag{5.42}$$

In the gradient BIE it produces, for each stress component ij,

$$\gamma\sigma_{ij} \equiv \gamma \cdot 0 \equiv \int_S D_{ijk} \cdot 0 - S_{ijk}\overline{u_k}\, dS \equiv -\int_S \overline{u_k} S_{ijk}\, dS \quad (5.43)$$

$$\Leftrightarrow \quad \left\{ \begin{array}{l} \text{Generic modal integral (5.2), with} \\ f = -S_{ijk}\overline{u_k},\ C = 0 \end{array} \right\} \quad (5.44)$$

$$\int_{S_1} -S_{ijk}\overline{u_k}\, dS = \gamma \cdot 0 - \int_{S_2} -S_{ijk}\overline{u_k}\, dS \quad (5.45)$$

$$\Leftrightarrow \quad \left\{ \begin{array}{l} \text{Factor } -\overline{u_k} \text{ to isolate purely geometric} \\ \text{integral} \end{array} \right\} \quad (5.46)$$

$$\boxed{\int_{S_1} S_{ijk}\, dS = -\int_{S_2} S_{ijk}\, dS} \quad (5.47)$$

Constant Strain (Linear Displacement) Mode Consider a solid body subjected to a deformation in which the displacement components $u_i(\mathbf{x})$ vary linearly with respect to some point $\overline{\mathbf{x}}$ according to

$$\begin{array}{rcll} u_i(\mathbf{x}) & \equiv & \overline{A_{ij}}(x_j - \overline{x_j}) & \text{for each } i \\ \dfrac{\partial u_i}{\partial x_j} & \equiv & \overline{A_{ij}} & \text{for each } i \text{ and } j \end{array} \quad (5.48)$$

This may also be described as a 'uniform stress' or 'uniform strain' field. The stress components at any point, and the tractions on a surface through that point, are determined by the A_{ij} and elasticity relation

$$\begin{array}{rcccl} \sigma_{ij}(\mathbf{x}) & \equiv & E_{ijmn}\dfrac{\partial}{\partial x_n}u_m(\mathbf{x}) & \equiv & E_{ijmn}\overline{A_{mn}} \\ p_i(\mathbf{x},\mathbf{n}) & \equiv & \sigma_{ij}n_j & \equiv & E_{ijmn}\overline{A_{mn}}n_j \end{array} \quad (5.49)$$

This deformation satisfies the elasticity equations identically in any region. Therefore, independent of any particular field problem, we can write the gradient boundary integral for each stress component $\sigma_{ij}$and over any surface S, using the expressions with A_{ij} for both the left side results and the surface displacements and tractions in the integrands. This produces

$$\gamma\sigma_{ij} \equiv \gamma E_{ijmn}\overline{A_{mn}} \tag{5.50}$$

$$\equiv \int_S D_{ijk}E_{klmn}n_l\overline{A_{mn}} - S_{ijm}\overline{A_{mn}}(y_n - \overline{x_n})\,dS \tag{5.51}$$

$$\Leftrightarrow \left\{ \begin{array}{l} \text{Generic modal integral (5.2), with} \\ \quad f = D_{ijk}E_{klmn}n_l\overline{A_{mn}} \\ \qquad -S_{ijm}\overline{A_{mn}}(y_n - \overline{x_n}) \\ \quad C = E_{ijmn}\overline{A_{mn}} \end{array} \right\} \tag{5.52}$$

$$\int_{S_1} D_{ijk}E_{klmn}n_l\overline{A_{mn}} - S_{ijm}\overline{A_{mn}}(y_n - \overline{x_n})\,dS \tag{5.53}$$

$$= \gamma E_{ijmn}\overline{A_{mn}} \tag{5.54}$$

$$- \int_{S_2} D_{ijk}E_{klmn}n_l\overline{A_{mn}} - S_{ijm}\overline{A_{mn}}(y_n - \overline{x_n})\,dS \tag{5.55}$$

$$\Leftrightarrow \left\{ \begin{array}{l} \text{Factor } \overline{A_{mn}} \text{ to isolate a purely geometric} \\ \text{integral} \end{array} \right\} \tag{5.56}$$

$$\boxed{\begin{array}{l} \int_{S_1} D_{ijk}E_{klmn}n_l - S_{ijm}(y_n - \overline{x_n})\,dS \\ \quad = \gamma E_{ijmn} - \int_{S_2} D_{ijk}E_{klmn}n_l - S_{ijm}(y_n - \overline{x_n})\,dS \end{array}} \tag{5.57}$$

The linear field has zero displacement at $\overline{\mathbf{x}}$, so the primary BIE is

$$\gamma u_i(\mathbf{x}) = \int_S U_{ik}p_k - P_{im}u_m\,dS \tag{5.58}$$

$$\Leftrightarrow \left\{ \text{Substitute} \begin{array}{rcl} u_m & \equiv & \overline{A_{mn}}(y_n - \overline{x_n}) \\ p_k & \equiv & E_{klmn}\overline{A_{mn}}n_l \\ u_i & \equiv & \delta_{im}\overline{A_{mn}}(x_n - \overline{x_n}) \end{array} \right\} \tag{5.59}$$

$$\gamma\delta_{im}(x_n - \overline{x_n})\overline{\mathbf{A}_{mn}} = \tag{5.60}$$

$$\int_S U_{ik}E_{klmn}\overline{A_{mn}}n_l - P_{im}\overline{A_{mn}}(y_n - \overline{x})\,dS \tag{5.61}$$

$$\Leftrightarrow \left\{ \begin{array}{l} \text{Remove common factor } \overline{A_{mn}} \text{ to isolate a} \\ \text{purely geometric integral} \end{array} \right\} \tag{5.62}$$

$$\gamma\delta_{im}(x_n - \overline{x_n}) = \int_S U_{ik}E_{klmn}n_l - P_{im}(y_n - \overline{x})\, dS \tag{5.63}$$

$$\Leftrightarrow \quad \left\{ \begin{array}{l} \text{Generic modal integral (5.2), with} \\ f = U_{ik}E_{klmn}n_l - P_{im}(y_n - \overline{x}), \\ C = \gamma\delta_{im}(x_n - \overline{x_n}) \end{array} \right\} \tag{5.64}$$

$$\boxed{\begin{aligned} &\int_{S_1} U_{ik}E_{klmn}n_l - P_{im}(y_n - \overline{x})\, dS \\ &\quad = \gamma\delta_{im}(x_n - \overline{x_n}) \\ &\qquad - \int_{S_2} U_{ik}E_{klmn}n_l - P_{im}(y_n - \overline{x})\, dS \end{aligned}} \tag{5.65}$$

5.4 Discussion of the Modal Existence Proof

The modal approach to singular integrals is significantly different than the algebraic methods of Chapter 4. Rather than picking the kernels apart term-by-term, it treats the entire BIE as a whole and converts the 'hard' integral over S_1 to essentially the same integral over S_2.

Assumptions about S_1, S_2, and $\overline{\mathbf{x}}$ The only explicit requirements for surface patch S_1 are that it contain $\overline{\mathbf{x}}$ and that it join with S_2 to enclose volume.

The later condition that $\overline{\mathbf{x}}$ be a nonzero distance away from S_2 allows the additional inferences that (a) S_1 is a *finitely large* patch of surface and (b) $\overline{\mathbf{x}}$ is a strictly interior point of S_1, i.e. *not* on the shared boundary between S_1 and S_2. Violation of either of these inferences would allow $\overline{\mathbf{x}}$ to be arbitrarily close to S_2.

Fig. 5.3 indicates some geometries that *are* valid. Patch S_1 may be flat, curved, and may have corners at $\overline{\mathbf{x}}$ itself or elsewhere. Patch S_2 may be a single smooth surface or a collection of several surfaces. The surfaces may have self-crossings (loops in 2D); the boundary integrals will evaluate to 0 over the boundary of any enclosed region not containing $\mathbf{x}$, so the loop has no effect. The general requirement is that the surface be orientable and that the general winding number of $\mathbf{x}$ with

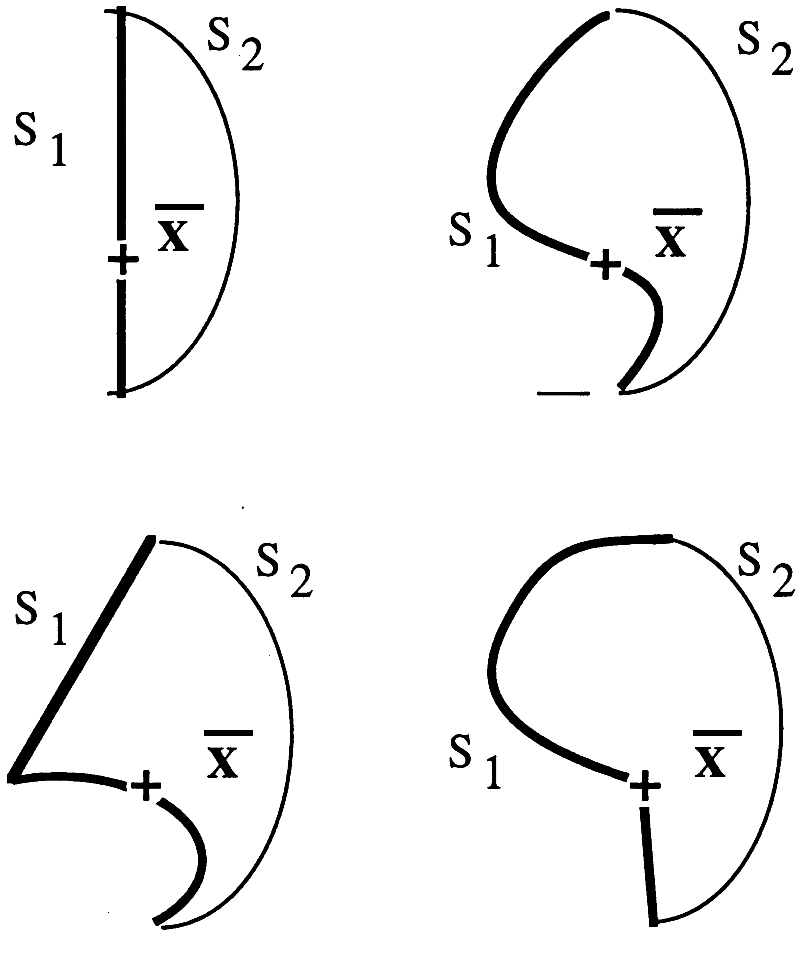

Figure 5.3: Different surfaces S_1 with same closure surface S_2

(continued on next page)

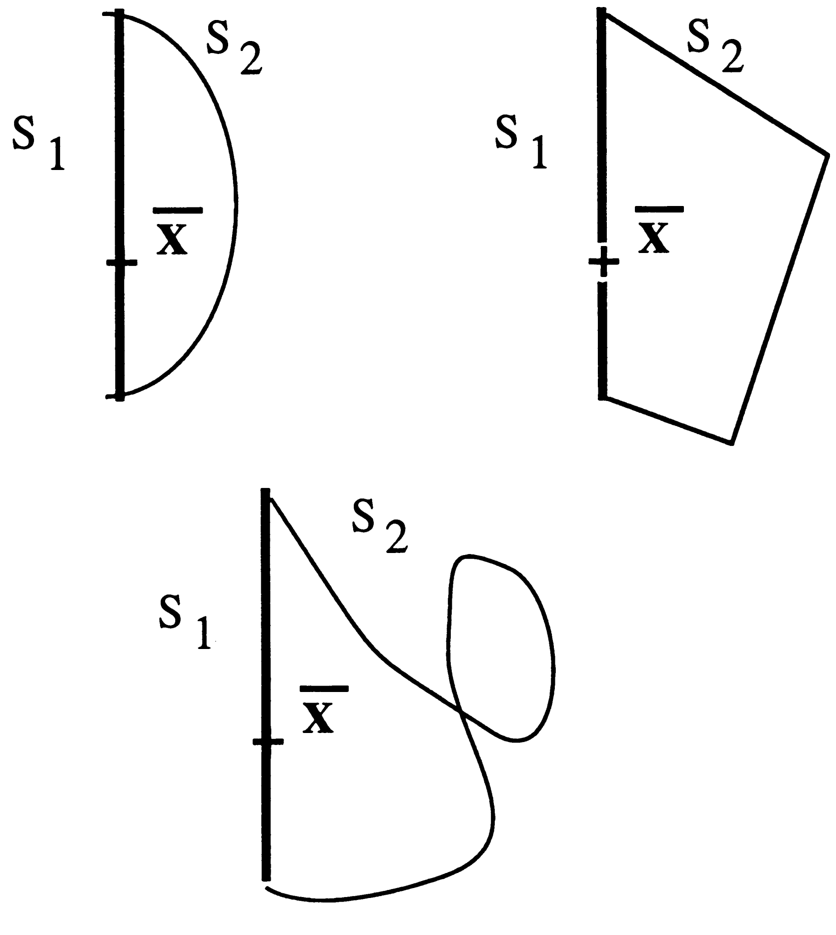

Fig. 5.3 (continued from previous page) Different closure surfaces S_2 for a single patch S_1

respect to the surface (i.e. the difference between outward and inward boundary crossings encountered by a ray from $\mathbf{x}$ to infinity) must be known to be used as γ in the modal formula.

Interdependence of elements The modal formula produces a single composite value for the integral over all of S_1. If S_1 is a union of several smaller patches (i.e., in the BEM/FEM style of geometry, as several elements), the modal formula does *not* give an individual contribution of each element.[1] For instance, in Fig. 5.4, the construction will provide the values of the integrals over the entire patch of 5 elements, but *not* over the single highlighted element.

This conclusion is also found in the algebraic analyses. In the 3D version Gray's method, it took the form of the requirement that the integration over θ be taken over the full range 0 to 2π. In Rizzo's finite parts analysis, the cancellation of interior and exterior integrals over the exclusion zone occurred as a net result for the entire integral, not as a local effect each surface differential $dS(\mathbf{y})$.

The absence of per-element values is not a detriment to application of the method. Even for less singular kernels that *can* be evaluated on each element, the per-element values are only temporary quantities that are summed to obtain final matrix entries equal to the full-patch values.

Interdependence of Kernels For the *constant* solution mode, the modal method gives formulas for the $\mathbf{P}$ and $\mathbf{S}$ kernels, without reference to $\mathbf{D}$ or $\mathbf{U}$. For the *linear* solution modes, the modal method gives a *combined* formula for the $\mathbf{D}$ kernel and

[1] Both the implementation in Chapter 8 and the earlier one by Martha [Mar89] are structured as a loop over incident elements. However, the computation done at each element is ultimately determined only by the (far) *edge* of the element, and not by the element surface. The loop-over-elements is only a convenient superstructure for the real work of doing computations on the *edges* of the elements.

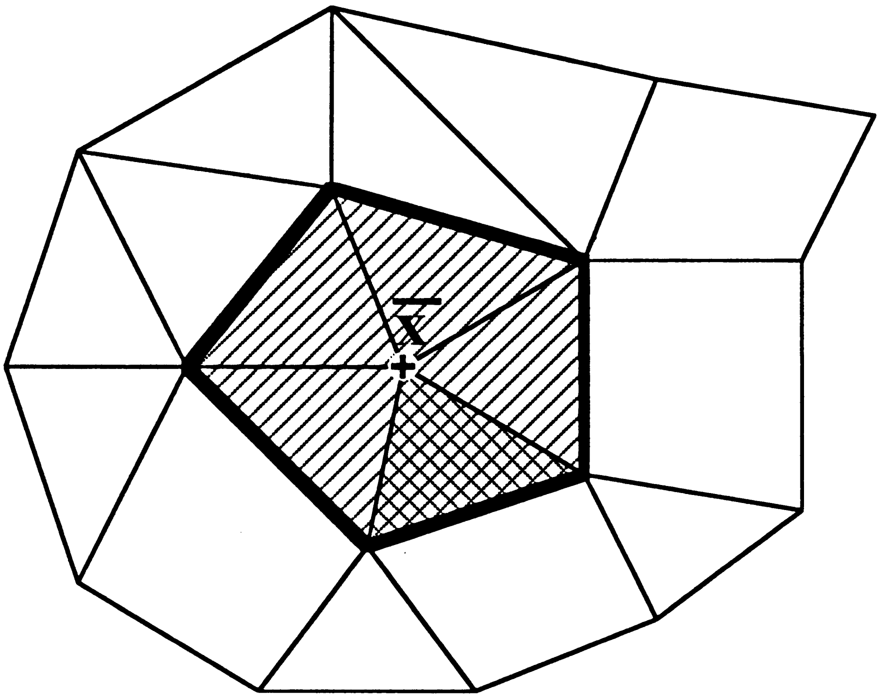

Figure 5.4: Patch of elements around a singular point

a product of **S** and a cartesian linear term.

This is contrary to the usual boundary element practice of integrating the two kernels independently of one another. The integrals over S_2 can still be performed independently, but there is no way to take those results and apportion them as distinct **D** and **S** integrals on S_1.

This is also consistent with the results of Gray's method, in which cancellation of infinite terms on opposite sides of an edge was found to depend on simultaneous treatment of the same terms in their algebraic forms.

Continuity Conditions The requirement of a series expansion with a continuous *cartesian* (not parametric) gradient is extremely important in all analyses of the gradient BIE. Extension of standard finite element methods (e.g., as in [Boi89]) to higher order continuity leads to very high order parametric functions for limited additional continuity. More modern surface fitting methods ([BFK]) may be more useful, but the method of producing continuity 'across a sharp corner' where the underlying geometry is not smooth means that there is more involved than simply applying spline methods that produce smooth surfaces.

For the case of purely planar cracks, Gray, Martha, and Ingraffea [GMI90] achieved very good results by using only C^0 approximation but applying a least-squares procedure to obtain an approximate gradient at the nodes. Because it was done only at smooth surface points with known traction, the least squares process could be applied exclusively to interpolation of displacement. Extension to corners requires the least squares process to consider tractions and displacements simultaneously. It is also difficult to construct a closure surface at an arbitrary re-entrant corner.

The entire problem is bypassed if one does not attempt to evaluate the integrals at nodes and edges of the surface mesh. This is easily done by (a) choosing a 'non-conforming' surface function representation that allows even the primary **u** function to be discontinuous across element boundaries and (b) enforcing integral conditions only at points strictly *interior* to surface elements that are individually smooth. This has the undesirable effects that (a) it produces more equations than nodal collocation, (b) the displacement discontinuity is physically unrealistic. An especially difficult technical problem is that collocation points 'inside the element but near the node' are quite close to neighboring surfaces of both the real geometry and of closure surfaces constructed temporarily for modal integrals. [2]

The results in Chapter 8, along with those of [CN90] and [KSRR90] clearly indicate that the non-conforming method can produce excellent results despite the difficulties.

5.5 Obtaining a Closure Surface

In order to take advantage of the modal formula for the Cauchy and hypersingular singularities, we must be able to produce the closure surface S_2 for any given singular surface S_1.

When singular point $\overline{\mathbf{x}}$ is on an *external* (i.e. non-crack) surface and S_1 contains all elements that are incident to $\overline{\mathbf{x}}$, we may simply use all remaining including (including crack elements) as the closure surface. This is indicated in Fig. 5.5 for a smooth surface point and Fig. 5.6. For these non-crack cases, combined contribution of crack faces is zero because of antisymmetry properties (Section 2.5), so results are not affected by including or omitting the crack face.

When $\overline{\mathbf{x}}$ is on a crack surface, this fails because the 'remaining elements' left after those that are topologically adjacent to the singular point are excluded include those on the opposite crack face, which passes through the singular point geometrically.

[2]A somewhat heated discussion of these issues may be found in [MB86] and [BN87].

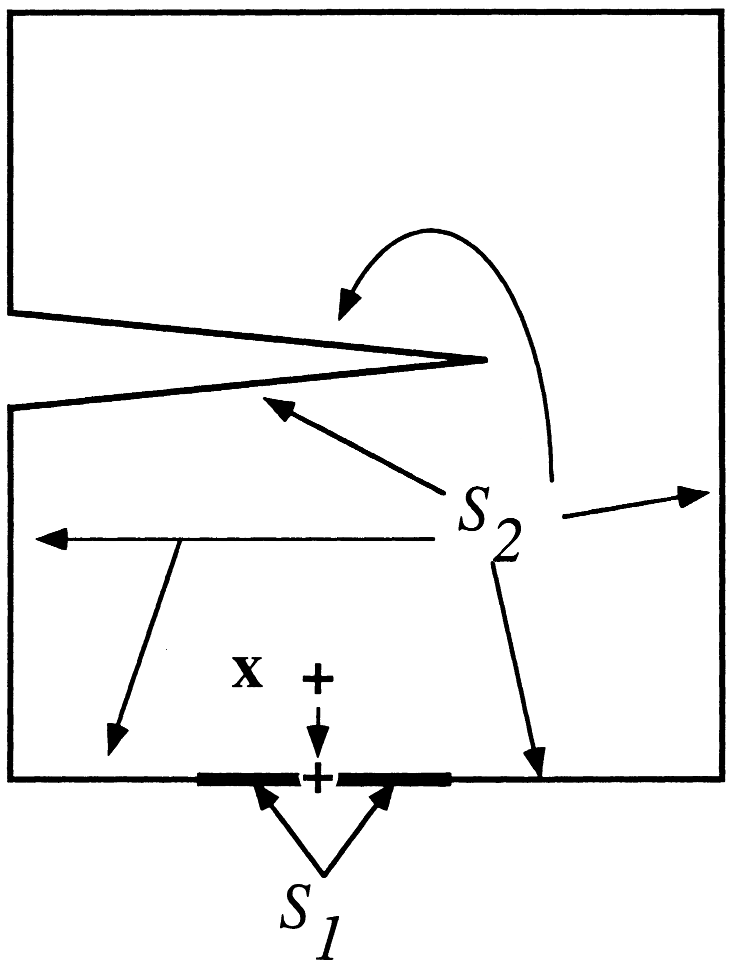

Figure 5.5: Closure surface for a smooth non-crack point

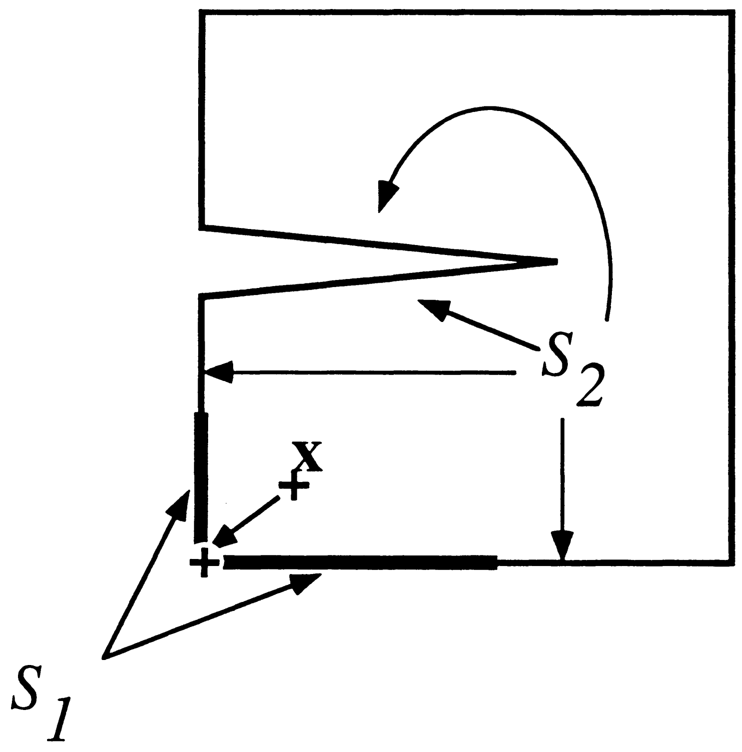

Figure 5.6: Closure surface for a corner non-crack point

The condition that surface S_2 be a nonzero distance away from $\overline{\mathbf{x}}$ is violated. Hence we cannot simply use the 'other elements' to compute *any* of the singular integrals. Such an *incorrect construction* is given in Fig. 5.7.

This problem is resolved by taking advantage of the fact that the modal summation properties apply to not just to the real surface of the object but to *any* surface S_2 that joins with S_1 to enclose volume. The functions that the modal integrals require to be integrated are cartesian polynomials that have nothing to do with either the actual geometry or the basis functions being used on the actual surface. They are well defined whether the artificial surface is inside, outside, or crosses the boundaries of **S**. Fig. 5.8 shows a small tent constructed so that it and patch S_1 on the crack surface enclose a region for modal integration.

In 3D, a trial closure surface can be constructed by choosing any point in space and drawing a 'ruled surface' between that point and the boundaries of S_1. Fig. 5.9 illustrates the construction when $\overline{\mathbf{x}}$r is on the interior of a mildly curved surface that is typical of boundary element approximations to geometry. When (a) $\overline{\mathbf{x}}$ is at corner or (b) S_1 is highly curved, it is possible that such a closure surface will itself contain $\overline{\mathbf{x}}$, or that it does not close off a simply connected surface. The equations still remain valid in these cases if (a) a second closure surface is recursively constructed to avoid the singularity at $\overline{x}$ and (b) we compute γ as a more general *winding number* that counts the difference between the number of outward and inward boundary crossings encountered by a ray from $\overline{\mathbf{x}}$ to infinity.

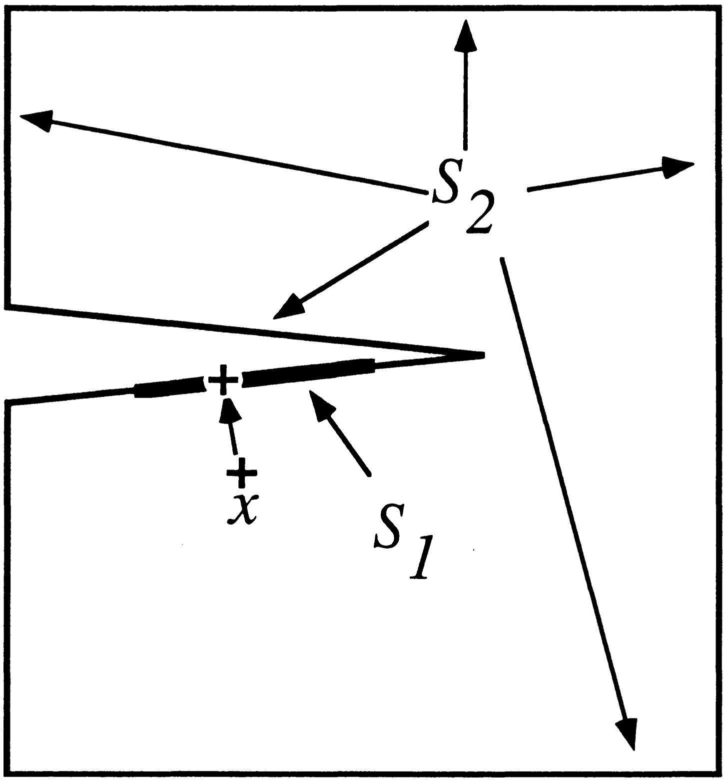

Figure 5.7: An incorrect closure surface around a 2D crack point

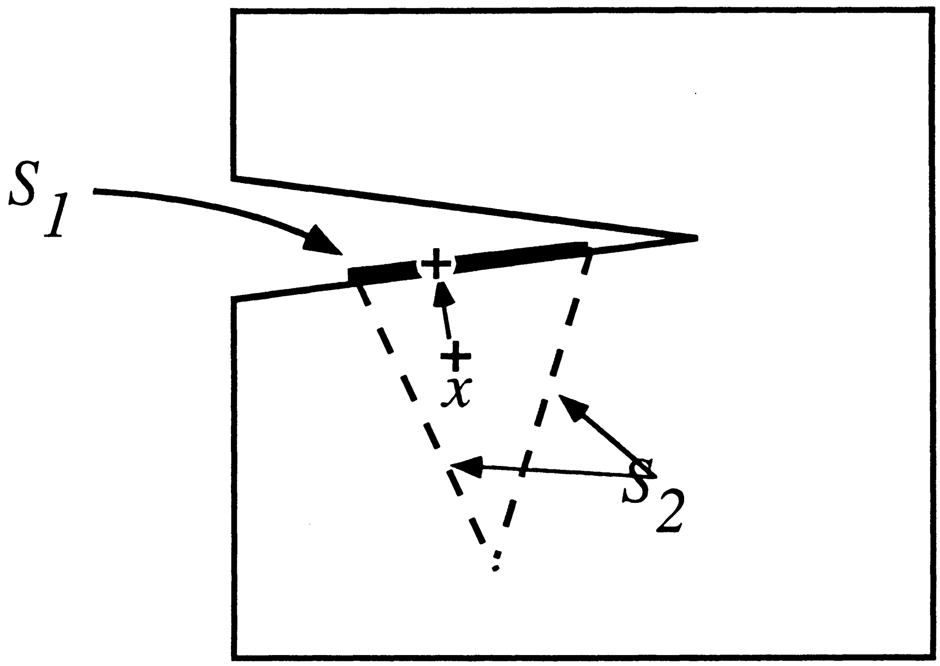

Figure 5.8: A closure surface around a 2D crack point

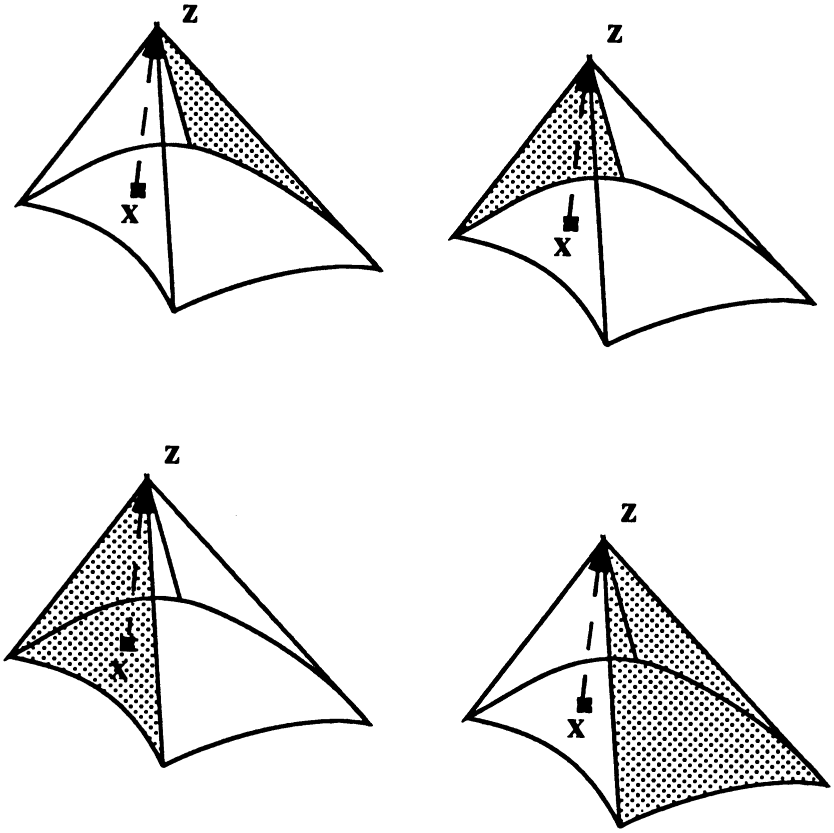

Figure 5.9: A closure surface over a 3D surface patch

Chapter 6

Singular Integration III: Further Uses of Modal Analysis

This chapter presents some theoretical results that follow from the modal method of computing singular integrals. These are not immediately useful for an isoparametric BEM implementation. However, they identify particular open problems whose solution may allow simpler implementations in the future.

6.1 A Conversion Theorem

The discussion of what surfaces could be treated by modal integrals is filled with disclaimers about geometric factors that do *not* affect the results of a modal integral. The following theorem identifies the factors that *do* affect the results:

Theorem: (Edge Theorem) Let $f(\mathbf{y})$ be any function whose integral over a closed surface is known *a priori* to be

$$\int_S f(\mathbf{y})\, dS(\mathbf{y}) = \gamma(\mathbf{x})C(\mathbf{x}) \tag{6.1}$$

for $C(\mathbf{x})$ independent of the surface S. Then the integral of f over any subset S_1 of S depends only on $\mathbf{x}$ and the boundary of S_1.

Proof: Let S_2, S_3, and S_4 be any surfaces that share the boundary of S_1, such that $\gamma(\mathbf{x})$ is invariant when computed for the (closed) surface formed by joining one of S_1 and S_3 with one of S_2 and S_4. Let $I(f,S_i)$ denote the integral of f over surface S_i. Applying the known integration value over various combinations yields

$$I(f,S_1) + I(f,S_2) = \gamma C = I(f,S_3) + I(f,S_2) \tag{6.2}$$

$$= \left\{ \text{Eliminate common term I}(f,S_3) \right\} \tag{6.3}$$

$$I(f,S_1) = I(f,S_3) \tag{6.4}$$

and

$$I(f,S_1) + I(f,S_2) = \gamma C = I(f,S_1) + I(f,S_4) \tag{6.5}$$

$$= \left\{ \text{Eliminate common term I}(f,S_3) \right\} \tag{6.6}$$

$$I(f,S_2) = I(f,S_4) \tag{6.7}$$

The only geometric data common to all of these equalities are (a) point $\mathbf{x}$, and (b) the shared boundary. Therefore, the integrals $I(f,S_1)..I(f,S_4)$ 'are functions of' $\mathbf{x}$ and the boundary, and of nothing else. **QED**

The implications of this are as follows:

- In 3D, we should be able to convert any modal integral to a contour integral over the edge of the patch. This conversion would be extremely useful, for contour integrals can be done much more systematically than surface integrals. Unfortunately, the theorem does not explicitly produce the integrands to be evaluated along the edge. We still need to produce, for each modal integrand f, a 'Stokes vector' $\mathbf{F}$ such that $f = \nabla \times \mathbf{F} \cdot \mathbf{n}$, so that we can apply Stokes theorem in the form

$$\int_S \nabla \times \mathbf{F} \cdot \mathbf{n}\, dS = \oint_{\partial S} \mathbf{F} \cdot \mathbf{T}\, dl \tag{6.8}$$

where **T** is the (non-unit) tangent vector to the parameterized edge ([Gas58]).

- In 2D, a modal integral only depends on the *endpoints* of the curve segment. That is, the integral is 'path independent', and there is some function $V(x,y)$ such that

$$
\begin{aligned}
& \int_S \mathbf{F} \cdot \mathbf{n}\, dS && (6.9)\\
= \quad & \left\{ \begin{array}{l} \text{Expand vector components with path} \\ \text{parameterized from } s{=}0 \text{ to } s{=}1\text{, with} \\ \text{(non-unit) tangent vector } \mathbf{T} \end{array} \right\} && (6.10)\\
& \int_0^1 (F_x n_x + F_x n_y)|\mathbf{T}|\, ds && (6.11)\\
= \quad & \left\{ \begin{array}{l} \text{The tangent and unit normal vectors to a 2D} \\ \text{curve are related by } (n_x, n_y) = \dfrac{(-T_y, T_x)}{|\mathbf{T}|} \end{array} \right\} && (6.12)\\
& \int_0^1 - F_y T_x + F_x T_y\, ds && (6.13)\\
= \quad & \{ \text{ The integral is path independent } \} && (6.14)\\
& = V(x_1, y_1) - V(x_0, y_0) && (6.15)
\end{aligned}
$$

From vector calculus, the path independence condition is equivalent to saying the V and **F** are related by

$$\frac{\partial V}{\partial x} = -F_y and \frac{\partial V}{\partial y} = F_x \tag{6.16}$$

The edge theorem is a proof that (depending on the dimension) Stokes vectors and endpoint functions must exist. This is another instance of the distinction between algebraic and generalized analysis of the BIE. By analyzing the BIE as a single unit, rather than as a collection of complex, unrelated terms, we obtain a very powerful property. Conversely, it is suggested (but not proven) that this property might *not* apply to any smaller portion of the equation.

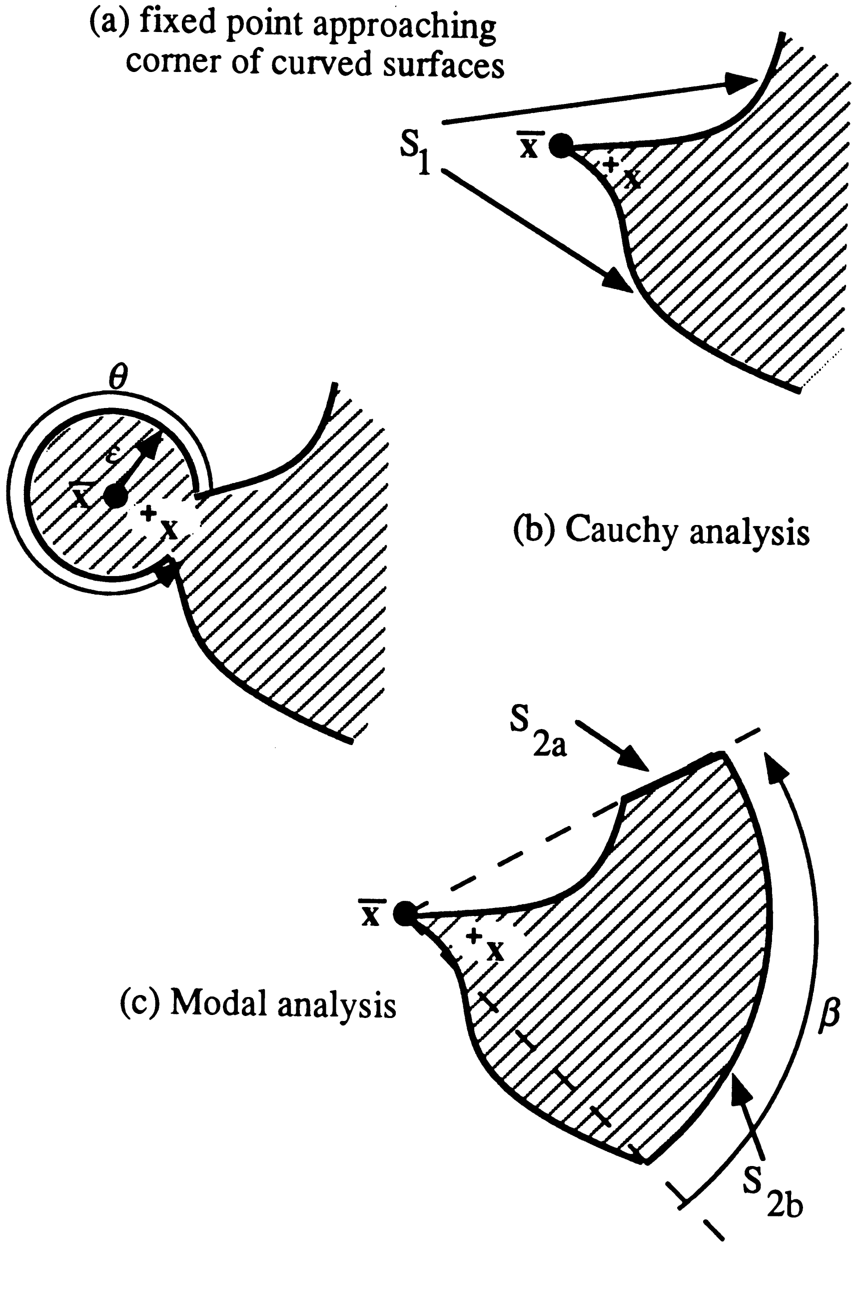

Figure 6.1: Comparison of Cauchy and Modal Analysis of a Corner

6.2 Example: The Solid Angle Kernel

To illustrate the ideas of modal integration and the edge theorem, consider the H kernel of the Laplace equation when x approaches a corner point $\overline{\mathbf{x}}$ of a curved surface, as in Fig. 6.1. A Cauchy analysis defines this singular integral as

$$\int_{S_1} \frac{\mathbf{r}\cdot\mathbf{n}}{2\pi r^2}\, dS \tag{6.17}$$

$$= \left\{ \begin{array}{l} \text{Cauchy analysis (see Chapter 4), with} \\ \theta\text{=corner angle, } \epsilon\text{=size of exclusion zone} \end{array} \right\} \tag{6.18}$$

$$\frac{\theta}{2\pi} + \lim_{\epsilon\to 0} \int_{S_1 - S_\epsilon} \frac{\mathbf{r}\cdot\mathbf{n}}{2\pi r^2}\, dS \tag{6.19}$$

For modal analysis, construct a closure surface using (a) a radial line segment from the nearer endpoint out to the radius of the farther endpoint of S_1, and (b) a circle of radius R to the other endpoint. The modal integral is

$$\int_{S_1} \frac{\mathbf{r}\cdot\mathbf{n}}{2\pi r^2}\, dS \tag{6.20}$$

$$= \left\{ \begin{array}{l} \text{Constant potential modal analysis (Section} \\ \text{5.2); } \mathbf{x} \text{ is inside the closure, so } \gamma = 1 \end{array} \right\} \tag{6.21}$$

$$1 - \int_{S_{2a}} \frac{\mathbf{r}\cdot\mathbf{n}}{2\pi r^2}\, dS + \int_{\mathbf{S}_{2b}} \frac{\mathbf{r}\cdot\mathbf{n}}{2\pi r^2}\, dS \tag{6.22}$$

$$= \left\{ \begin{array}{lll} \text{Geometric analysis of } S_{2a} \text{ and } S_{2b} \text{ when } \mathbf{x} \text{ is} & & \\ & \frac{\mathbf{r}\cdot\mathbf{n}}{r^2} \approx 0 & \text{on } S_{2a} \\ \text{near } \overline{\mathbf{x}}\text{:} & \mathbf{r}\cdot\mathbf{n} \approx R & \text{on } S_{2b} \\ & r^2 \approx R^2 & \text{on } S_{2b} \\ & dS \approx R\, d\theta & \text{on } S_{2b} \end{array} \right\} \tag{6.23}$$

$$1 - \int_{S_{2a}} 0\, dS + \int_{S_{2b}} \frac{d\theta}{2\pi} \tag{6.24}$$

$$= \left\{ S_{2b} \text{ is an arc of angle } \beta \right\} \tag{6.25}$$

$$1 - \frac{\beta}{2\pi} \tag{6.26}$$

The Cauchy analysis gives a clear interpretation of the exclusion zone integral as the corner angle at $\overline{\mathbf{x}}$ itself, but no particular explanation of the limit integral over S_1 minus the exclusion zone. The modal analysis says the net value of the integral over S_1 is exactly *the angle between the lines from* $\overline{\mathbf{x}}$ *to the endpoints.* Hence the Cauchy limit integral is just the correction factor that accounts for the difference between the local and outer angles. Both the local angle θ and the curvature or additional corners elsewhere on S_1 are irrelevant to the result; any surface the gets from $\overline{\mathbf{x}}$ to those corners subtends the same angle.

The edge theorem says that we do not need to depend on finding some particularly convenient closure surface to verify that the result depends only on the endpoints.

The 3D analogy of this example is that the H kernel integral is the solid angle of the outer contour of S_1. The Cauchy analysis again calls for explicit computation of the the local solid angle, to be augmented by a limit integral that gives the difference between the local and total angle.

For this to be useful, we must actually produce the endpoint functions or Stokes vectors. The following sections will identify cases where these functions are known and unknown. For the Laplace equation, nearly all cases are known; derivations are quite systematic in 2D, but largely *ad hoc* in 3D. For elasticity, there are only a few known cases. Systematic derivation of all of these results is an issue for future research.

Section 3 discusses the (rather incomplete) status of 3D Stokes vectors. Section 4 discusses the more systematic 2D Laplace cases, with each Laplace result followed by an outline of corresponding 3D and elasticity analysis.

6.3 Stokes Vectors

Stokes vectors are actually available only for a subset of the modal integrals given in Chapter 5. The cases (a) known from literature and (b) newly derived under the stimulus of the theorem are:

BIE	Solution mode	Status
Laplace primary	constant	known
Laplace primary	linear	new
Laplace gradient	constant	known
Laplace gradient	linear	new
Elasticity primary	constant	known
Elasticity primary	linear	(??)
Elasticity gradient	constant	new
Elasticity gradient	linear	(??)

The Laplace equation vectors are as follows:

- Ghosh and Muhkerjee[GM87] give a spherical coordinate system in which the primary BIE H kernel constant term (Cauchy singularity) is

$$H \equiv \nabla G \cdot \mathbf{n} \equiv \nabla \times [(1 - \frac{\mathbf{e} \cdot \mathbf{r}}{r}) \frac{\mathbf{e} \times \mathbf{r}}{|\mathbf{e} \times \mathbf{r}|^2}] \cdot \mathbf{n} \tag{6.27}$$

  This can be interpreted as a computation of the solid angle θ subtended by the cone (ruled surface) defined by the boundary of the surface patch and the singular point. The vector $\mathbf{e}$ is the north pole vector of a spherical coordinate system. For a given surface patch, any $\mathbf{e}$ is valid so long as (a) it does *not* pass through the edge of the patch and (b) the south pole vector -$\mathbf{e}$ does not pass through the surface patch. Violation of the second condition makes the integration produce the complementary solid angle $\theta - 4\pi$.

- For each direction k, the primary BIE linear term integrand is

$$(G\delta_{ik} - G_{,i}(y_k - x_k))n_i = \nabla \times (e_k \times \nabla r) \cdot \mathbf{n} \tag{6.28}$$

For example, the x direction Stokes vector is $[0, -z/r, y/r]$.

When the primary BIE is differentiated in direction j, the constant and linear term Stokes vectors are the respective partials of those of the primary BIE. The hypersingular kernel can also be derived in a generalized sense (i.e. without algebraic expansion of (6.27)) (Krishnasawamy, Schmerr, Rudolphi, and Rizzo [KSRR90]) as

$$\frac{\partial^2 G}{\partial n \partial y_j} = \nabla \times (-\mathbf{e}_j \times \nabla G) \tag{6.29}$$

By differentiating (6.28), the direction-j gradient BIE with a linear solution mode varying in direction k is

$$-G_{,j} n_k + H_{,j}(y_k - \overline{x_k}) = \nabla \times [\frac{\partial}{\partial x_j}(e_k \times \nabla r)] \cdot \mathbf{n} \tag{6.30}$$

This set of Stokes vectors completely covers the singular cases in Chapter 5.

For elasticity, only the constant term cases have been determined. Ghosh and Muhkerjee[GM87] give a collection of vector quantities $\mathbf{F}_{ik}$ such that the P_{ik} kernel is $P_{ik} = \nabla \times \mathbf{F}_{ik} \cdot \mathbf{n}$. The derivation is by serendipitous analysis of a spherical coordinate system. A new derivation in Appendix B gives the surprisingly simple expression for the gradient of P_{ik} as

$$\frac{\partial}{\partial y_j} P_{ik} = \nabla \times (-\mathbf{e}_j \times m \, D_{imk}) \tag{6.31}$$

The full S_{ijk} kernel is $\frac{\partial}{\partial x_j} P_{ik} + \frac{\partial}{\partial x_i} P_{jk}$ multiplied by material constants, so this formula for one directional derivative of P_{ik} also provides the Stokes vector for the S_{ijk} kernel. [1]

[1]The full formula for S_{ijk} in terms of derivatives of P_{ik} includes an additional term $P_{lk,l}$ (summed over l). Appendix B shows that this 'trace' term vanishes identically.

For a purely linear displacement field, the open problem of finding a Stokes vector is to determine some collection of vectors $\mathbf{G}_{imn}$ to generate the primary BIE, i.e.

$$\nabla \times \mathbf{G}_{imn} \cdot \mathbf{n} = (U_{ik} E_{klmn} - D_{ilm} y_n) n_l \tag{6.32}$$

The Stokes vector for the gradient BIE will follow by differentiation.

Properties of Stokes Vectors Each Stokes vector is one degree of singularity *lower* than the integrand it generates. This reduction exactly balances the lowered dimension of the integration, so the initial classification of the singularity as hypersingular or Cauchy remains unchanged. However, the lower-dimension integration domain is substantially easier to deal with numerically. The single-parameter quadrature formulae in Chapter 7 can be applied exactly in the lower dimension. In addition, the construction of a closure surface S_2 is completely avoided.

The derivations of these formulae illustrate again the distinction between generalized and algebraic analysis of the kernels. The Stokes vectors for the hypersingular kernels $\frac{\partial}{\partial y_j} P_{ik}$ and $\frac{\partial^2 G}{\partial n \partial y_j}$ rely only on general properties that occur because the primary kernel (U_{ik} or G, respectively) is a solution of the PDE away from the singular point. In contrast, the derivations for P_{ik} and H rely on (a) expanding the kernels algebraically in a particular coordinate system and (b) term-by-term manipulation.

Application of Stokes Vectors In the implementation of Chapter 8, Stokes vectors would be useful to eliminate construction of the 'closure surface' needed to evaluate modal integrals in a crack.

More broadly, it may be possible to construct 3D BIE analysis in which *all* integrals are converted to contour integrals. The following section gives some analysis leading towards this goal.

Ghosh and Muhkerjee[GM87] used the Stokes vectors for the constant term to convert the primary BIE to another BIE in which the displacements **u** are replaced by tangential derivatives of displacements. In their case, the Stokes vectors remain in the integral as *surface* (rather than contour) integrands multiplying the tangential derivatives. Okada, Rajiyah, and Atluri [ORA88] derive (using integration by parts rather than Stokes theorem) an analogous form of the gradient BIE. The relationship among these forms has not been fully explored.

6.4 Some Analysis of a BEM Using Implicit Functions

This section discusses systematic construction of cartesian basis functions and their coupling to the edge theorem.

Cartesian Basis Functions for 2D Laplace Fenner and Watson [FW88] give the sequence of polynomials that satisfy the 2D Laplace equation exactly. Fig. 6.2 gives (a) these functions $u(x,y)$ up to cubic and (b) the corresponding functions $V(x,y)$ that satisfy (6.15) are also given. In general, there are (only) two linearly independent basis polynomials for degree k ($k > 0$) polynomials that satisfy the 2D Laplace equation. [2]

A parametric BEM formulation needs to be transformed so that its surface potential and flux are a a sum of these Cartesian functions. If the parametric

[2]S.Vavasis observes that these polynomials for degree k are exactly the real and imaginary parts of the complex variable $\mathbf{z}_k = (x+iy)^k$. The functions $V(x,y)$ corresponding to $\mathbf{Re}(\mathbf{z}_k)$ and $\mathbf{Im}(\mathbf{z}_k)$ are, respectively, $(-1^k)\mathbf{Im}(\mathbf{z}_k)(\ln(r^{-1})+1/k)$ and $\mathbf{Re}(\mathbf{z}_k)(\ln(r^{-1})+1/k)$.

$u(x,y)$	$V(x,y)$
1	$\arctan\frac{y}{x}$
x	$-y(\ln(r^{-1})+1)$
y	$-\ (\ln(r^{-1})+1)$
x^2-y^2	$2xy(\ln(r^{-1})+\frac{1}{2})$
$2xy$	$(x^2-y^2)(\ln(r^{-1})+\frac{1}{2})$
x^3-3xy^2	$-(3x^2y-y^3)(\ln(r^{-1})+\frac{1}{3})$
$3x^2y-y^3$	$(x^3-3xy^2)(\ln(r^{-1})+\frac{1}{3})$

Figure 6.2: Polynomial solutions of 2D Laplace equation

functions express u and $\frac{\partial^2 u}{\partial y \partial f}$or an element on the x axis as

$$u = a_0 + a_1 x + a_2 x^2 \quad \text{and} \quad \frac{\partial u}{\partial y} = b_0 + b_1 x \tag{6.33}$$

the same a_i and b_i may be considered to be the coefficients of the Cartesian function

$$u = a_0 + a_1 x + b_0 y + b_1 xy + a_2(x^2 - y^2) \tag{6.34}$$

That is, since the parametric formulation does not explicitly constrain second derivatives in the y direction we can assume that $\frac{\partial^2 u}{\partial^2 y}$ takes on whatever value is needed to satisfy the PDE.

Using these cartesian functions[3] the linearized BIE over a boundary contour S_1 is written (without need for a separate approximating function for the surface flux) as

$$\int_{S_1} G\frac{\partial u}{\partial \mathbf{n}} - Hu\, dS \tag{6.35}$$

$$= \left\{ \text{Substitute expansion of } u \text{ and } \frac{\partial u}{\partial \mathbf{n}} \right\} \tag{6.36}$$

$$a_0 \int_{S_1} -H\, dS \tag{6.37}$$

$$+ a_1 \int_{S_1} Gn_x - Hx\, dS + a_2 \int_S Gn_y - Hy\, dS \tag{6.38}$$

$$+ a_3 \int_{S_1} 2G(yn_x + xn_y) - 2Hxy\, dS \tag{6.39}$$

$$+ a_4 \int_{S_1} 2G(xn_x - yn_y) - H(x^2 - y^2)\, dS \tag{6.40}$$

$$= \left\{ \begin{array}{l} \text{Substitute point functions from Fig. 6.2} \\ \text{evaluated at line endpoints } (x_1, y_1) \text{ and} \\ (x_0, y_0) \end{array} \right\} \tag{6.41}$$

$$\sum_{i=0}^{i=5} b_i (V_i(x_1, y_1) - V_i(x_0, y_0)) \tag{6.42}$$

[3]The origin of these functions is the fixed point $\mathbf{x}$. If potential is expressed in local coordinates of an element, translations and rotations must be applied.

Cartesian Basis Functions for 2D Elasticity Any combination of a_0, a_1, a_2, b_0, b_1, and b_2 in the linear expression

$$\begin{aligned} u_x &= a_0 + a_1 x + a_2 y \\ u_y &= b_0 + b_1 x + b_2 y \end{aligned} \tag{6.43}$$

satisfies the differential equation of elasticity. Quadratic basis functions are developed from the differential equation as follows:

$$\tag{6.44}$$

$$= \left\{ \begin{array}{l} \text{Differential equation} \\ u_{i,jj} + (1-2\nu)u_{j,ji} = 0 \text{ for each } i \end{array} \right\} \tag{6.45}$$

$$\begin{array}{rcrcrcl} (2-2\nu)u_{x,xx} & + & u_{x,yy} & + & (1-2\nu)u_{y,xy} & = & 0 \\ (1-2\nu)u_{x,xy} & + & u_{y,xx} & + & (2-2\nu)u_{y,yy} & = & 0 \end{array} \tag{6.46}$$

$$\Rightarrow \left\{ \text{Choose} \begin{array}{rcl} u_x &=& a_3 x^2/2 + a_4 xy + a_5 y^2/2 \\ u_y &=& b_4 x^2/2 + b_4 xy + b_5 y^2/2 \end{array} \right\} \tag{6.47}$$

$$\begin{array}{rcrcrcl} (2-2\nu)a_3 & + & (1-2\nu)a_5 & + & b_4 & = & 0 \\ a_4 & + & (1-2\nu)b_3 & + & (2-2\nu)b_5 & = & 0 \end{array} \tag{6.48}$$

Given two constraints on the six coefficients, we can choose four freely and have the remaining two fixed. For instance, a_3, a_5, b_3, and b_5 can be freely chosen, and b_4 and a_4 will be fixed by the differential equation.

Cartesian Basis Functions for 3D Laplace The 3D constant, linear, and quadratic basis functions that identically satisfy the Laplace equation are:

zero order	1		
linear	x	y	z
quadratic	xy $x^2 - z^2$	yz $y^2 - z^2$	xz

If u and $\frac{\partial u}{\partial z}$ are interpolated parametrically on an element in the xy plane in the form

$$u = a_0 + a_1 x + a_2 x^2 + a_3 xy + a_4 y^2 \quad \text{and} \quad \frac{\partial u}{\partial y} = b_0 + b_1 x + b_2 y \qquad (6.49)$$

the same a_i and b_i may be considered to be the coefficients of the Cartesian function

$$u = a_0 + a_1 x + b_0 z + b_1 xz + b_2 y_z \qquad (6.50)$$

$$+ a_2(x^2 - z^2) + a_3 xy + a_4(y^2 - z^2) \qquad (6.51)$$

Cartesian Basis Functions for 3D Elasticity The constant and linear basis functions for elasticity are

$$u_x = a_0 + a_1 x + a_2 y + a_3 z \qquad (6.52)$$

$$u_y = b_0 + b_1 x + b_2 y + b_3 z \qquad (6.53)$$

$$u_z = c_0 + c_1 x + c_2 y + c_3 z \qquad (6.54)$$

For quadratic functions, setting each of u_x, u_y, and u_z equal to a linear combination of the 6 terms x^2, y^2, z^2, xy, xz, and yz provides 18 degrees of freedom. Enforcing the differential equation simultaneously in x, y, and z directions provides 3 constraints and reduces the number of free coefficients to 15.

6.5 Conclusion of Singular Integration Analysis

This chapter has proposed that the parametric aspects of the boundary element method may be unnecessary. We have shown that a certain class of integrals can be computed independent of the parameterized geometry, and that the necessary conditions for those formulae can be met by either (a) pure cartesian functions or (b) transformations of parametric surface functions.

Practical use of this method for elasticity is not yet possible because certain of the abstract formulae are not yet known. Determination of these formulae is a research problem.

The move from parametric approximation of surface functions to cartesian functions is a natural analog to recent research (e.g. [Baj90]) aimed at using implicit, rather than parametric, surfaces for approximating geometry. As with the implicit surface research, the goal of replacing well-established parametric technology requires extensive theoretical and practical effort.

The edge theorem discussion complete the three chapters on singular integration. Chapter 4 dealt with the intensively algebraic past methods. Chapter 5 gave a concise and powerful alternative by high level reasoning about known modes of behavior. This chapter used the modal notions to prove, albeit non-constructively, that a further simplification is possible via reduction of the geometric dimension of the integrals. Formulae that achieve this reduction were actually produced for the Laplace equation.

The next three chapters will deal with issues that arise in implementing the modal method, and give computational results.

Chapter 7

Near Singular Integration

Quadrature, or numerical integration, refers to approximation of an integral by a weighted sum of function values, as in

$$\int f(s)ds = \Sigma A_i f(s_i) \tag{7.1}$$

The weights and evaluation points for such quadrature rules are chosen so that some polynomial approximation of the function is integrated exactly, either over the entire interval or piecewise over several subintervals. The accuracy of the rule is determined by how closely that polynomial approximates the actual function.

Quadrature is widely used for the kernel integrals in boundary integral equations. However, the presence of singularities in the kernels causes severe errors when the computations are done naively. Section 1 contains background information on quadrature methods, with particular emphasis on (a) the special properties of Gaussian quadrature rules and (b) the quite different ways that these properties are exploited by the finite element method on one hand and the boundary element method on the other.

Section 2 identifies conditions under which BIE kernels can exploit the optimality properties of Gaussian quadrature. This method was initially published for

2D elasticity in Lutz [Lut91][LWI90]. Because it relies directly on the derivation of Gauss quadrature rules, it provides exact results for certain geometries and certain polynomial integrands. The cost of this optimality is that the quadrature rules apply only at specific distances from the surface; the distance to the surface acts as a (continuously varying) parameter that determines the (continuously varying) evaluation points and weights of the rule.

Section 3 extends the optimum results to surface integrals in the 3D BIE. It is shown that an *on-surface* integral with a r^{-1} (weak) singularity can be optimally integrated by a transformation that uses the 1D parameterized rule for one direction of integration and a conventional rule for the other direction. Finally, we give transformations that allow approximate (not exactly) use of the parameterized quadrature rules for 'near surface' integrals in 3D.

7.1 Numerical Integration

Integration of smooth functions – those with no large low-order derivatives – is considered to be one of the easier problems of numerical analysis. Intuitively, errors between the approximating polynomial and the actual function in one portion of the interval are often canceled by oppositely-signed errors in other parts of the interval. Comparison of values produced by similar rules applied with different subdivisions provides accurate bounds on the error of the computed integral. This leads to 'adaptive' quadrature methods in which the interval is progressively subdivided to obtain higher and higher accuracy. This refinement is done selectively so evaluations are concentrated where the function varies most rapidly. For many applications, these methods seem to have an ideal combination of efficiency (due to selective refinement) and robustness (due to accurate error estimates).

The kernel functions in the BIE violate most or all of the conditions that lead up to the conclusion that integration is an easy numerical problem. In particular,

1. The kernel functions in the BIE are not smooth.
2. The apparently modest overhead cost of the adaptive algorithms becomes a large efficiency penalty if incurred at each of thousands of integrations.

Because of these factors, the boundary element method benefits substantially from careful analysis of the particular problems of its integrations.

Quadrature with Weighted Integrands For many integration problems, the integrand $f(s)$ can be written as a product $f(s) = w(s)g(s)$, where $w(s)$ (a) is known *a priori* and (b) does not change sign on the interval. This additional knowledge allows quadrature rules to be constructed with the behavior of the weight function 'built into' the weights A_i and evaluation points s_i in such a way that the quadrature rule requires evaluation only of $g(s)$, i.e.

$$\int w(s)g(s)\,ds = \Sigma A_i g(s_i) \tag{7.2}$$

'Non-weighted' quadrature rules, i.e. those with no weight function, are a special case of weighted quadrature where the weight function is identically $w(s) \equiv 1$.

Aside from the convenience of not having to evaluate $w(s)$ at the quadrature points s_i, weighted quadrature rules have the significant advantage that their accuracy depends primarily on the smoothness of $g(s)$. The effects of $w(s)$ are incorporated into the placement and weights of the quadrature rule.

Gauss Quadrature Rules The most accurate quadrature rules for a given weight function are the 'Gauss' rules derived from the roots of orthogonal polynomials based on the weight function. These rules have the following formal property:

- *Exactness property of Gauss quadrature:* A k-point Gauss rule for weight $w(s)$ produces an *exact* integral of any function g that is a polynomial of degree $2k-1$ or less. This is optimal in the sense that no other rule of fewer points is exact for all polynomials of this degree.

In addition, Gauss rules tend to provide remarkably good results for integrands that are of degree slightly *higher* than the $2k$-1 exactness limit. Stroud and Seacrist [SS66] gives a formal claim that Gauss rules are essentially always as good as or better than any other quadrature rules with the same number of points.

The polynomials $P_i(a)$ that determine the weights and evaluation points are defined by a two term recurrence relationship as follows:

$$\begin{aligned} i=0: \quad P_0(s) &= 1 \\ i=1: \quad P_1(s) &= (s-b_0) \\ i\geq 2: \quad P_{i+1}(s) &= (s-b_i)P_i(s) - c_iP_{i-1} \end{aligned} \tag{7.3}$$

where the coefficients b_i and c_i are defined by:

$$b_i = \frac{\int_a^b w(s)sP_i^2(s)\,ds}{\int_a^b w(s)P_i^2(s)\,ds} \tag{7.4}$$

$$c_i = \frac{\int_a^b w(s)P_i^2(s)\,ds}{\int_a^b w(s)P_{i-1}^2(s)\,ds} \tag{7.5}$$

Since the recursion coefficients b_i and c_i depend only on preceding polynomials P_i and P_{i-1}, a polynomial of any desired degree can be computed explicitly by computing the given integrals of prior polynomials in the series.

The evaluation points of the k-point Gauss quadrature rule are exactly the roots of $P_k(s)$. The weight A_i for point s_i is obtained by integrating the weight function times the (Lagrangian) polynomial whose value is 1 at s_i and 0 at the other $k-1$ roots of P_k:

$$A_i = \int_a^b w(s)\Pi_{i\neq j}\frac{s-s_j}{s_i-s_j}\,ds \tag{7.6}$$

Both the roots and weights can also be determined by efficient algorithms based on finding eigenvalues and eigenvectors of a related tridiagonal matrix, as described in Golub and Welsch [GW69].

Determination of the coefficients b_i and c_i appears to be a direct, exact process, since the formulas involve only previously determined polynomials. On the other hand, as indicated by Gautschi [Gau70] and Danloy [Dan73], integrals of $P_i^2(s)w(s)$ and $sP_i^2(s)w(s)$ for high degrees are difficult to compute to high precision, either analytically or numerically. For example, analytic evaluation of

$$\int_0^1 \frac{s}{\sqrt{c^2+s^2}}\, ds = \sqrt{1+c^2} - c \tag{7.7}$$

results in cancellation of 5 significant digits for c=100. In limited-precision arithmetic even a 2- or 3- point Gauss rule will give better results in this case than the analytic result.[1]

Hence although Gauss rules are easy to obtain in principle, the initial analysis needed to obtain them is still not a trivial matter, except in a small number of cases where there are explicit formulas (e.g. see Davis [Dav75]) for the b_i and c_i.

Historical Notes In the era of hand computation, both initial computation of Gauss rules and subsequent use were difficult. Computation of the s_i and A_i requires high accuracy evaluation of the integrals in (7.4) and (7.5), followed by extraction of roots of high-order polynomials. Once rules were computed and tabulated, practical use was further limited by the fact that essentially all weights and evaluation points are irrational numbers and therefore quite difficult to work with by hand.

[1]The cancellation in the analytic example can be avoided by rewriting it as

$$\sqrt{1+c^2} - c = \sqrt{1+c^2}(1-\cos(\theta) = \sqrt{1+c^2}(2\sin^2(\theta/2))$$

where $\theta =$ atan$(1/c)$. Obtaining accurate forms when x and r are raised to arbitrary powers is a substantial algebraic task.

An additional drawback of Gauss formulas is the fact that they do not produce error estimates as a side effect of the computation. This is because there are no common evaluation points when one applies either (a) two formulas of different order, or (b) the same formula on an original interval and then again on both parts of a halved interval. Patterson [Pat89] has recently shown a general method of adding points to existing rules, obtaining rules with some Gauss-like optimality and some error estimation properties.

The relative significance of these issues have changed with use of digital computers. There is no longer any penalty for computing with weights and evaluation points that are not simple integers or fractions. *If* the character of the integrand is well known, Gauss quadrature offers guaranteed accuracy for significantly less cost than a safe-but-cautious adaptive method that must do extra function evaluations and summations in order to obtain error estimates.

Finite element computations are able to benefit from both the exactness property and the informal robustness of Gauss rules. On the other hand, boundary element computations have in the past used exactness only in the special case of a logarithmic (weak) line singularity. The remainder of this chapter identifies a number of cases where it is possible to use the exactness property for boundary integrals, at the cost of precomputing and managing a large number of Gauss rules.

The Finite Element Case Integration of finite element stiffness matrices is an extreme example of a case where Gaussian quadrature works effectively. The standard isoparametric finite element formulation ([CMP89]) reduces each entry K in a stiffness matrix to the form

$$K = \int_0^1 \int_0^1 \frac{p(\xi,\eta)q(\xi,\eta)}{|J(\xi)|}\, d\xi\, d\eta \qquad (7.8)$$

where $p(\xi)$, $q(\xi)$, and $|J(\xi)|$ are polynomials known to be of a low degree. For perfectly regular elements – e.g. a 4-noded rectangular element – the $|J(\xi)|$ term is a constant, and the entire integrand is a polynomial of known degree. Practical experience has shown that the error that is introduced by non-constant $|J(\xi)|$ is quite tolerable even when the quadrature rule only has enough points to nominally exactly integrate the other parts of the integrand. In addition, it has been found that it is often beneficial to intentionally *underintegrate*, i.e. choose a Gauss formula with *fewer* points than are necessary to exactly integrate $p(\xi)q(\xi)$. The resulting errors occur in a predictable direction and are often of the right magnitude to cancel (in a useful way) other errors in the approximation.

The boundary element case In the boundary element method, integrands are *never* exactly polynomials. For a portion of surface on the boundary of a 2D region, the integrals for the 2D BIE kernels are of the form

$$\int_0^1 \ln(r^2) g(s)\, ds \qquad \text{or} \qquad \int_0^1 \frac{g(s)}{r^n}\, ds \tag{7.9}$$

where r is the distance from the fixed point of the integration to the element at parametric coordinate s and n is some (even) power. In the simplest case of a perfectly linear boundary element, the worst case numerator term (for the S_{ijk} elasticity kernel) might be a degree 6 polynomial formed from the product of a quadratic displacement function and a degree 4 geometric polynomial taken from the kernel. Since the distance r from a fixed space point to points on the element is non-constant, the denominator is always non-constant, and the entire integrand is rational. Hence a unit-weight quadrature rule will never give an exact result.

It is conventional to classify the severity of the variation into the three cases of 'far field', 'near singular', and 'singular' integrations. When singular point $\mathbf{x}$ is far from the surface patch, r is nearly constant over the surface, and (inverse) powers of r introduce only mild variation in a kernel. When $\mathbf{x}$ is very close to the surface patch, distance to various surface points may vary by orders of magnitude. This causes severe difficulty in numerical integration. The problem is captured by Fig. 7.1, which shows the function $f(s) = \frac{1}{c^2 + s^2}$ for various values of c. At c=4, the function is nearly constant. At small c the spike at s=0 grows as $1/c^2$. Any quadrature rule with fixed evaluation points will either (a) underestimate (due to missing the spike) if there is no evaluation at s=0 or (b) overestimate if it evaluates at s=0.

Gauss integration of the far field case BIE integral – which should be the easiest of all BIE integrations – is extremely accurate, but never *exact.* On the other hand, for the *on-element* case of integrating the $\ln(r^2)$ kernel, multiplied by a low order polynomial, along a straight line segment, as in Fig. 7.2(a), a weight function that defines an exact Gauss rule is isolated by the transformations

$$\int_0^1 \ln(r^2) g(s)\, ds \tag{7.10}$$

$$= \left\{ \begin{array}{l} \text{Substitute } r = sL \text{ and simplify log of} \\ \text{product:} \end{array} \right\} \tag{7.11}$$

$$\int_0^1 (\ln(s^2) + \ln(L^2)) g(s)\, ds \tag{7.12}$$

$$= -\tfrac{1}{2}\int_0^1 \ln(1/s) g(s)\, ds + \ln(L^2) \int_0^1 g(s)\, ds \tag{7.13}$$

In the final form, the second integral has no singularity at all and can be integrated by unit-weight Gauss quadrature. In the first integral, the factor $\ln(1/s)$ is always non-negative for $0 \le s \le 1$. The Gauss rule for this special case is tabulated in boundary element texts. These rules provide an *exact*, not approximate, result when $g(s)$ is a polynomial of degree up to $2k$-1.

This derivation has highlighted the oddity that the *hardest* case is treated exactly, but the easiest case only approximately, by quadrature rules. It seems peculiar that a method strong enough to handle a true singularity should fail so badly for very closely related problems that are only nearly singular.

Figure 7.1: Typical 2D nearly singular function

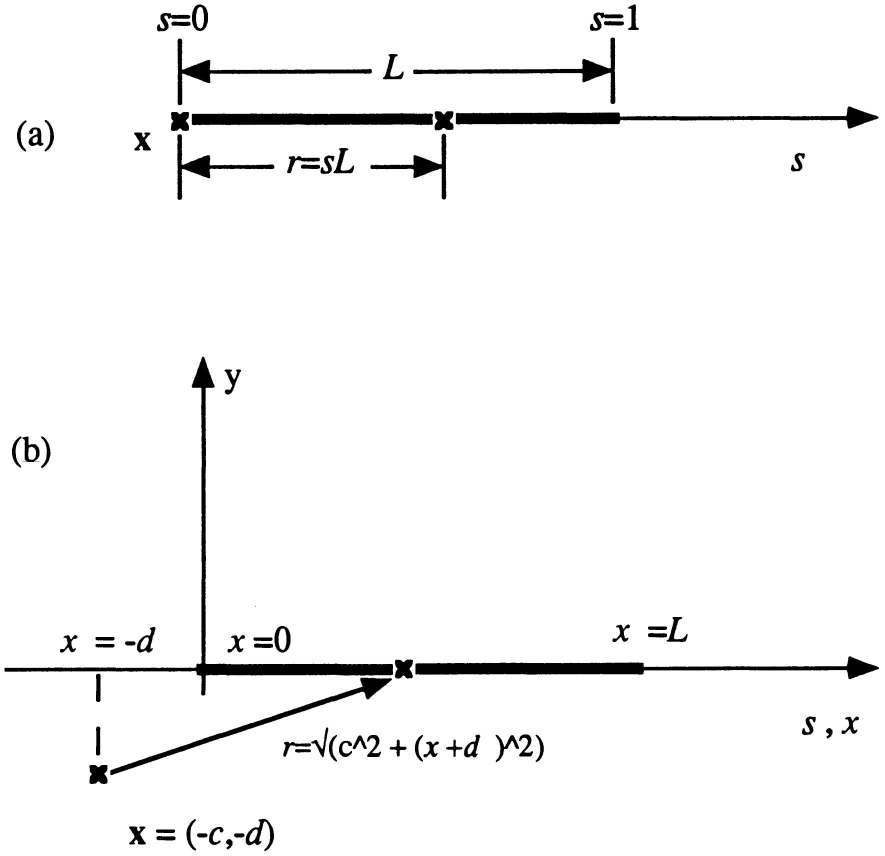

Figure 7.2: Special geometries for Gauss rule construction

7.2 Gaussian Solutions for BIE Kernels

Now consider a case where the fixed point $\mathbf{x}$ is located as in Fig. 7.2(b), at a distance c from the line containing the surface element and a distance d from the origin of the s axis. The best we can do at isolating the kernel is

$$\int_0^1 \ln(r^2) g(s)\, ds \tag{7.14}$$

$$= \left\{ \text{Substitute } r^2 = L^2(s^2 + (c^2 + d^2)) \right\} \tag{7.15}$$

$$\ln(L^2c^2)\int_0^1 g(s)\, ds + \int_0^1 \ln(1 + \frac{(d+s)^2)}{c^2}) g(s)\, ds \tag{7.16}$$

The c and d terms, which will be different for every fixed point, cannot be isolated from the s term. Hence there is no single weight function for which a Gauss rule can be derived.

On the other hand, consider a single fixed point for which c and d are given. Then c and d are constants, so $\ln(1 + (d+s)^2/c^2)$ is a function of s only, and also does not change sign. Hence a Gauss rule can be computed for that particular point.

For a point with c=0, there is only one free parameter d, and the evaluation points are a function of that one parameter. For $c \neq 0$ a non-zero d parameter is eliminated by projecting $\mathbf{x}$ to the element and integrating separately to each endpoint, as derived in Fig. 7.3. The transformed integrand has fixed integration limits and a constant-signed weight function depending only on s and c.

Fig. 7.4 and Fig. 7.5 show the variation of evaluation points and weights for 1 to 4 point rules for weights $1/\sqrt{(s^2 + c^2)}$ and $1/(s^2 + c^2)$ when Gauss points computed for various values of c. The following behavior is typical of rules for different powers of r:

$$
\begin{aligned}
& \int_0^L f(x,r)\,dx && (7.17)\\
= \quad & \{ \text{ split integration domain } \quad \} && (7.18)\\
& \int_{-d}^L f(x,\mathrm{r})\,dx - \int_{-d}^0 f(x,r)\,dx && (7.19)\\
= \quad & \left\{ \begin{array}{l} \text{reparameterize first integral} \\ x = s(L+d) - d, \text{ second by } x = d(s-1) \end{array} \right\} && (7.20)\\
& (L+d)\textstyle\int_0^1 f(s(L+d)-d, \sqrt{(c^2+s^2(L+d)^2})\,ds && (7.21)\\
& -d\textstyle\int_0^1 f(d(1-s), \sqrt{(c^2+s^2d^2)^2})\,ds && (7.22)\\
= \quad & \left\{ \text{ Define } \overline{c_1} = c/(L+d) \text{ and } \overline{c_2} = c/d \right\} && (7.23)\\
& (L+d)\textstyle\int_0^1 f(s(L+d)-d, c\sqrt{(1+s^2/\overline{c_1}^{\,2}})\,ds && (7.24)\\
& -d\textstyle\int_0^1 f(d(1-s), c\sqrt{(1+s^2/\overline{c_2}^{\,2})^2})\,ds && (7.25)
\end{aligned}
$$

Reparameterized forms of typical singularities

$\int g(x)\ln(r^2)\,dx$	$\ln(c)\int_0^1 g(s)\,ds + \int_0^1 g(s)\ln(1+s^2/\bar{c}^2)\,ds$
$\int \frac{g(x)}{r^n}\,dx$	$c^{-n}\int_0^1 \frac{g(s)}{(1+s^2/c^2)^n}\,ds$

Figure 7.3: Domain splitting to eliminate d from the weight function

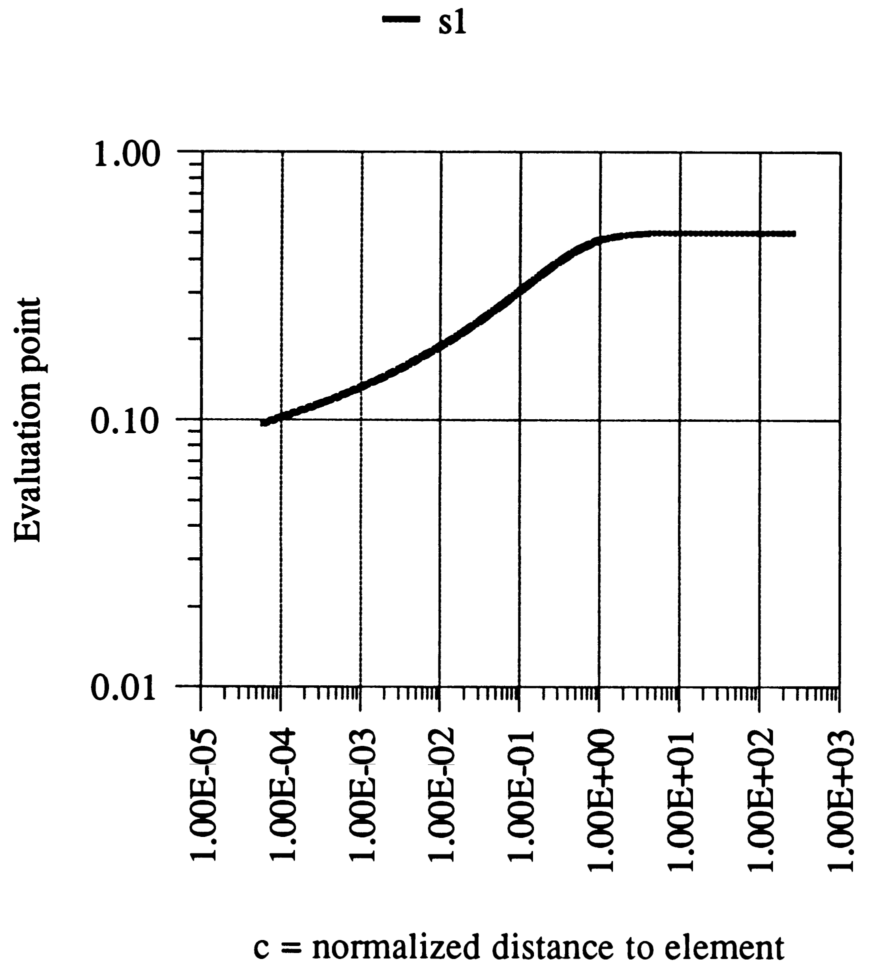

Figure 7.4: 1 point quadrature rules for weight $w(s) = \frac{1}{(s^2 + c^2)^{1/2}}$ (Normalized weights identically 1)

(continued on next page)

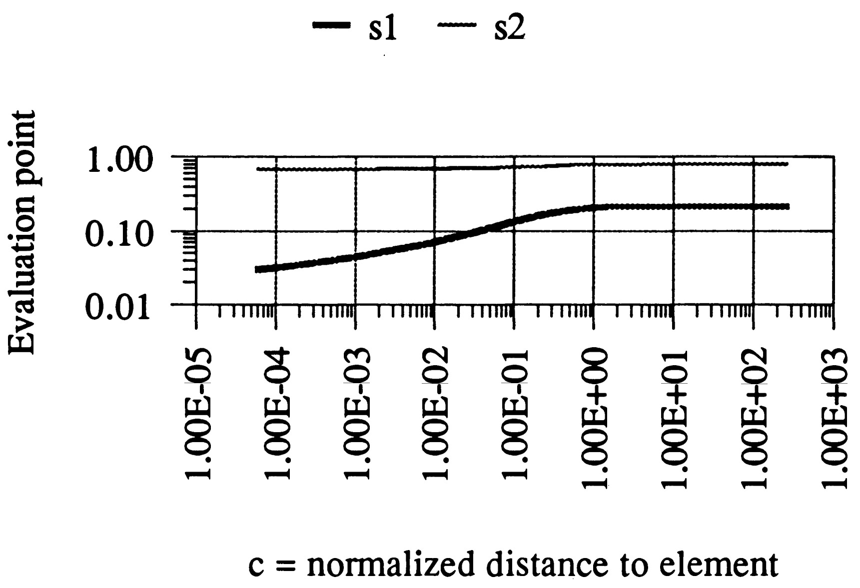

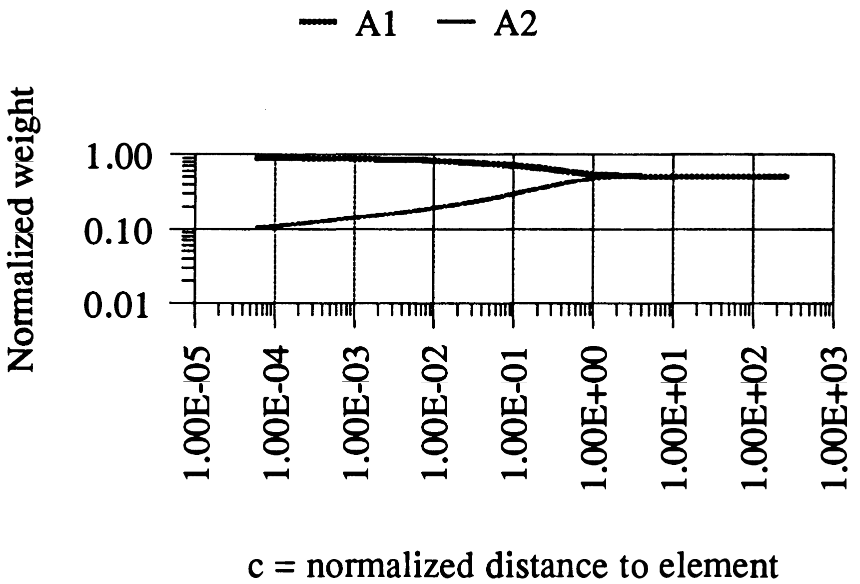

Fig. 7.4 (continued from previous page) 2 point quadrature rules for weight

$$w(s) = \frac{1}{\sqrt{s^2 + c^2}}$$

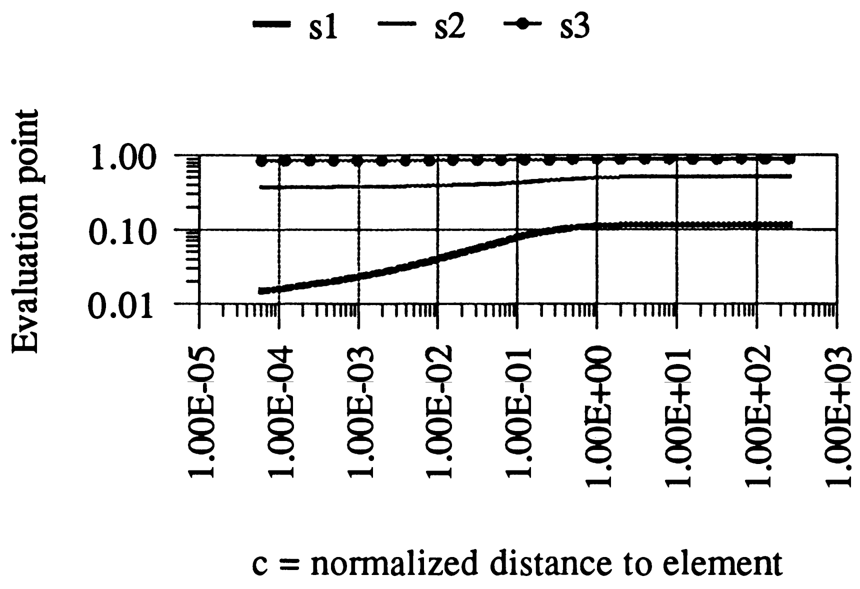

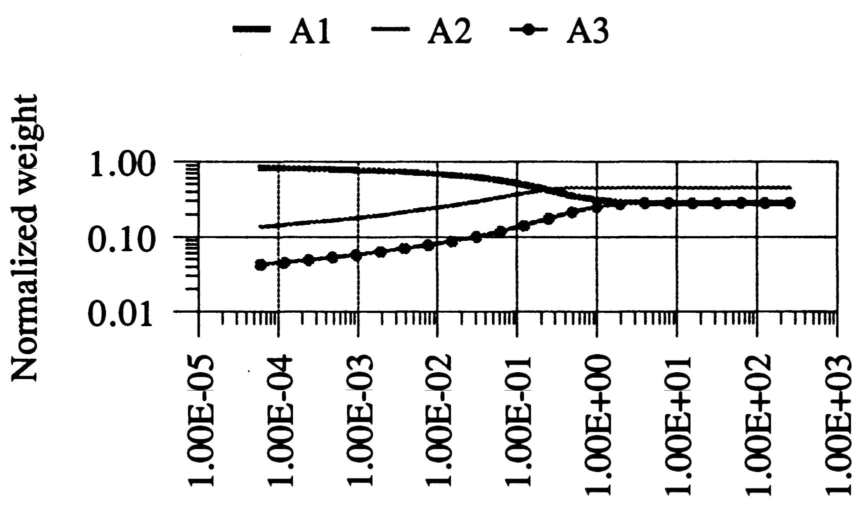

Fig. 7.4 (continued from previous page) 3 point quadrature rules for weight

$$w(s) = \frac{1}{\sqrt{s^2 + c^2}}$$

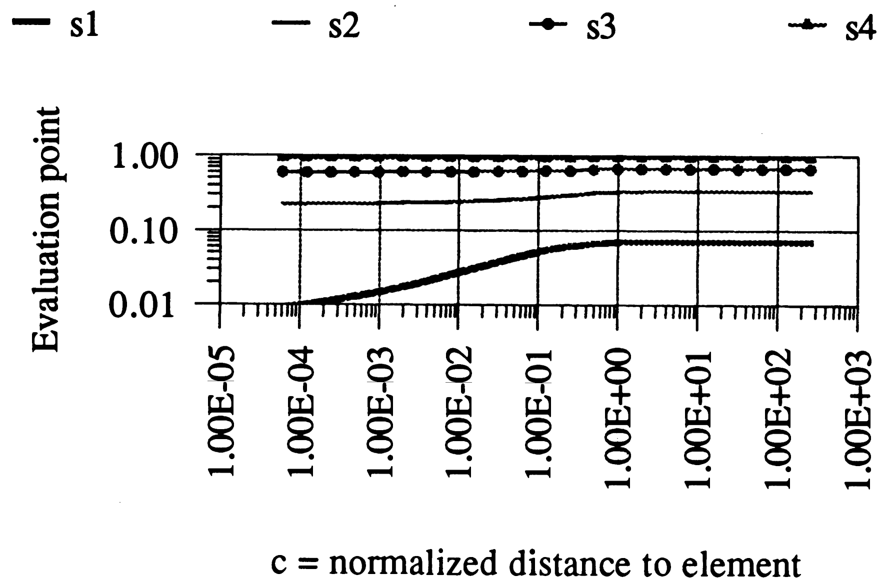

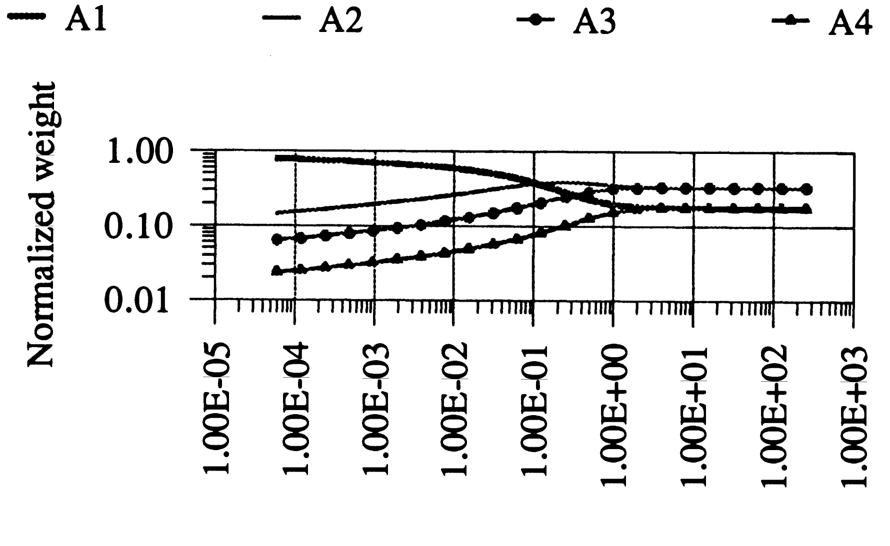

Fig. 7.4 (continued from previous page) 4 point quadrature rules for weight

$$w(s) = \frac{1}{\sqrt{s^2 + c^2}}$$

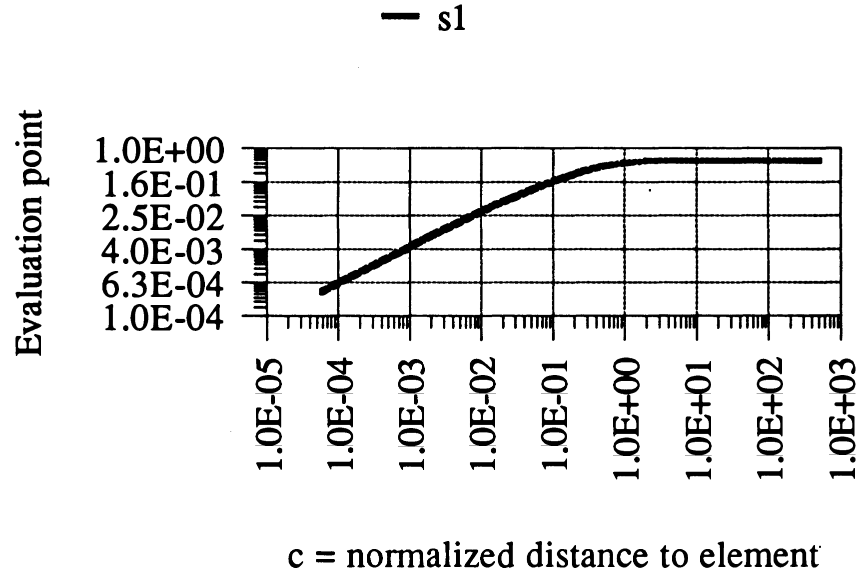

Figure 7.5: 1 point quadrature rules for weight $w(s) = \frac{1}{s^2 + c^2}$ (Normalized weights identically 1)

(continued on next page)

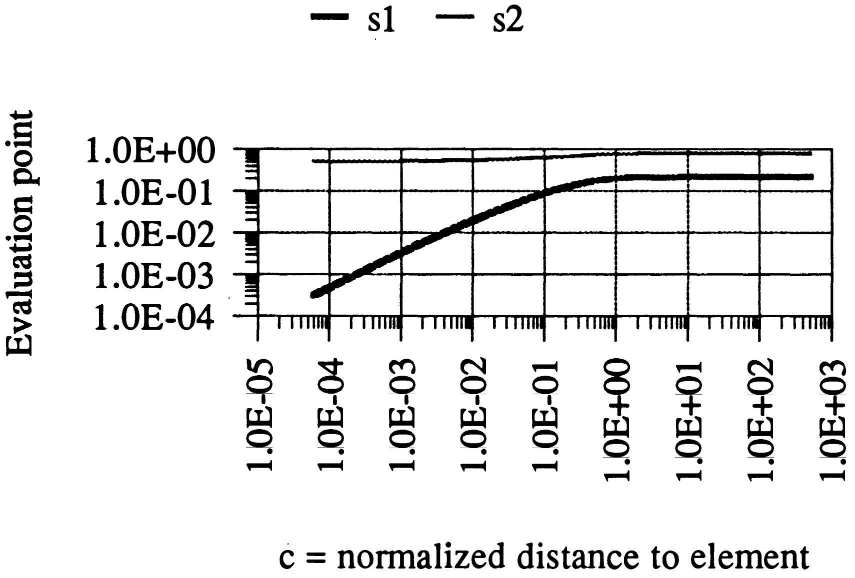

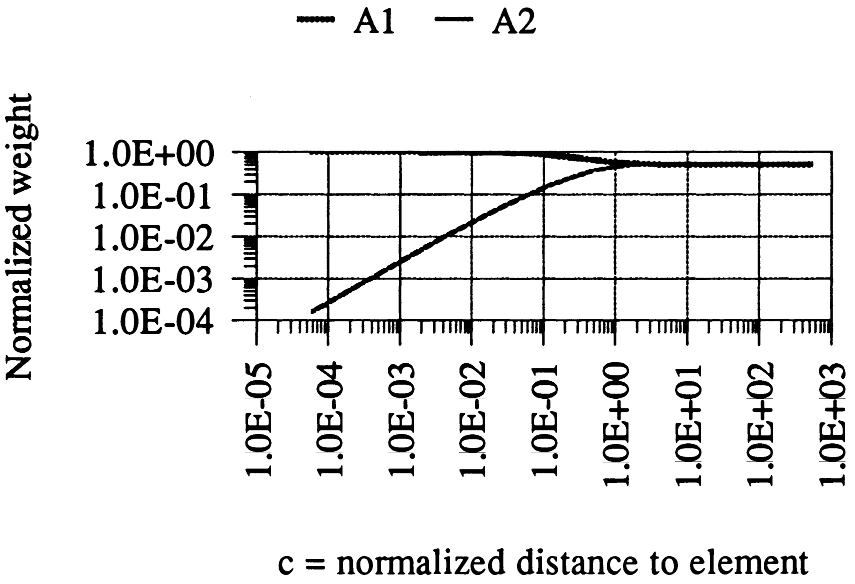

Fig. 7.5 (continued from previous page) 2 point quadrature rules for weight

$$w(s) = \frac{1}{s^2 + c^2}$$

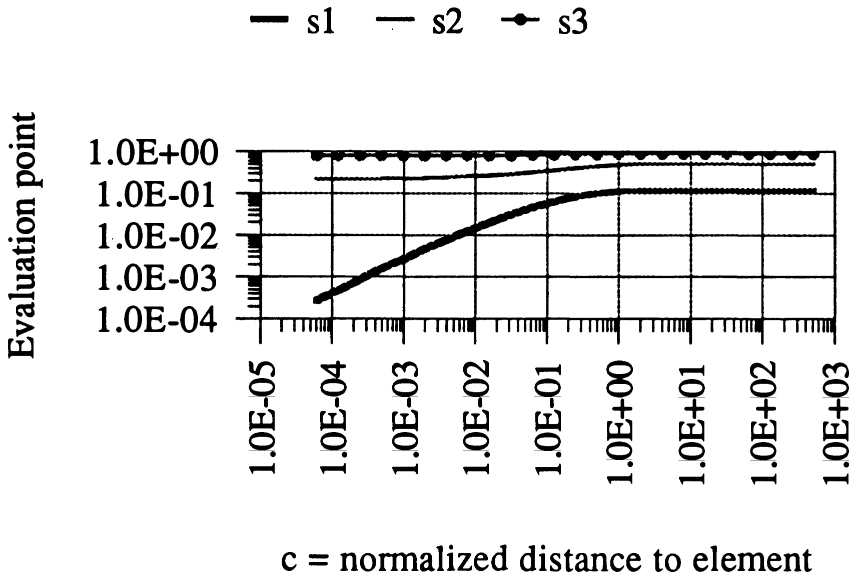

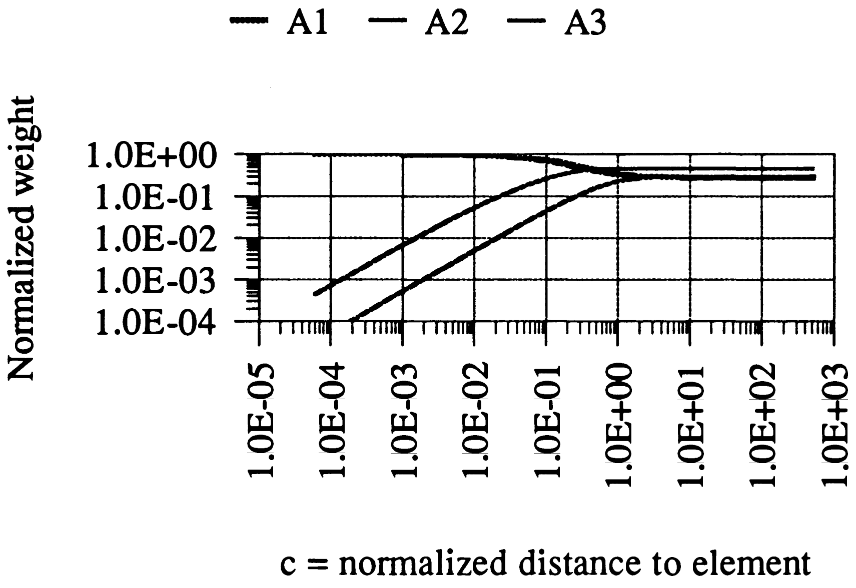

Fig. 7.5 (continued from previous page) 3 point quadrature rules for weight

$$w(s) = \frac{1}{s^2 + c^2}$$

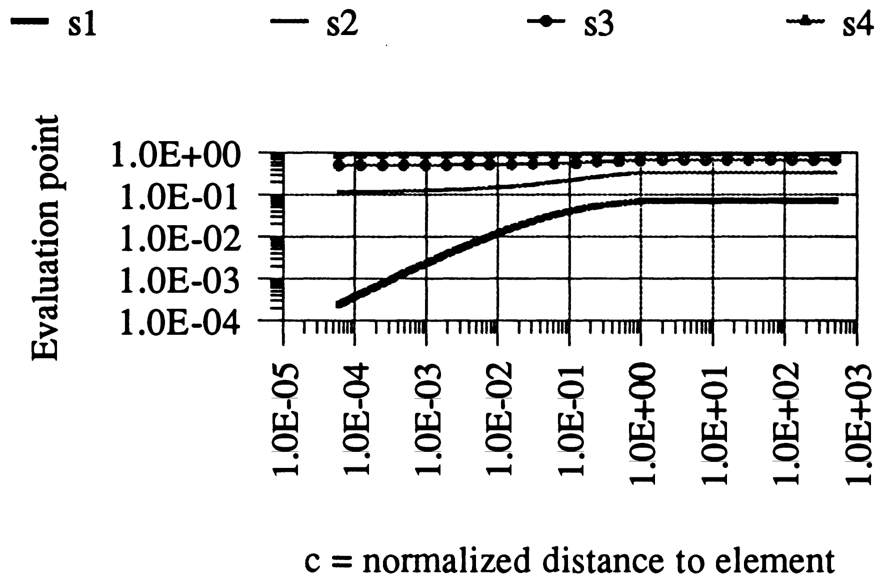

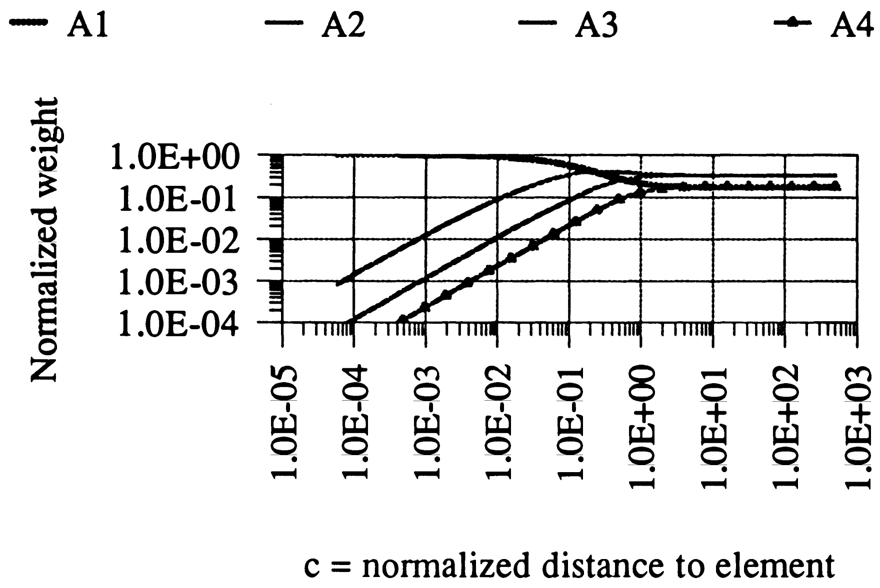

Fig. 7.5 (continued from previous page) 4 point quadrature rules for weight

$$w(s) = \frac{1}{s^2 + c^2}$$

1. For large c, both the weights and evaluation points converge to unit-weight ($w(s)$ Gauss rules.
2. For small c, function values near the origin are emphasized by both (a) clustering of evaluation points and (b) higher weighting of the points nearest to the origin.
3. The clustering effect is more pronounced for higher powers of r.

Other approaches The notion of distance-sensitive quadrature rules is present in methods proposed by [HB88] and [Tel87]. Their methods apply a distance-sensitive change of variables to map the integrand to a different domain where it is smoother; a conventional Gauss rule is then applied. Because the transformed integrand is not a polynomial, the result is never exact.

7.3 Integration on Surfaces in 3D

Although there are numerous special-case formulas ([SS66],[Str71],[NVB90]) for multidimensional integrals with various weight functions and domains, there is no systematic process for obtaining surface integration formulas with an arbitrary weight, domain, and degree of accuracy. The following paragraphs give special-case transformations that convert certain BIE kernel integrals over surface patches into repeated 1D integrals that can be systematically treated by parameterized methods.

Weak (r^{-1}) singularities on a triangle Consider a right triangle with leg lengths cL and L, as in Fig. 7.6, with the singular point $\overline{\mathbf{x}}$ of a BEM kernel integral placed at the origin. An integral of a r^{-1} singularity over the triangle is

$$\int \frac{g(x,y)}{r}\,dx\,dy \tag{7.26}$$

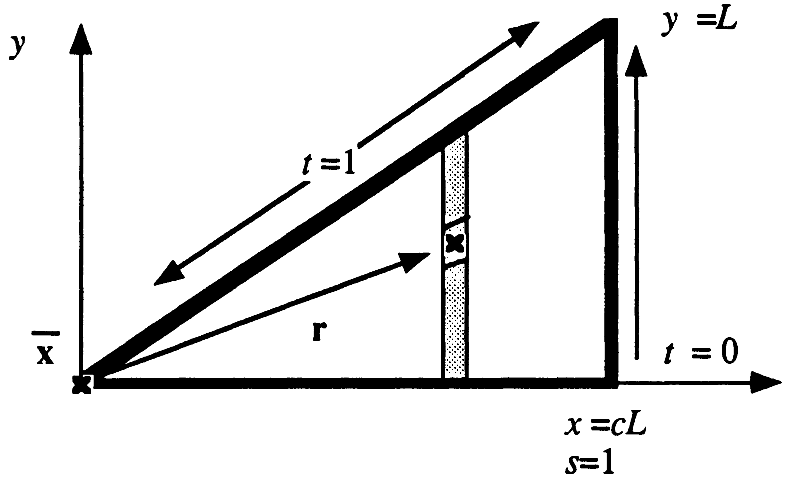

Figure 7.6: Geometry for quadrature rules for weak singularities over a triangle.

$$= \left\{ \text{Transformation} \left\{ \begin{array}{c} x = scL \\ y = stL \\ dx\,dy = cL^2 s\,ds\,dt \\ r = scL\sqrt{1+t^2/c^2} \end{array} \right. \right\} \quad (7.27)$$

$$L \int_0^1 \int_0^1 \frac{g(x,y)}{\sqrt{1+t^2/c^2}}\,dt\,ds \quad (7.28)$$

$$\approx \left\{ \begin{array}{l} \text{At each particular } s\text{, approximate inner} \\ \text{integral by } k_1\text{-point parameterized} \\ \text{quadrature rule with weight } 1/\sqrt{1+t^2/c^2}. \end{array} \right\} \quad (7.29)$$

$$L \int_0^1 \Sigma_{1 \le i \le k_1} A_i g(scL, st_i L)\,ds \quad (7.30)$$

$$= \left\{ \begin{array}{l} \text{Parameter } c \text{ is independent of } s\text{, so } A_i \text{ and } t_i \\ \text{are the same at all } s \text{ and the summation and} \\ \text{integration can be reversed.} \end{array} \right\} \quad (7.31)$$

$$L \Sigma_{1 \le i \le k_1} A_i \int_0^1 g(scL, st_i L)\,ds \quad (7.32)$$

$$\approx \left\{ \begin{array}{l} \text{Approximate each } s \text{ integral (at constant } t_i\text{)} \\ \text{by } k_2\text{-point unit-weight Gauss rule with} \\ \text{weights } B_j \text{ and evaluation points } s_j \end{array} \right\} \quad (7.33)$$

$$L \Sigma_{1 \le i \le k_1} \Sigma_{1 \le j \le k_2} A_i B_j g(s_j cL, s_j t_i L) \quad (7.34)$$

If $g(x,y)$ is exactly a polynomial, the transformed integrand is also a polynomial (in s and t) at every step. Hence both the first parameterized integral and the subsequent conventional integral are exact if a sufficient number of points is used.

The interpretation of this transformation is that the inner t integral sweeps along a straight line at constant x coordinate. A small triangle aspect ratio c makes x small in comparison to the line length, so r behaves like that of a nearly-singular contour integral in the 2D BEM.

The kernels for elasticity have a leading r^{-1} singularity that is further multipled by various partial derivatives of r. The partial derivatives add powers of r to the denominator and powers of x and y to the numerator. The same transformation applied to r^{-1} gives

$$\int\int \frac{x^m y^n g(x,y)}{r^{m+n+1}}\,dx\,dy \tag{7.35}$$

$$\approx \int_0^1 \int_0^1 \frac{L}{c^{n+1}} \Sigma_{1\le i\le k_1} \Sigma_{1\le j\le k_2} A_i B_j g(s_j cL, s_j t_i L) \tag{7.36}$$

where A_i and t_i are from a parameterized rule for $w(t) = (1 + t^2/c^2)^{-(m+n+1)}$.

This applies to all weakly singular BIE integrals that remain after singular parts are subtracted off.

Near-Surface Integrals When the singular point is off of the surface, a single-parameter formula cannot exactly capture both a geometric parameter (such as the triangle aspect ratio above) *and* the distance to the surface. Fig. 7.7 gives geometry for a transformation to capture *one* direction of integration as a parameterized rule, leaving the other for conventional integration. Singular point $\overline{\mathbf{x}}$ is placed a distance d from a vertex of a surface triangle, and the triangle is determined by two vectors $\mathbf{u}$ and $\mathbf{v}$ along the indicated edges. A nearly singular integral over the triangle can be written

$$\int\int_S \frac{g(\mathbf{y})}{r^n}\,dS(\mathbf{y}) \tag{7.37}$$

$$= \left\{ \text{Transformation} \left\{ \begin{array}{c} \mathbf{y} = s\mathbf{u} + st\mathbf{v} \\ dS(\mathbf{y}) = s|\mathbf{u}\times\mathbf{v}|\,ds\,dt \end{array} \right. \right\} \tag{7.38}$$

$$\int_0^1 \int_0^1 \frac{sg(s\mathbf{u} + t\mathbf{v})}{d^{n/2}(1 + s^2|\mathbf{u} + t\mathbf{v}|^2/d^2)^{n/2}} |\mathbf{u}\times\mathbf{v}|\,ds\,dt \tag{7.39}$$

$$= \left\{ \text{Define } \overline{c}(t) = (1 + s^2|\mathbf{u} + t\mathbf{v}|^2/d^2)^{n/2} \right\} \tag{7.40}$$

$$\int_0^1 \int_0^1 \frac{sg(\mathbf{u} + t\mathbf{v})}{d^{n/2}(1 + s^2/\overline{c}^2)^{n/2}} |\mathbf{u}\times\mathbf{v}|\,ds\,dt \tag{7.41}$$

At a particular t, the integral along the ray from the origin to $\mathbf{u}+t\mathbf{v}$ is nearly singular, with a relative distance $\overline{c}(t)$ (valid *only* at this t) determined by d and

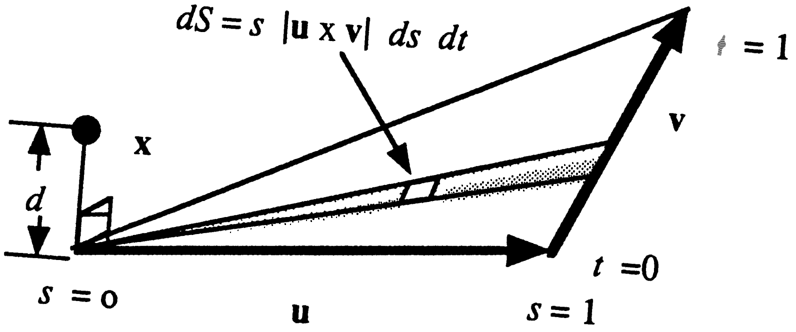

Figure 7.7: Geometry for near-singular integration over a triangle.

the length of the ray. Parameterized quadrature based on $\bar{c}(t)$ will give an accurate integral along the ray. The placement and weight of s points for different t values will be different, and are not polynomially related. An approximation to the integral can be obtained by using some quadrature method (e.g. unit weight quadrature) for the outer t integral and a parameterized rule for each inner s integral at each t value:

$$\int\int_S \frac{g(\mathbf{y})}{r^n dS(\mathbf{y})} \approx \Sigma_{1\leq j\leq k_2} B_j I(t_j) \tag{7.42}$$

where (7.43)

$$I(t_j) \quad = \Sigma_{1\leq i\leq k_1} A_i(t_j) \frac{g(s_i(t_j)\mathbf{u} + t_j v)}{d^{n/2}} |\mathbf{u}\times\mathbf{v}| \tag{7.44}$$

The $A_i(t_j)$ and $s_i(t_j)$ must be determined separately at each individual t_j for weight function $w(s) = s/(1+s^2/\bar{c}^2)^{n/2}$.

It is emphasized that for this case the quadrature rule is only approximate. The parameterized rule covers only the variation due to d. Variation due to c is not covered.

7.3.1 Curved Surfaces

For curved geometry, the r terms of the BIE kernels reduced to simple functions of a non-dimensional integrand and non-dimensional geometric parameter. However, in each of the geometries considered above the nondimensional parameter c can be interpreted as

$$c \sim \frac{\text{distance } d \text{ from singular point to integration line}}{\text{length of integration path}} \tag{7.45}$$

The analogous integration path on curved geometry (Fig. 7.8) is a (non-linear) function $\mathbf{y}(s)$ of the parameter s measured along the path, with tangent vector $\mathbf{T} = \frac{\partial}{\partial s}\mathbf{y}(0)$. If we define $\bar{c} = d/|\mathbf{T}|$ the quantity $q = \sqrt{1+s^2/\bar{c}^2}$ is very nearly

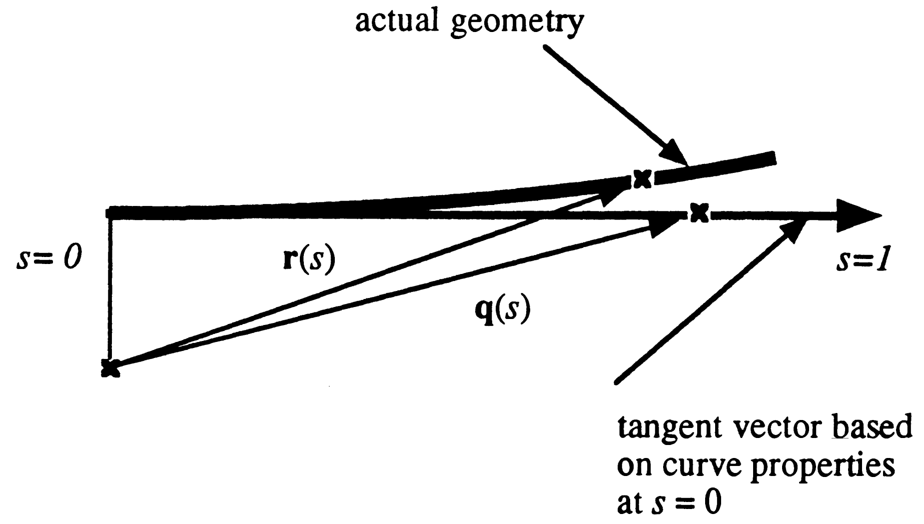

Figure 7.8: Geometry for near-singular integration over a curve.

proportional to $\mathbf{r}$ between $\overline{\mathbf{x}}$ and $\mathbf{y}(s)$. Then

$$\int_0^1 \frac{g(\mathbf{y})}{r^n}\, ds \equiv \int_0^1 \frac{1}{q^n} \frac{q^n}{r^n} g(\mathbf{y})\, ds \tag{7.46}$$

The ratio q/r will be nearly unit for mildly curved surfaces. Hence the integrand is transformed to a single-parameter singularity in q multiplying a non-polynomial but smooth function[2]. This step of multiplying and dividing by q is useful even in the planar case, for it gets the *form* of the singularity into the integrand without the tedious powers of L and c that appeared in the direct geometric derivations.

For working purposes, since q is a function of only s and c, the numerator term q^n can be built into the weights of the quadrature rule, so that the working form of the rule is

$$\begin{aligned}
& \int_0^1 \frac{1}{q^n} \frac{q^n}{r^n} g(\mathbf{y})\, ds && (7.47)\\
\approx\quad & \left\{ \begin{array}{l} \text{Apply quadrature rule with weights } A_i \text{ and} \\ \text{points } s_i \end{array} \right\} && (7.48)\\
& \textstyle\sum_{1\le i\le k} A_i \frac{q(s_i)^n}{r^n} g(s) && (7.49)\\
=\quad & \left\{ \text{Define working weights } B_i = A_i * q(s_i)^n \right\} && (7.50)\\
& \textstyle\sum_{1\le i\le k} B_i \frac{g(s)}{r^n} && (7.51)
\end{aligned}$$

Note that $f(s) = g(s)/r^n$ is present in its *original form*, i.e. with its singularity. With the modified weights B_i, the quadrature rule that cancels a weight of $1/q^n$ can be applied to any $f(s)$ without the need to explicitly separate the weight from the smooth part.

[2]The hypothetical line segment is *not* the projection of the curve to its tangent line. The line segment is on the (unbounded) tangent line, but has length determined only by the magnitude of the tangent vector at s=0. Changes in the tangent magnitude along the curve cause $\mathbf{r}(s)$ to be different from the projection of the curve point to the tangent line.

7.3.2 Mixed Degrees of Singularity

Each elasticity kernel has a leading singularity multiplying a sum of partial derivatives. Several different powers of r appear to be present in the terms of the sum. This seems to call for separate quadrature on each term. Since the various powers always differ by an even degree, multiplying and dividing the lower power terms by r^2 makes the sum uniform, as in (ignoring constant factors)

$$U_{ik} \approx \frac{1}{r}((3-4\nu)\delta_{ik} + r_{,i}r_{,k}) = \frac{1}{r^3}((3-4\nu)r^2\delta_{ik} + r_{,i}r_{,k}) \tag{7.52}$$

This manipulation does not actually have to be coded. It simply shows that U_{ik} 'has the form' of a r^{-3}singularity. The modified weights defined for curved surfaces can be applied directly to U_{ik} in its usual form.

Chapter 8

Implementation

This chapter describes design decisions required to apply hypersingular integrals to problems that include (1) cracks, (2) multiple material regions, and (3) boundary conditions expressed independent of global axes.

Chapter 1 gave a 6-part outline of the design decisions that lead to approximate methods of solving boundary value problems. In this implementation of a BIE-based method, these decisions are made as follows:

- **Issue:** Choose a physical condition to be enforced

  Decision: We will enforce a boundary integral condition, using both the primary and gradient forms of the integral.

- **Issue:** Linearize the physical condition

  Decision: Boundary integrals are linearized as described in Chapter 2

- **Issue:** Choose a geometry representation

  Decision: Surface geometry is represented by triangular and quadrilateral faces parameterized by linear or quadratic shape functions. Both faces of each crack must be present as separate geometrical entities; the meshing of opposing faces must be identical. Construction of this geometry is done in the FRANSYS (Fracture Analysis System) described by Martha [Mar89].

- **Issue:** Choose a representation of the unknown function

  Decision: Within each face, displacement and traction are represented as vector functions of the parametric coordinate within the face. This is carried out entirely independently on each face; both displacements and tractions at face boundaries (i.e. at common vertices and edges) may be *different* on each incident face. The construction generates (exactly) one displacement function and one basis function for each 'vertex-face use' of the solid topology.

- **Issue:** Define the boundary conditions

  Decision: At each vertex-face use of the surface, boundary conditions define 3 simultaneous linear equations among the 6 components of displacement and traction vectors.

- **Issue:** Enforce the physical condition in terms of the approximated function and boundary conditions

  Decision: The boundary integral equation and (in a crack) its gradient are enforced by collocation at certain points on the surface. Two methods are used to determine the points. The 'non-conforming displacement' method is guaranteed to produce the correct number of independent equations regardless of complexities due to cracks, assemblies of multiple regions with shared surfaces, and difficult combinations of boundary conditions. The collocations that it produces are always at smooth surface points, which assures that the derivative continuity conditions in the hypersingular gradient BIE will be met. For some geometric conditions, a 'conforming displacement method' is applied. This produces fewer and more numerically stable collocations, but cannot be applied in the cases noted above.

8.1 Geometry and Surface Representation

A 3D surface is represented by a collection of quasi-disjoint faces, as described for finite element analysis by Hughes [Hug87] and in boundary element analysis by Perucchio [Per84] and Gerstle [Ger86]. Each face is parameterized by a 1:1 mapping from a region of a reference ξ-η plane (Fig. 8.1). Each parametric coordinate (ξ,η) in the parametric domain is explicitly mapped to some geometric point $(x_1, x_2, x_3) = \mathbf{x}(\xi,\eta)$. Finite and boundary element methods have been strongly tied to this representation because of the ability to perform integrals and graphics display operations in terms of the coordinates in the simple squares and triangles of the parametric domain.

The mapping functions used are Lagrangian and 'serendipity' polynomial interpolation functions. Each geometric point $\mathbf{x}$ on the surface is given by

$$\mathbf{x}(\xi,\eta) = \Sigma_a N_a(\xi,\eta)\mathbf{x}_a \tag{8.1}$$

where the summation index a ranges over all the vertices of the parametric region, and the $N_a(\xi,\eta)$ are low order polynomials. Derivatives of the mapping define two in-surface tangents $\mathbf{t}_1$ and $\mathbf{t}_2$ and an (oriented) surface normal $\mathbf{n}$ by

$$\mathbf{t}_1(\xi,\eta) = \frac{\partial\mathbf{x}(\xi,\eta)}{\partial\xi} \quad \mathbf{t}_2(\xi,\eta) = \frac{\partial\mathbf{x}(\xi,\eta)}{\partial\eta} \quad \mathbf{n}(\xi,\eta) = \frac{\mathbf{t}_1 \times \mathbf{t}_2}{|\mathbf{t}_1 \times \mathbf{t}_2|} \tag{8.2}$$

Traction and displacement within a face are defined by the same basis functions as

$$\mathbf{u}(\mathbf{x}) = \Sigma_a N_a(\xi,\eta)\mathbf{u}_a \qquad \mathbf{p}(\mathbf{x}) = \Sigma_a N_a(\xi,\eta)\mathbf{p}_a \tag{8.3}$$

The quantities $\mathbf{u}_a$ and $\mathbf{p}_a$ are the degrees of freedom in the linearized BIE (Chapter 2). We will refer to them as control point values (rather than nodal values).

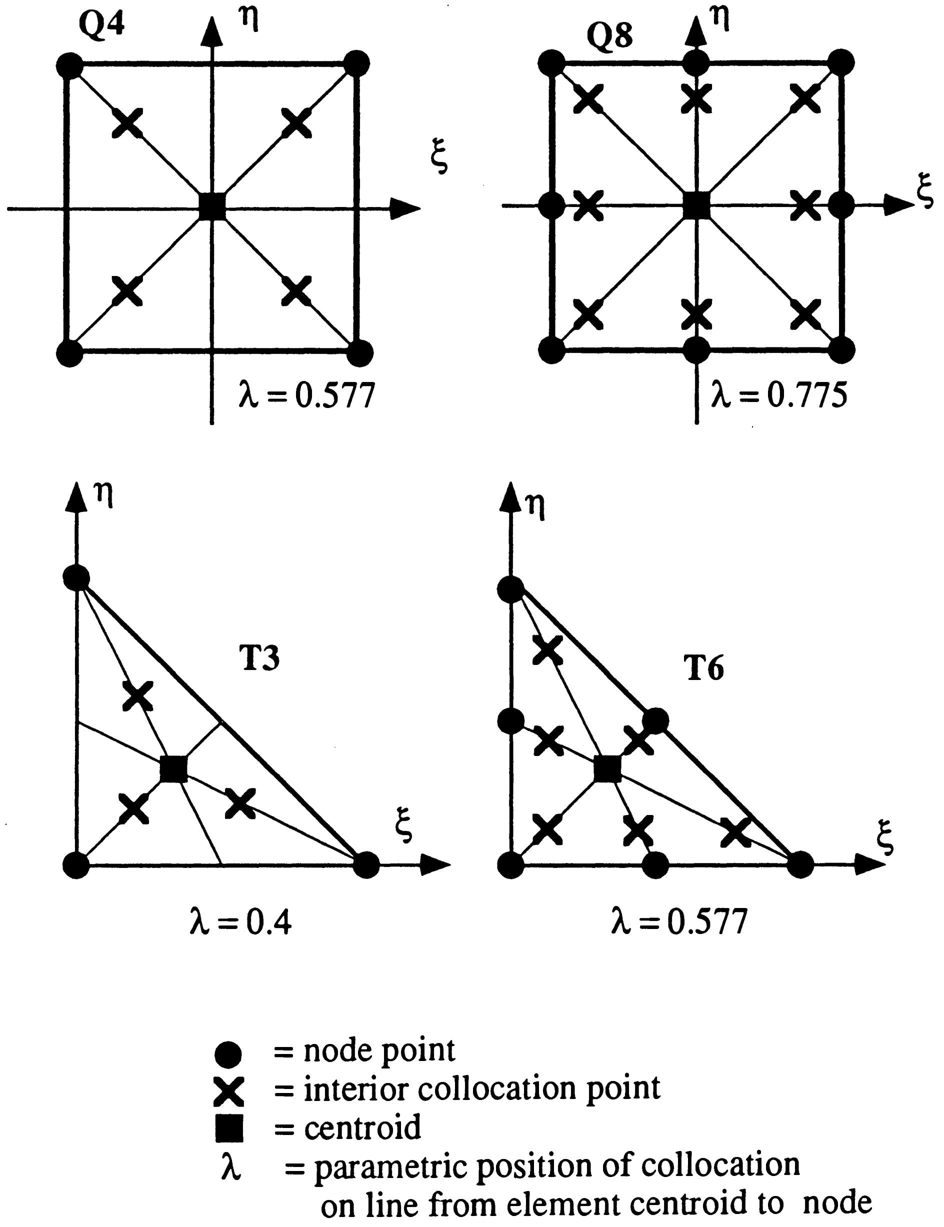

Figure 8.1: Parametric element types

When multiple faces share a single vertex, each face has its own degrees of freedom 'at the node' and (generally unequal) values of $\mathbf{u}(\mathbf{x})$ and $\mathbf{p}(\mathrm{x})$. To distinguish among the multiple values, we use the notion of a *vertex use* as given by Weiler [Wei86]. A vertex use is an artificial entity associated with the use of a vertex by a face (or vice versa). It may be thought of as a point in the interior of the face but arbitrarily close to the vertex. If $\overline{\mathbf{a}}$ denotes one such vertex use, we refer to the associated face, vertex, vertex coordinates, and normal of the face as $\overline{\mathbf{a}}$.face, $\overline{\mathbf{a}}$.vertex, $\overline{\mathbf{a}}.\mathbf{x}$, $\overline{\mathbf{a}}.\mathbf{n}$. Similarly, $\mathbf{v}$.VertexUses and $\mathbf{f}$.VertexUses will denote the (sets of) vertex uses associated with vertex $\mathbf{v}$ and face $\mathbf{f}$.

In a physical solution, *displacements* are always continuous at a vertex. *Tractions* have a more complicated physical relationship. Tractions can be discontinuous along a surface line passing through at vertex if (a) the surface tangent is discontinuous or (b) boundary conditions are discontinuous.

Parametric geometry and function representations allow C^0 continuity to be obtained by choosing any one incident vertex face use whose values are to be independent and constraining all others to match it. Higher order continuity, such as the C^1 continuity required for the hypersingular BIE, is significantly more difficult to obtain [Boi89].

When permitted (see below), function continuity is enforced among the various incident faces. However, we consider it a *normal* situation to have unequal function values on various incident elements.

8.2 Boundary Conditions

A boundary condition is a linear relationship between the traction and displacement vectors at a surface point. At a surface point $\mathbf{y}$ with surface normal $\mathbf{n}(\mathbf{y})$, boundary conditions are stated as a set of linear equations

$$\mathbf{Au} + \mathbf{Bp} = \mathbf{c} \tag{8.4}$$

where $\mathbf{A}$ and $\mathbf{B}$ are 3-by-3 and $\mathbf{c}$ is a 3 vector. $\mathbf{A}$, $\mathbf{B}$, and $\mathbf{c}$ are functions of the surface coordinates and normal. For example, a fixed displacement condition has $\mathbf{A}$=$\mathbf{I}$ and $\mathbf{B}$=$\mathbf{0}$, with $\mathbf{c}$ as the displacement value. A fixed traction condition has $\mathbf{A}$=0 and $\mathbf{B}$=$\mathbf{I}$, with $\mathbf{c}$(y) as the traction value. Cases where both $\mathbf{A}$ and $\mathbf{B}$ have nonzero entries (e.g. a 'roller' condition on an arbitrarily oriented surface) are summarized in Fig. 8.2 and Fig. 8.3.

8.3 Constraint equations

In a model with N_v vertex-face uses, the (non-conforming) definition of surface displacement and traction functions produces $2N_v$ unknown coefficients. We must produce $2N_v$ conditions that we wish the surface functions to satisfy. Cracks, multiple materials, and mixed boundary conditions make this process less than straightforward. Three types of 'validity' must be satisfied:

Structural Validity: A set of equations is structurally valid if it contains the same number of equations as unknowns.

Computability: A set of equations is computable if all of its coefficients can be computed.

Nonsingularity: A set of equations is nonsingular if its matrix has full row rank.

Structural validity is simply a counting property. Since we know *a priori* that there are exactly 2 (vector) control point values per vertex-face use, we can redefine structural validity as:

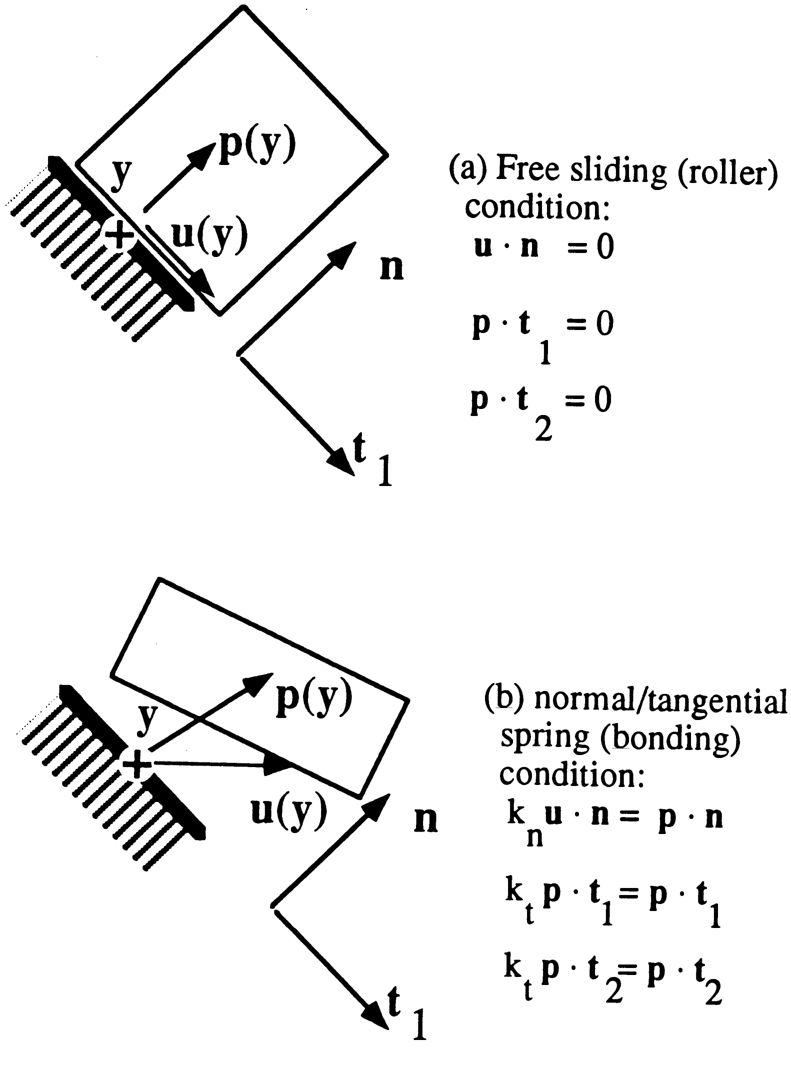

Figure 8.2: Examples of boundary conditions expressed relative to normal and tangential orientations

Condition	$\mathbf{A}$	$\mathbf{B}$	$\mathbf{c}$
Displacement $\overline{\mathbf{u}}$ in global coordinates	$\mathbf{I}$	$\mathbf{0}$	$\overline{\mathbf{u}}$
Traction $\overline{\mathbf{p}}$ in global coordinates	$\mathbf{0}$	$\mathbf{I}$	$\overline{\mathbf{p}}$
Pressure a on surface	$\mathbf{0}$	$\begin{bmatrix} \mathbf{n}^T \\ \mathbf{t}_1{}^T \\ \mathbf{t}_2{}^T \end{bmatrix}$	$\begin{bmatrix} -a \\ 0 \\ 0 \end{bmatrix}$
roller	$\begin{bmatrix} \mathbf{n}^T \\ \mathbf{0} \\ \mathbf{0} \end{bmatrix}$	$\begin{bmatrix} \mathbf{0} \\ \mathbf{t}_1{}^T \\ \mathbf{t}_1{}^T \end{bmatrix}$	$\begin{bmatrix} 0 \\ 0 \\ 0 \end{bmatrix}$
normal spring stiffness k_n, tangential spring stiffness k_t	$\begin{bmatrix} k_n \mathbf{n}^T \\ k_t \mathbf{t}_1{}^T \\ \mathbf{k}_t t_2{}^T \end{bmatrix}$	$-\begin{bmatrix} \mathbf{n}^T \\ \mathbf{t}_1{}^T \\ \mathbf{t}_2{}^T \end{bmatrix}$	$\begin{bmatrix} 0 \\ 0 \\ 0 \end{bmatrix}$

Figure 8.3: Boundary condition matrices

Structural Validity (vertex-face use version) A set of equations is structurally valid if and only if it contains exactly 2 (vector) equations for each vertex-face use.

Computability depends on the singular integration analysis of Chapter 4 and Chapter 5:

The integrals in the primary BIE are computable for surface point $\bar{\mathbf{x}}$ if the primary unknown $\mathbf{u}$ has C^0 continuity at $\bar{\mathbf{x}}$.

The integrals in the gradient BIE are computable for surface point $\bar{\mathbf{x}}$ if the primary unknown $\mathbf{u}$ has C^1 continuity in a cartesian (not parametric) Taylor series centered at $\bar{\mathbf{x}}$.

Nonsingularity depends on the rows of the matrix being based on physically independent conditions. For non-crack problems, collocations at distinct points in distinct regions are independent. In a crack, a primary and gradient BIE are independent of one another.

We present 3 methods of constructing sets of equations. The 'non-conforming' Method 1 satisfies all validity conditions. However, it has numerous undesirable computational properties. Method 2 is a more conventional node-based 'conforming' construction. It is invalid for certain combinations of geometry and boundary conditions. Method 3 combines the two, choosing one or the other on a vertex-by-vertex basis.

Types of Equations Five types of equations are available: boundary conditions, displacement and traction continuity, and collocation of the primary and gradient

BIE. Fig. 8.4 describes parameters necessary to apply each of these. There are important differences among the conditions under which each of the equation constructions can proceed. Continuity procedures can be applied arbitrarily; boundary conditions require only the availability of the boundary condition coefficients $\mathbf{A}$, $\mathbf{B}$, and $\mathbf{c}$. Primary and BIE equations require, respectively, C^0 and C^1 continuity of the surface functions at the surface point where they are constructed.

Method 1: Nonconforming Constraints There is one displacement unknown $\mathbf{u}_a$ and one traction unknown $\mathbf{p}_a$ for each vertex-face use. An equal number of constraint equations is obtained by constructing (a) one boundary integral condition for each of the (one or two) incident material regions and (b) a boundary condition equation for the non-material side of the face. Fig. 8.5 summarizes the decision process at each vertex-face use.

If the procedure is applied to *all* vertex-face uses in a model, the resulting equations have guaranteed structural validity because exactly two equations are constructed for each vertex use.

The equations that are constructed are guaranteed to be linearly independent as long as the collocation points are distinct at all vertex-face uses. This condition is assured by placing the collocation point for vertex-face use **a** along the (parametric space) line from the vertex to the face centroid. The parametric coordinates of this point **a**.collocation_pt are

$$(\overline{\xi,\eta}) = (\xi,\eta)_{\mathbf{v}} + \lambda((\xi,\eta)_{\mathbf{c}} - (\xi,\eta)_{\mathbf{v}}) \tag{8.5}$$

where **c** and **v** identify parametric coordinates of the vertex and the centroid and $0 < \lambda < 1$. The parameters λ is chosen to place the collocation points close to the evaluation points for a quadrature rule with the same number of points as there are vertex-face uses on the face (see Fig. 8.1).

Parameter	Description
$\mathbf{a}$	vertex-face use
$\bar{\mathbf{a}}$	vertex face use
$\mathbf{A}$,$\mathbf{B}$,$\mathbf{c}$	Matrices and vectors of boundary conditions
$\bar{\mathbf{x}}$	surface point
$\mathbf{f}$	face

Equation Type	Equation Constructed	Continuity Requirements
Boundary condition	$\mathbf{Au}(\mathbf{a}) + \mathbf{Bp}(\mathbf{a}) = \mathbf{c}$	
Traction continuity	$\mathbf{p}(\mathbf{a}) = \mathbf{p}(\bar{\mathbf{a}})$	
Displacement continuity	$\mathbf{u}(\mathbf{a}) = \mathbf{u}(\bar{\mathbf{a}})$	
Primary BIE collocation	$\mathbf{u}(\bar{\mathbf{x}}, \mathbf{f}) = \int_S \mathbf{Up} - \mathbf{Pu}\, dS$	C^0
Gradient BIE collocation	$\mathbf{p}(\bar{\mathbf{x}}, \mathbf{f}) = \int_S \mathbf{Dp} - \mathbf{Su}\, dS$	C^1

Figure 8.4: Types of equations

The resulting equations are undesirable in that (a) they allow physically nonrealistic discontinuities in the displacement function, (b) they are placed very close to edges, leading to difficult 'nearly singular' integrals over adjacent faces and over closure surfaces.

Method 2: Conforming Construction Under certain circumstances, it is possible to require that (a) displacements $\mathbf{u}_a$ on vertex-face uses incident to a common vertex be identical, and (b) tractions on adjacent vertex-face uses with a common surface normal be identical.

At a smooth vertex, these continuity requirements provide equations for all but one unknown traction and displacement at a vertex. A single boundary condition and collocation complete the set of equations for the vertex.

At a non-smooth vertex (i.e. a corner or edge), each incident surface will have (a) a boundary condition equation and (b) a traction vector independent of the others. The determination of which tractions are eliminated by the boundary conditions and which remain independent can be done on a face-by-face and axis-by-axis basis only for special cases. A more general solution is to (a) construct a matrix that contains all incident boundary conditions and (b) use the rank of the matrix to determine whether the boundary conditions eliminate enough tractions to allow collocation *at* the vertex instead of *around* the vertex.

Definition: A *traction sector* is a set of contiguous vertex-face uses that have the same boundary conditions and identical surface normal at their shared vertex.

Definition: The composite boundary condition equations at a vertex are the

```
procedure Non-Conforming Constraints(A)
  Uses arguments or global quantities:
    A — Set of vertex uses
  Computes: Linear constraint equations at each vertex use a in A
  Precondition: Two (2) degrees of freedom are defined
    for each a in A.
  Postcondition: Two (2) linear equations are defined
    for each a in A.
  for each  vertex-face use a do
    for each  region R in {f.InsideRegion,f.OutsideRegion} do
      if     R is a boundary condition region then
        Enforce boundary condition equation
          at a.vertex on a.face
      elseif R is a material region then
        if     a.face is a non-crack face or a main crack face then
          Enforce primary boundary integral
            over the surface of R
            for point x̄=a.collocation_pt
        elseif x̄ is a secondary crack surface then
          Enforce primary boundary integral
            over the surface of R
            for point x̄=a.collocation_pt
        endif
      endif
    endfor
  endfor
```

Figure 8.5: Construction of equations for non-conforming surface functions

equations

$$\mathbf{D}\begin{bmatrix}\mathbf{u}\\ \mathbf{p}_1\\ \mathbf{p}_2\\ \mathbf{p}_3\\ \vdots\end{bmatrix} = \begin{bmatrix}\mathbf{A}_1 & \mathbf{B}_1 & 0 & 0 & \cdots\\ \mathbf{A}_2 & 0 & \mathbf{B}_2 & 0 & \cdots\\ \mathbf{A}_2 & 0 & 0 & \mathbf{B}_3 & \cdots\\ \vdots & & & & \end{bmatrix}\begin{bmatrix}\mathbf{u}\\ \mathbf{p}_1\\ \mathbf{p}_2\\ \mathbf{p}_3\\ \vdots\end{bmatrix} = \begin{bmatrix}\mathbf{c}_1\\ \mathbf{c}_2\\ \mathbf{c}_3\\ \vdots\end{bmatrix} \tag{8.6}$$

where $\mathbf{A}_i$, $\mathbf{B}_i$, and $\mathbf{c}_i$ are the boundary condition matrices for the traction sectors around the vertex, $\mathbf{u}_1$ is the displacement of an arbitrarily chosen vertex-face use, and $\mathbf{p}_i$ a traction in some arbitrarily chosen vertex-face use on sector i. The size of this matrix $\mathbf{D}$ for a vertex with n traction sectors is $3n \times (3n+3)$.

A single collocation 'at a node' is sufficient to restrain the degrees of freedom at all incident vertex-face uses if and only if the rank of the composite matrix plus the number of collocation equations (number of incident regions) equals the total number of traction and displacement unknowns on all incident sectors, i.e.

$$\text{rank}(\mathbf{D}) + 3n_R = 3 + n_T$$

where n_R and n_T are the number of material regions and traction sectors at the vertex.

The algorithm in Fig. 8.6 constructs a single BIE equation and the composite boundary condition equations at a vertex.

The algorithm always produces a structurally valid set of equations. However, the equations are physically valid if and only if all rows of the composite boundary condition matrix are linearly independent.

Method 3: Mixed Construction A mixed conforming/non-conforming construction is obtained by deciding, on a vertex-by-vertex basis, whether all the con-

```
procedure Conforming Constraints(v)
    Uses arguments or global quantities:
        v — Vertex
        v.VertexUses — the set of vertex-face uses at v
        v.TractionSectors — the set of traction sectors (sets of vertex-face uses) at v.
    Computes: Equations to enforce boundary conditions, continuity, and BIE
        at a vertex, using generalized rank analysis
    Precondition: Two (2) degrees of freedom are defined
        for each vertex-face use around v.
    Postcondition: Two (2) linear equations are defined
        for each vertex use around v.
    — Enforce displacement continuity by equating all
    — displacements to one arbitrarily chosen displace-
        ment
    choose any ā from v.VertexUses
    for each region R incident to v do
        Enforce the primary boundary integral over region R at v
    endfor
    for each a in v.VertexUses-{ā} do
        Enforce displacement compatibility equation u(a) = u(ā)
    endfor
    for each A in v.TractionSectors do
        choose any ā from v.VertexUses
        Enforce boundary condition equation
            Au(a) + p(a) = c
        for each a in A do
            Enforce traction compatibility equation p(a) = p(ā)
        endfor
    endfor
```

Figure 8.6: Construction of conforming nodal equations with general boundary conditions

ditions necessary for nodal collocation are satisfied. The selection of conforming or non-conforming equations is then

```
for each vertex v do
   if    Boundary condition equations have full row rank
     and v is not a crack surface or crack edge point then
       Conforming Constraints(v)
   else
       Non-conforming Constraints(v.VertexUses)
   endif
endfor
```

8.4 Linear System Solution

The constraint construction described above defines a valid set of equations for a more general selection of boundary conditions and special geometries than is usually considered by boundary element programs. The immediate cost of this generality is that the full set of equations for a model with N vertex-face uses contains $6N$ scalar equations, whereas a boundary element method is usually claimed (e.g. [BB81]) to produce 'only' $3M$ equations, where M, the number of *vertices* (rather than face uses) is typically a factor of 4 to 6 *smaller than* N.[1]. Hence a full matrix form of the equations will have the number of equations, the storage requirements, and the factorization time increased by a factor of 8, 64, and 512 (for quadrilaterals) and 12, 144, and 1728 (for triangles).

This problem is addressed by treating the matrix factorization as a two step process. The first step treats only the sparse equations due to boundary conditions and explicit continuity conditions. The collocation equations, whose matrix rows are dense, are treated in a second step. Because the boundary conditions and con-

[1]A regular quadrilateral mesh has 4 vertex-face uses per vertex. Adding a diagonal to each quadrilateral raises this (on average) to 6.

tinuity equations are extremely sparse, the NP-complete worst-case characteristics of sparse factorization (George and Liu [GL81]) are never encountered, and the overhead of the sparse factorization is minimal.

Suppose that a linear system **Ax=b** is partitioned as

$$\mathbf{Ax} = \begin{bmatrix} \mathbf{A}_{aa} & \mathbf{A}_{ab} \\ \mathbf{A}_{ba} & \mathbf{A}_{bb} \end{bmatrix} \begin{bmatrix} \mathbf{x}_a \\ \mathbf{x}_b \end{bmatrix} = \begin{bmatrix} \mathbf{b}_a \\ \mathbf{b}_b \end{bmatrix} = \mathbf{b} \tag{8.7}$$

where $\mathbf{A}_{aa}$ and $\mathbf{A}_{ab}$ are sparse and the diagonal blocks $\mathbf{A}_{aa}$ and $\mathbf{A}_{bb}$ are square and nonsingular. If $\mathbf{A}_{aa}$ and $\mathbf{A}_{ab}$ have full row rank, the upper portion may be prefactored , leaving a smaller system

$$\mathbf{Bx}_b = \mathbf{d}_b \tag{8.8}$$

to be solved, where $\mathbf{B}$, $\mathbf{x}_b$, and $\mathbf{d}_b$ are as defined in Fig. 8.7. If $\mathbf{A}_{aa}$ and A_{ab} are 'sparse' and $\mathbf{A}_{ba}$ and $\mathbf{A}_{bb}$ are 'dense', this factorization allows separate handling of the two parts without resorting to axis-specific reasoning that is usually used to reduce a boundary element method to solution of a small, dense set of equations.

When solving a BIE problem for a single set of boundary conditions, the constraint equations are divided between 'sparse' and 'dense' parts of the matrix as follows:

$$\begin{bmatrix} \mathbf{A}_{aa} & \mathbf{A}_{ab} \\ \mathbf{A}_{ba} & \mathbf{A}_{bb} \end{bmatrix} \begin{bmatrix} \mathbf{x}_a \\ \mathbf{x}_b \end{bmatrix} = \begin{bmatrix} \mathbf{b}_a \\ \mathbf{b}_b \end{bmatrix} \tag{8.9}$$

$$\Leftrightarrow \quad \{ \text{ Linear algebra, assuming } A_{aa} \text{ nonsingular } \} \tag{8.10}$$

$$\mathbf{x}_a = \mathbf{A}_{aa}{}^{-1}\mathbf{b}_a - \mathbf{A}_{aa}{}^{-1}\mathbf{A}_{ab}\mathbf{x}_b \tag{8.11}$$

$$(\mathbf{A}_{bb} - \mathbf{A}_{ba}\mathbf{A}_{aa}{}^{-1}\mathbf{A}_{ab})\mathbf{x}_b = \mathbf{b}_b - \mathbf{A}_{ba}\mathbf{A}_{aa}{}^{-1}\mathbf{b}_a \tag{8.12}$$

$$\Leftrightarrow \quad \left\{ \text{Define} \left\{ \begin{array}{rcl} \mathbf{C} & = & \mathbf{A}_{aa}{}^{-1}\mathbf{A}_{ab} \\ \mathbf{c} & = & \mathbf{A}_{aa}{}^{-1}\mathbf{b}_a \\ \mathbf{B} & = & (\mathbf{A}_{bb} - \mathbf{A}_{ba}\mathbf{C}) \\ \mathbf{d}_b & = & \mathbf{b}_b - \mathbf{A}_{ba}\mathbf{c} \end{array} \right. \right\} \tag{8.13}$$

$$\mathbf{B}\mathbf{x}_b = \mathbf{d}_b \tag{8.14}$$

Figure 8.7: Isolating a small dense system from **Ax=b**

Equation type	matrix assignment
Displacement continuity	sparse
Traction continuity	sparse
Boundary conditions	sparse
Primary Collocations	dense
Gradient Collocations	dense

Assembly Logic The matrices $\mathbf{A}_{ab}$ and $\mathbf{A}_{aa}$ are substantially smaller than the overall matrix. However, they are still so large that full storage is impossible.

Therefore, a procedure that generates $\mathbf{A}_{ba}$ and $\mathbf{A}_{bb}$ must be able to add each entry directly to $\mathbf{B}$ and $\mathbf{b}$. The logic for this operation is:

procedure Assemble Coefficient to Linear System(a)
Uses arguments or global quantities:
a — coefficient of $\mathbf{A}_{ab}$ or $\mathbf{A}_{bb}$
Computes: Assembles one coefficient into the $\mathbf{B}$ matrix
Precondition: a is a part of $\mathbf{A}_{ba}$ or $\mathbf{A}_{bb}$
Postcondition: a is accumulated to $\mathbf{B}$ and $\mathbf{d}_b$
if a is entry ij of $\mathbf{A}_{bb}$ **then**
Add **a** directly to entry ij of $\mathbf{B}$
elseif a is entry ij of $\mathbf{A}_{bb}$ **then**
Subtract ac_j from $\mathbf{d}_{bi}$
Subtract a·(row j of $\mathbf{C}$) from row i of $\mathbf{B}$
endif
end procedure

Comparison to Usual Analysis For the special case when boundary conditions vectors are stated only as fixed values of x, y, and z components of $\mathbf{u}$ and $\mathbf{p}$ (i.e. if we do not allow sliding conditions or other general boundary conditions on general planes), the $\mathbf{A}_{aa}$ part of the sparse matrix is just an identity, the $\mathbf{A}_{ab}$ part is zero, and the right hand side $\mathbf{b}_a$ contains the fixed traction and displacement components. The final dense system $\mathbf{B}\mathbf{x}_b=\mathbf{d}_b$ simplifies to

$$\mathbf{A}_{bb}\mathbf{x}_b = \mathbf{b}_b - \mathbf{A}_{ba}\mathbf{b}_a \tag{8.15}$$

Applying the general analysis thus produces the same dense system as is normally obtained, but allows more general boundary conditions to be applied.

Implementation of Sparse Matrix Handling The sparse matrix handling is implemented using sparse matrix software described in Kundert [Kun86]. This

General Form	Factored Form
$\overline{\mathbf{A}} = \begin{bmatrix} \mathbf{A}_{aa} & \mathbf{A}_{ab} \end{bmatrix}$	$\overline{\mathbf{A}} = \mathbf{L}\begin{bmatrix} \mathbf{U}_{aa} & \mathbf{U}_{ab} \end{bmatrix}$ (**L** lower triangular) ($\mathbf{U}_{aa}$ upper triangular)
$\mathbf{A}_{aa}{}^{-1}$	$\mathbf{U}_{aa}{}^{-1}\mathbf{L}^{-1}$
$\mathbf{c} = \mathbf{A}_{aa}{}^{-1}\mathbf{b}_a$	$\mathbf{c} = \mathbf{U}_{aa}{}^{-1}\mathbf{L}^{-1}\mathbf{b}_a$
$\mathbf{C} = \mathbf{A}_{aa}{}^{-1}\mathbf{A}_{ab}$	$\mathbf{C} = \mathbf{U}_{aa}{}^{-1}\mathbf{U}_{ab}$
$\mathbf{x}_a = \mathbf{A}_{aa}{}^{-1}\mathbf{b}_a - \mathbf{A}_{aa}{}^{-1}\mathbf{A}_{ab}\mathbf{x}_b$	$\mathbf{x}_a = \mathbf{c} - \mathbf{C}\mathbf{x}_b$ $= \mathbf{L}^{-1}\mathbf{U}_{aa}{}^{-1}\mathbf{b}_a$ $-\mathbf{U}_{aa}{}^{-1}\mathbf{U}_{ab}\mathbf{x}_b$

Figure 8.8: **C** and *c* expressed in terms of factored form of sparse part of matrix

produces an **LU** factorization of the sparse portion of the matrix. Fig. 8.8 gives expressions for the **C** and **c** of Fig. 8.7 in terms of the **LU** factorization.

If multiple cases are to be run with different values of the right-hand sides of selected boundary conditions, those boundary condition equations are placed in the dense portion and treated as full equations.

Chapter 9

Examples of 3D Crack Computations

The critical test of a linear crack analysis method is its ability to compute *stress intensity factors* that quantify the stress state around the crack front. Section 1 describes stress intensity factors and how they are computed from displacements received from analysis using the hypersingular integration methods.

Sections 2, 3, and 4 consider three calibration problems for which accurate analytic results are known:

- Elliptical Interior Crack in an infinite medium with given far field stress
- Semicircular surface crack with internal pressure
- Compact Tension Test specimen

Section 5 is an analysis of possible crack growth in the shuttle fuel door hinge mount used as an example in Chapter 1.

The conclusions reached on the benchmarks are as follows:

- The method is able to produce K factors accurate to within a few percent.

- The meshes required for accurate results are remarkably coarse. It must be remembered that the use of nonconforming surface functions introduces roughly 4 times as many degrees of freedom per vertex as conforming methods, so a nonconforming computation has as many degrees of freedom as a conforming method with a more refined mesh.

- The convergence characteristics – i.e. relationship of mesh size to accuracy – are not always consistent. Results from the semicircular surface crack show regular improvement with mesh refinement. The interior elliptical crack has only 1% error on its coarsest mesh, but slightly larger errors with some refined meshes.

These results reinforce the basic principles that (1) all finite and boundary element solutions should be compared to some other estimate, however crude, that provides an order of magnitude check on validity, and (2) one should always perform several analyses to get a feel for mesh sensitivity.

9.1 Stress Intensity Factors

Exact analysis of the stress field in the vicinity of cracks in simple geometries under the assumption of purely linear elastic material behavior shows two critical characteristics. First, stress front are infinite for points approaching the crack front. Second, a series expansion of the displacement and stress fields in a polar coordinate system centered at the crack tip takes the form

$$\text{displacement component } i = \textstyle\sum_{m\in\{I,II,III\}} K_m f_{im}(\theta)\sqrt{r} \tag{9.1}$$

$$\text{stress component } ij = \textstyle\sum_{m\in\{I,II,III\}} \frac{K_m g_{ijm}(\theta)}{\sqrt{r}} \tag{9.2}$$

The terms K_I, K_{II}, and K_{III} are determined by the crack geometry and loading, but are independent of r and θ. The functions f_{im} and g_{ijm} contain angular effects. *All* stress components are (under the assumption of linear behavior at all stress levels) driven to infinity by the division by $\sqrt{r}$.

The terms K_I, K_{II}, and K_{III} have interpretations as the 'stress intensity factors' due to particular types of loading. K_I is related to loads normal to the crack face, K_{II} to shearing along the crack face and normal to the crack front, and K_{III} due to shearing along the crack face and tangent to the crack front.

Real materials are never able to duplicate these infinite stresses exactly. However, it is experimentally observed that under a given loading condition a crack will either grow or remain stable depending on the relationship of K_I, K_{II}, and K_{III} to threshold levels that are material properties. These factors, rather than absolute stress levels, are thus the interesting measurable quantity for crack geometries. The following analogy holds between stress components σ_{ij} and stress intensity factors K_m:

Case	Quantity determined by geometry and loading	Material Property	"Failure condition"
stress field away from all crack tips	maximum principle stress σ_{11}	σ_{yield} (yield strength)	$\sigma 11 \geq \sigma_{\text{yield}}$
crack-tip stress field	mode I SIF K_I	K_{Ic} (Fracture toughness)	$K_I \geq K_{Ic}$

In each of the test cases described below, displacements are computed by collocation of the primary and gradient BIE conditions, implemented as described in

Chapter 8. These displacements are returned to the FRANSYS interactive modeling system.[1] FRANSYS computes approximate K_I, K_{II}, and K_{III} factors for the given displacements by applying the approximations

$$\begin{bmatrix} K_I \\ K_{II} \\ K_{III} \end{bmatrix} = \begin{bmatrix} \Delta u_n \\ \Delta u_t \\ \Delta u_s(1+\nu) \end{bmatrix} \frac{E}{4(1-\nu^2)} \sqrt{\frac{\pi}{2r}} \tag{9.3}$$

where r is distance from the crack front to a point on the crack face, u_n is crack opening normal to the face, and u_t and u_s are tangential displacements of top and bottom face points in directions normal and parallel to the crack front, respectively.

In the examples that follow, formulae in (9.3), are applied using displacements in the first row of nodes behind the crack front to determine Δu_n, Δu_t, and Δu_s. Geometric manipulations to support this are described in Sousa [SMWI89].

9.2 Interior Elliptical Crack

Fig. 9.1 shows a large block containing a small elliptical crack at its center. The block is loaded in pure tension, with the tension oriented at 45 degrees from the crack face. Analytic results for this geometry and load are found in Tada, Paris, and Irwin [TPI73].

Fig. 9.2 shows 4 meshes on the crack face. The base mesh (a) has 12 elements around the circumference and 2 bands of quadrilateral elements around a central transition mesh. Meshes (b) and (c) add rows of quadrilaterals. Mesh (d) has the number of elements along the crack front doubled.

Figures 9.3, 9.4, and 9.5 show the analytic and computed K_I, K_{II}, and K_{III} for the four meshes, obtained using linear elements. Fig. 9.6 shows the K_I values

[1] FRANSYS (FRacture ANalysis SYstem) has no relationship to ANSYS, a product of Swanson Analysis Systems.

Table 9.1: Extreme K values on elliptical crack

Case	min K_I	max K_I	max K_{II}	max K_{III}
Analytic	.183	.259	.224	.238
(a)	.178	.261	.225	.244
(b)	.181	.269	.231	.252
(d)	.176	.262	.225	.245
(c)	.188	.269	.236	.251
(a) quad	.174	.257	.234	.238
(b) quad	.180	.260	.230	.252

for meshes (a) and (b) using quadratic elements. Numeric values of the extrema are in Table 9.1.

In the angular refinement sequence (meshes (a), (b), and (c)), the coarsest and finest meshes produce peak K_I within 2% of the analytic results. Both the intermediate mesh (b) and the angular refinement (d) are in error by about 4%. The quadratic versions of (a) and (b) are within 2% of maximum K_I. Minimum K_I have somewhat larger error. K_{II} and K_{III} have comparable accuracy.

9.3 Semicircular Surface Crack

Fig. 9.7 shows a semicircular surface crack in a half-infinite medium. The surface containing the crack edge has roller boundary conditions (fixed displacement normal to the surface, no tangential traction). The crack is loaded by uniform internal pressure. Because of symmetry, the crack behaves like half of a full circular crack in an infinite medium. For pressure p and radius a, analytic results ([TPI73]) give $K_I = 2p\sqrt{a/\pi}$. For $a = 1$ and $p = 4$, this is $K_I = 2.256$. K_{II} and K_{III} are both

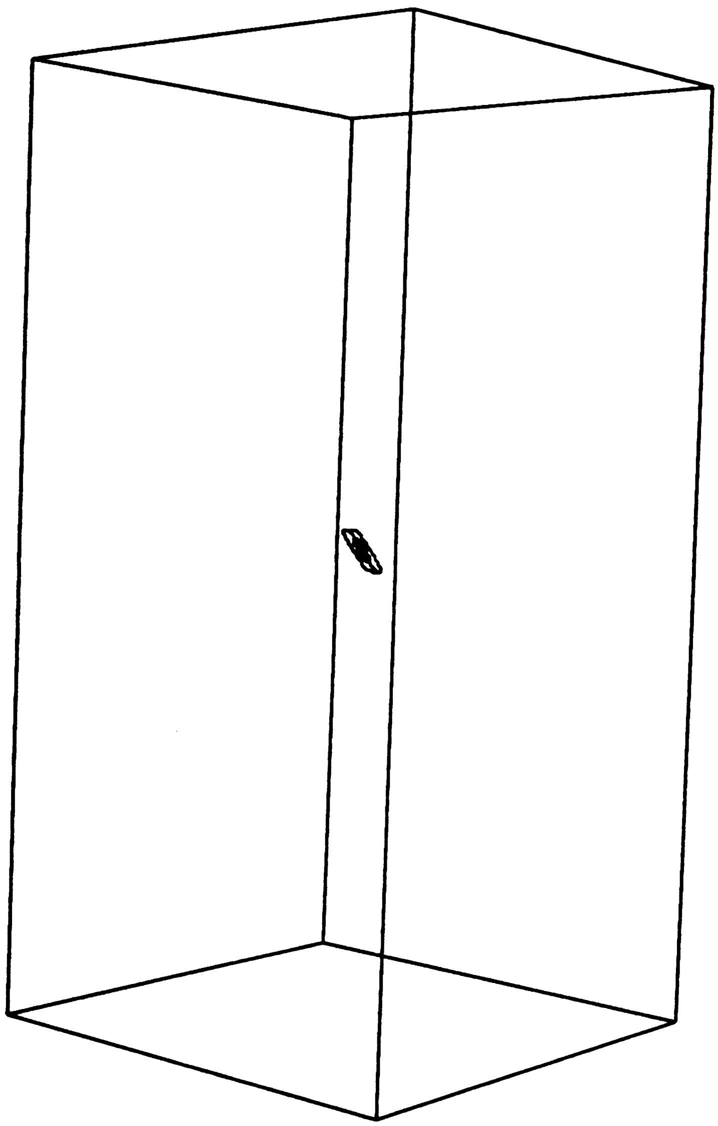

Figure 9.1: Internal elliptical crack

(continued on next page)

edge view of axis AA

plane of ellipse

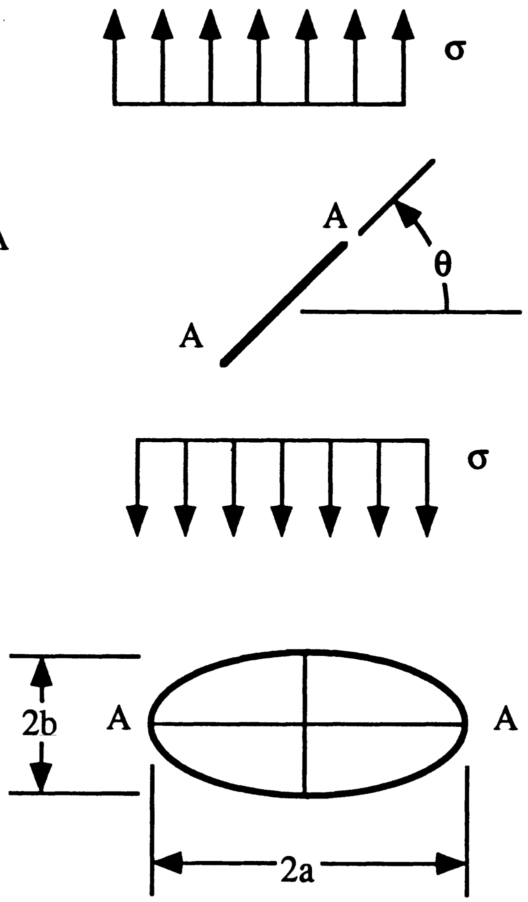

dimensions

σ	1	free field stress
θ	$\pi/4$	inclination
a	0.25	major semiaxis
b	0.125	minor semiaxis
E	10000	elastic modulus
ν	0.25	poisson's ratio

Fig. 9.1 (continued from previous page) Internal elliptical crack

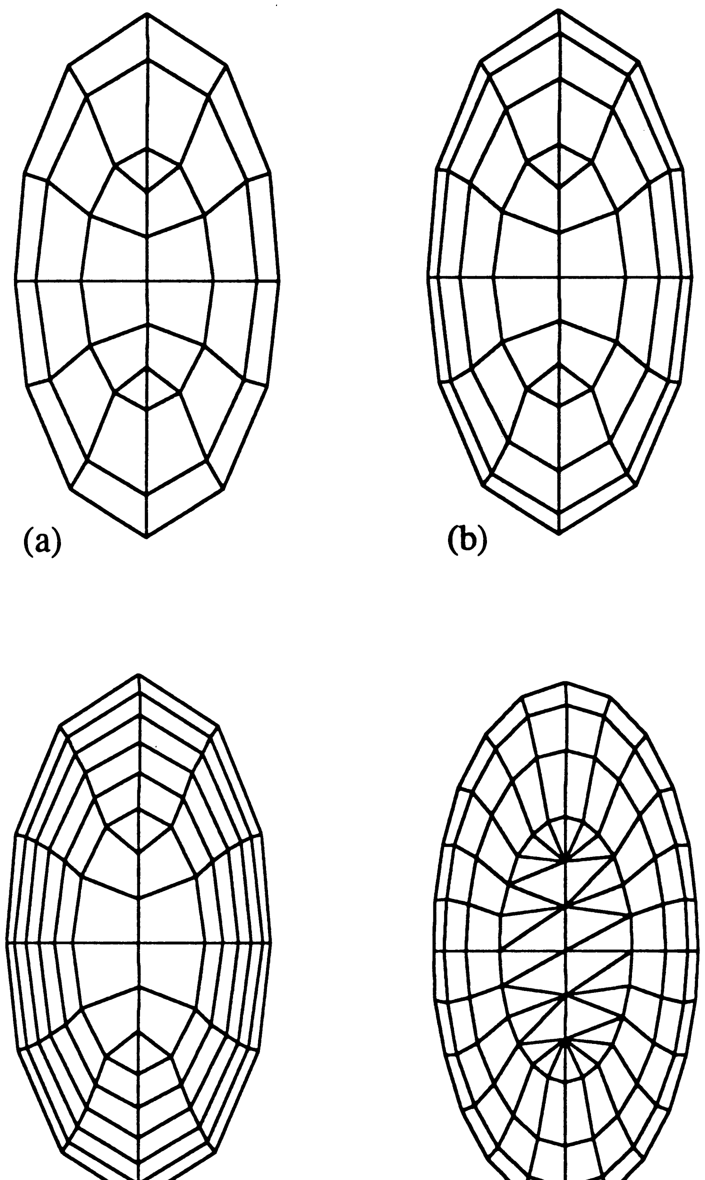

Figure 9.2: Meshes on elliptical crack

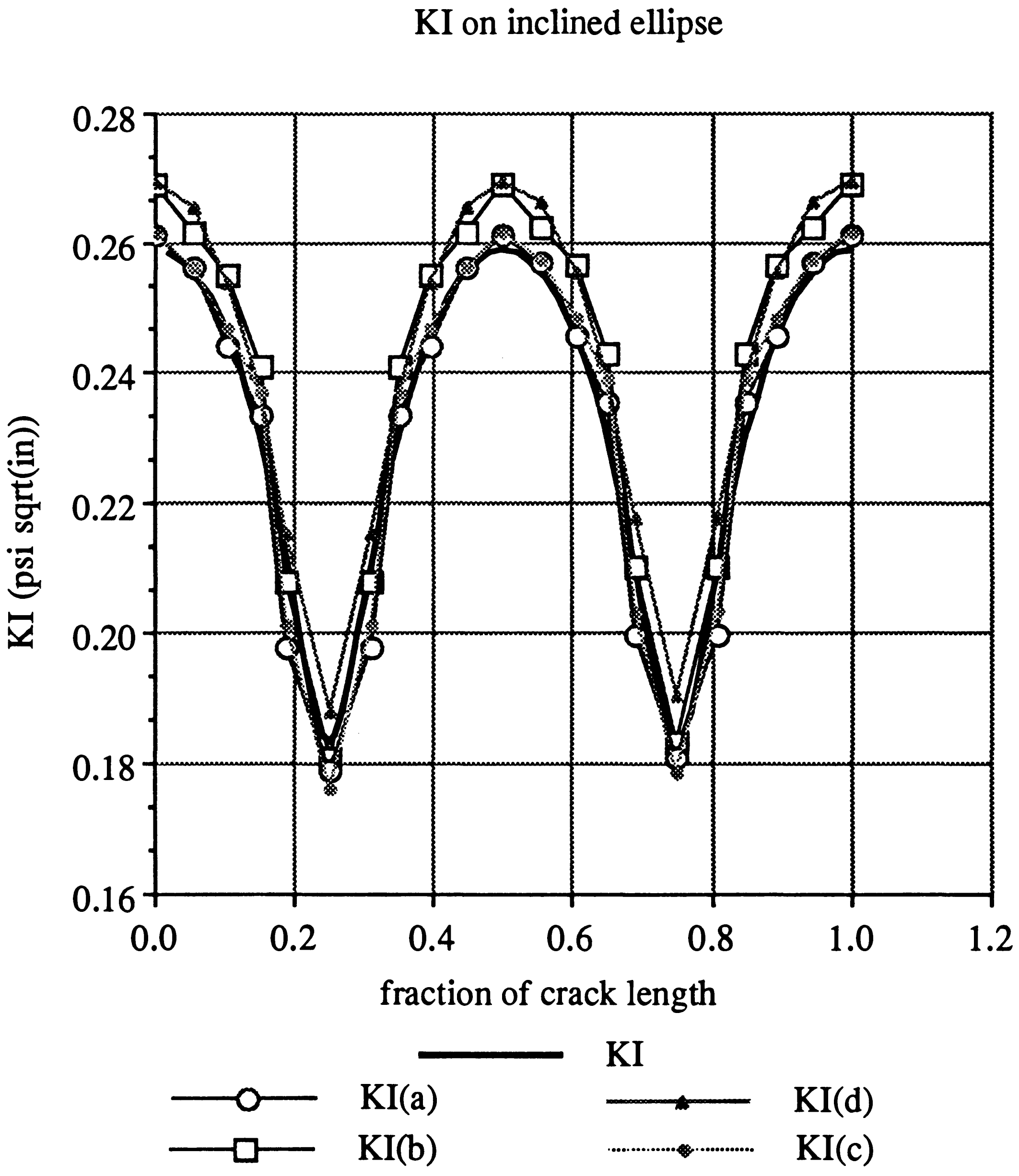

Figure 9.3: K_I on elliptical crack

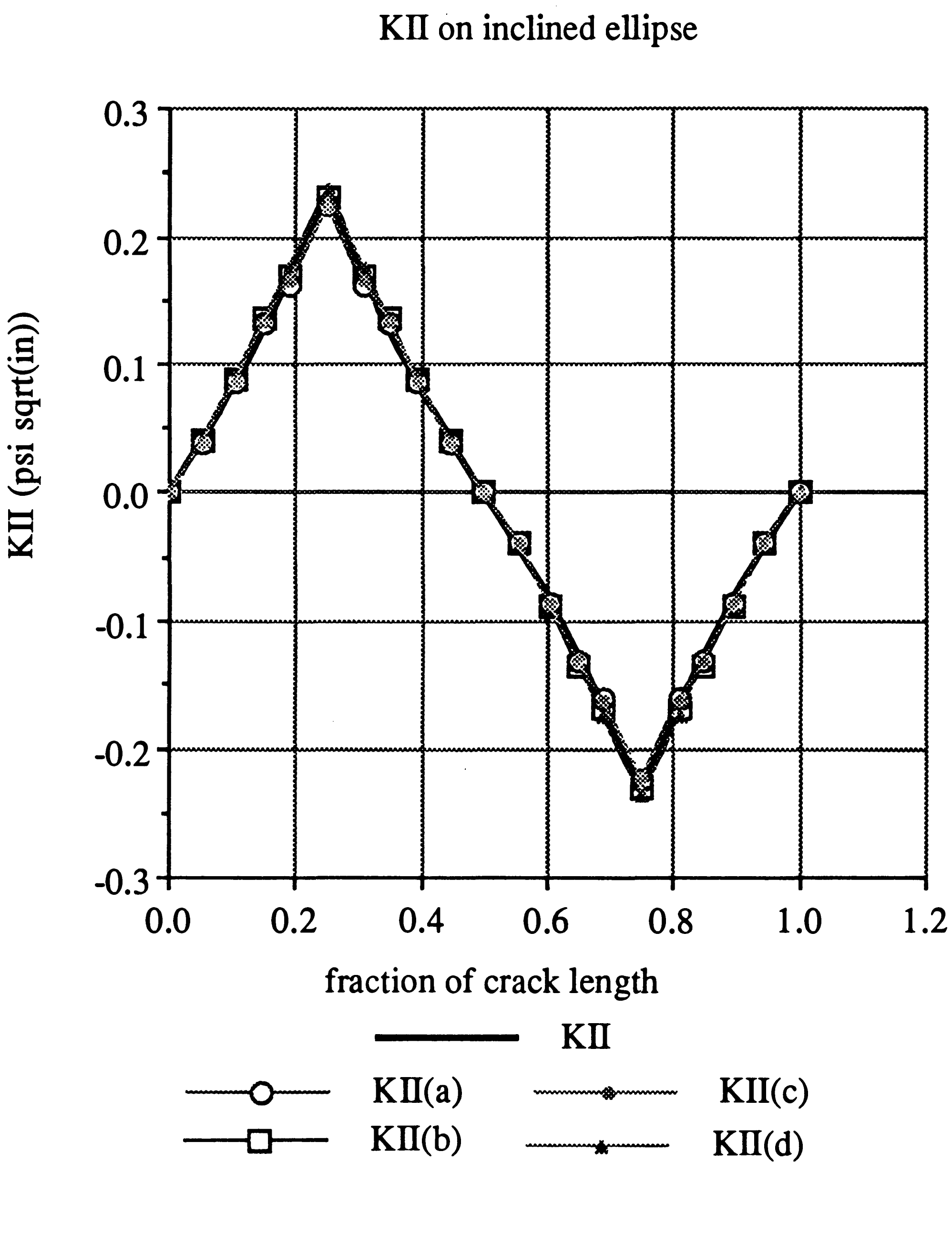

Figure 9.4: K_{II} on elliptical crack

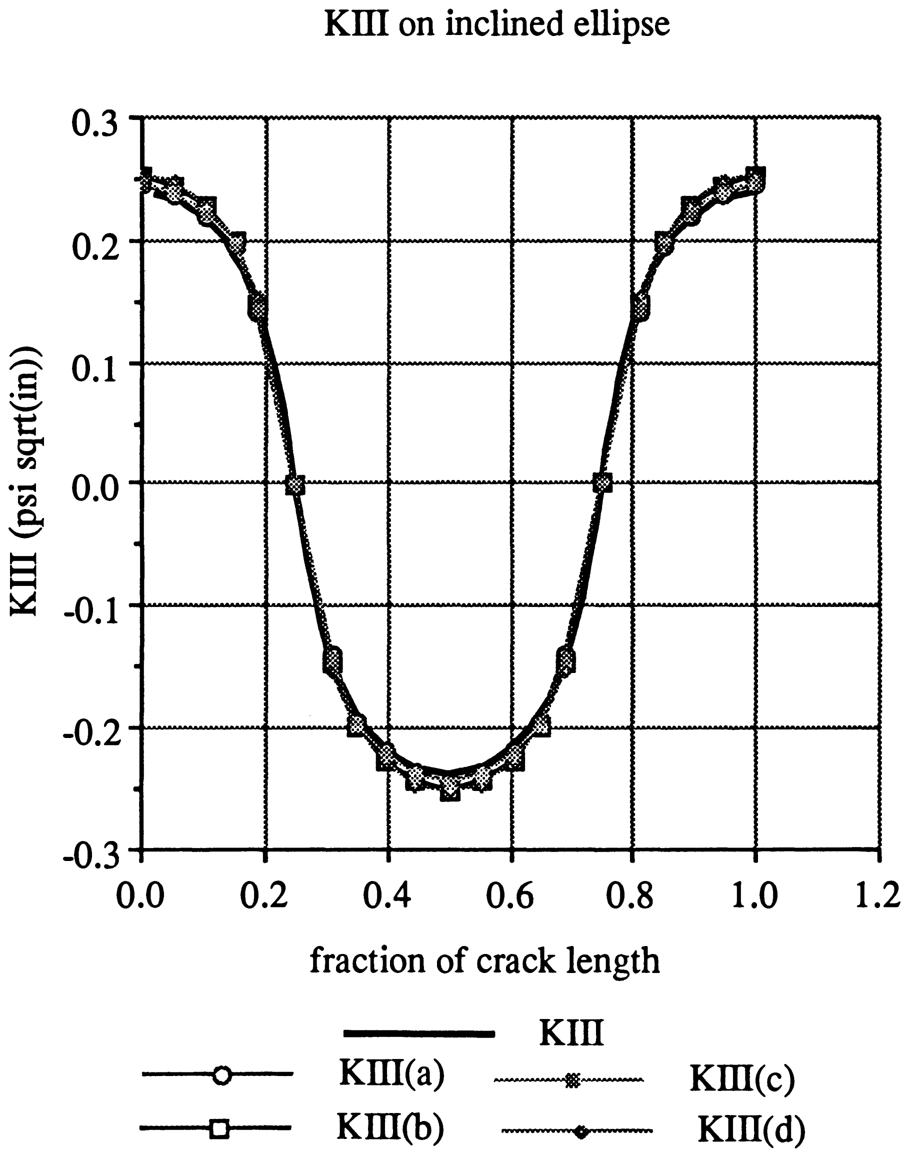

Figure 9.5: K_{III} on elliptical crack

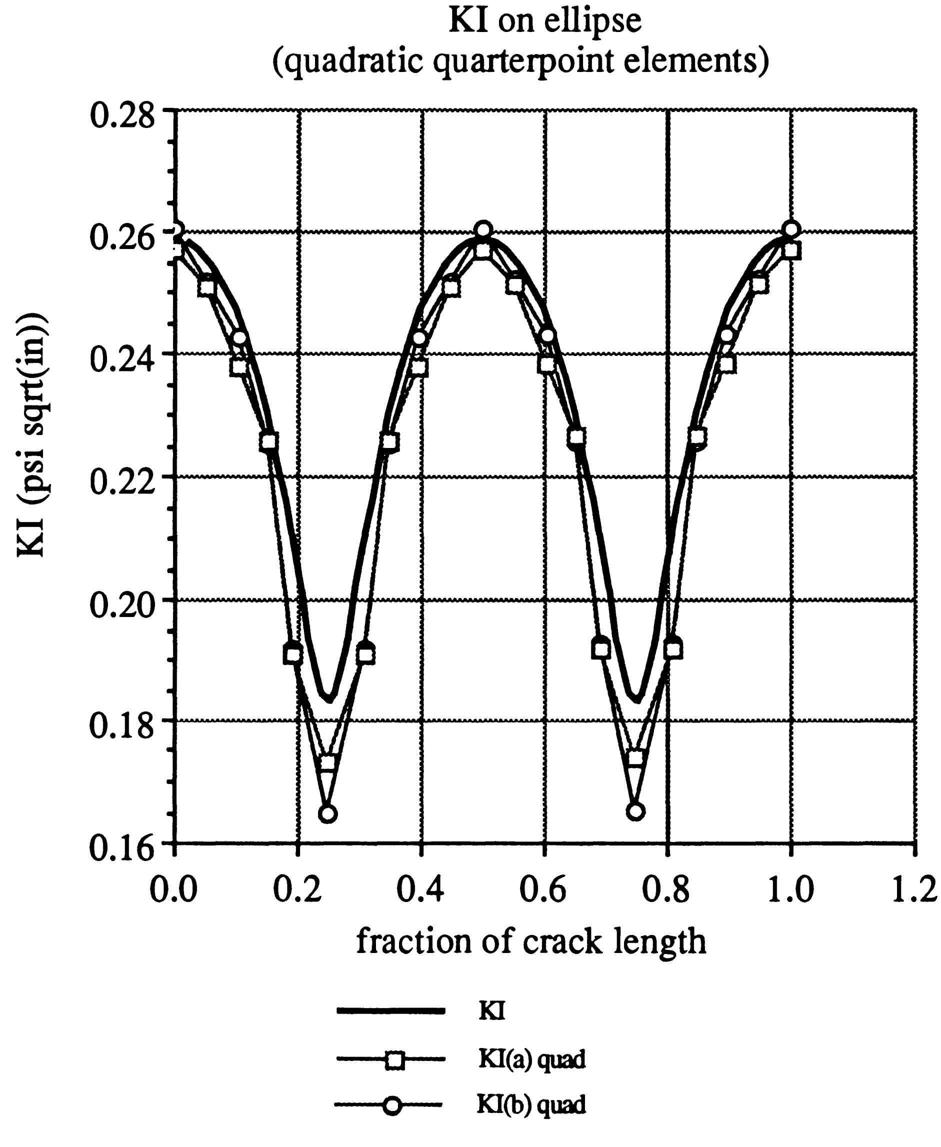

Figure 9.6: K_I on elliptical crack (quadratic element solutions)

zero.

Fig. 9.8 shows several discretizations of the crack. Mesh (a) is extremely coarse, with only 6 elements (30 degrees each). Meshes (b) and (c) are refined, respectively, in the angular and radial directions. Mesh (d) is refined in both directions.

Fig. 9.9 shows K_I computed along the crack front for mesh (a). The maximum error at any point along the crack front is less than 2.5%. The noticeable variation within each element is due primarily to variation of the r values, which are measured exactly normal to the crack front for midpoints of each element but at an angle to the front at the nodes where two elements join. Fig. 9.10 and Fig. 9.11 show results for all four meshes; in each case these figures show a band of K_I values, with the upper and lower limits taken from the top and bottom of the oscillations. Angular refinement significantly reduces the range of the oscillations within each element (compare (a) to (b) and (c) to (d)). At the middle of the crack front, the K_I bands for coarse radial meshes (a) and (b) are mostly above the correct value. In the radially refined meshes (c) and (d) the minimum and maximum values are nearly symmetric about the correct answer.

The K_I values at the crack tip are consistently higher than the correct result, but are quite close to those at interior points. The normal traction variation on the sliding surface should go to infinity at the crack tip; however, it is not modeled by the linear elements, and it is not surprising that mid-crack results are better than those at the free surface.

Computed K_{II} and K_{III} are 4 orders of magnitude smaller than computed K_I in all cases, and may be considered zero.

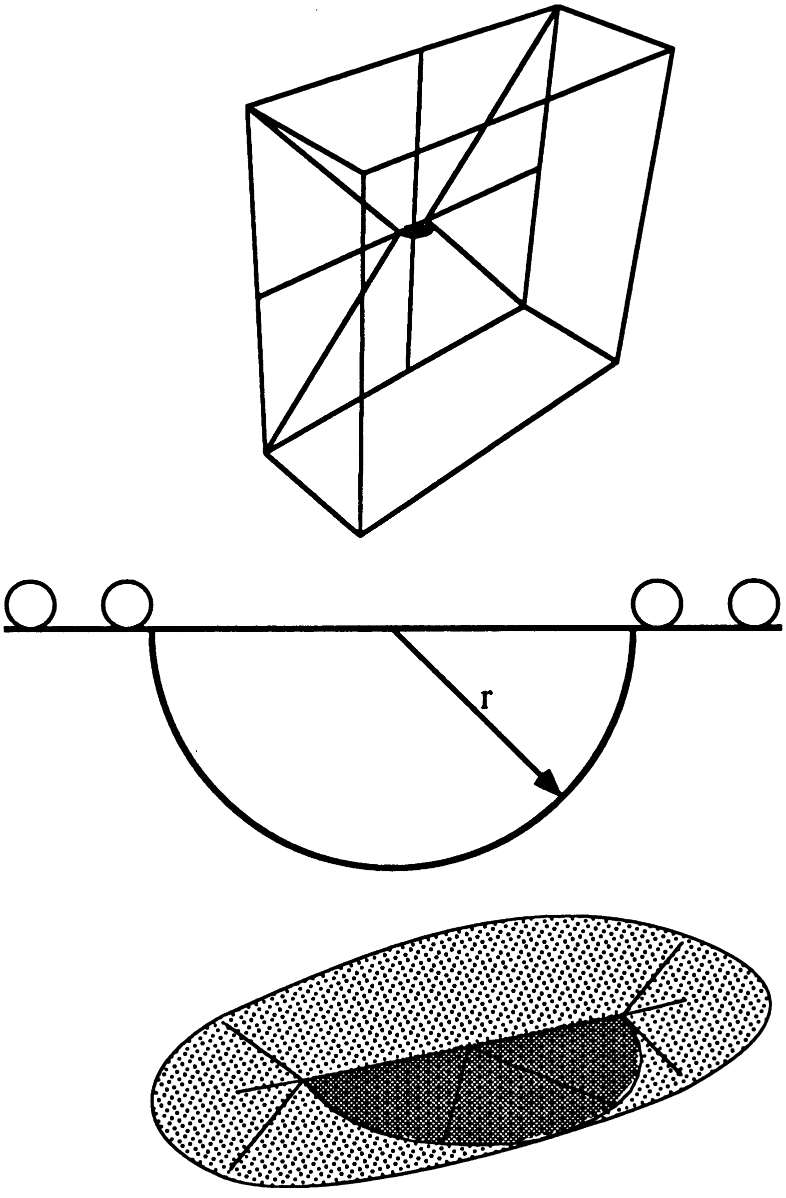

Figure 9.7: Geometry for semicircular surface crack

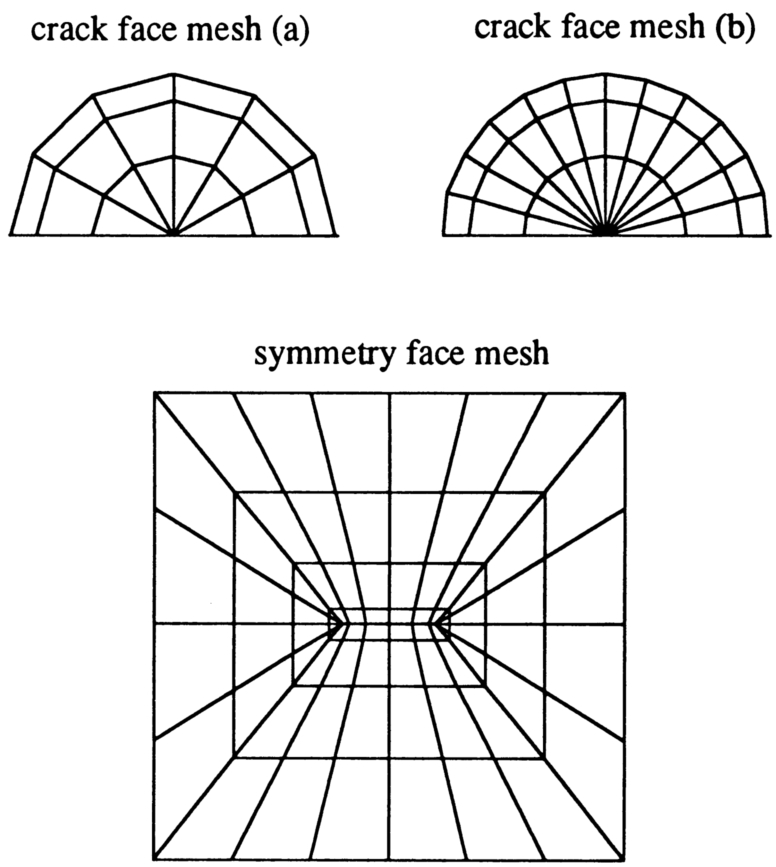

Figure 9.8: Meshes on semicircular crack

(continued on next page)

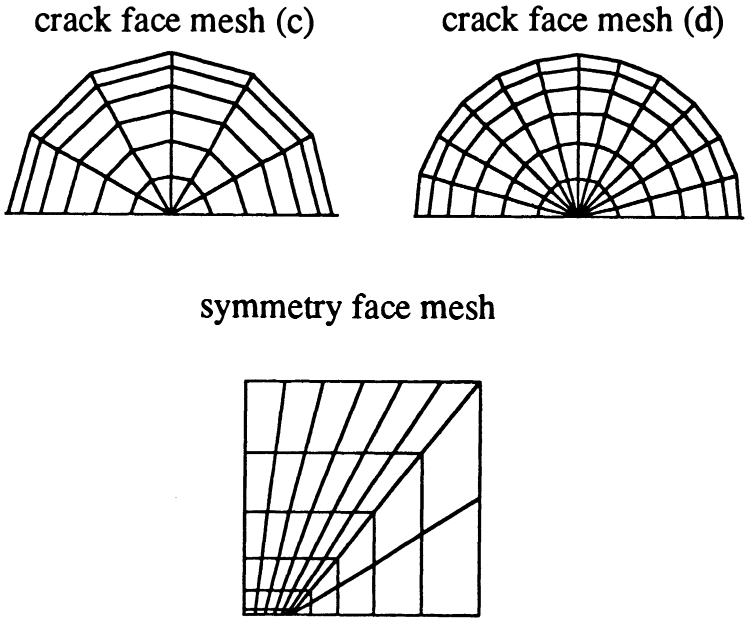

Fig. 9.8 (continued from previous page) Meshes on semicircular crack

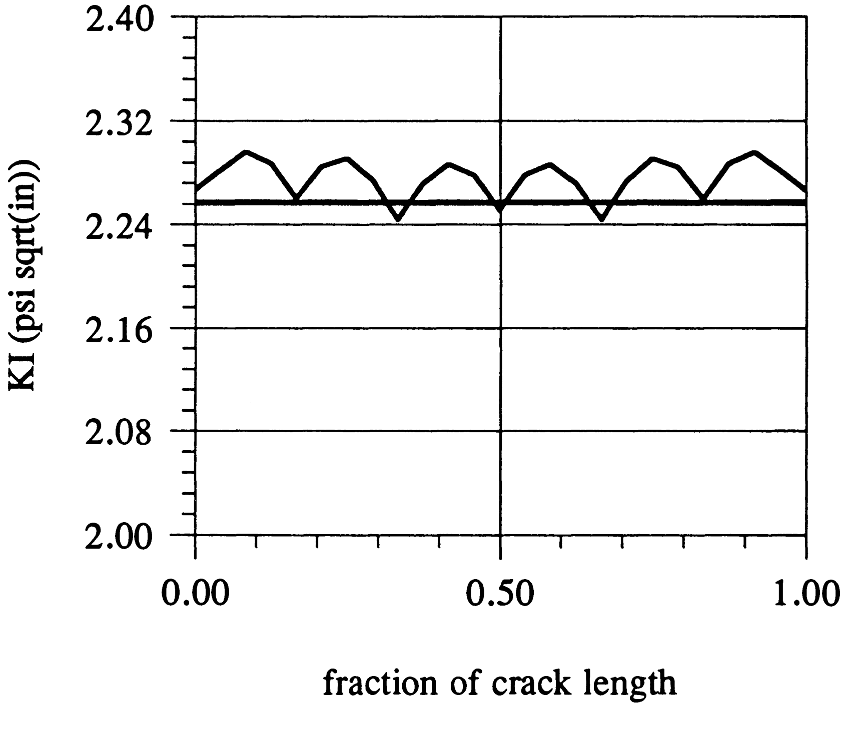

Figure 9.9: K_I computed point-by-point along semicircular crack front

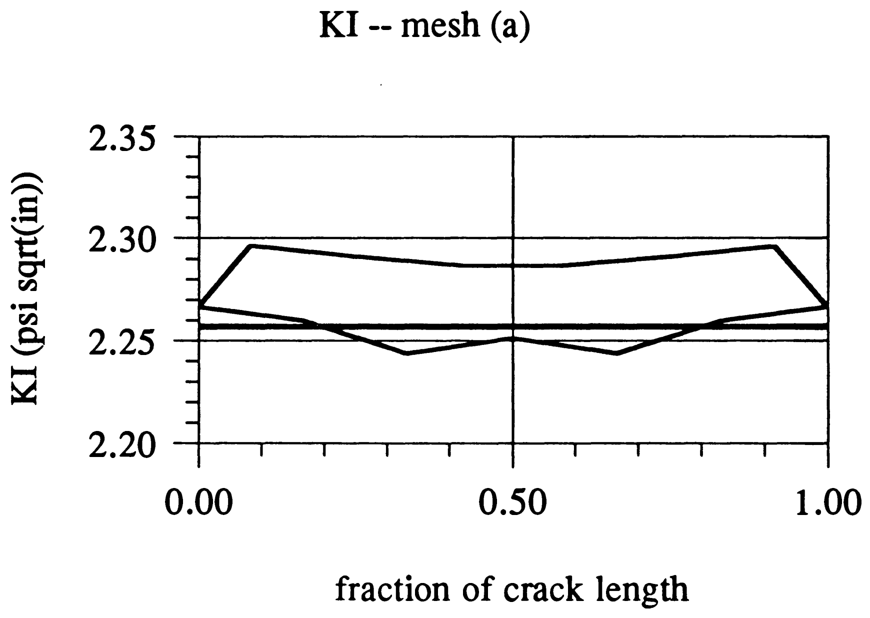

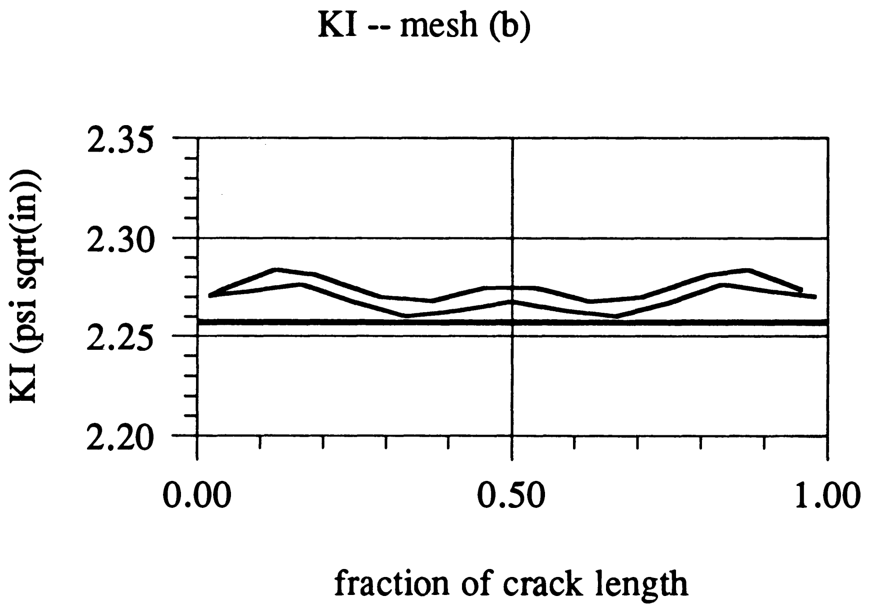

Figure 9.10: K_I upper and lower bands computed along semicircular crack front

KI - mesh (c)

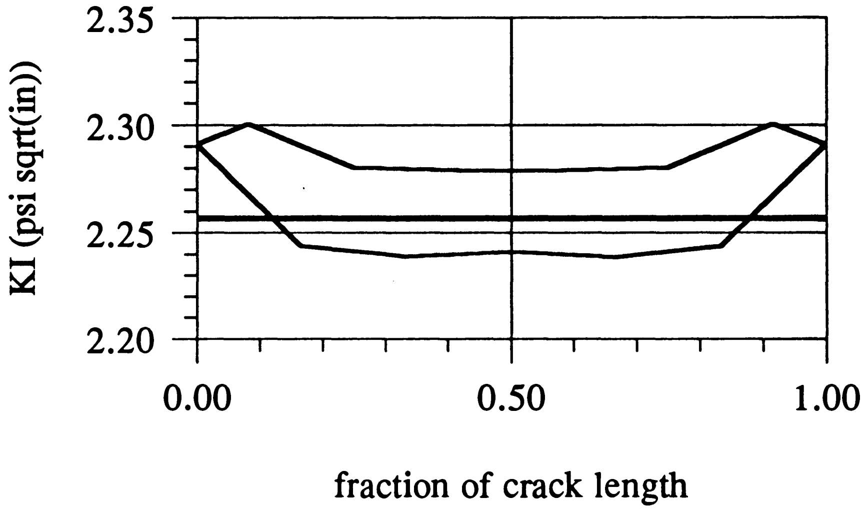

KI -- mesh (d)

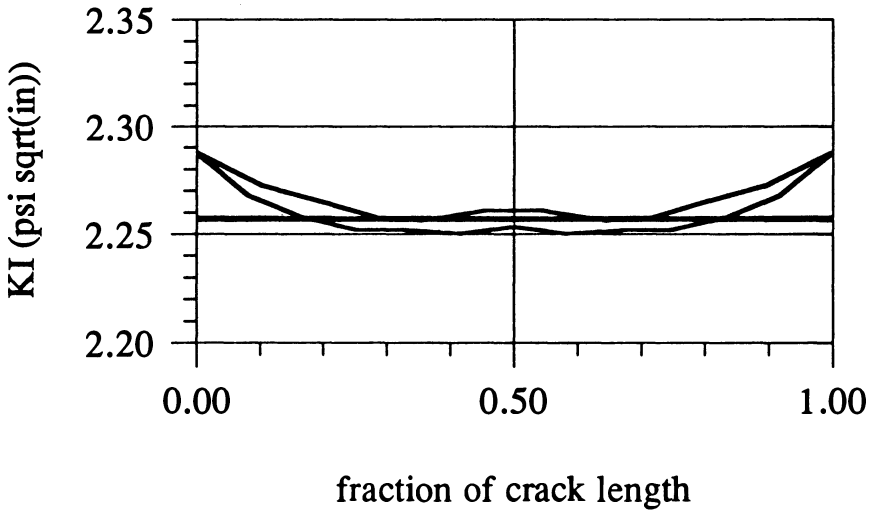

Figure 9.11: K_I upper and lower bands computed along semicircular crack front

9.4 Compact Tension Test Specimen

The compact tension test specimen is a rectangular block with a through-crack cut from one surface, as in Fig. 9.12. Experimental specimens are loaded by pins to create a strong K_I. For analysis and numerical simulation, the load is applied uniformly on an (artificial) surface passing through the pin location of the real specimen.

For an infinitely-thick specimen, mode I stress intensity factor of K_I=7.14 is given in (Tada, Paris, and Irwin [TPI73]). Actual results are expected to differ due to 3D effects not accounted for in the 2D analytic result.

Fig. 9.13 shows the mesh for a numerical simulation with thickness $T = 10$. Computed K_I along the crack front is shown in Fig. 9.14. The midline value of 7.05 is in good agreement with the analytic result.

Fig. 9.15 shows 4 meshes for numerical simulation of a specimen with thickness $T = 1$. Base mesh (a) has 4 elements along the crack front and 5 on the edge leading away from the crack front. Mesh (b) has 8 along the front, and mesh (c) has 8 along the edge. Mesh (d) has only 3 along the edge.

K_I values for all 4 meshes are in Fig. 9.16. All indicate a higher K_I at midcrack than near the edges, which is typical of this geometry ([Bro82]). The close agreement between meshes (a) and (b) indicates that 4 elements along the crack front is adequate. The K_I magnitudes consistently decline as the mesh is refined. This is consistent with results in Perucchio [Per84], where an example shows that linear boundary elements with crude meshes tend to overestimate displacements for a beam loaded in shear on the free surface. Each half of the compact specimen is effectively a short beam loaded in shear.

(a) Test specimen. Unit load applied through pin holes

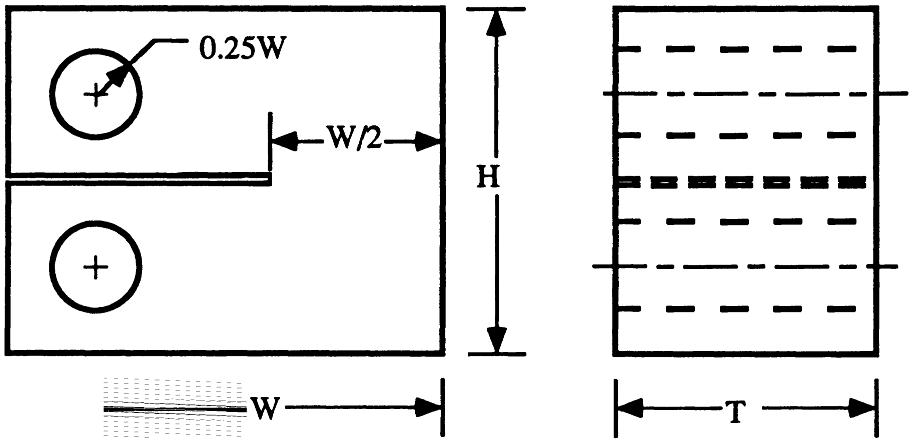

(b) Analyzed geometry Unit shear load on face at nominal pinhole center. (All tests use H=W=2)

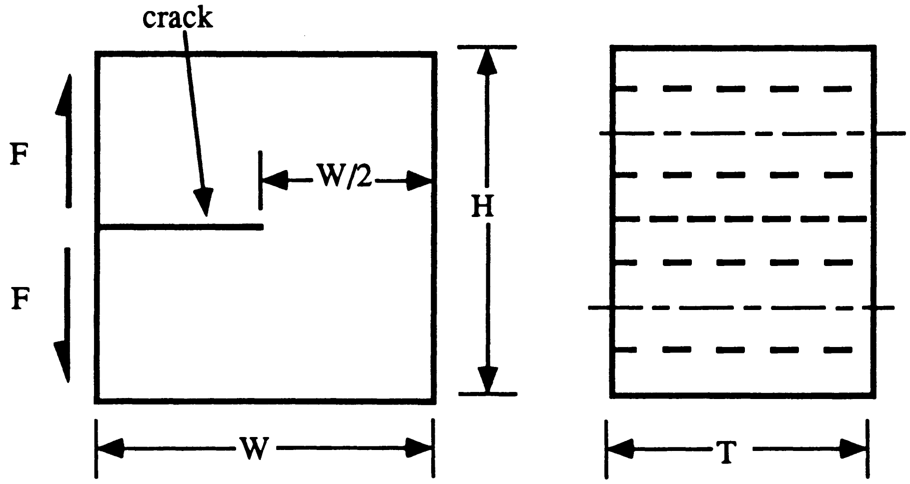

Figure 9.12: Compact test specimen

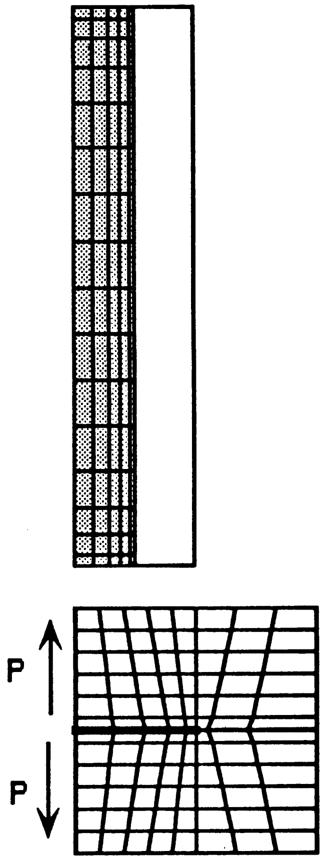

Figure 9.13: Mesh on thick compact test specimen

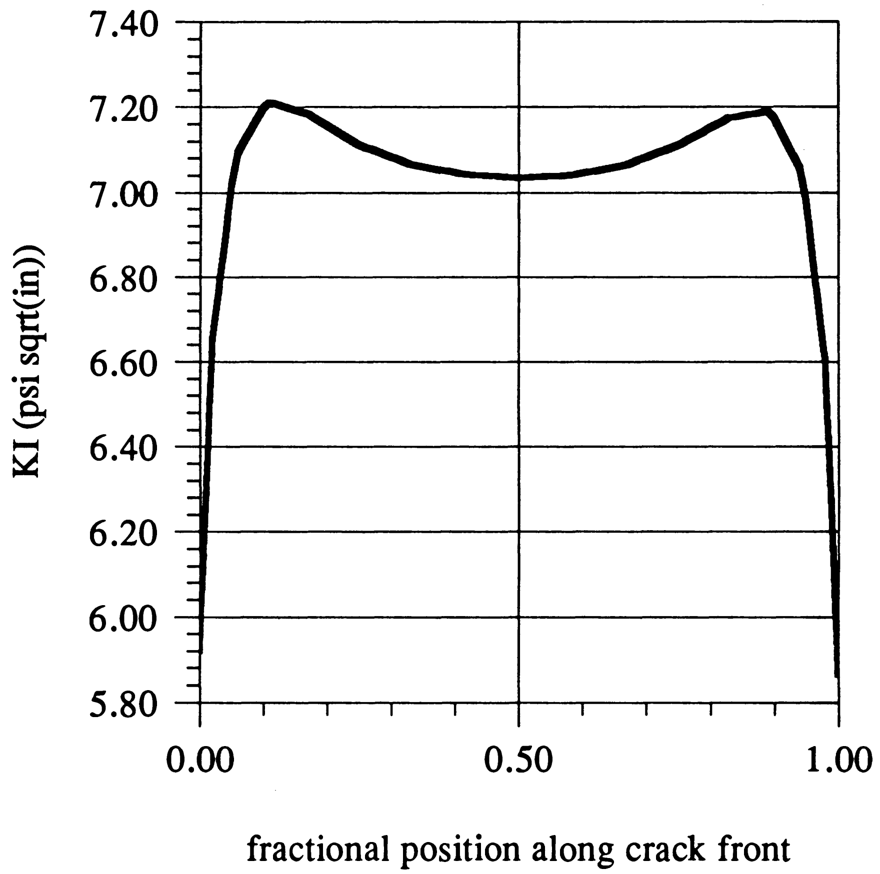

Fig. 9.14 KI for thick specimen (T=10)

Figure 9.14: K_I on compact test specimen (T=10)

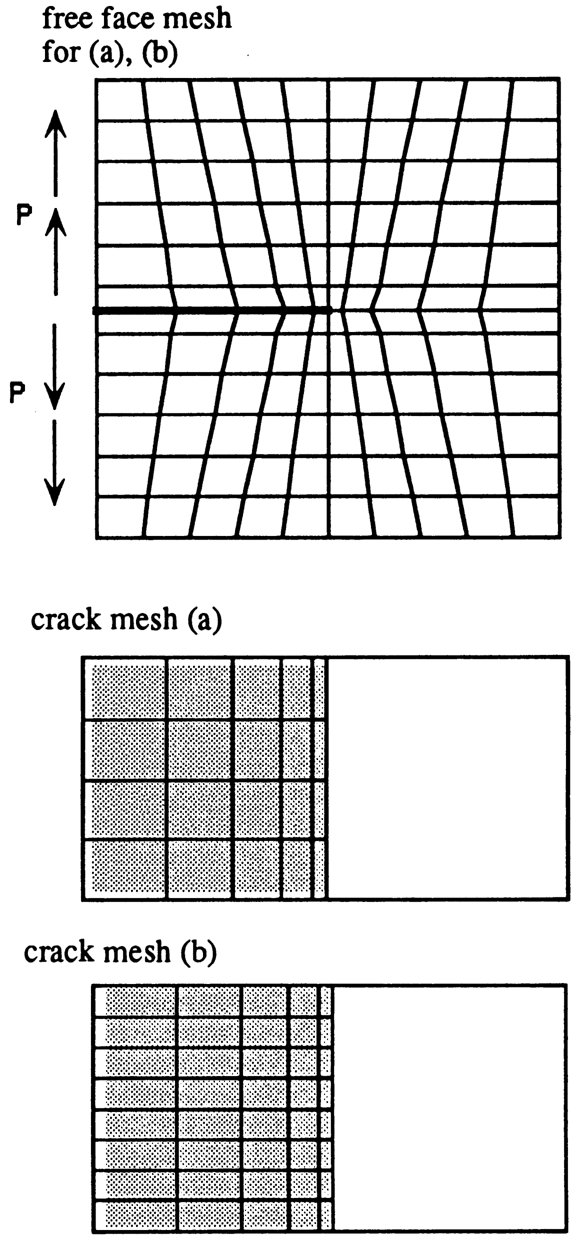

Figure 9.15: Meshes on compact test specimen (T=1)

(continued on next page)

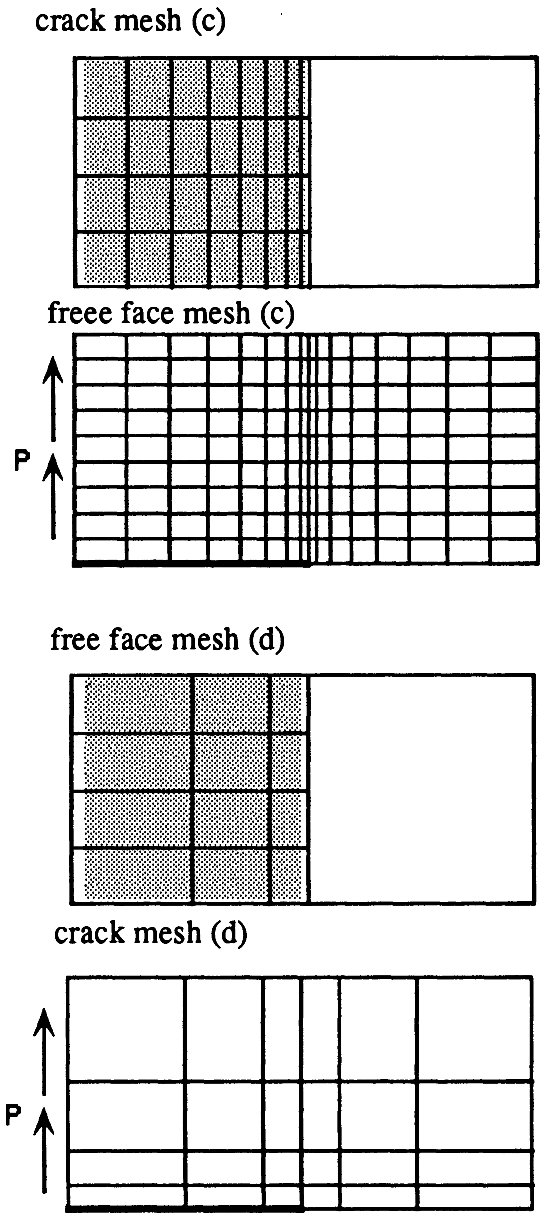

Fig. 9.15 (continued from previous page) Meshes on compact test specimen

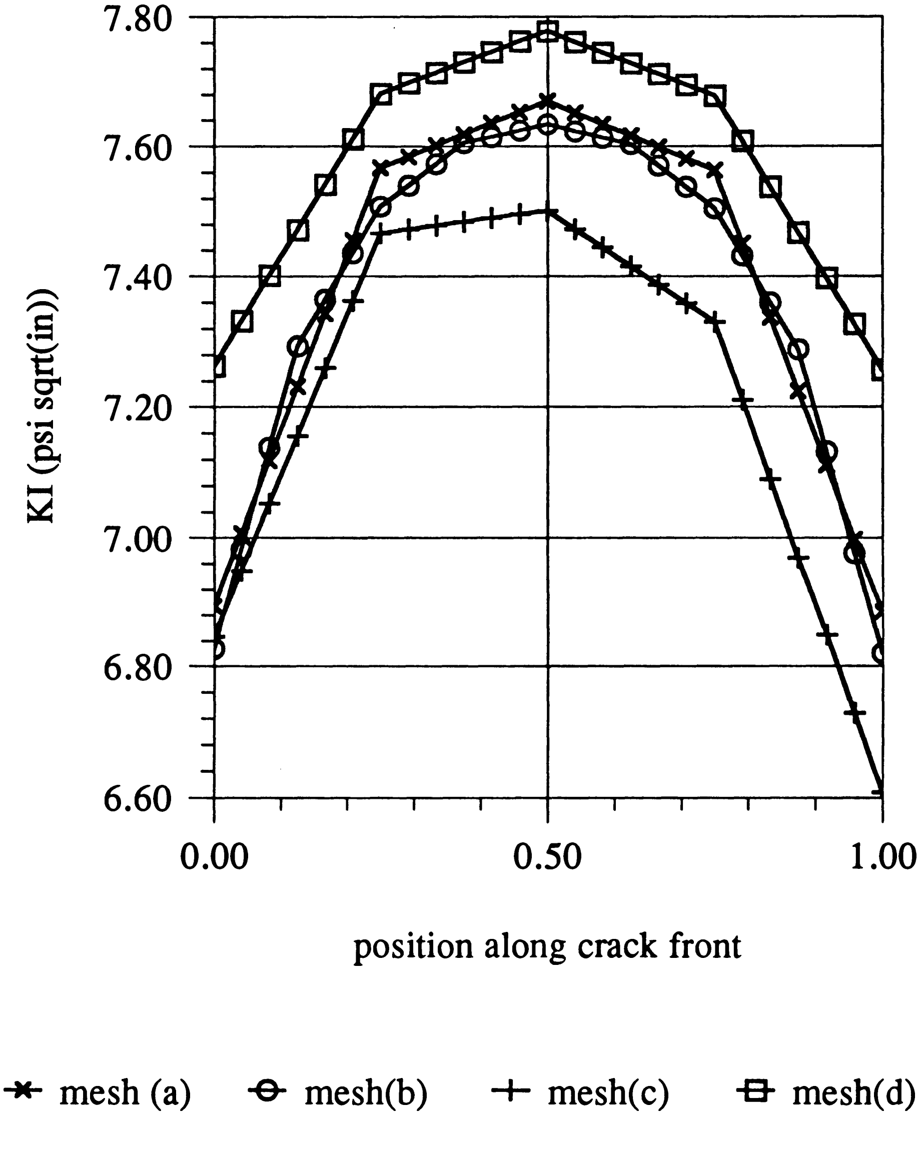

Fig. 9.16 : KI on compact test specimen, T=1

Figure 9.16: K_I on compact test specimen (T=1)

9.5 Shuttle Hinge Crack

This section describes a simulation of crack growth in the shuttle fuel door hinge part of Fig. 1.1. In that isometric figure, the region at the base of the lug is noted as being a high stress region when an upward or rearward load is applied at the pin in the lug. The analysis below considers a unit load applied in the rearward direction.

Fig. 9.17 shows a view looking through the interior of the part towards the base of the lug. Fig. 9.21 shows the same region from the above and in front of the right platform. An initial crack (dark shading in Fig. 9.17) is defined penetrating just under half the thickness of the horizontal platforms to the left and right of the lug. At the left of the lug, the exterior edge of the crack runs 0.050 inches down the vertical step surface between the left and right platforms. The initial crack front, labeled (1), runs from left to right under the full width of the lug. At the far right of the lug, it turns upward and joins the upper platform surface at the front right corner of the lug.

This initial crack is an estimate of how a small crack might be shaped. For this shape, we would like to know the K factors at each point along the crack front. Knowing K factors, the direction and rates of crack growth can be predicted using methods described by Martha [Mar89]. Crack fronts labeled (2), (3), and (4) are the result of this process.

Fig. 9.18, Fig. 9.19, and Fig. 9.20 show the K factors at each step. The significant characteristics are:

1. When multiplied by typical loads (on the order of 3000 lb.), the K_I values are in the vicinity of critical K_{Ic} for the aluminum used for the part.
2. K_I monotonically increases at corresponding points on successive

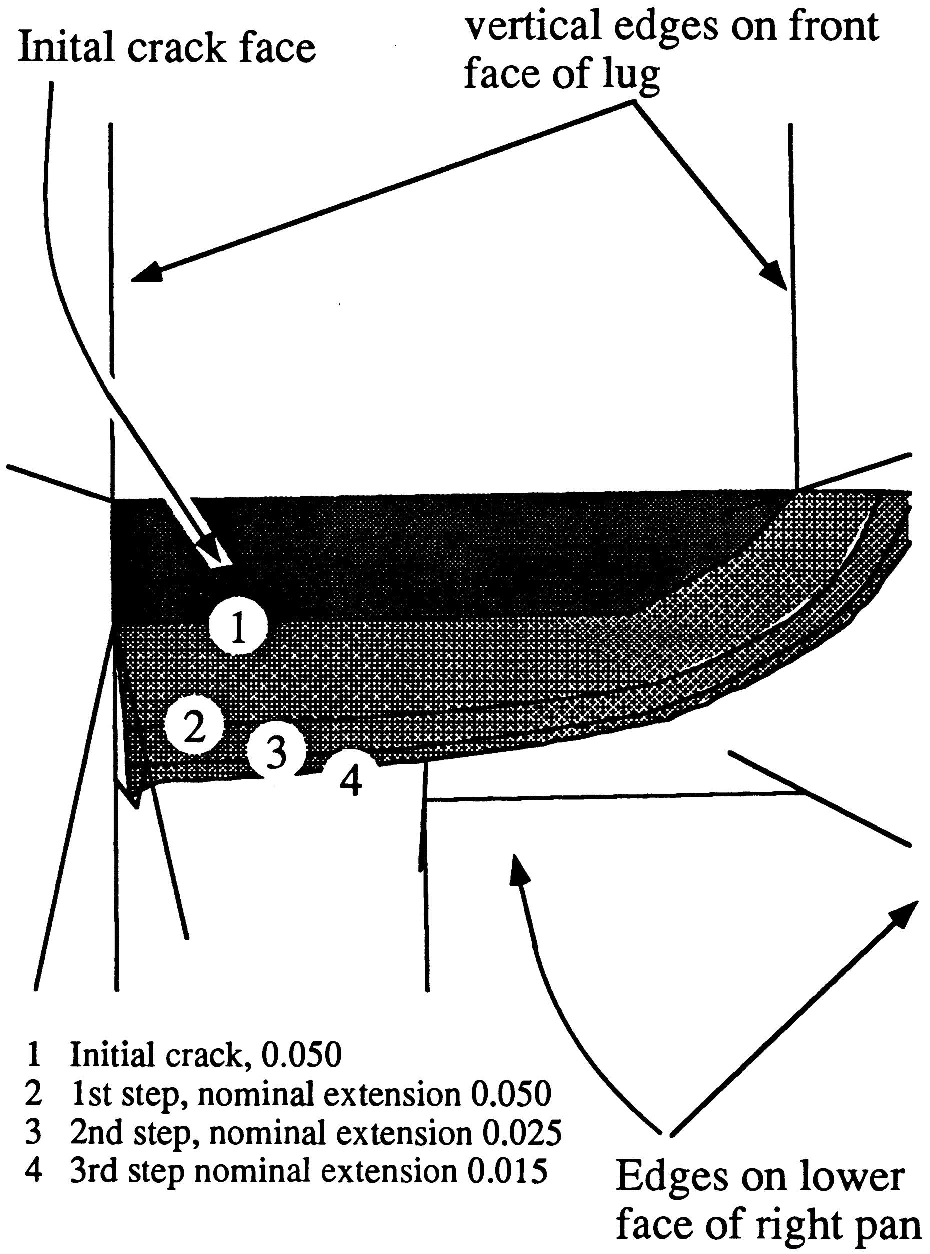

Figure 9.17: Cracks at base of lug in shuttle fuel door hinge mount. View through interior of vertical support under lug.

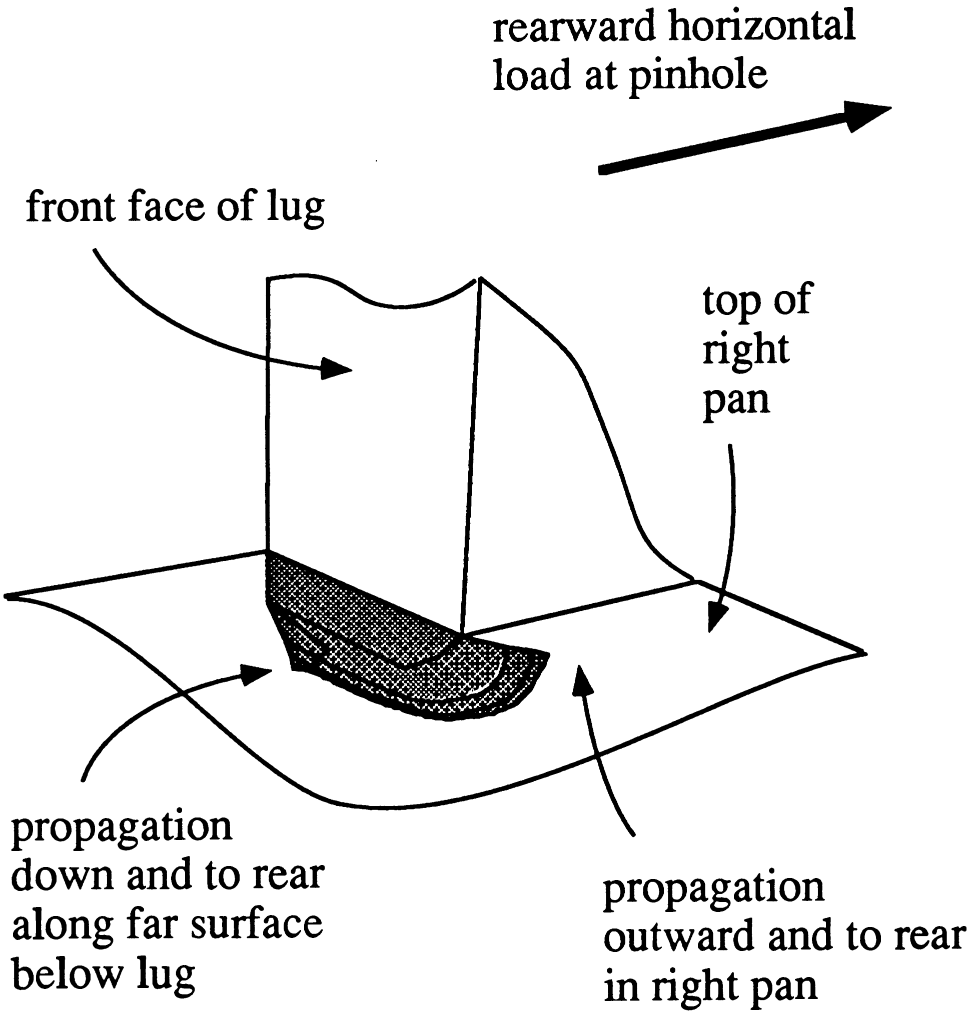

Figure 9.18: Cracks at base of lug in shuttle fuel door hinge mount. View from above and in front of right platform.

crack fronts.

3. The magnitude of K_{II} is large all the way across crack front (1). During the first propagation step, the crack turns rearward (see Fig. 9.21). The turning has the effect of reducing K_{II}. K_{II} is an order of magnitude smaller on the straight portions of fronts (2) and (3).
4. K_{III} changes sign on the initial front and is relieved on successive fronts.
5. Both K_{II} and K_{III} are larger at the right end, where the crack front is turning up to meet the surface.

This analysis involves numerous approximations. The geometry and fixity conditions are not exact. The steady rearward load is just one of many loading configurations. The assumed initial crack shape is not one actually observed, but simply an informed estimate of how a crack might have started. The method of estimating distance and direction of propagation at each point on the crack front is based on a hypothesis about the way the material yields under load.

Because of these estimates, a designer would not use these calculations alone as grounds to make critical design decisions. However, the calculations provide a way to compare the relative effects of various design ideas.

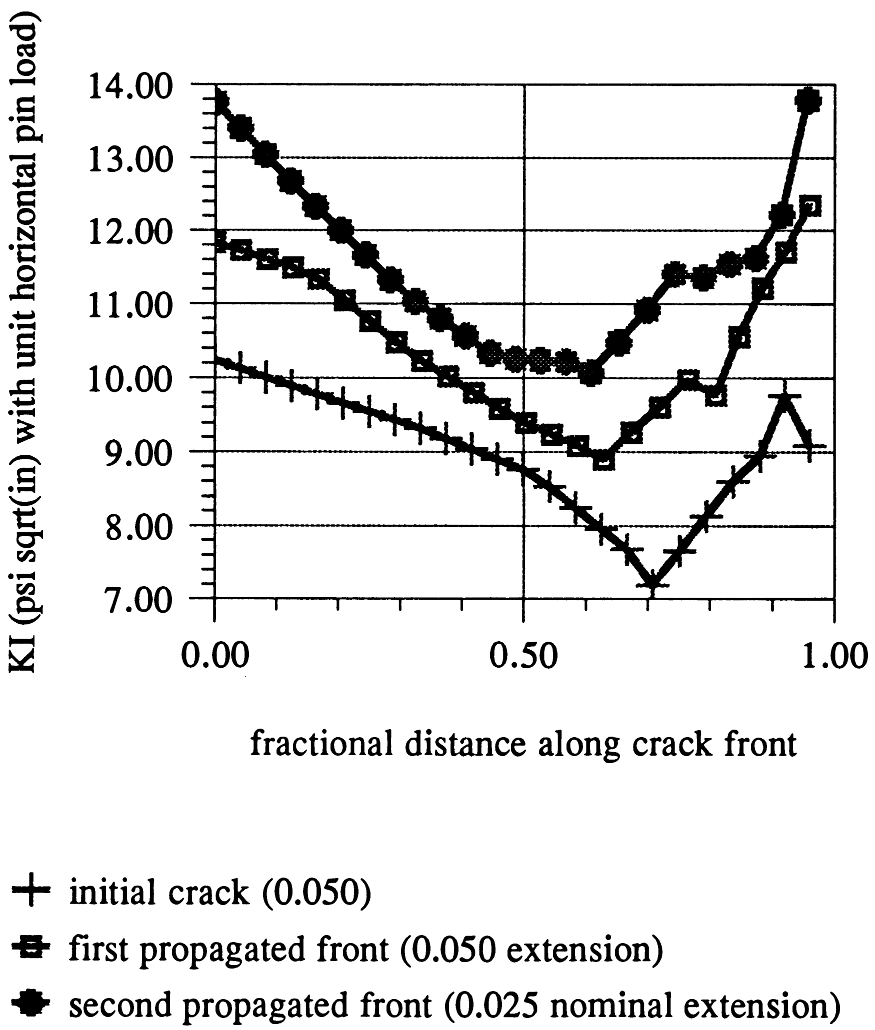

Figure 9.19: K_I on crack fronts at base of lug

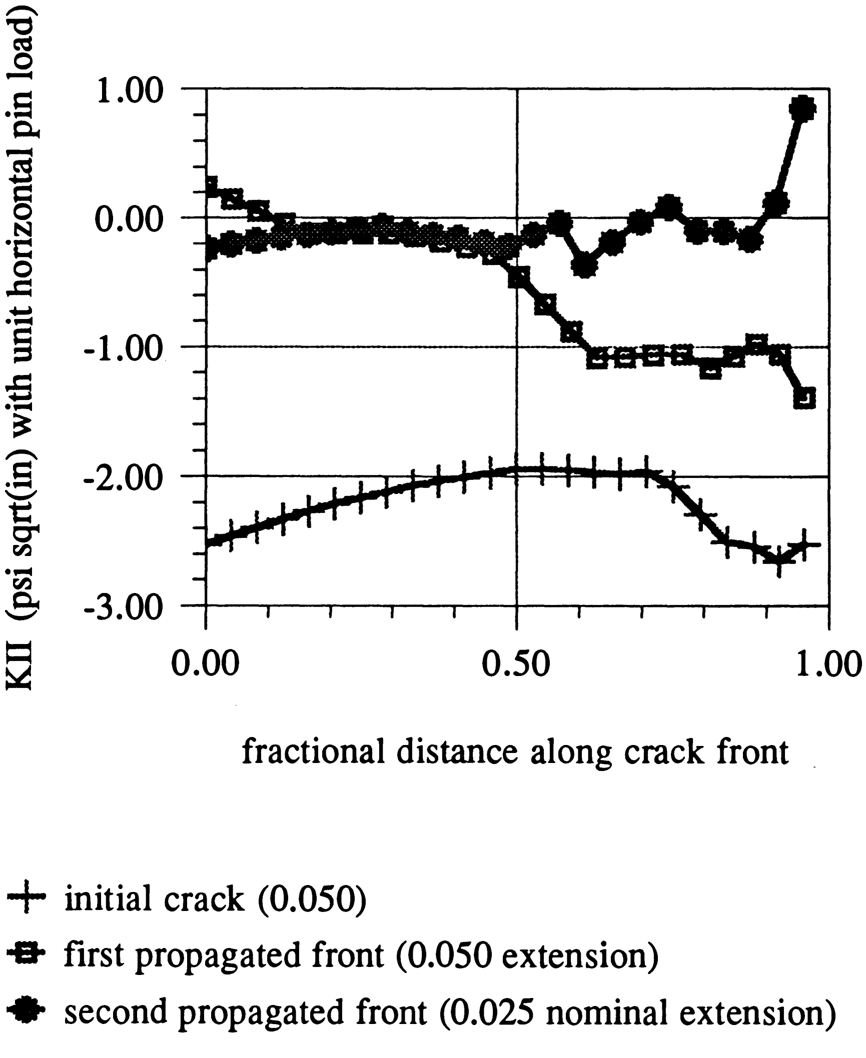

Figure 9.20: K_{II} on crack fronts at base of lug

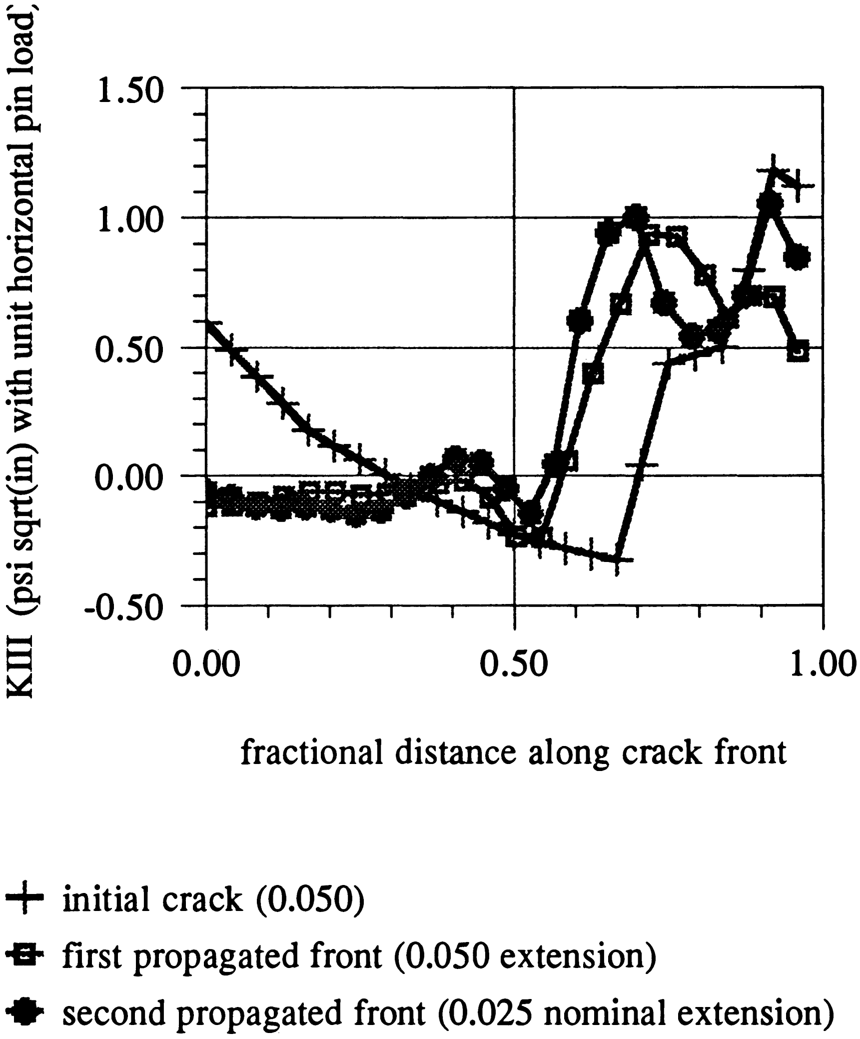

Figure 9.21: K_{III} on crack fronts at base of lug

Chapter 10

Conclusions

The first section below outlines the contributions made in this thesis, first as an itemized review of technical results and then from a higher level view that emphasizes use of high level principles in place of special cases. The second section considers areas for further research.

10.1 Contributions in this Thesis

As a result of the analysis in this thesis, it is now possible to perform 3D fracture analysis (and other crack-like field problems involving the Laplace equation) using only the actual geometry of the external surface and the crack. This result is due to the following specific theoretical contributions:

- The modal integration formulae in Chapter 5 provide a complete explanation of both existence and practical computation of all singular integrals appearing in boundary integrals. They are dramatically shorter than prior analyses, apply in both 2D and 3D, and apply to curved surfaces and corners.

- The conversion theorem in Chapter 6 shows that it should be possible to systematically reduce surface integrations to contour integrations.

- Chapter 7 showed numerous cases where the optimum exactness properties of Gaussian quadrature can be applied to BIE kernels.

- Chapter 8 outlined an implementation that takes advantage of the modal integration and parameterized quadrature.

- Examples in Chapter 9 showed that these methods produce accurate results for both analytic benchmarks and real problems.

A common feature of these results is the view that tedious case analysis can be replaced by higher level analysis. Examples of this are:

- The modal integration method applies properties of the BIE itself to solve singular integration problems. This replaces term-by-term analysis of the kernels and case-by-case treatment specific surfaces.

- The conversion theorem shows that conversion to contour integrals is not a fortuitous algebraic coincidence, but should be possible for *all* integrations. This result depends only on the properties of modal integration, and not algebraic case analysis.

- Parameterized quadrature addresses the near-singular integration problem by exactness properties of Gaussian quadrature, rather than the more pessimistic view that calls for intensive search operations by adaptive quadrature methods.

- The formulation of constraint equations applied linear algebra at a block matrix level in place of case-by-case analysis of various combinations of boundary conditions and geometry.

- The presentation of Gray's limiting process Chapter 4 views this process as a method to be applied to *all* singular integrals, rather than something that happens to work for the hardest of all integrals.

10.2 Further Research

Even with a relatively fast computer[1], 3D stress analysis using these methods is a compute-bound 'batch' computation. Small models (several hundred nodes and elements, 1000 unknowns in the final linear system) are solved in 10 to 30 minutes. Large models (1000 nodes and elements, 3000 to 4000 unknowns) require 4 hours. The three steps of propagation analyzed for the space shuttle fuel door hinge (Chapter 9) averaged 1.5 hours of processing time each.

It is almost predictable that careful code optimization and faster computers will improve performance of a compute-bound program by a factor of 10 every few years. However, increasing problem size will demand more fundamental changes to the method. The following paragraphs outline some areas where such fundamental changes may be possible.

10.2.1 Systematic Determination of Stokes Vectors

Chapter 6 outlined a broad goal of converting all 3D BIE integrals to contour integrals, and completely eliminating surface representation from the method. Attaining this goal requires finding of certain 'Stokes vectors' whose existence was demonstrated only implicitly.

[1]An FPS/Celerity 500EA computer with 140Mbyte of real memory. Benchmark tests show 15 million floating point operations per second in sustained boundary element computations.

10.2.2 Closer Coupling of Solid Modeling and Solution of Boundary Value Problems

The standard implementation of the boundary element method is intimately coupled with (a) parametric representations of surface functions, (b) independent representation of primary and gradient unknowns, (c) independent integration of the two kernels in each BIE (primary and gradient), and (d) separate integration over each element.

This thesis showed that the gradient BIE becomes tractable when one (a) applies a *cartesian* function for the primary unknown, (b) directly differentiates that primary function to obtain surface gradients, (c) integrates the entire gradient BIE integrand (**Dp-Su**) as a unit, and (d) evaluates integrals over a complete patch, rather than over individual elements. Further, it showed that in principle applying these conditions to higher order solution fields provides sufficient conditions for conversion of all BIE surface integrals to contour integrals. If this hypothetical possibility can be achieved, even the parametric representation of surface geometry will be bypassed.

These conditions are so far afield from the basic parameterized BEM that one should ask whether any part of the parameterized formulation is absolutely essential. That is, we ask whether there might be some (possibly very different) representation scheme that will provide a similar or superior combination of the following services:

- Accurate, unambiguous, and convenient modeling of changing geometry.
- Differentiable basis functions defined over all of space, rather than just the surface.
- Addressability of surface points (so that boundary conditions can be specified).

- Topological information that is needed for integrations and construction of constraint equations.

Appendix A

Storage and factorization costs of FEM and BEM

The following paragraphs derive order-of-magnitude estimates of storage use and operation counts for the finite and boundary element methods.

As in Fig. A.1, consider a square (geometric dimension=d=2) and a cube (d=3), each with a regular mesh based on n nodes per edge. We will compare certain data and operation counts for (a) finite element analysis using the entire mesh and (b) boundary element analysis using only the boundary portions of each mesh. Both Laplace (k=1 degrees of freedom per scalar) and elasticity (k=3 degrees of freedom per vector unknown) equations will be considered.

Finite Element Method A finite element model has $N_1 = n^d$ nodes and $N_2 = (n-1)^d$ elements. There are $N_3 = kN_2 \approx kn^d$ nodal unknowns. Each (linear) element has $N_4 = 2^d$ nodes, hence $N_5 = kN_4 = k2^d$ nodal unknowns in its local $\mathbf{Ku} = \mathbf{f}$ stiffness formulation.

A single element stiffness matrix has (taking advantage of symmetry) $N_6 = N_5{}^2 = \frac{1}{2}k^2 2^{2d}$ entries. Computing stiffness matrices for all elements requires

Figure A.1: Finite and boundary element analysis of a square and cube

$N_7 = N_2 N_6 \approx \frac{1}{2} n^d k^2 2^{2d}$ entries in per-element-stiffness matrices.

The assembled (symmetric) matrix has bandwidth $b = kn^{d-1}$. Banded storage (including zeros) requires $N_8 = bN_3 = k^2 n^{2d-1}$ entries. A banded symmetric factorization has $N_9 \approx b^2 N_3 = 2k^3 n^{3d-2}$ arithmetic operations.

Boundary Element Method A surface mesh has $N_1 = 2dn^{d-1}$ nodes and $N_2 = 2d(n-1)^{d-1} \approx 2dn^{d-1}$ elements. There are $N_3 = kN_2 = 2dn^{d-1}$ total nodal unknowns. A (linear) has $N_4 = 2^{d-1}$ nodes, hence $N_5 = kN_4 = k2^{d-1}$ nodal unknowns. A single integration from one element to one node point has $N_6 = k^2 N_4 = k^2 2^{d-1}$ entries for each of two kernels. Integrating from each element to each node point requires

$$N_7 = N_1 N_2 (2N_6) = (2dn^{d-1})(2dn^{d-1})(2k^2 2^{d-1}) = 8dk^2 2^{d-1} n^{2d-2} \qquad \text{(A.1)}$$

entries to be computed.

The matrix is fully populated, so the total matrix size is $N_8 = N_9$. A dense Gaussian elimination factorization has $N_9 = \frac{2}{3} N_3{}^3$ operations.

Summary The number of nonzero matrix entries (N_7) for each case are:

	FEM	BEM	FEM/BEM
Laplace 2D	$8n^2$	$32n^2$	$\frac{1}{2}$
Laplace 3D	$32n^3$	$96n^4$	$\frac{1}{3n}$
Elasticity 2D	$32n^2$	$128n^2$	$\frac{1}{2}$
Elasticity 3D	$288n^3$	$864n^4$	$\frac{1}{3n}$

The total matrix storage (N_8) for each case are:

	FEM	BEM	FEM/BEM
Laplace 2D	n^3	$32n^2$	$\frac{n}{32}$
Laplace 3D	n^5	$96n^4$	$\frac{n}{96}$
Elasticity 2D	$4n^3$	$128n^2$	$\frac{n}{32}$
Elasticity 3D	$9n^5$	$864n^4$	$\frac{n}{96}$

The matrix factorization steps (N_9) for each case are:

	FEM	BEM	FEM/BEM
Laplace 2D	n^4	$43n^3$	$n/43$
Laplace 3D	n^7	$144n^6$	$n/144$
Elasticity 2D	$8n^4$	$341n^3$	$n/43$
Elasticity 3D	$27n^7$	$3888n^6$	$n/144$

The hoped-for 'dimension reduction' advantage of the boundary element method appears as a single order-n factor in overall factorization steps. The breakeven point occurs at n=144, which would require nearly 3 million finite elements and 125,000 boundary elements (!!).

There are reasons to suggest that both problem itself and the solution methods are skewed in favor of the boundary element method. A 'real' problem would be expected to have less volume per unit surface area. At the other extreme, if the cube is replaced by a plate one element thick with $n \times n$ nodes on each face, both methods have $N_1 = 2n^2$ nodes and $N_3 = 2kn^2$ degrees of freedom. The FEM bandwidth decreases to n, while the BEM system is dense.

This comparison makes no accounting of the relative cost of matrix entries for FEM and BEM. During use of both methods, it is observed that the matrix factoring time is often less than the time to compute coefficients. The coefficient counts (N_7) above show that BEM always has more coefficients, but does not indicate the fact that each BEM coefficient is far more expensive to compute than each FEM coefficient.

Appendix B

Stokes Vectors for the S_{ijk} Kernel

Stokes' theorem provides a way to convert certain surface integrals to path integrals along the edge of the surface. To apply the theorem, one must show that the integrand can be expressed as the curl of some other integrand. Cruse and Novati [CN90] have applied this to hypersingular integrals in the displacement discontinuity formulation of a crack. Krishnasawamy, Schmerr, Rudolphi, and Rizzo [KSRR90] has applied it to the Green's function for wave scattering in an elastic material.

This section derives the Stokes theorem form for hypersingular elasticity kernels. The derivation given here is different from those previously mentioned in that it refers to the general properties that the elasticity kernels inherit from the differential equation, but never deals with the algebraic expression for the kernels.

The primary result is a path integral for a derivative of the T_{ik} kernel in terms of the (weaker) D_{ijk} kernel:

Theorem:

$$\int_S \frac{\partial}{\partial x} T_{ik} \, dS = \oint_{\partial S} (-\mathbf{e}_x \times {}_j D_{ijk}) \cdot \mathbf{V} \cdot \mathbf{T} \, dl \qquad \text{(B.1)}$$

where $\mathbf{V}$ is a tangent vector along the boundary of the surface patch.

Similar results apply in the y and z directions. Recombining these with elastic tensor constants gives the S_{ijk} kernels. The most general form of this summation is

$$\int_S S_{ijk}\, dS = E_{ijmn} \oint_{\partial S} \frac{\partial}{\partial x_n} T_{mk} \cdot \mathbf{V} \cdot \mathbf{T}\, dl \tag{B.2}$$

$$= E_{ijmn} \oint_{\partial S} (-\mathbf{e}_n \times {}_l D_{mlk}) \cdot \mathbf{V} \cdot \mathbf{T}\, dl \tag{B.3}$$

Due to the special structure of E_{ijmn} and the D_{ijk} kernel, the summation over all values of m and n simplifies to

$$S_{ijk} = G\left(\frac{\partial}{\partial x_j} T_{ik} + \frac{\partial}{\partial x_j} T_{jk}\right) \tag{B.4}$$

The proof of these results follows. We first give Stokes' theorem, then derive some useful properties relating D_{ijk} and T_{ik}, and observe that the final properties of D_{ijk} and T_{ik} are in exactly the form needed for Stokes' theorem.

Theorem: (Stokes) Let $\mathbf{f}$ and $\mathbf{F}$ be vector functions such that

$$\mathbf{f} \equiv \nabla \times \mathbf{F} \tag{B.5}$$

Then for a surface patch S with boundary ∂S and boundary tangent $\mathbf{V}$,

$$\int_S \mathbf{f} \cdot \mathbf{N}\, dS \equiv \int_S \nabla \times \mathbf{F} \cdot \mathbf{N}\, dS \equiv \oint_{\partial S} \mathbf{F} \cdot \mathbf{V} \cdot \mathbf{T}\, dl \tag{B.6}$$

The kernel manipulations that introduce the cross products and differentiations into the kernel are as follows:

Property 1: T_{ik} has a surface normal embedded in its algebraic form. If the surface normal is written with components N_j, T_{ik} can be written in terms of D_{ijk} as

$$T_{ik} \equiv D_{ijk} N_j \tag{B.7}$$

Property 2: For each k, the ij stress tensor formed from the ij components of D_{ijk} satisfy the differential equation $\sigma_{ij,j} = \sigma_{ij,i}$ of elasticity. Hence we can write

$$D_{ijk,j} = 0 \tag{B.8}$$
$$= \quad \{ \text{ Expand } j \text{ index } \} \tag{B.9}$$
$$(D_{ixk}),_x + (D_{iyk}),_y + (D_{izk}),_z = 0 \tag{B.10}$$
$$= \quad \{ \text{ Algebra } \} \tag{B.11}$$
$$(D_{ixk}),_x = -(D_{iyk}),_y - (D_{izk}),_z \tag{B.12}$$

Property 3: Let $\mathbf{e}_x$ be the x-direction unit vector. Then

$$\frac{\partial}{\partial x} D_{ijk} = \nabla \times (-\mathbf{e}_x \times {}_j D_{ijk}) N_j \tag{B.13}$$

($\times$ denotes cross product; the j subscript on $\times_j$ indicates that the j subscript of the D_{ijk} operand is the one used for the cross product) This is established by applying Property 2 in the expansion of the cross product:

$$\nabla \times (-\mathbf{e}_x \times {}_j D_{ijk}) \tag{B.14}$$
$$= \quad \{ \text{ expand inner cross product } \} \tag{B.15}$$
$$\nabla \times [0, -D_{izk} + D_{iyk}] \tag{B.16}$$
$$= \quad \{ \text{ expand cross product: } \} \tag{B.17}$$
$$[(-D_{iyk,y} - D_{izk}), D_{iyk},_x, D_{izk},_x] = \tag{B.18}$$
$$= \quad \{ \text{ Property 2: } \} \tag{B.19}$$
$$[D_{ixk},_x, D_{iyk},_x, D_{izk},_x] \tag{B.20}$$
$$= \quad \{ \text{ Generalize subscripts } \} \tag{B.21}$$
$$D_{ijk},_x \tag{B.22}$$

This leads to a similar property of the T_{ik} kernel:

Property 3a:

$$\frac{\partial}{\partial x} T_{ik} \tag{B.23}$$
$$= \quad \{ \text{ Property 1: } \} \tag{B.24}$$
$$\frac{\partial}{\partial x}(D_{ijk} N_j) \tag{B.25}$$
$$= \quad \{ \text{ subscript manipulation: } \} \tag{B.26}$$
$$(\frac{\partial}{\partial x} D_{ijk}) N_j \tag{B.27}$$
$$= \quad \{ \text{ Property 3: } \} \tag{B.28}$$
$$\nabla \times (-\mathbf{e}_x \times {}_j D_{ijk}) \cdot \mathbf{N} \tag{B.29}$$

This form has the necessary cross products and derivatives for Stokes' theorem:

Proof of Theorem:

$$\int_S \frac{\partial}{\partial x} T_{ik} \, dS \tag{B.30}$$
$$= \quad \{ \text{ Substitute by Property 4: } \} \tag{B.31}$$
$$= \int_S \nabla \times (-\mathbf{e}_x \times {}_j D_{ijk}) \cdot \mathbf{N} \, dS \tag{B.32}$$
$$= \quad \left\{ \text{ Stokes theorem with } \mathbf{F} = -\mathbf{e}_x \times {}_j D_{ijk} \right\} \tag{B.33}$$
$$= \oint_{\partial S} (-\mathbf{e}_x \times {}_j D_{ijk}) \cdot \mathbf{V} \cdot \mathbf{T} \, dl \tag{B.34}$$

QED

The usual form of recombining derivatives of T_{ik} to obtain S_{ijk} is

$$S_{ijk} = G(\frac{2\nu}{1-2\nu} \delta_{ij} T_{lk,l} + T_{ik,j} + T_{jk,i}) \tag{B.35}$$

The Stokes' theorem results can be applied to this as written, giving S_{ijk} as a sum of several edge integrals. However, the term $T_{lk,l}$ (summed over l) can be shown to be identically zero and can be omitted:

Property 4: $T_{ik,i} \equiv 0$

$$T_{lk,l} = \tag{B.36}$$

$$
\begin{aligned}
= \quad & \{\ \text{Property 1} \qquad\qquad\qquad\qquad\qquad\qquad\qquad \} && \text{(B.37)}\\
& (D_{ijk}N_j)_{,i} && \text{(B.38)}\\
= \quad & \{\ \text{Subscript manipulation} \qquad\qquad\qquad\qquad \} && \text{(B.39)}\\
& D_{ijk,i}N_j && \text{(B.40)}\\
= \quad & \left\{ \begin{array}{l} D_{ijk,i} \equiv 0 \text{ because } D_{ijk} \text{ satisfies the} \\ \text{differential equation for indices } ij \end{array} \right\} && \text{(B.41)}\\
& 0 && \text{(B.42)}
\end{aligned}
$$

Bibliography

[Ame77] W.F. Ames. *Numerical Methods for Partial Differential Equations.* Academic Press, 1977.

[Baj90] C. Bajaj. Surface fitting using implicit algebraic surface patches. Technical Report CSD-TR-1001, Purdue University Computer Sciences Department, 1990.

[BB81] P.K. Banerjee and R. Butterfield. *Boundary Element Methods in Engineering Science.* McGraw Hill, 1981.

[BD88] C.A. Brebbia and X.Y. Dominguez. *Boundary Elements: An Introductory Course.* Computational Mechanics Publications (McGraw-Hill), 1988.

[BFK] W. Bohm, G. Farin, and J. Kahmann. A survey of curves and surface methods in CAGD. *Computer Aided Geometric Design*, 1:1–60.

[BIL81] G.E. Blandford, A.R. Ingraffea, and J.A. Liggett. Two dimensional stress intensity factor computations using the boundary element method. *International Journal for Numerical Methods in Engineering*, 17:387–404, 1981.

[BN87] C.A. Brebbia and S.M. Niku. Conforming versus non-conforming boundary elements in three-dimensional elastostatics. *International Journal for Numerical Methods in Engineering*, 24:283–287, 1987.

[Boi89] J.M. Boisserie. A new C1 finite element: Full heptic. *International Journal for Numerical Methods in Engineering*, pages 667–677, 1989.

[Bro82] D. Broek. *Elementary Fracture Mechanics.* Nijhof, 1982.

[BTW84] C.A. Brebbia, J.C.F. Telles, and L.C. Wrobel. *Boundary Element Techniques - Theory and Applications in Engineering.* Springer-Verlag, 1984.

[Bui77] H.D. Bui. An integral equation for solving the problem of plane crack of arbitrary shape. *J. Mech. Physics and Solids*, 25:23–39, 1977.

[CMP89] R.D. Cook, D.S. Malkus, and M.E. Plesha. *Concepts and Applications of Finite Element Analysis.* Wiley, 1989.

[CN90] T.A. Cruse and G. Novati. Traction BIE formulations and applications to non-planar and multiple cracks. In *22nd ASTM Conference on Fracture Mechanics.* ASTM, 1990.

[Cru69] T.A. Cruse. Numerical solutions in three dimensional elastostatics. *International Journal of Solids and Structures*, 5:1259–1274, 1969.

[Cru88] T.A. Cruse. *Boundary Element Analysis in Computational Fracture Mechanics.* Kluwer, 1988.

[CVB71] T.A. Cruse and W. Van Buren. Three-dimensional elastic stress analysis of a fracture specimen with an edge crack. *International Journal of Fracture Mechanics*, 7:1–15, 1971.

[CWB90] J.J.S.P. Cabral, L.C. Wrobel, and C.A. Brebbia. A BEM formulation using b-splines: I- uniform blending functions. *Engineering Analysis*, 7:136–144, 1990.

[CZ57] A.P. Calderon and Zygmond. Singular integral operators and differential equations. *American Journal of Mathematics*, 79:901–921, 1957.

[Dan73] B. Danloy. Numerical construction of gaussian quadrature formulas for logarithmic and exponential weights. *Mathematics of Computation*, 27:861–869, 1973.

[Dav75] P.J. Davis. *Interpolation and Approximation.* Dover, 1975.

[DS90] E.W.D. Dijkstra and C.S. Scholten. *Predicate Calculus and Program Semantics.* Springer-Verlag, 1990.

[FW88] R.T. Fenner and J.O. Watson. A local boundary integral equation method for potential problems. *International Journal for Numerical Methods in Engineering*, 26:2517–2529, 1988.

[Gas58] R.E. Gaskell. *Engineering Mathematics.* Holt, Reinhart, and Winston, 1958.

[Gau70] W. Gautschi. On the construction of gaussian quadrature rules from modified moments. *Mathematics of Computation*, 24:245–259, 1970.

[GC87] Massimo Guiggiani and Paolo Casalini. Direct computation of cauchy principal value integrals in advanced boundary elements. *International Journal for Numerical Methods in Engineering*, 24:1711–1720, 1987.

[Ger86] W.H. Gerstle. *Finite and Boundary Element Modeling of Crack Propogation in Two- and Three-Dimensions Using Interactive Computer Graphics.* Ph.D. dissertation, Cornell University, Ithaca, NY, USA, 1986.

[GL81] A. George and J. Liu. *Computer Solution of Large Sparse Positive Definite Systems.* Prentice-Hall, 1981.

[GL90] L.J. Gray and E.D. Lutz. On the treatment of corners in the boundary element method. *Journal of Computational and Applied Mathematics*, 32:369–386, 1990.

[GM87] N. Ghosh and S. Muhkerjee. A new boundary element method formulation for three dimensional problems in linear elasticity. *Acta Mechanica*, 67:107–119, 1987.

[GMI90] L.J. Gray, Luiz F. Martha, and A.R. Ingraffea. Hypersingular integrals in boundary element fracture analysis. *International Journal for Numerical Methods in Engineering*, 29:1135–1158, 1990.

[Gra91] L.J. Gray. Evaluation of hypersingular integrals in the boundary element method. *Computers and Mathematics with Applications*, 1991. (In Press).

[Gri90] D. Gries. Teaching calculation and discrimination early in the curriculum. Technical Report TR 90-1110, Cornell University Dept. of Computer Science, 1990.

[GW69] G.H. Golub and J.H. Welsch. Calculation of gaussian quadrature rules. *Mathematics of Computation*, 24:221–230, 1969.

[HB88] K. Hayami and C.A. Brebbia. Quadrature methods for singular and nearly singular integrals in 3-D boundary element method. In *Boundary Elements X.* Computational Mechanics Publications (Springer-Verlag), 1988.

[Hug87] T.J.R. Hughes. *The Finite Element Method.* Prentice-Hall, 1987.

[IP88] N.I. Ioakimidis and M.S Pitta. Remarks on the gaussian quadrature rule for finite-part integrals with a second-order singularity. *Computer Methods in Applied Mechanics and Engineering*, 69:325–343, 1988.

[Jas63] M.A. Jaswon. Integral equation methods in potential theory, i. *Proceedings of the Royal Society*, 275:23–32, 1963.

[KSRR90] L.W. Krishnasamy, L.W. Schmerr, T.J. Rudolphi, and F.J. Rizzo. Hypersingular boundary integral equations: Some applications in acoustic and elastic wave scattering. *Journal of Applied Mechanics*, 57:404–414, 1990.

[Kun86] K.S. Kundert. Sparse matrix techniques. In *Circuit Analysis, Simulation and Design*. North-Holland, 1986.

[Kup65] V.D. Kupradze. *Potential Methods in the Theory of Elasticity*. D. Davey, 1965.

[Lea81] M.H. Lean. *Electromagnetic Field Solution with the Boundary Element Method.* Ph.D. dissertation, University of Manitoba, Winnipeg, Canada, 1981.

[Lea91] William E. Leary. NASA delays shuttle launching to repair cracks on door hinges. *New York Times*, March 1, 1991.

[Lut91] E.D. Lutz. Exact gaussian quadrature rules for near-singular integrals in the boundary element method. *Engineering Analysis with Boundary Elements*, 1991. (accepted for publication, Oct. 1990).

[LW76] J.C. Lachet and J.O. Watson. Effective numerical treatment of boundary integral equations: A formulation for three-dimensional elastostatics. *International Journal for Numerical Methods in Engineering*, 10:991–1005, 1976.

[LWI90] E.D. Lutz, P. Wawrzynek, and A.R. Ingraffea. Implementation of parameterized gaussian quadrature in the 2D BEM for elasticity. In A.H.D. Cheng, C.A. Brebbia, and S. Grilli, editors, *Computational Engineering with Boundary Elements: Vol. 2: Solid and Computational Problems.* Computational Mechanics Publications, 1990.

[Mar89] L.F.M. Martha. *Topological and Geometrical Modeling Approach to Numerical Discretization and Arbitrary Fracture Simulations in Three-Dimensions.* Ph.D. dissertation, Cornell University, Ithaca, NY, USA, 1989.

[MB86] G.D. Manolis and P.K Banerjee. Conforming versus non-conforming boundary elements in three-dimensional elastostatics. *International Journal for Numerical Methods in Engineering*, 23:1885–1904, 1986.

[Mik64] S.G. Mikhlin. *Variational Methods in Mathematical Physics.* MacMillan, 1964.

[Mik65] S.G. Mikhlin. *Multidimensional Singular Integrals and Singular Integral Equations.* Pergamon Press, 1965.

[Muh82] S. Muhkerjee. *Boundary Element Methods in Creep and Fracture.* Applied Science Publishers, 1982.

[Mus63] N.I. Muskhelishivili. *Some Basic Problems of the Mathematical Theory of Elasticity.* Noordhoff, 1963.

[NVB90] M. Nooijen, T.E. Velde, and E.J. Baerends. Symmetric numerical integration formulas for regular polygons. *SIAM Journal on Numerical Methods*, 27:198–218, 1990.

[ORA88] H. Okada, H. Rajiyah, and S.N. Atluri. A novel displacement gradient boundary element method for elastic stress analysis with high accuracy. *Transactions of the ASME, Journal of Applied Mechanics*, 55:786–794, 1988.

[Pat89] T.N.L. Patterson. An algorithm for generating intepolatory quadrature rules of the highest degree of precision with preassigned nodes. *ACM Transactions on Mathematical Software*, 15:123–136, June 1989.

[PCH87] E.Z. Polch, T.A. Cruse, and C.-J. Huang. Traction BIE solutions for flat cracks. *Computational Mechanics*, 2:253–267, 1987.

[Per84] R. Perucchio. *An Integrated Boundary Element Analysis System with Interactive Computer Graphics for Three-Dimensional Linear-Elastic Fracture Mechanics.* Ph.D. dissertation, Cornell University, Ithaca, NY, USA, 1984.

[Pol88] C. Polizzotto. An energy approach to the boundary element method. *Computer Methods in Applied Mechanics and Engineering*, 69:167–184, 1988.

[Riz69] F.J. Rizzo. An integral equation approach to boundary value problems of classical elastostatics. *Quarterly of Applied Mathemathics*, 25:83–95, 1969.